Electronic Transport Properties of Thin Films of Amorphous Silicon.

A thesis presented by

Henry Silvio Fortuna

(sponsoring establishment

Dundee College of Technology

collaborating establishment

Sheffield University)

to the CNAA

in partial fulfilment of the

requirements for the degree of

Doctor of Philosophy

November 1984.

To Colette, Nicola and Paul.

DECLARATION

I declare that while registered as a candidate for the degree for which this thesis is presented I have not been a candidate for any other award. I further declare that except where stated the work contained in this thesis is original and was performed by the author. The author is grateful to Dr. A. Long of Glasgow University who helped with the structural and chemical analyses of the Silicon films and to Mr. L. Arcari who assisted with the preparation of the computer programs.

Signed 

Henry Silvio Fortuna.

ADVANCED STUDIES

In addition to the original research reported in this thesis the author followed a program of postgraduate study. This program included attendance at the lectures and tutorials of the Joint Scottish Universities M.Sc course in the Physics and Technology of Amorphous Materials held at Dundee University during 1980 - 81. In addition the author attended the Chelsea Meeting on Liquid and Amorphous Semiconductors in 1980 and 1981, and participated in the Ninth International Conference on Amorphous and Liquid Semiconductors held in Grenoble, France in 1981.

ACKNOWLEDGEMENTS

I would like to express my gratitude to my supervisor Dr. Joseph M. Marshall for his constant interest, guidance, encouragement and friendship during the period of this study. Thanks are also due to Dr. Charles Main and Dr. Malcolm J. Thompson for stimulating discussions and constructive critisisims on the work presented in this thesis.

The assistance and co - operation of many members of the academic and technical staff of Dundee College of Technology is gratefully acknowledged, in particular Mr. J. Higgins and Mr. J.C. Anderson.

A further debt of thanks is due to Lindsay Arcari, Alan Sharp, Raymond Barclay, Charles Bullock and Catherine Dunn for their much appreciated friendship and assistance.

I thank the Science and Engineering Research Council for the provision of a Research Studentship, and the staff of the computer centre of Dundee College of Technology for their assistance in the preparation of this document.

Most of all, I wish to thank my wife Colette and my daughter Nicola for enduring my absence during the writing of this thesis.

ELECTRONIC TRANSPORT PROPERTIES OF THIN FILMS OF AMORPHOUS SILICON

HENRY SILVIO FORTUNA

The work reported in this thesis was carried out at the Physics Department of Dundee College of Technology between May 1980 and October 1983. The aims of the work were; (i) to develop a computer - based system for the capture and analyses of fast transient waveforms, with particular emphasis on the "Time of Flight" experiment, (ii) to commission an r.f. sputter - deposition system capable of producing thin films of amorphous Silicon, and to evaluate the electronic transport properties of the material prepared over a wide range of deposition conditions, and (iii) to investigate the electronic transport properties of thin films of co - sputtered Silicon - Aluminium and Silicon - Antimony, and to evaluate the effectiveness of Aluminium and Antimony as electronic dopants.

The apparatus constructed consists of an electron - gun capable of firing a pulsed electron beam, in the energy range 4 - 15 keV, at the top metallic contact of a semiconductor specimen. A Datalab DL905 transient recorder was used to capture and digitise the characteristic waveforms, these waveforms being sent to the College's Dec - System - 20 mainframe computer for analyses, via a NASCOM microcomputer. Computer programs were developed for the control of the experimental equipment and for the capture and analyses of the transient waveforms.

Dark d.c. conductivity, electron drift mobility, transient and steady state photoconductivity and optical absorption experiments were carried out on thin films of amorphous Silicon. These measurements reveal wide variations in the electronic transport properties of specimens of amorphous Silicon prepared under seemingly identical deposition conditions. The experimental results are interpreted in terms of localised conduction band tail states extending to approximately 0.2 eV below the conduction band mobility edge, and a discrete set of localised states situated at 0.4 eV below the conduction band mobility edge. It is suggested that the extent of the tail states and the density of the discrete states are critically dependent upon the conditions of film deposition and upon the level of impurity atoms within the material.

Silicon - Aluminium films were found to contain crystalline Aluminium islands embedded within an amorphous lattice. Silicon - Antimony films appeared homogeneous to a resolution of 50 Angstroms. The addition of Aluminium or Antimony to the amorphous Silicon was seen to increase the room temperature conductivity and decrease the conductivity activation energy and the optical band gap. It is suggested that neither Aluminium or Antimony act as effective substitutional dopants for the particular films of amorphous Silicon prepared in this laboratory.

CONTENTS

CHAPTER 1

AMORPHOUS SEMICONDUCTORS

1.1 INTRODUCTION

Today's interest in amorphous semiconductors stemmed from the pioneering work of Kolomiets and co - workers (1,2) at the Leningrad school in the early fifties. Since then, research in several countries has been directed towards deepening the understanding of the structural, electrical, optical and other properties of these materials, in an attempt to approach the present level of understanding of crystalline materials.

Early research in the field was stimulated by the successful use of amorphous selenium in the Xerox reprographic process. This prompted further research through fundamental scientific interest. In 1968, Ovshinsky (3) detailed various types of switching phenomena that occurred in a large class of amorphous solids and the subsequent publicity, describing many potential applications of these phenomena, prompted many laboratories to turn their attention to the study of amorphous materials.

A further surge of interest occurred in 1975 when Spear and Le Comber (4,5) reported the successful doping of amorphous Silicon, both n - type and p - type. This discovery offered a reasonable chance that at least some aspects of this field of research could lead to highly profitable new applications in solid state electronics.

Prior to 1975, the commercial applications of amorphous semiconducting materials had been limited to only a few areas, with reprographics being of major importance. However, the field is rapidly advancing and new commercial applications of amorphous semiconducting materials (especially amorphous Silicon) are just beginning to be realised. Products containing amorphous Silicon photovoltaic cells and thin film transistors are now on the market.

1.2 STRUCTURE

Prior to the early 1900's, solids were designated amorphous if they had a formless fracture surface. With the advent of X - rays and their use in studying crystalline materials, it was found that most solids characterised amorphous by fractography were also non - crystalline as evidenced by X - ray diffraction. That is, they did not exhibit the sharp reflections associated with crystalline materials but instead exhibited a few broad halos (6). Amorphous and non - crystalline are in present terminology synonymous. Thus, we can structurally classify materials either as crystalline or non - crystalline (amorphous).

An IDEAL crystal is defined as a substance consisting of atoms arranged in a pattern that repeats periodically in three dimensions (7). In the idealised mathematical description of a crystal, a given lattice point is in exactly the same environment as any other equivalent lattice point, and the contents of every unit cell, (called the basis), are identical to those of every other unit cell. The cells extend infinitely in all directions and the crystal is said to

possess long range order (LRO). The immediate surroundings of a given atom, such as the number of nearest and next nearest neighbours and their distances, are identical to those of any corresponding atom in any other unit cell, and this is called the short range order (SRO).

In practice, ideal crystals do not exist since no real material can satisfy the condition specified by infinite long range order. REAL crystals, therefore, are materials of finite dimensions. Under normal circumstances (i.e. when the crystal extends in all directions by many interatomic spacings), this dimensional limitation is of minor importance and only leads to small perturbations from the ideal crystalline theory.

Amorphous solids differ from crystalline materials in that there is no long range order. There is no periodicity and no way of defining an extended regular lattice as a realistic description of the structure. Nevertheless, the same chemical properties of the individual atoms still control the local interactions and environment and most of the chemical bonds will be satisfied. This forces some similarity with the crystalline phase, in-so-far as it is compatible with the loss of long range order. There remains a short range order which extends only to distances of a few interatomic spacings. Thus, an amorphous material may be conveniently defined as one without long range order.

The nature of short - range order in amorphous materials has been extensively studied, especially by X - rays and electron diffraction. Figure 1.1 shows a typical example of the radial distribution function for amorphous Germanium (a-Ge). The vertical lines indicate the

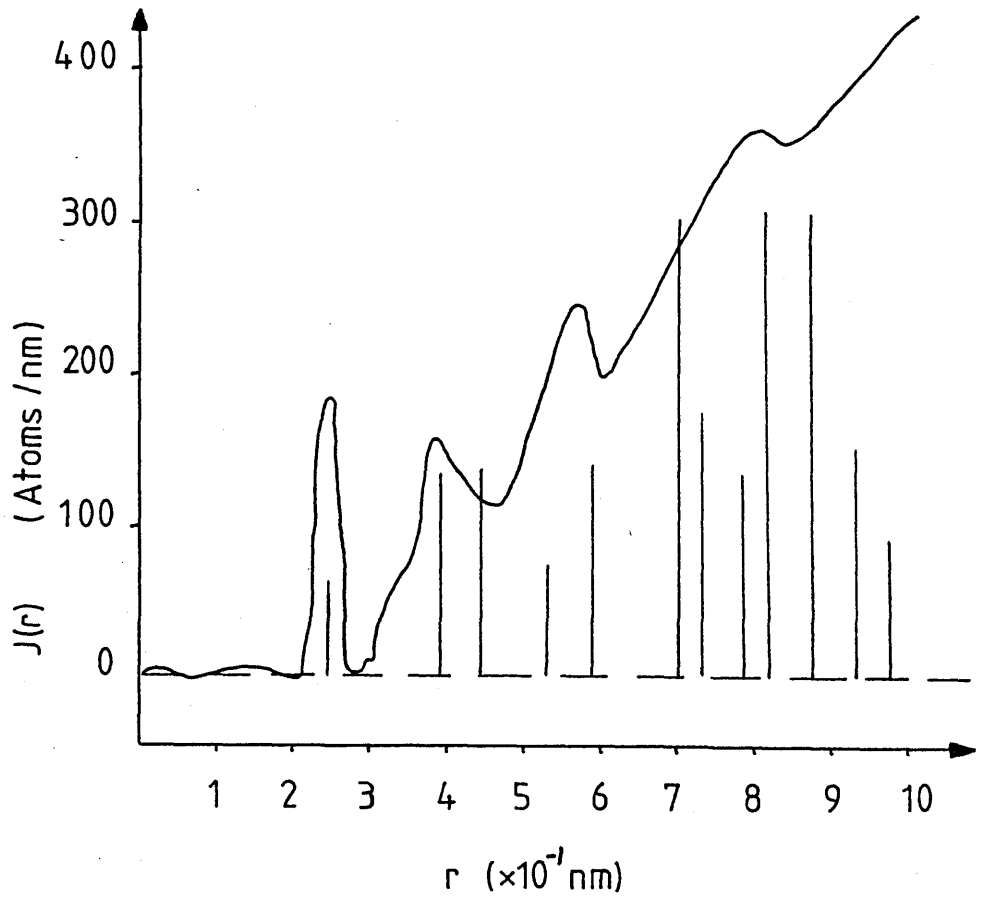

Figure 1.1. Radial Distribution Function determined for a - Ge. Vertical lines indicate sharp peaks expected in crystalline Ge.

position of sharp peaks expected in crystalline Ge. The figure shows clearly that the short - range order extends to about 1 nm, (that being about three nearest - neighbour distances), and then merges into the statistical background. Most amorphous materials produce radial distribution functions with features similar to figure 1.1.

In an attempt to determine the procedures by which materials with no long range order can arise, model amorphous structures have been generated, relaxed and optimised by computer, then analysed. Using such techniques it has been shown that the observed radial distribution function for tetrahedrally co-ordinated materials such as a-Si and a-Ge can be explained quite satisfactorily by a relatively small spread in bond angle distribution and the break down of the rigid configuration of the tetrahedral unit.

An important concept arising out of such structural work is that of a CONTINUOUS RANDOM NETWORK. This ideal amorphous structure represents a fundamental concept on which many theoretical considerations are based. The major reason, however, why theory and experiment do not agree in many cases is because it has now been realised that materials prepared experimentally have structures which deviate from the ideal continuous random network. In fact, structures of amorphous tetrahedral semiconductors often contain an appreciable density of defects of the vacancy type, and the unsaturated bonds associated with these defects introduce electronic states into the system which can completely dominate the observed properties.

1.3 ELECTRONIC STRUCTURE AND THE EFFECT OF DISORDER

The theoretical treatment of crystalline solids is generally based on the assumption of perfect structural periodicity (or long - range order). Bloch wavefunctions extend throughout the infinite lattice, leading to a completely delocalised description of the electron. In other words, an electron can take up any position in the lattice with finite probability, just as in the free electron case. Occasionally scattering (by lattice vibrations or structural imperfections) limits the lifetime in the Bloch states, but this can be treated as a perturbation in the theory. The delocalised treatment applies in the case where the mean free path, L, of the carriers is much greater than the lattice spacing, a, i.e. $L \gg a$.

The first steps towards a development of a theory for the electronic structure of disordered solids were not taken until almost 20 years after the work of Bloch, when Frohlich (1947) (8) pondered the nature of the eigenstates in the tails of the bands. It was not until much later that Mott (1967) (9) combined these ideas with the work of Anderson (1958) (10) on the absence of diffusion in a three dimensional random potential to give a simple model containing the essential features common to all disordered systems.

The model starts with the theory of a perfect crystalline lattice and investigates what happens when an increasing amount of disorder is progressively introduced (say by elementary particle irradiation of a crystalline semiconductor). As disorder increases, the periodic potential of the lattice will be disturbed, the scattering will be

enhanced and the carrier mean free path reduced. As the limiting condition, $L \simeq a$, is approached, the Bloch wavefunctions will loose their phase coherence in a few interatomic spacings and the wavefunctions representing the electron will look like that shown in figure 1.2(a). It is interesting to note that even though the phase coherence has been lost, the wavefunction still extends throughout the complete disordered structure without attenuation.

If the disorder (and hence the random potential fluctuations) in the structure is increased further, a fundamental change in the form of the wavefunction takes place. Figure 1.2 (b) and (c) refer to this situation and show that the wavefunction becomes modulated by an exponentially decaying envelope. It means that the electron has become localised in space, no longer having finite probability of taking up any position in the lattice.

The transition from extended to localised states is one of the most important aspects in the treatment of non - crystalline materials and will be reviewed on a more quantitative basis below.

1.3.1 ANDERSON LOCALISATION

The first paper to prove and to give a quantitative criterion for disorder induced localisation was that by Anderson (10) (1958). The theoretical approach is based on the tight - binding approximation and is applicable when the electron wave functions are weakly overlapping and bands are narrow. It can be shown that the bandwidth, B, is given by

$$B = 2zJ \qquad - (1.1)$$

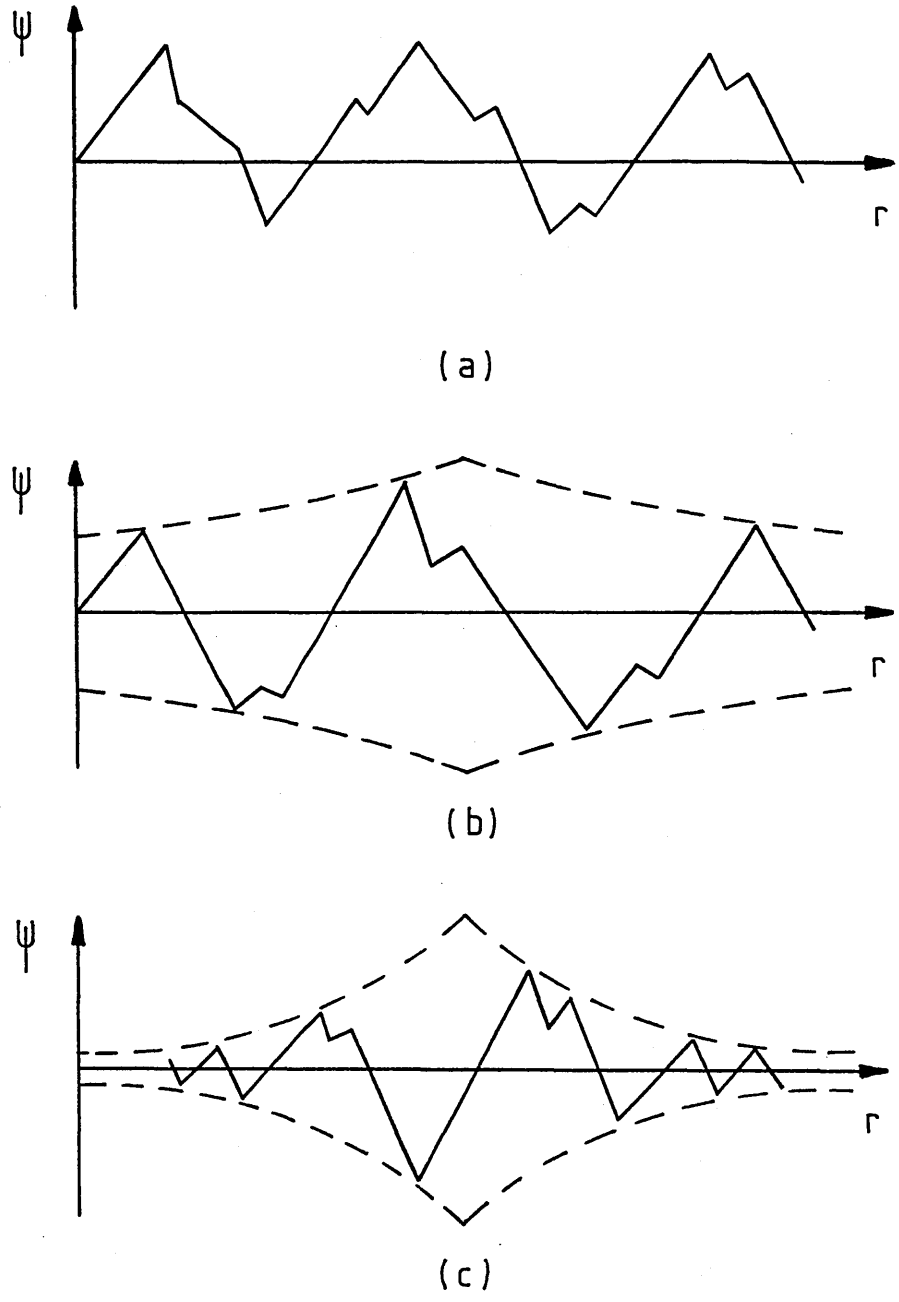

Figure 1.2. Form of the wavefunctions in an amorphous solid. (a) Delocalised. (b) Weak localisation. (c) Strong localisation.

where J is the two site exchange integral, (essentially a measure of the wavefunction overlap of electron states on nearest - neighbour atoms) and z is the co-ordination number.

The tight - binding approach is often applied to a three dimensional crystalline solid with rectangular potential wells each containing a bound electron state (figure 1.3(a)). Disorder is introduced by distributing the energies of the sites over a range, Vo, as indicated in figure 1.3(b), resulting in a broadening of the density of states spectrum, (no attempt is made in the model to account for disorder in position of the potential wells). Using scattering theory, the effective mass approximation and the results of the tight - binding approximation, Mott (9) derived the expression

$$\frac{a}{L} = \frac{1}{16\pi}\left(\frac{V_o}{J}\right)^2 = \frac{4z^2}{16\pi}\left(\frac{V_o}{B}\right)^2 \qquad - (1.2)$$

This equation brings out the importance of the ratio Vo/J (or Vo/B) to the problem. As the limiting case a/L = 1 is approached (Vo/B = 0.6 using z = 6 for a simple cubic lattice) the electron wavefunctions loose phase coherence and begin to look as in figure 1.2(a).

The difficult theoretical problem, first considered by Anderson (10), was what value of Vo/B is necessary to produce complete localisation at T = 0? His calculations suggest that localisation throughout the narrow band would occur when

$$\frac{V_o}{B} = 5 \qquad - (1.3)$$

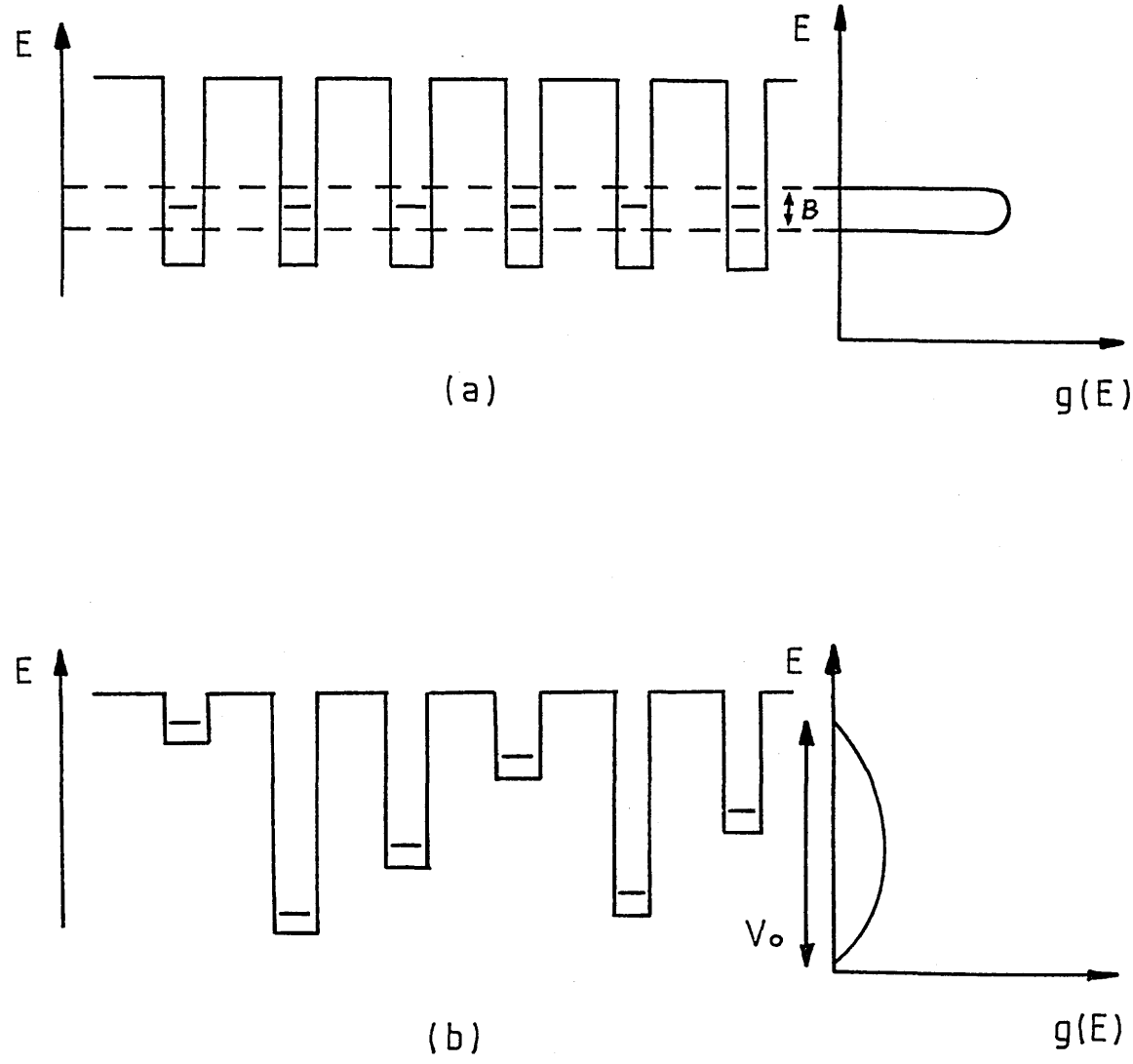

Figure 1.3. Tight - binding model showing potential wells for (a) Crystalline solid (b) Disordered solid.

More recent work (11,12) has given a smaller critical value of about 2.

The important result, however, is that "Anderson localisation" sets in when the ratio Vo/B exceeds a critical value. All states in the narrow tight - binding band will then be localised as shown in figure 1.2(b) and (c), implying that at T = 0, the ensemble average over a transport quantity such as conductivity must vanish, i.e.

$$\langle \sigma \rangle = 0 \quad \text{at } T=0$$

A second important concept arising out of the Anderson criterion for localisation is that of a "minimum metallic conductivity". Mott (13), has shown that when Vo/B reaches the critical value for localisation, the conductivity is given by

$$\sigma_{min} = \frac{\pi e^2}{4z\hbar a}\left(\frac{B}{V_o}\right)_{crit} \qquad - (1.4)$$

were a is the interatomic spacing and z the co - ordination number. Taking values of (Vo/B)crit = 2 and z = 6 results in a conductivity of

$$\sigma_{min} = \frac{61}{a} \quad (\Omega\, cm)^{-1} \qquad - (1.5)$$

where a is in nanometers. The importance of these relationships is that when Vo/B exceeds the critical value, the conductivity drops discontinuously to zero. Thus, in non - crystalline materials where the value of conductivity tends to a finite value as temperature tends

to zero, σ_{min} is the smallest value of conductivity that the material can have.

1.3.2 THE MOBILITY EDGE

It was stated in the above section that in order to obtain Anderson localisation of a complete band, the bandwidth, B, must be small. In an amorphous semiconductor, however, wide conduction bands are generally found. How then can Anderson localisation be applied to these wide band materials ?

Figure 1.4 shows the density of states, g(E), plotted against energy for an amorphous semiconductor. The important fact to recognise about this distribution is that the two site exchange integral, J, will vary throughout the band, since it is critically dependent upon the separation of the states. The electron wavefunction overlap will be much smaller in the "tails" of the band, (where g(E) is small), so that Vo/J will reach the critical value for localisation first in the tail states. States away from the edge of the band will remain delocalised. For the purpose of illustration, consider the conduction band, and suppose that localisation sets in when the density of states falls below a value corresponding to energies, Ec, at the top and bottom of the band. Considering only the bottom of the band (the top of the band being insignificant as far as conduction is concerned), at energies $E > Ec$, there are extended states in which conduction can take place, even at $T = 0$. For energies $E < Ec$, the ensemble average of conductivity will be zero at

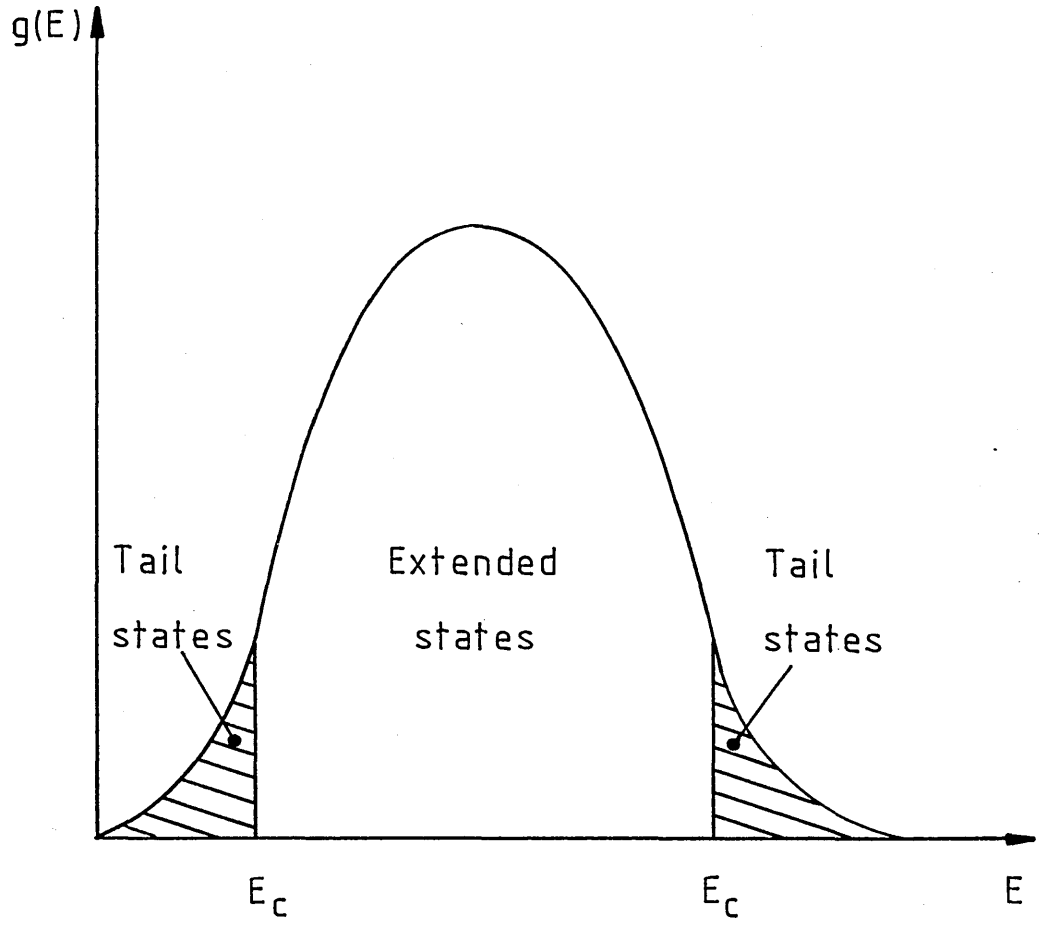

Figure 1.4. Density of states in a wide conduction band amorphous semiconductor. The tail states are localised.

T = 0, and the mobility must vanish. The existence of an energy such as Ec, was first pointed out by Mott (9,14), and its existence in non - crystalline semiconductors implies a "mobility edge" which takes the place of (for many practical purposes) the density of states edge in crystalline semiconductors.

1.4 SUMMARY

The above description of an "ideal" amorphous semiconductor forms the basis on which the electrical and optical properties of real amorphous semiconductors may be understood. There is a great deal of experimental evidence to support the existence of bands in amorphous semiconductors dating from the pioneering work of Kolomiets and co - workers (1,2) in the 1950's. There is also a large amount of experimental evidence to support the presence of mobility edges (the position of which may be temperature dependent), which has been reviewed by a number of authors (15). The sharpness of the mobility edge, however, as well as the existence of a "minimum metallic conductivity" at low temperature still remains controversial.

Detailed measurements of drift mobility, field effect, photoconductivity, etc., on a variety of materials have subsequently verified the existence of fairly discrete levels, or at least structure, in the distribution of the density of states throughout the mobility gap of some amorphous semiconductor. The existence of these localised defect and tail states, together with extended band states and the concept of mobility edges, will be assumed in the following

section in order to describe the transport properties of amorphous semiconductors.

1.5 ELECTRONIC TRANSPORT IN AMORPHOUS SOLIDS

For the purpose of discussion, the schematic density of states distribution shown in figure 1.5 will be used. The diagram shows the density of states, g(E), from just above the lower edge of the conduction band to just below the upper edge of the valence band. The energy spectrum is divided according to the electronic character of the states; namely extended states (E), band tail states (T), and gap states (G). The states shown shaded in figure 1.5 are localised.

Two main conduction mechanisms are generally observed in amorphous materials, namely extended - state conduction and localised - state conduction. These mechanisms will be discussed below.

1.5.1 EXTENDED STATE CONDUCTION

Extended state conduction occurs for electrons at energies above Ec, and for holes below Ev. In these regions the effect of the random potential and of fluctuations in the interatomic distance dominates the transport. In the case of electrons, the mean free path just above Ec, and the coherent length of the electrons' wavefunction approach the interatomic separation, so that one can no longer regard transport as band motion with occasional scattering. Cohen (16),

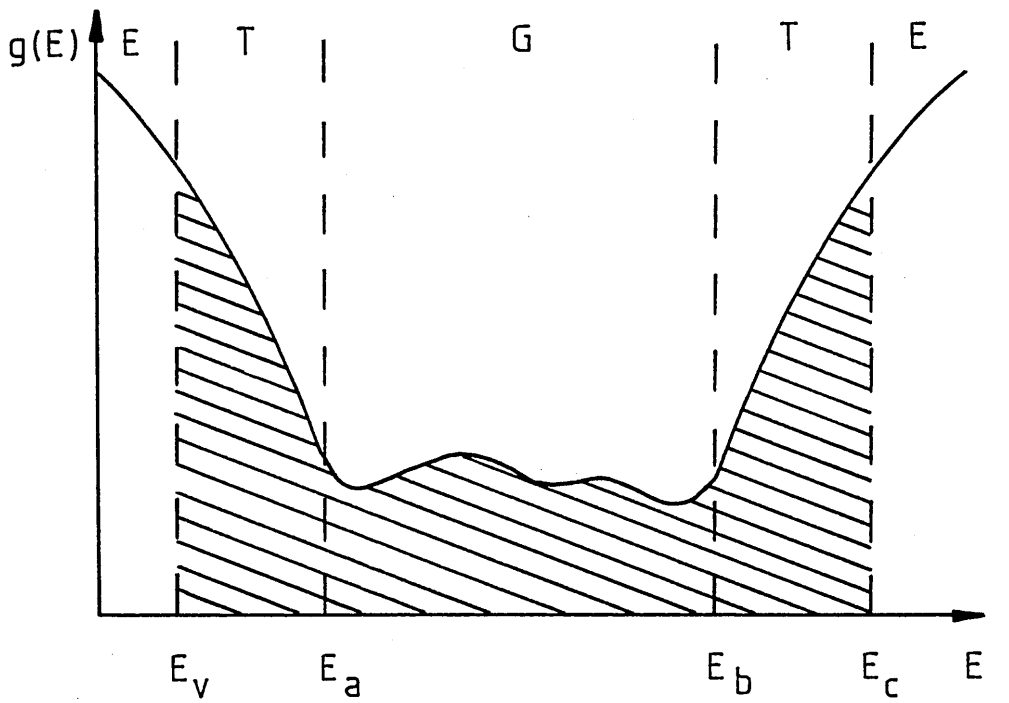

Figure 1.5. Schematic density of states distribution in an amorphous semiconductor. States are localised in the shaded part of the distribution.

pointed out that in this region of extended states, conduction is essentially a diffusive process, quite similar to Brownian Motion. The electron can be envisaged as jumping from site to site with an atomic frequency ν_{el}, but without any thermal activation. Adopting such a classical picture Cohen derived an expression for the mobility, i.e.

$$\mu = \frac{1}{6}\left[\frac{ea^2}{kT}\right]\nu_{el} \qquad - (1.6)$$

Where a is the average interatomic distance and ν_{el} is an electronic jump frequency of the order of 10^{15} sec^{-1}. An estimated drift mobility of about 10 $cm^2 V^{-1} s^{-1}$ is obtained using equation (1.6).

A more exact analysis of the transport just above Ec, is based on the so called "random phase" model (17,18). In this model a mean free path of the order of the lattice spacing is represented by a loss of phase memory of the electron wavefunction as it moves from site to site. Assuming a constant density of states at the mobility edge g(Ec), Friedman (18) derived the following expression for the mobility in the extended states near Ec or Ev.

$$\mu = \frac{2\pi}{3} \cdot \frac{ea^2}{h} \cdot z \cdot \frac{J}{kT} \cdot a^2 J g(E_c) \qquad - (1.7)$$

Here z is the co-ordination number, J is the two site exchange integral and a is the interatomic spacing. Equation (1.7) yields a value of 5 $cm^2 V^{-1} s^{-1}$ for the mobility at room temperature, a value not significantly different from that obtained by the simple estimate of equation (1.6).

1.5.2 LOCALISED STATE CONDUCTION.

Conduction through localised tail or defect states takes place only with phonon assistance. The mobility, $\mu(E)$, for this thermally assisted tunnelling transport, at an energy E, is normally written in the form:

$$\mu(E) = \frac{1}{6}\left(\frac{eR^2}{kT}\right)\nu_{ph}\exp(-2\alpha R)\exp\left(\frac{-W}{kT}\right) \quad - \quad (1.8)$$

As illustrated in figure 1.6, R = Ro is the average nearest - neighbour hopping distance, which depends on the density of states distribution, and is thus a function of energy. The term $\exp(-2\alpha R)$ describes the overlap of the wavefunctions on neighbouring hopping sites, with the parameter $1/\alpha$ representing the range of spatial decay of a localised wavefunction. ν_{ph} is a phonon "attempt to escape" frequency, and $\exp(-W/kT)$ represents the probability that an electron will gain an energy W, in order to move from one site to another. Equation (1.8) predicts hopping mobilities at room temperature of 10^{-2} $cm^2 V^{-1} s^{-1}$ or less. Comparing this value with the mobility obtained for extended state conduction just above Ec (or below Ev), suggests that at Ec (and Ev) the mobility drops by something like three orders of magnitude at the "mobility edge".

In general, there are many current paths through the localised states, all of which can contribute to the observed electrical properties. A common simplifying assumption which is normally used, however, is that at any given temperature one of these paths will

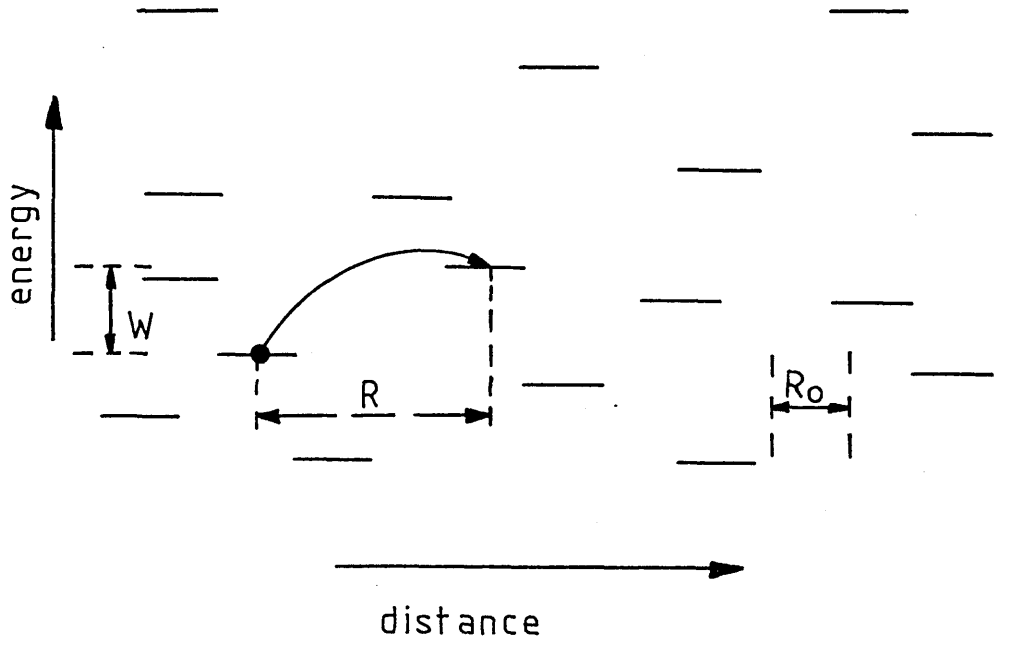

Figure 1.6. Nearest - neighbour hopping transport in an amorphous semiconductor.

predominate. This theme will be investigated further in Chapter 2, where a complete analysis of the temperature dependence of the conductivity of amorphous semiconductors will be presented.

REFERENCES CHAPTER 1

(1) Kolomiets B.T., Phys. Stat. Sol. 7, 359, (1964).

(2) Kolomiets B.T., Phys. Stat. Sol. 7, 713, (1964).

(3) Ovshinsky S.R., Phys. Rev. Lett. 21, 1450, (1968).

(4) Spear W.E., Le Comber P.G., Solid State Comm. 17, 1193, (1975).

(5) Spear W.E., Le Comber P.G., Phil. Mag. 33, 935, (1976).

(6) Olley J.A., Ph.D Thesis, University of Cambridge (1972).

(7) Barrett C.S., Structure of Metals, 2nd ed.
(Mc Graw Hill Book Co., New York), (1952).

(8) Frohlich H., Proc. R. Soc. A 188, 521, (1947).

(9) Mott N.F., Adv. Phys. 16, 49, (1967).

(10) Anderson P.W., Phys. Rev. 109, 1492, (1958).

(11) Edwards J.T., Thouless D.J., J. Phys. C 5, 807, (1972).

(12) Herbert D.C., Jones R., J. Phys. C 5, 4, 1145, (1971).

(13) Mott N.F., Phil. Mag. 26, 1015, (1972).

(14) Mott N.F., Phil. Mag. 13, 989, (1966).

(15) Mott N.F., Pepper M., Pollitt S., Wallis R.H.,
Adkins C.J., Proc. R. Soc. A 345, 169, (1975).

(16) Cohen M.H., J. Non-Cryst. Sol. 4, 391, (1970).

(17) Hindley N.K., J. Non-Cryst Sol. 5, 17, 31, (1970).

(18) Friedman L., J. Non-Cryst. Sol. 6, 329, (1971).

CHAPTER 2

EXPERIMENTAL STUDY OF AMORPHOUS SEMICONDUCTORS.

This chapter deals with the main experimental methods that are used in studying the transport and optical properties of amorphous semiconductors, and discusses, with examples, the information that can be obtained from the results.

2.1 ELECTRICAL CONDUCTIVITY AND ITS TEMPERATURE DEPENDENCE.

Electrical conductivity is determined by the number of free carriers at each energy and their mobility. Thus in the dark, conductivity is given by

$$\sigma = e\int_0^\infty g(E)\mu(E)f(E)\,dE \qquad - (2.1)$$

where e is the electronic charge, g(E) the density of states, μ(E) the mobility of a carrier at energy E and f(E) the probability that a state at energy E is occupied by an electron. f(E) is the so - called Fermi - Dirac function and is given by

$$f(E) = \frac{1}{1 + \exp\left[\frac{E - E_f}{kT}\right]} \qquad - (2.2)$$

where the energy corresponding to E_f is called the Fermi level. Conduction at energies below the Fermi level is normally considered to be due to positive holes. The probability of a state at energy E not being occupied by an electron, i.e. of containing a hole, is

$$\overline{f(E)} = 1 - f(E) \qquad - \quad (2.3)$$

From equation 2.1 it can be seen that the conductivity of any solid is intimately related to the electronic density of states, g(E), for that material. Thus, in order to aid a description of the conduction mechanisms which may occur in an amorphous solid, the density of states distribution shown in figure 2.1 (a) will be employed. This distribution is of interest since it illustrates the main conduction processes which can take place in an amorphous solid, but is of no other significance. In order to aid clarity, the discussion will also be restricted to electrons, but unless otherwise stated, the equations and situations described are equally applicable to holes.

Figure 2.1 shows the expected variation of the functions $\mathcal{N}(E)$, f(E) and $\sigma(E)$ with energy, for the case of the given distribution g(E) at a number of temperatures. Since g(E) is temperature independent and $\mathcal{N}(E)$ is likely to vary only slowly with temperature, it is f(E) (with its strong temperature dependence given by equation 2.2) which will determine how the energy of the dominant conduction path, and hence the dominant conduction mechanism, is likely to vary with temperature.

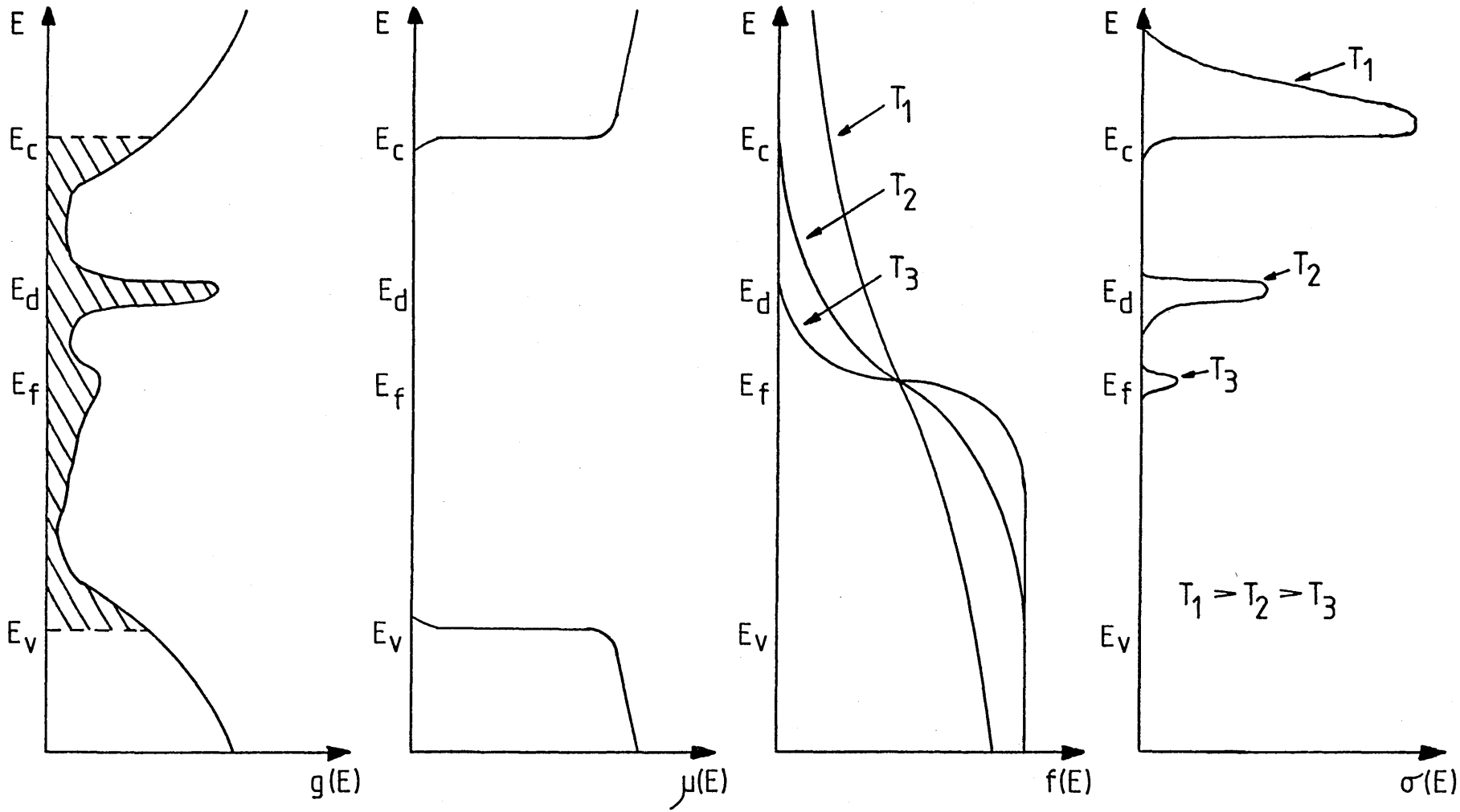

Figure 2.1. Energy dependence of the mobility μ(E), occupation function f(E) and conductivity σ(E), for the given density of states distribution g(E), at a number of temperatures. Graph (d) considers electrons only and shows the dominant conduction path which exists at the temperatures indicated.

At high temperatures (T_1 in figure 2.1) the conductivity is dominated by electrons thermally activated to extended states above the mobility edge at E_c. Under these conditions, the electrical conductivity can be written, just as in the crystalline case as

$$\sigma = n e \mu \qquad - (2.4)$$

where n is the electron density in extended states and μ_c is the electron mobility at E_c as described by equation 1.6 or 1.7. If $(E_c - E_f) \gg kT$ and g(E) does not vary too much in the neighbourhood of E_c, where it has a value $g(E_c)$, then

$$n = g(E_c)\, kT \exp\left[-\frac{E_c - E_f}{kT}\right] \qquad - (2.5)$$

The extended state conductivity of electrons above E_c can therefore be written

$$\sigma = g(E_c)\, kT e \mu_c \exp\left[-\frac{E_c - E_f}{kT}\right] \qquad - (2.6)$$

One feature of the conductivity not accounted for by equation 2.6 is the variation in the width of the mobility gap with temperature. If this is taken to be linearly dependent on temperature with coefficient δ such that

$$(E_c - E_f)_T = (E_c - E_f)_0 - \delta T \qquad - (2.7)$$

then the expression for extended state conductivity becomes

$$\sigma = \sigma_o \exp\left[-\frac{(E_c - E_f)_o}{kT}\right] \qquad - (2.8)$$

with

$$\sigma_o = g(E_c) kT \mu_c e \exp\left[\frac{\delta}{k}\right] \qquad - (2.9)$$

It is important to note that for a material having conductivity characterised by equation 2.8, a graph of $\ln(\sigma)$ versus $1/T$ will yield a straight line with activation energy $(E_c - E_f)o$, the position of the Fermi level relative to the mobility edge, extrapolated to $T = 0$. The intercept on the $\ln(\sigma)$ axis at $1/T = 0$ will provide the constant σ_o.

The value of σ_o is not strongly dependent on individual material parameters and for most amorphous semiconductors lies in the range 10^2 to 10^4 $(\Omega.cm)^{-1}$. Many examples of this are cited by Fritzsche (1) and by Mott and Davis (2). A particular example is the case of the temperature dependence of the conductivity of the chalcogenide glass $Tl_2 Se\ As_2(Te_x Se_{1-x})_3$ studied by Andriesh and Kolomiets (3) and shown in figure 2.2. It is clear from figure 2.2 that as the material composition is changed the activation energy for conductivity changes, but the pre - exponential factor, σ_o, does not vary much.

Returning to figure 2.1, as the temperature is lowered, the number of electrons thermally activated to E_c reduces and the contribution to the total conductivity of electrons in extended states diminishes. Under such reduced temperatures it is possible for the

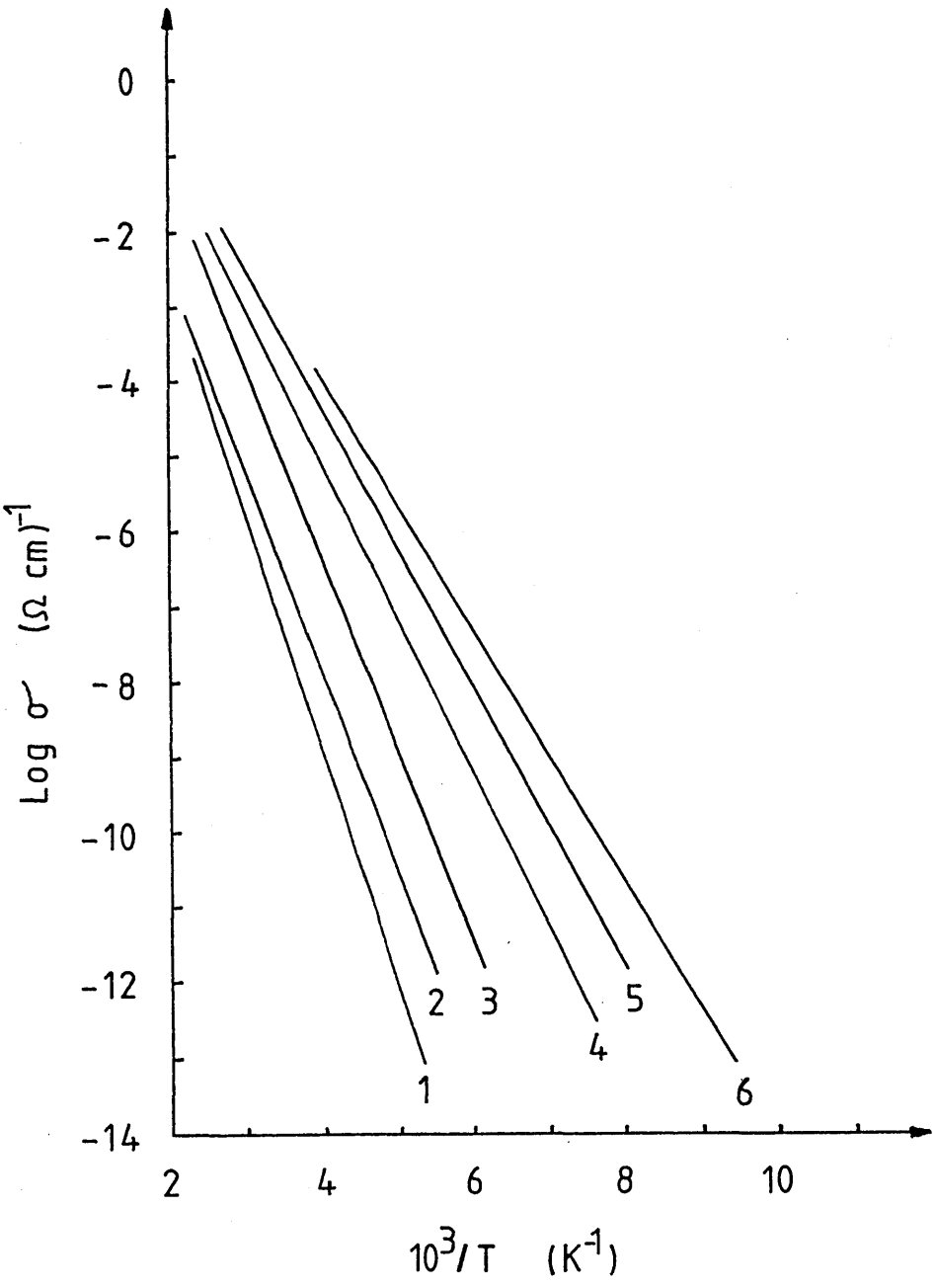

Figure 2.2. Temperature dependence of the conductivity of $Tl_2 Se_3 As_2 (Te_x Se_{1-x})_3$ where x = 0, 0.2, 0.4, 0.6, 0.8 and 1.0 in curves 1 to 6 respectively. (After ref. 3).

dominant conduction path to move from its position in extended states to a location between E_c and the Fermi level. This can only occur, however, when there exists a region in the mobility gap where the variation in the magnitude of the density of states with energy is greater than the corresponding variation of the occupation probability with energy. Such a region is depicted by the feature at energy E_d in figure 2.1 (a).

In order to determine whether the conduction path through states at E_d dominates the total conductivity at any given temperature, the contribution to the total conductivity of the path at E_d must be evaluated. This can be accomplished using the integral

$$\sigma_{E_d} = e\int_{E_d-\Delta E/2}^{E_d+\Delta E/2} g(E)\,\mu(E)\,f(E)\,dE \qquad - \quad (2\cdot10)$$

where ΔE is the width of the feature in the density of states at E_d. If at any given temperature $\sigma_{E_d} \simeq \sigma$, where σ is the total conductivity given by equation 2.1, then it may be concluded that the total conductivity is dominated by the conduction path at E_d.

Since all the states in the mobility gap are localised, conduction at E_d must be via a hopping mechanism. Furthermore, if the width of the feature in the density of states extends over only a small range of energy, then it may be assumed that carriers move between sites of effective density $g(E_d)$ and average separation $R = [g(E_d)]^{-\frac{1}{3}}$. Under these conditions the total conductivity may be written in the form

$$\sigma = \sigma_1 \exp\left[-\frac{(E_d - E_f)_o + W_1}{kT}\right] \qquad - \quad (2\cdot11)$$

where $(E_d - E_f)o$ is the position of the dominant conduction path relative to the Fermi level at T = 0, and W_1 is a hopping energy. The pre - exponential σ_1 is given by

$$\sigma_1 = g(E_d)\mu_d e \exp\left[\frac{\delta_1}{K}\right] \qquad - \qquad (2.12)$$

where μ_d is a hopping mobility, and δ_1 is a coefficient which characterises the variation in the band gap with temperature. The magnitude of σ_1 is not expected to exceed 10^{-1} $(\Omega.cm)^{-1}$, and using computer simulations Marshall (4) has shown that the hopping energy W_1 is likely to take a value of approximately half the energy spread of the feature under consideration, i.e. $W_1 \simeq \Delta E/2$.

As the temperature is lowered further, the occupation probability of states at E_d is reduced, resulting in a corresponding reduction in the contribution to the total conductivity of the path at E_d. Since (in figure 2.1 (a)) there is a continuous fall in the density of states from E_d to the Fermi level a critical temperature will exist where below that temperature the dominant conduction path will switch from hopping at E_d to hopping at the Fermi level. Carriers moving at the Fermi level require no energy to activate them to their conduction path, so the conductivity may be expected in the form

$$\sigma = \sigma_2 \exp\left(-\frac{W_2}{KT}\right) \qquad - \qquad (2.13)$$

with

$$\sigma_2 = g(E_s) e \mu_f \qquad - \qquad (2.14)$$

$g(E_f)$ is the effective density of states at the Fermi level, μ_f is the carrier mobility at the Fermi level and W_2 is a hopping energy with a form similar to that described for the case of hopping at E_d. The magnitude of σ_2 is normally expected to be less than σ_1 (i.e. $\sigma_2 < \sigma_1$) since both the density of states and the mobility at the Fermi level are expected to be less than their respective values at the energy E_d.

At even lower temperatures it can become energetically more favourable for carriers to hop large distances in order to find final sites close in energy ($\simeq kT$) to their initial sites. Thus conduction occurs close to the Fermi level by so - called variable range hopping. Under these circumstances, Mott (5,6) has shown that for three dimensional hopping within a density of states $g(E_f)$, the conductivity is given by

$$\sigma = \sigma_3 \exp\left(\frac{T_o}{T}\right)^{-\frac{1}{4}} \qquad - (2.15)$$

with

$$T_o = \frac{18\alpha^3}{k\, g(E_f)} \qquad - (2.16)$$

This is known as Mott's $T^{-\frac{1}{4}}$ law.

As described by equation 2.1, the total conductivity for all processes is obtained as an integral over all available energy states and the manner in which this conductivity is expected to vary with temperature is illustrated in a plot of $\ln(\sigma)$ versus $1/T$ shown in

figure 2.3. On the basis of this model, the expected temperature dependence of the drift mobility and thermopower (discussed in the following sections) are also schematically illustrated in figure 2.4.

2.1.1 HIGH FIELD EFFECTS.

At high electric fields the enhanced emission of carriers into extended conduction band or valence band states from localised states (the Poole - Frenkel effect), or from metal electrodes (the Shottky effect), can occur. Other high electric field effects exist such as field assisted hopping, hot carriers and field stripping of traps. All of these lead to an electric field dependent conductivity.

(a) The Poole - Frenkel Effect (7).

In the Poole - Frenkel effect, depicted in figure 2.4, the ionisation energy of a localised center subject to a coulombic potential is reduced by the application of an external field. In a simple one - dimensional treatment the potential energy of an electron a distance x from a localised center is given by the expression $-e^2/4\pi\varepsilon\varepsilon_0 X$, where ε is the relative high frequency dielectric constant and ε_0 is the permittivity of free space. In the absence of an applied field, a trapped carrier must surmount a barrier E_t in order to enter the band. The application of an electric field, F, lowers the barrier, in the direction of the field, by an amount -Fex and a maximum down field barrier is obtained at X_m. The barrier is smaller than its original height by an amount $\beta F^{\frac{1}{2}}$ where

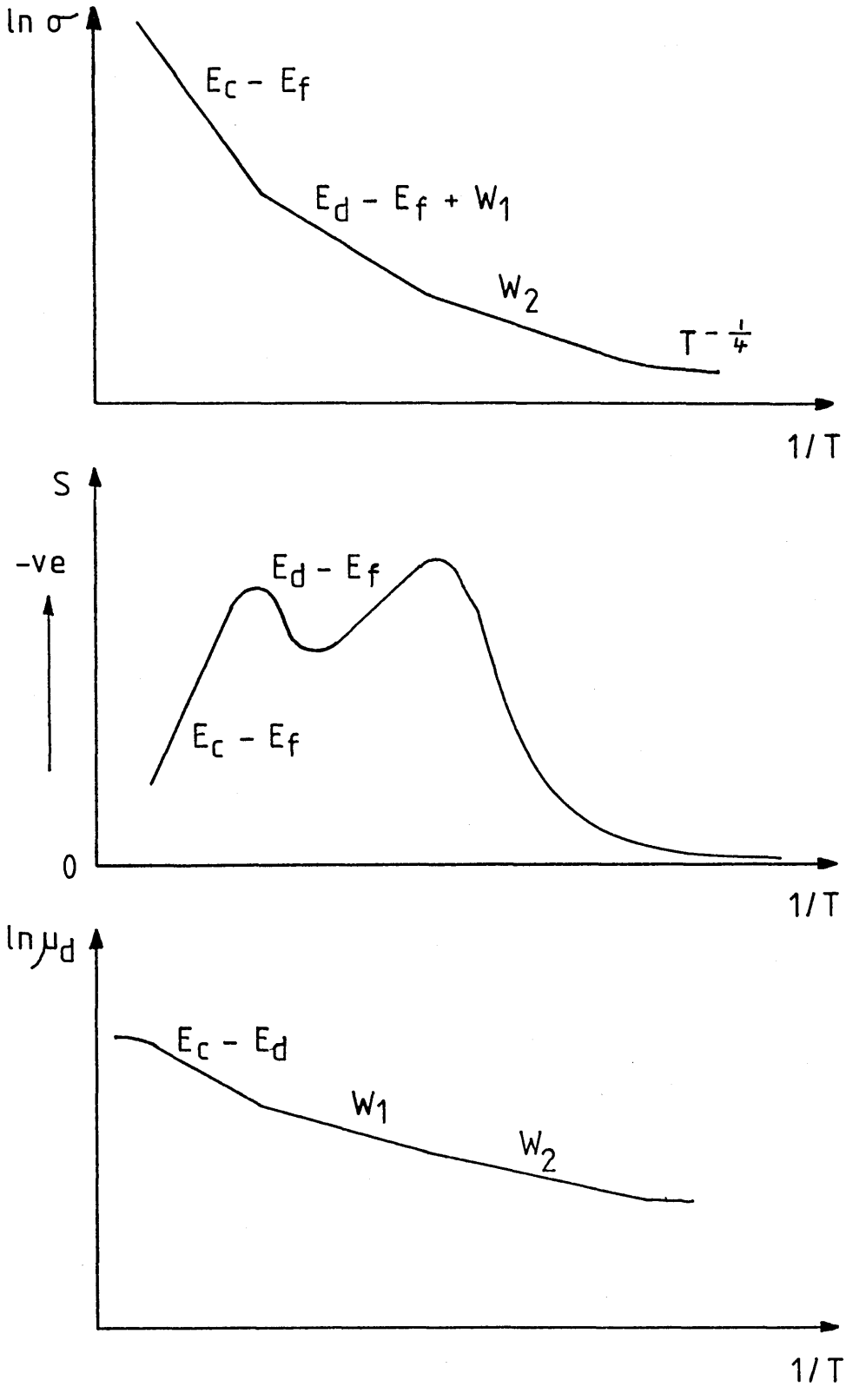

Figure 2.3. Temperature dependence of the conductivity, thermoelectric power and drift mobility on the basis of the transport model discussed in the text, and the density of states distribution of figure 2.1(a).

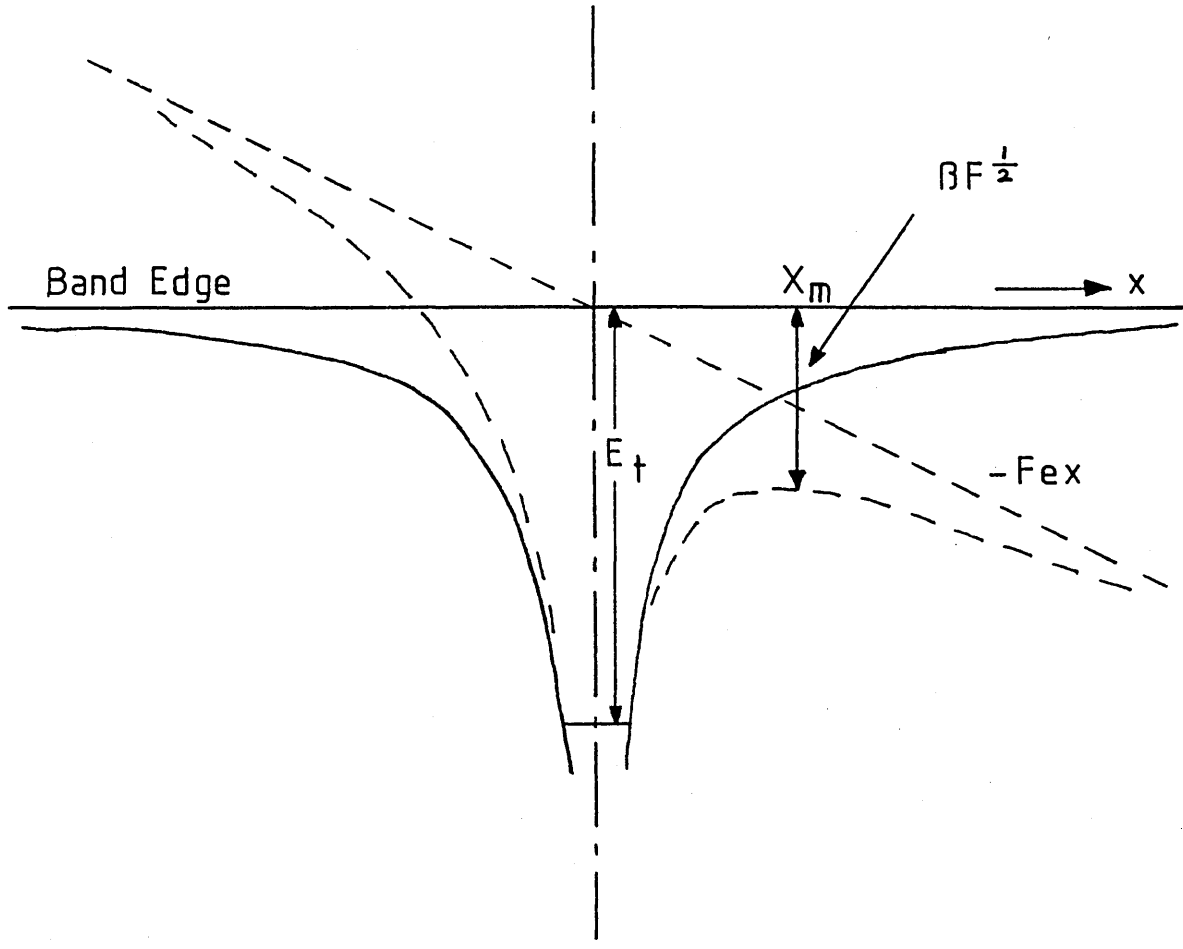

Figure 2.4. Mechanism of the Poole Frenkel effect.

$\beta = (e^3/\pi\varepsilon\varepsilon_0)^{1/2}$. The trapped carrier release probability is therefore increased by the factor $\exp(\beta F^{\frac{1}{2}}/kT)$ and the field dependence of the conductivity due to this effect can be given by

$$\sigma(F) = \sigma(0)\exp\left(\frac{\beta F^{\frac{1}{2}}}{kT}\right) \qquad - \quad (2.17)$$

where $\sigma(0)$ and $\sigma(F)$ are the conductivities at zero field and a field of F Vm^{-1} respectively.

Other treatments exist where three dimensional geometry has been assumed (8,9) and carrier emission in all directions has been dealt with (9).

(b) The Schottky Effect (10).

The Schottky effect, depicted in figure 2.5, gives results similar to the Poole - Frenkel effect. The applied electric field lowers the barrier by an amount -Fex, in the direction of the field, and again a maximum down - field barrier is obtained at X_m. The conceptional difference between these two effects is that the potential barrier is due to the metal - semiconductor work - function in the Shottky effect, but coulombic in the Poole - Frenkel effect.

(c) Field Assisted Hopping.

Various authors (11,12,13) have discussed the effect of high electric fields on hopping conduction. Essentially, the applied field lowers the energy barrier for a given down - field hop, and raises the barrier for a given up - field hop. Equation 2.11 (and 2.12)

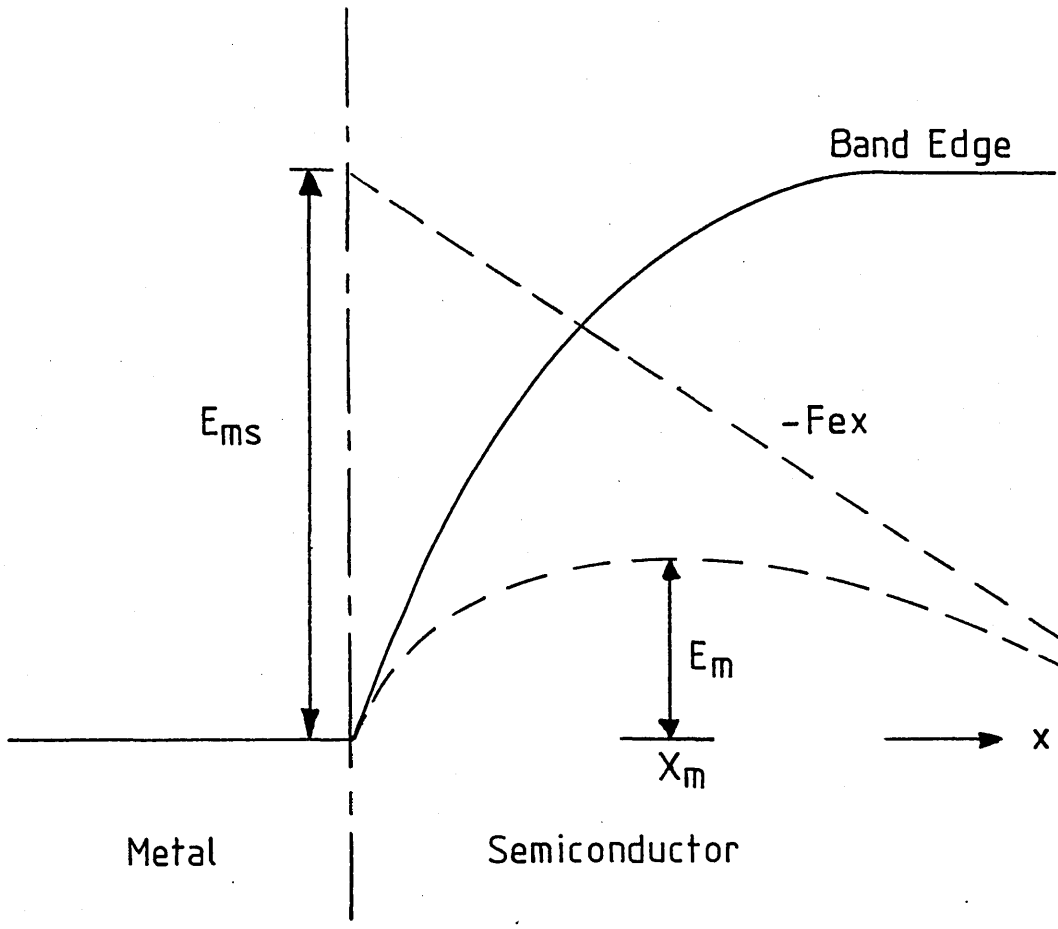

Figure 2.5. Mechanism of the Shottky effect. E_{ms} is the metal - semiconductor work function which exists with no externally applied field and E_m is the maximum down field barrier produced when a field of F Vm^{-1} is applied.

describing hopping conductivity is modified to

$$\sigma(F) = \sigma(0) \sinh\left(\frac{eFR}{2kT}\right) \qquad - \quad (2.18)$$

where $\sigma(0)$ and $\sigma(F)$ are the conductivities at zero field and a field of F Vm^{-1} respectively, and $R \simeq [g(E_d)]^{-\frac{1}{3}}$. At sufficiently high fields equation 2.18 predicts a conductivity which is exponentially dependent on field.

(d) Hot Carrier Effects.

At sufficiently high electric fields, carriers in extended states may gain energy faster than they lose it by emission of phonons. If the mean free time between carrier scattering events is τ , then a critical field above which this occurs is given approximately by (13)

$$F_{crit} = \left(\frac{kT}{2\tau e \mu_o}\right)^{1/2} \qquad - \quad (2.19)$$

where μ_o is the free carrier mobility. As this occurs, carriers move into extended states of higher energy, and if the mobility in the band increases with energy (14), the conductivity can rise rapidly with electric field.

(e) Field Stripping of Traps.

Trapped carriers may tunnel directly out of traps into extended states, through the intervening potential barrier in the down - field direction, when an electric field is applied. Mott (15), and Marshall

and Miller (13) have pointed out that carriers in localised band tails, close to the mobility edges, could be very susceptible to tunneling into extended states. Such field stripping of shallow traps effectively delocalises these states and can be interpreted as a lowering of the mobility edge, and hence changing the effective depth of deeper states. This effect results in an increasing conductivity with electric field.

2.1.2 SMALL POLARON FORMATION.

In the band theory of solids it is assumed that the presence or absence of an electron does not affect the positions of the atoms comprising the crystalline lattice. This is a justified approximation when the carrier's effective mass is sufficiently small (its mobility sufficiently large) to enable it to move many lattice spacings in the course of a single lattice vibration. Thus, the charge of the carrier is smeared out over many atoms and has little effect.

However, if the band is narrow, the carriers will have a much larger effective mass and move relatively slowly. Under these circumstances it may be that the carrier cannot traverse a distance of the order of a lattice spacing in a lattice vibration period, and the effect on the nearby heavy atom of an essentially point charge must be considered.

The charge can cause a deformation or polarisation of the surrounding lattice. This localised deformation moves with the carrier and the two together form a quasi - particle known as a molecular polaron. If the interaction is large compared to the band width, the carrier can become self - trapped and under these circumstances it is most likely that transport will be by hopping between such localised sites. If the extent of the lattice deformation produced by the carrier is largely confined to one atomic radius, the particle formed is said to be a small polaron.

Most theoretical studies of the motion of small polarons use a model called the Molecular Crystal Model (16), which considers a single excess carrier placed in an ordered array of deformable molecules. These studies have established that such polaron states are densely distributed energetically, and carrier motion proceeds via thermally activated hops between nearest neighbour sites. Consideration of the form of the conductivity (81) has led to the expression

$$\sigma = \left[\frac{Ne^2a^2\nu_o}{kT}\right] H \qquad - (2.20)$$

where N is the number of small polaron sites per cm^3, a is the site separation, ν_o is an optical phonon frequency and H is the hopping probability. The hopping probability is expected to be given by

$$H = P\exp\left[-\frac{W_P}{2kT}\right] \qquad - (2.21)$$

where W_p is the polaron binding energy. As far as P in the above expression is concerned, two extreme cases can be distinguished. In the adiabatic limit, the carrier adjusts rapidly to the motion of the lattice and is thus unlikely to miss any chance to hop to a nearest neighbour site; under these conditions p = 1. The opposite applies in the non - adiabatic case where the carrier adjusts itself too slowly and misses many chances to hop. In this case p is given by

$$P = \frac{2\pi}{h\nu_0}\left[\frac{2\pi}{W_p kT}\right]^{1/2} J^2 \ll 1 \quad - (2.22)$$

where J is the two - site transfer integral.

At sufficiently low temperatures carriers move from site to site without the aid of thermal activation. This transport corresponds to polaron band motion with an enhanced effective mass.

2.2 OPTICAL ABSORPTION.

Before discussing the optical absorption edge observed in amorphous semiconductors, a brief review will be given of the types of edges that are found in crystals.

Electronic transitions between the valence and conduction band in the crystal start at the absorption edge which corresponds to the minimum energy difference Eg, between the lowest minimum of the conduction band and the highest maxima of the valence band. If these extrema lie at the same point in k - space, the transitions are called

direct. If this is not the case, the transitions are possible only with phonon assistance and are called indirect. The rules governing these transitions are the conservation of momentum and energy during the transitions, either of electrons alone in direct transitions, or the sum of the electron and phonon in indirect transitions.

If exciton formation (electron - hole interaction) is neglected, the magnitude of the absorption co - efficient, α, as a function of photon energy, $h\nu$, depends on the energy dependence of the density of states, g(E), for the bands containing the initial and final states. For simple parabolic bands ($g(E) \propto E^{1/2}$), and for indirect and direct "allowed" transitions, (assuming the matrix element for transitions to be constant) the absorption co - efficient is given by

$$n_o h\nu\alpha = \text{const.}(h\nu - E_o)^{1/2} \quad \text{- direct} \quad - (2.23a)$$

$$n_o h\nu\alpha = \text{const.}(h\nu - E_o)^{2} \quad \text{- indirect} \quad - (2.23b)$$

where n_o is the refractive index and E_o is the optical gap (which in this case is the same as Eg as defined above).

Absorption at energies below the fundamental edge may occur due to exciton formation, where there is appreciable interaction between the electrons and holes created. For example a series of exciton absorption lines corresponding to different excited states of the pair may be observed at low temperatures, at energies less than E_o. These are normally broadened by interactions with phonons and imperfections, to give exciton "bands". The energy of an electron in such an excited

state may therefore lie within the forbidden gap.

A completely different type of absorption edge is observed in several materials (e.g. trigonal Selenium). This involves an absorption co - efficient which increases exponentially with photon energy, (for photon energies greater than the optical gap) and leads to a rapid rise of the absorption co - efficient over several orders of magnitude, within a few tenths of an electron volt near the energy gap. This is the so - called Urbach edge (17) which frequently obeys the empirical relationship

$$\alpha = \alpha_0 \exp\left[\frac{\gamma'(h\nu - E_0)}{kT}\right] \quad - \quad (2.24)$$

where γ' is a constant, and T is the absolute temperature down to a critical value T_0, and equal to T_0 for lower temperatures.

The optical gap in many semiconductors decreases linearly with temperature above about 50K, i.e.

$$E_0(T) = E_{0,0} - \gamma T \quad - \quad (2.25)$$

where $E_0(T)$ and $E_{0,0}$ are the optical gaps at temperature T and at absolute zero respectively. Below about 50K the variation normally flattens off, so that $E_0(0) < E_{0,0}$. This variation is due to thermal effects, e.g. expansion.

In amorphous semiconductors, a fundamental absorption edge is retained, but it is normally less steep than in crystalline semiconductors. A typical absorption edge, found in most amorphous compound semiconductors (e.g. As_2S_3) has the shape shown in figure 2.6. Three regions can be distinguished, A, the high absorption region, B, the exponential region, and C, the weak absorption region.

In the high absorption region (region A) the most common (although not universal) behavior of the absorption co - efficient, as a function of photon energy, is found to be

$$\alpha = \frac{\text{const.}(h\nu - E_o)^2}{h\nu} \qquad - \quad (2.26)$$

A number of examples of this behaviour are shown in figure 2.7, and by using equation 2.26 to fit these curves it is possible to define an optical gap, E_o. It is not known, however, whether E_o defined in this manner represents a true gap in the density of states, a mobility gap, or something relating to these energies. It is thought (18), however, that in the high absorption region, absorption occurs by excitation of electrons across the "gap" into band states. Thus, from plots similar to those shown in figure 2.7 it is possible to extract some information about the form of the density of states at the band edges.

If it is assumed that the k - conservation selection rule is relaxed, and the densities of states in the conduction and valence bands have power law energy dependences as shown in figure 2.8, then a relationship can be obtained linking the absorption co - efficient, α, with photon energy. The absorption co - efficient for a given photon

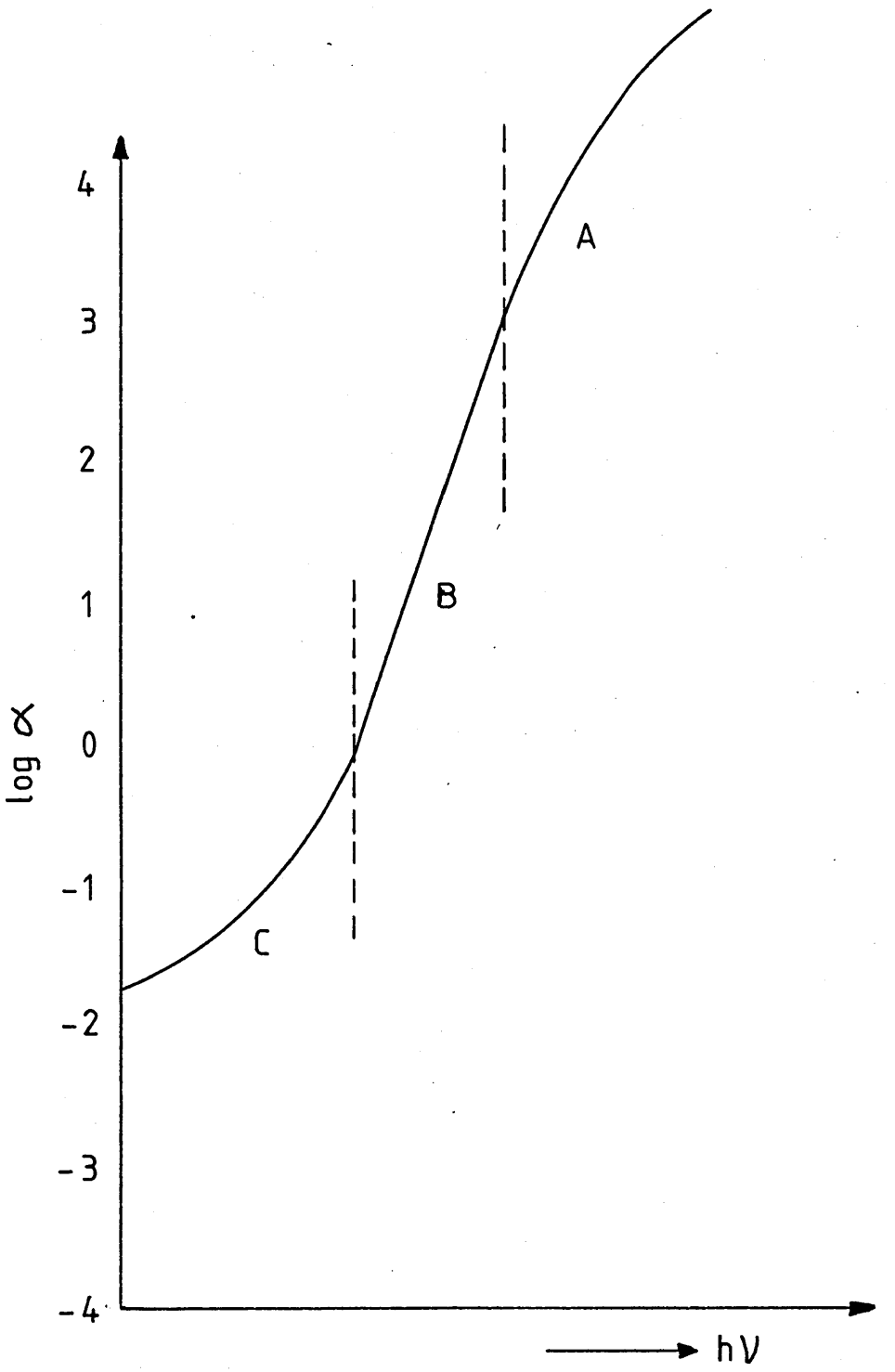

Figure 2.6. A typical absorption edge found in most amorphous compound semiconductors. Three regions can be distinguished:
(A). The high absorption region.
(B). The exponential region.
(C). The weak absorption region.

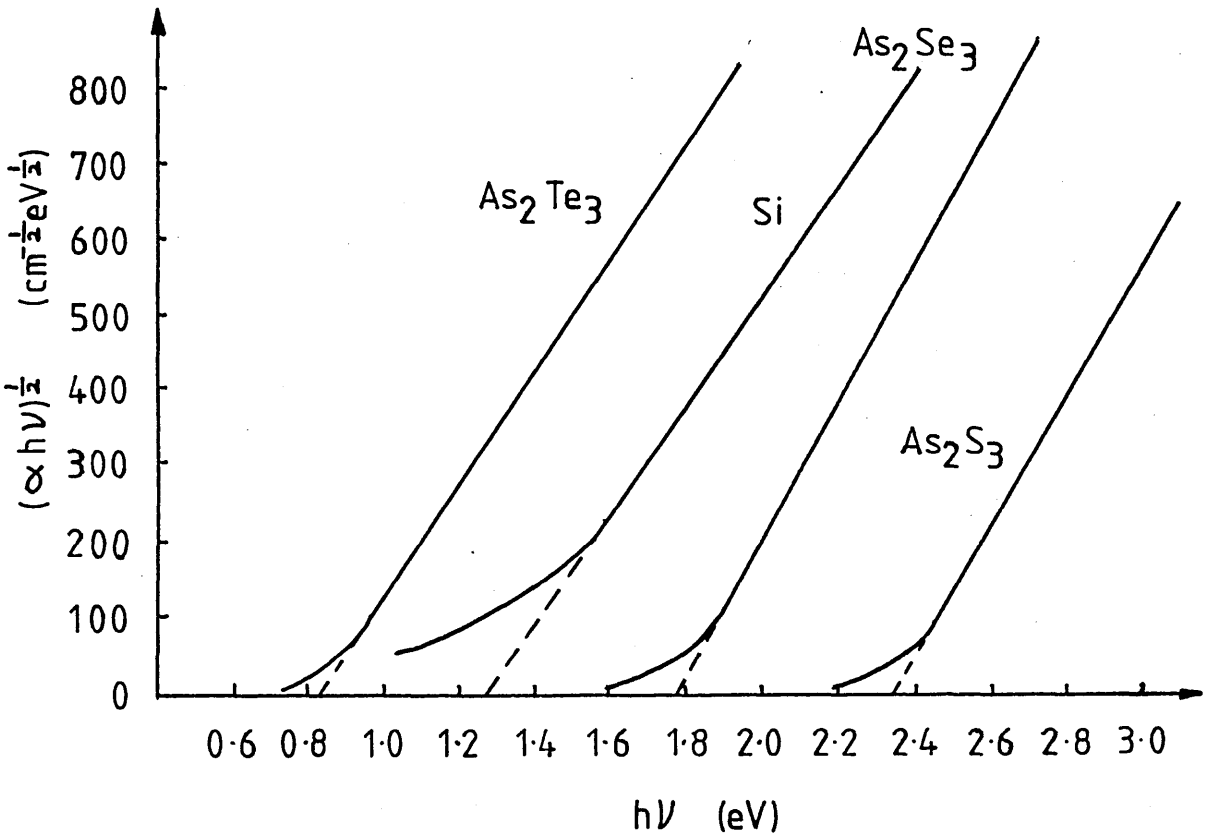

Figure 2.7. Examples of absorption edges whose functional dependence on photon energy is given by equation 2.26.

energy, $h\nu$, will be proportional to the weighted sum of all possible interband electron transitions. i.e.

$$\alpha(\nu) = \text{const.} \int_{\Delta E - h\nu}^{0} C(E)\, V(E)\, M\, dE \quad - (2.27)$$

where C(E), V(E) and ΔE are defined in figure 2.8, and M is a matrix element associated with specific electron transition probabilities. Assuming the matrix element to be constant, equation 2.27 can be evaluated (18) to give

$$\alpha(\nu) = \frac{\text{const.}\,(h\nu - \Delta E)^{s+p+1}}{h\nu} \quad - (2.28)$$

Using a result similar to equation 2.28, Tauc (19) interpreted the quadratic variation of $\alpha h\nu$ against $h\nu$ in terms of parabolic band edges, i.e. s = p = 1/2. Davis and Mott (20), however, interpreted the same behaviour using different assumptions. The assumed that the densities of states at the band edges were linear functions of energy and that transitions in which both the initial and final states were localised could be neglected. Such assumptions lead to s and p taking values of 0 and 1 respectively, thus leading to the same quadratic variation of $\alpha h\nu$ against $h\nu$.

The exponential region (region B) of the absorption edge is found to be a universal occurrence in amorphous semiconductors. This suggests that there must be something fundamental behind its formation, which is common to all of these materials. Tauc (19), suggested that the exponential tail results from electron transitions

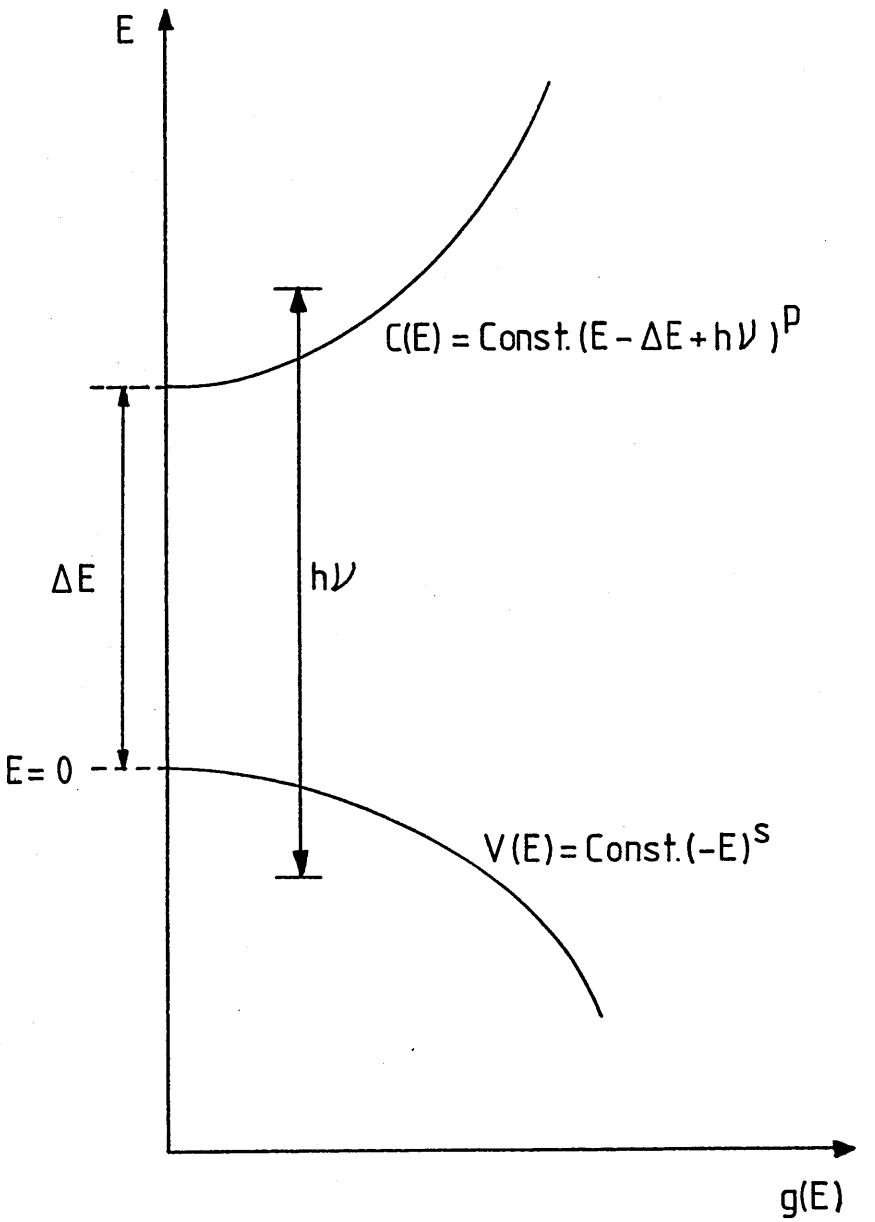

Figure 2.8. Energy dependence of the density of states in the valence band V(E) and the conduction band C(E). The minimum separation between the bands is ΔE and the k - conservation selection rule is relaxed.

involving localised states in exponentially distributed band tails. However, as pointed out by Davis and Mott (20), this is unlikely since plots of $\ln(\alpha)$ versus $h\nu$ obtained from studies of many amorphous semiconductors, exhibit approximately the same slope in the exponential region, thereby implying very similar tails of the density of states in all amorphous semiconductors.

An alternative explanation for the Urbach edge in amorphous semiconductors was put forward by Dow and Redfield (21). They treated the problem by calculating the absorption for direct electronic transitions in a uniform electric field. Their calculations show that the variation of the absorption co - efficient with photon energy, obtained in this manner, is accurately exponential. The problem that then arises, however, is where do these electric fields come from in the real material? One possibility is that the electric fields are present due to the inbuilt potential fluctuations within all amorphous semiconductors.

The weak absorption region (region C) is difficult to study due to the low absorption level. The magnitude of the absorption co - efficient, and the slope obtained from a plot of α versus $h\nu$, for any given material, are found to depend on preparation conditions, purity and the materials thermal history. Absorption in this region, however, has been attributed both to light scattering and to optical transitions between localised states and between localised and extended states.

2.3 PHOTOCONDUCTIVITY.

Under thermal equilibrium conditions, electrons are constantly being excited from the valence band to the conduction band with the absorption of energy from the lattice (phonons) or of black body radiation. There is a dynamic equilibrium which keeps the number of excited carriers constant (thermal fluctuations excepted). The principle of detailed balance applies, i.e. each entry - exit process proceeds equally fast in both directions. For example, the same number of photons are emitted in the form of black body radiation as are absorbed.

When this equilibrium is disturbed, e.g. by the introduction of additional external excitation, the principle of detailed balance no longer holds, although some fundamental parameters such as the capture cross section are usually unchanged. The history of an excited carrier, from the time it is generated to the time it returns to the original band, can be conveniently divided into generation and thermalisation, transport (with trapping and de - trapping) and recombination.

When the excitation is constant with time, a new dynamic quasi - equilibrium is established. Under these circumstances, the steady state number of photogenerated carriers, Δn, is defined as the difference between the number of carriers present with no externally applied excitation, n_d, and the number of carriers present under steady state illumination, n_i, i.e.

$$\Delta n = n_i - n_d \qquad - \quad (2.29)$$

In this section the concepts introduced above will be discussed.

2.3.1 EXCESS CARRIER GENERATION.

The principle methods for generating excess carriers are by absorption of light, or by injection at non - neutral contacts or junctions. Other methods include ionisation by high energy quanta or particles, and impact ionisation. Only the first will be considered here, although ionisation by electrons is important in drift mobility measurements in amorphous semiconductors.

Figure 2.9 illustrates all the possible electron transitions which can occur in a semiconductor with a single defect level, when it is illuminated. Transition No. 1 generates an electron - hole pair. Transitions No. 4 and 5 generate one free carrier each, and those No. 2 and 3 none at all. Generation of electron - hole pairs which are bound to each other (excitons) is also possible.

2.3.2 QUANTUM EFFICIENCY.

The quantum efficiency, η, is defined as the number of "free" electron - hole pairs produced per incident photon, "free" here meaning free to take part in photoconductivity. For a photon flux, F

$$G = \eta F \qquad - \quad (2.30)$$

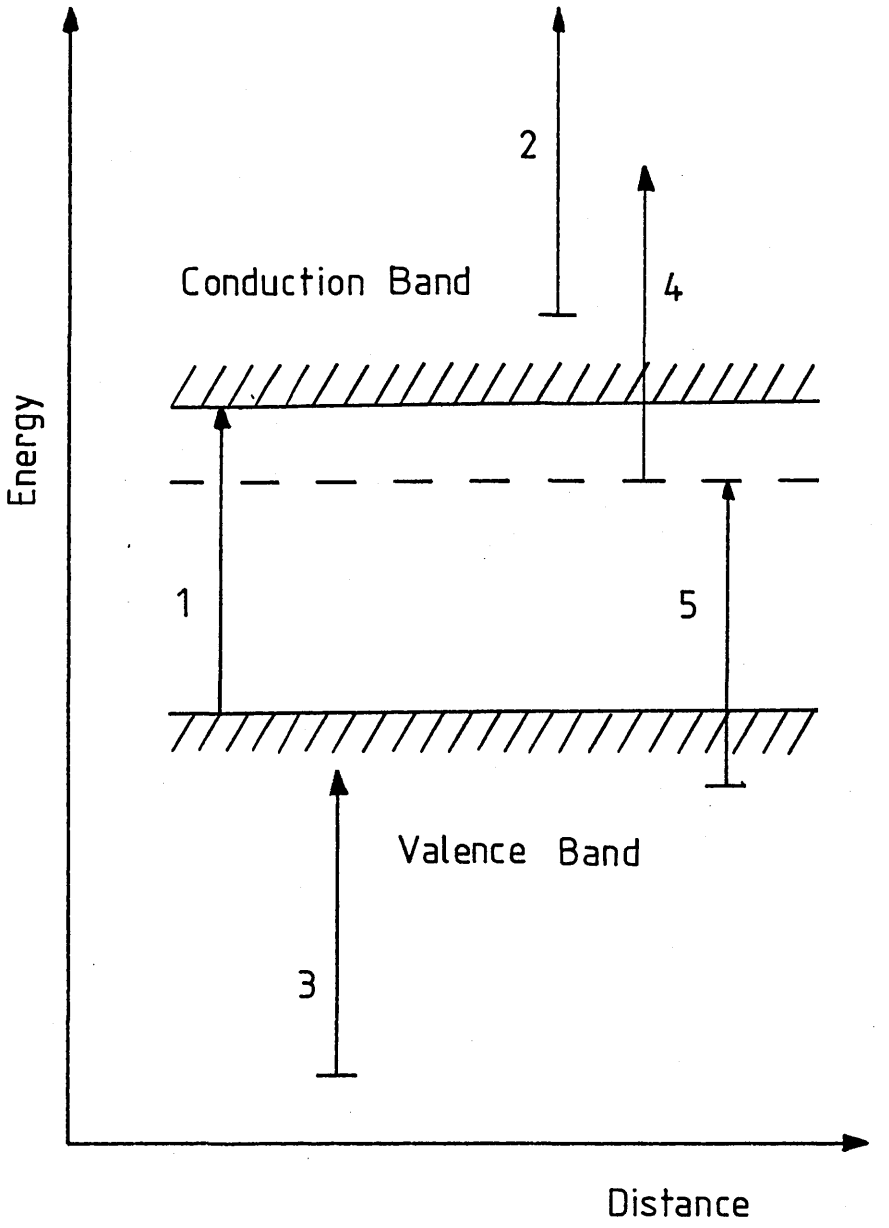

Figure 2.9. Possible electron transitions in the fundamental absorption region of a semiconductor with one set of defect states.

where G is the generation rate of free electron - hole pairs.

The quantum efficiency for a given semiconductor is a function of both its optical gap and the photon energy used for excitation. For photon energies less than the optical gap the quantum efficiency is usually much less than unity, and approaches unity for photon energies equal to the optical gap. In some cases, however, the quantum efficiency does not approach unity until the absorbed photon energy is considerably larger than the optical gap. This phenomenon has been observed in amorphous Selenium (22,23,24) where E_o is estimated as 2.1 eV (25), but η does not approach unity till photon energies of between 2.6 eV and 2.8 eV. This behavior is illustrated in figure 2.10 where the quantum efficiency and the absorption co - efficient for a - Se, are shown as a function of photon energy.

Several models have been proposed, varying in detail, to account for the behavior shown in figure 2.10. Hartke and Regensburg (24) proposed a two process model, an ordinary interband transition generating a free electron - hole pair with unity quantum efficiency, and a non - photoconducting generation of excitons which rapidly become self trapped and cannot be ionised. The quantum efficiency at photon energies, $h\nu$, is then

$$\frac{\varepsilon_2^P(\nu)}{\varepsilon_2^P(\nu)+\varepsilon_2^N(\nu)} \qquad - \quad (2.31)$$

where ε_2 is the imaginary part of the dielectric constant. The subscripts "P" and "N" refer to the photoconducting and non - photoconducting absorption processes respectively.

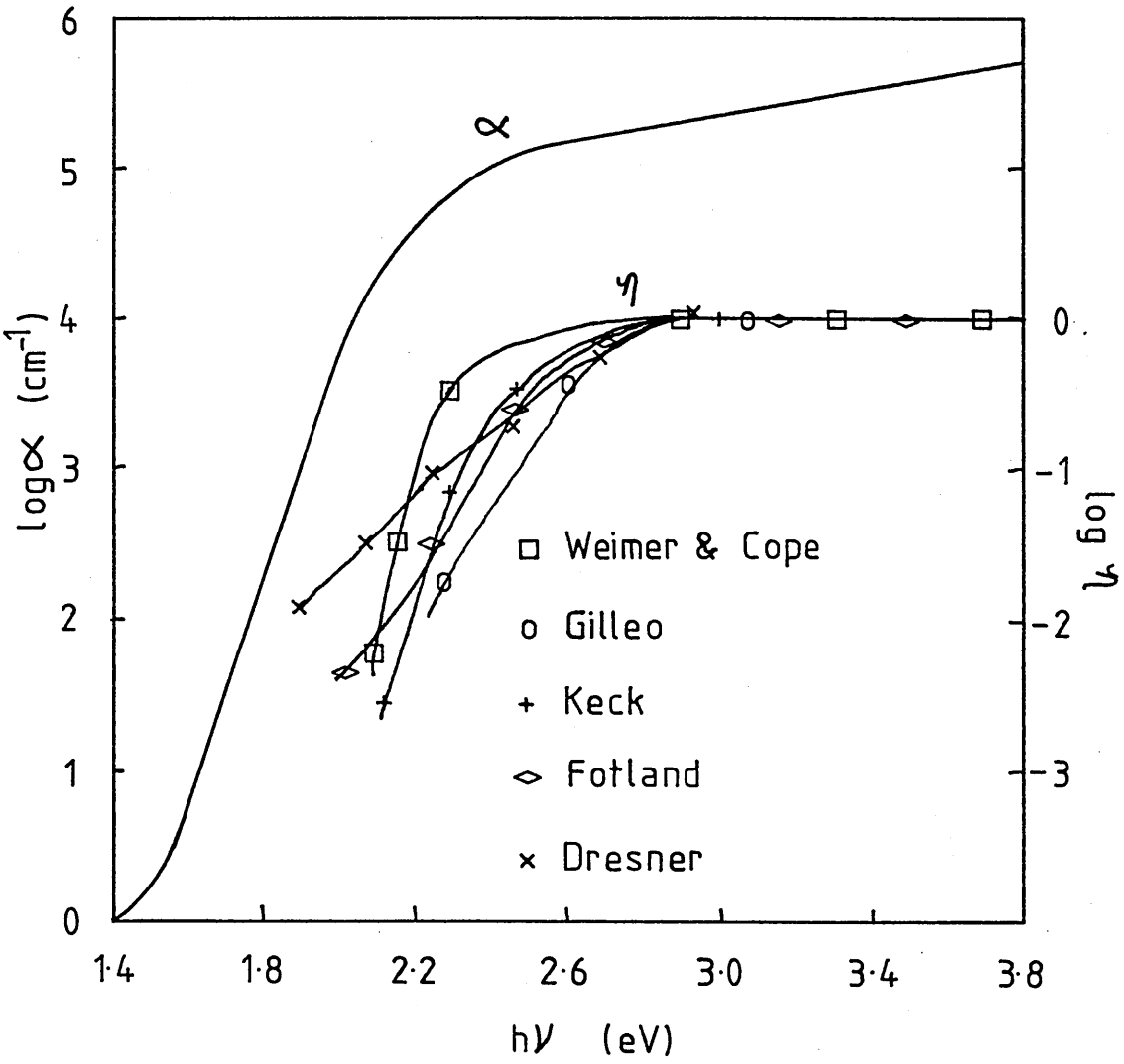

Figure 2.10. Optical absorption edge and quantum efficiency in amorphous Selenium at room temperature. (After ref. 24).

Most of the other models used to explain figure 2.10, involve the probability of separating a photogenerated electron - hole pair from the mutual coulombic attraction. Such models have been discussed by Tabak and Warter (22), Davis and Mott (20), and by Knights and Davis (26), and their main features are shown in figure 2.11. For an interband transition with photon energy, $h\nu$, the excess kinetic energy of the carrier over the local coulombic potential, is

$$K.E. = (h\nu - E_o) + \frac{e^2}{4\pi\varepsilon\varepsilon_o r} \qquad - \qquad (2.32)$$

This K.E. is lost by rapid thermalisation by phonon emission while the carriers move apart in diffusive motion with a short mean free path. When the k - selection rules are relaxed, the rate of emission of phonons is of the order of the phonon frequency. The time for the carrier to thermalise down to the bottom of the conduction band can thus be found, and random walk theory gives the separation of the carriers during that time. If the coulombic binding energy at that separation is of the order of kT or less, ionisation will be likely to take place and the quantum efficiency will approach unity for greater photon energies. For higher binding energies, the quantum efficiency depends upon the relative probabilities of ionisation (which is activated) and geminate recombination. An electric field will aid in the separation of the electron - hole pairs, both by modifying the random walk characteristics and by reducing the final ionisation barrier, whilst an increased temperature will enhance the probability of ionisation.

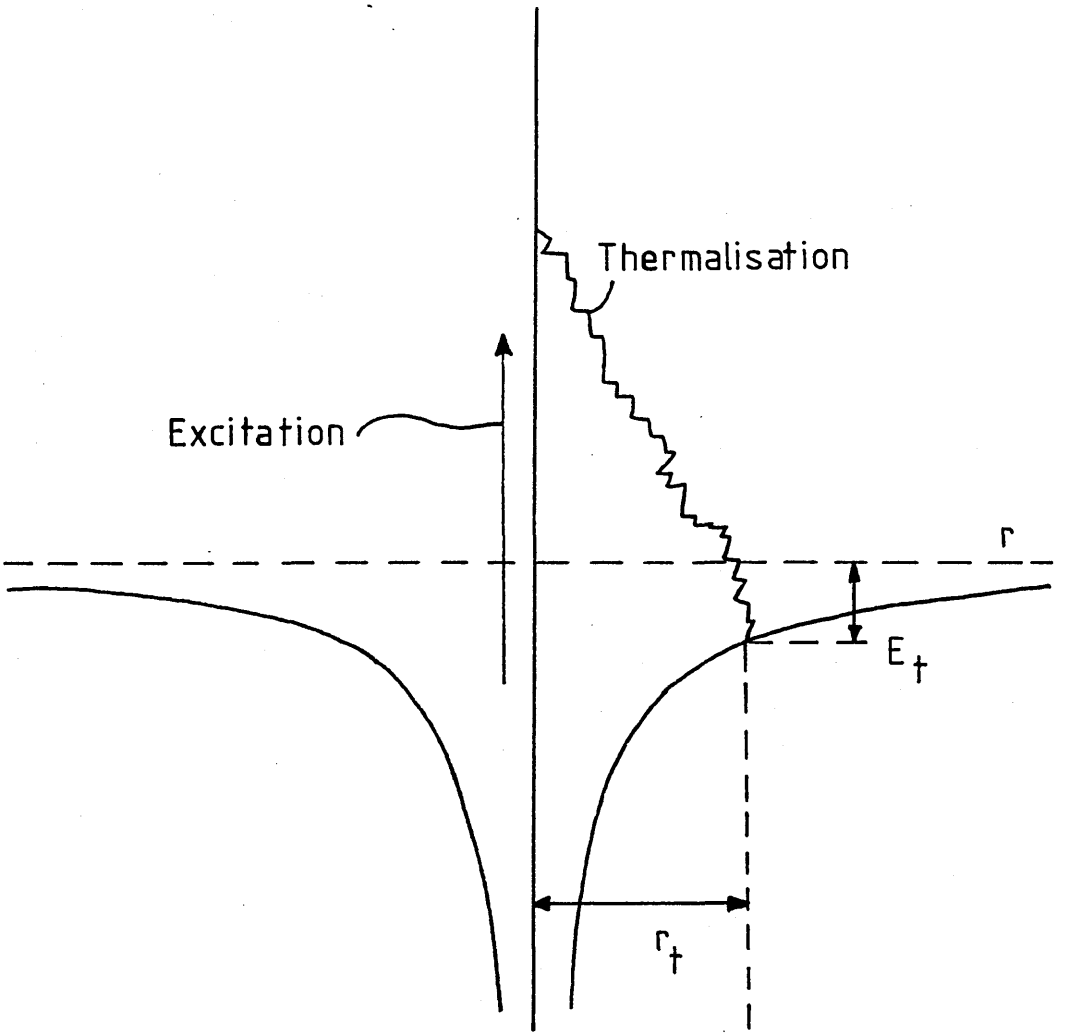

Figure 2.11. Thermalisation of an electron - hole pair in the mutual Coulombic field. (After ref. 26).

2.3.3 SIMPLE CARRIER KINETICS.

As a basic approach to the various types of photoconductivity kinetics, consider the simplest case possible; that of an intrinsic semiconductor with thermal and optical excitation of electrons from the valence band to the conduction band, as indicated in figure 2.12. Before proceeding with an analysis of this situation, three important concepts must be introduced.

(1). The principle of detailed balance which states that at equilibrium, the rate at which carriers enter a particular set of states, by all operative input paths, must be equal to the rate at which the carriers depart from the states, again including all operative exit paths.

(2). The principle of charge neutrality which states that internal thermal or optical carrier generation will yield equal numbers of hole and electron carriers so that the material will remain electrically neutral. Care is needed here to avoid the intervention of other effects (e.g. different rates of hole and electron diffusion from the photoexcited region, influence of contacts, etc.) which may perturb the analytically desirable neutrality condition.

(3). The concept of carrier lifetime, which correlates the steady state density of excess carriers, Δn, with the rate of excess carrier generation, G. i.e.

$$\Delta n = G\tau \qquad - \quad (2.33)$$

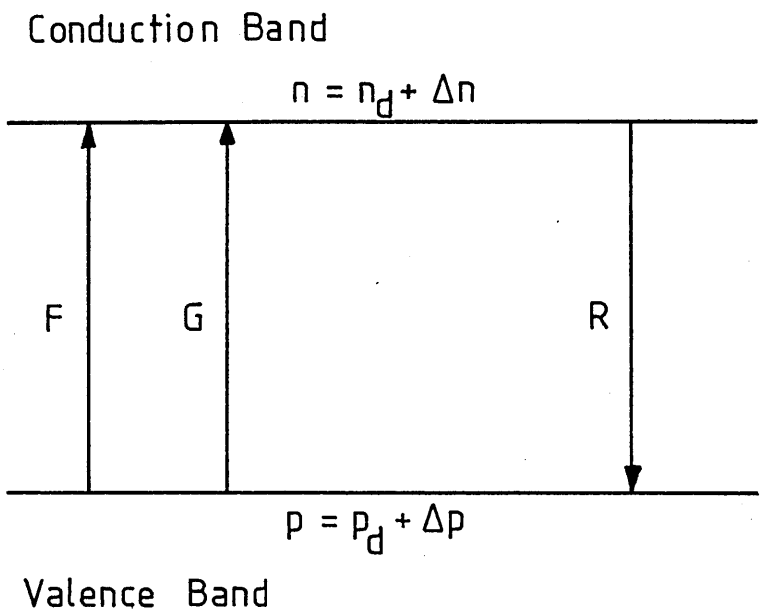

Figure 2.12. Thermal (F) and optical (G) generation of electrons and holes in an intrinsic semiconductor. n_d and p_d are the thermally generated density of carriers and Δn and Δp are the excess density of carriers. R is the recombination process.

where τ is the average lifetime of the excess carriers.

In figure 2.12, if the optical generation rate is G, and the thermal generation rate is F, then the rate of change of the free electron and hole concentration is given by

$$\frac{dn}{dt} = \frac{dp}{dt} = F + G - npC \qquad - \quad (2.34)$$

C is the capture coefficient for the recombination of a free electron with a free hole, and is defined as

$$C = vS \qquad - \quad (2.35)$$

where v is the carrier thermal velocity, and S is the band - to - band capture cross section. In thermal equilibrium in the dark

$$F = n_d p_d C = n_d^2 C \qquad - \quad (2.36)$$

where the subscript "d" refers to the electron and hole densities with no photoexcitation. The addition of photoexcitation gives

$$(F+G) = (n_d + \Delta n)^2 C \qquad - \quad (2.37)$$

Combining equation 2.36 and 2.37 yields

$$G = \Delta n(2n_d + \Delta n).C \qquad - \quad (2.38)$$

Two simple regimes can occur for this expression. The first is that for which $\Delta n \ll n_d$, when

$$\gamma = \frac{\Delta n}{G} = \frac{1}{2 n_d C} \qquad - (2.39)$$

Here, the lifetime is constant and depends upon the density of thermally generated carriers in the material. This is known as the MONOMOLECULAR REGION where the photoconductivity is found to vary linearly with excitation level. The second case is that for which $\Delta n \gg n_d$, when

$$\gamma = \frac{\Delta n}{G} = \frac{1}{\Delta n C} = \sqrt{\frac{1}{GC}} \qquad - (2.40)$$

In this case, known as the BIMOLECULAR REGION, the lifetime depends upon the excess carrier density, and the photoconductivity is found to vary as the square root of the excitation level. Figure 2.13 shows the expected illumination intensity dependence of the photoconductivity, over a range of excitation level which encompasses both the regimes introduced above.

When trapping and recombination centers are present in the forbidden gap, all possible transitions between states must be considered. Such an analysis is not appropriate here, however, since as the number of levels of localised states increases, the situation rapidly becomes mathematically complex. Main (27,28), however, applied the concepts introduced above to a material containing two levels of localised states in the forbidden gap, and used the results to explain the photoconductivity observed in some amorphous

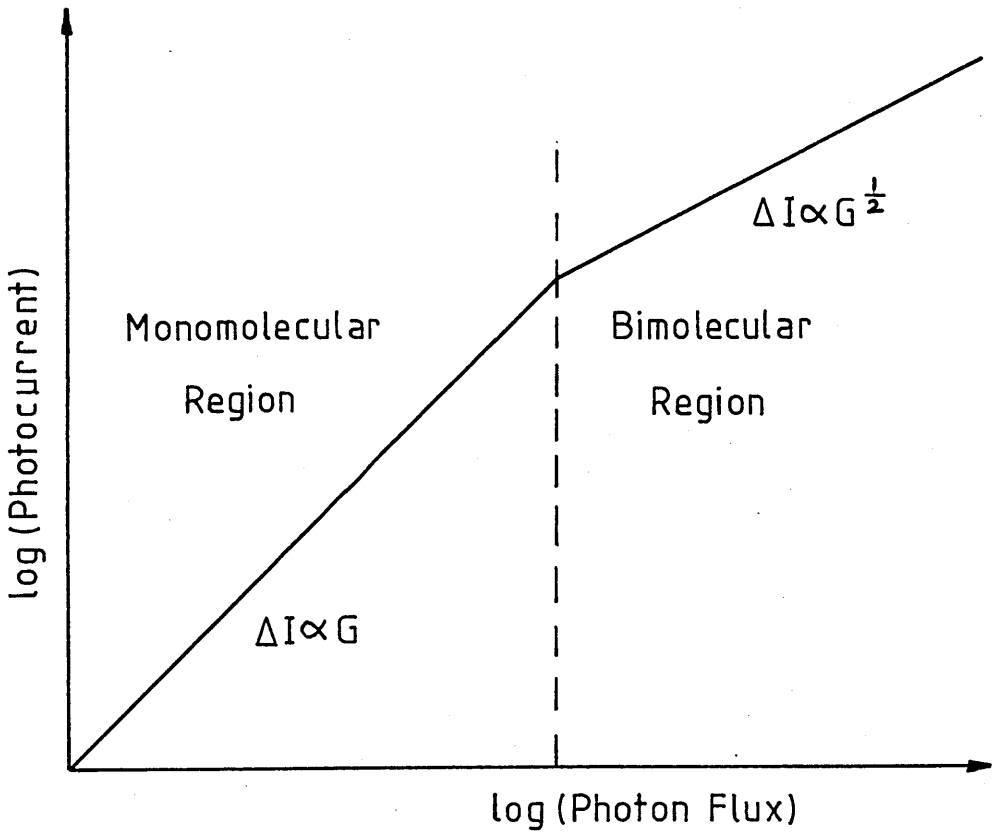

Figure 2.13. Dependence of the photocurrent on illumination intensity in both the monomolecular and the bimolecular regions.

chalcogenide semiconductors. A brief review of this work will be given in section 2.3.6.

2.3.4 QUASI - FERMI LEVELS.

The basic expressions relating the density of free electrons and holes to the position of the Fermi level in a semiconductor are

$$n = N_c \exp\left[-\frac{E_{fn}}{kT}\right] \quad - \quad (2.41a)$$

$$p = N_v \exp\left[-\frac{E_{fp}}{kT}\right] \quad - \quad (2.41b)$$

where $E_{fn} = E_c - E_f$ and $E_{fp} = E_f - E_v$. The product of these two expressions gives

$$E_{fn} + E_{fp} = kT \ln\left[\frac{N_c N_v}{np}\right] \quad - \quad (2.42)$$

Since the energy gap, $E_g = kT \ln(N_c N_v / n_d^2)$, then

$$E_{fn} + E_{fp} = E_g - kT \ln\left[\frac{np}{n_d^2}\right] \quad - \quad (2.43)$$

Now in thermal equilibrium, $np = n_d^2$, and so of course $E_{fn} + E_{fp} = E_g$ as expected.

Under a steady state situation, in the presence of photoexcitation, steady state Fermi levels describe the densities of free electrons and holes in the conduction band and valence band

respectively. They may also be expected to describe the occupation of all localised levels which are still essentially in thermal equilibrium with one or other of the bands. Thus, the occupation of levels in thermal equilibrium with the conduction band is given by E'_{fn}, whilst the parameter for the valence band and its effectively equilibrated localised states is E'_{fp}. The occupation of levels not in thermal equilibrium with one or other band will not be given by either of these terms.

Under photoexcitation, $np > n_d^2$, and equation 2.43 shows that the two steady state Fermi levels separate by an energy $kT.\ln(np/n_d^2)$, as illustrated in figure 2.14. For electrons

$$E'_{fn} - E_{fn} = kT \ln\left[\frac{n_d}{n_d - \Delta n}\right] \quad - (2.44)$$

with a corresponding expression for holes.

2.3.5 DEMARCATION LEVELS.

The occupation of levels in thermal equilibrium with one of the bands is given in terms of the corresponding steady state Fermi levels. The demarcation level defines the boundary between occupancy determined by effective thermal equilibrium with the nearest band, and occupancy determined by recombination kinetics. The location of the demarcation level depends upon the specific values of capture coefficient for the particular type(s) of localised states present. However, it is always true that $E_{dn} + E_{dp} = E'_{fn} + E'_{fp}$ where E_{dn} and

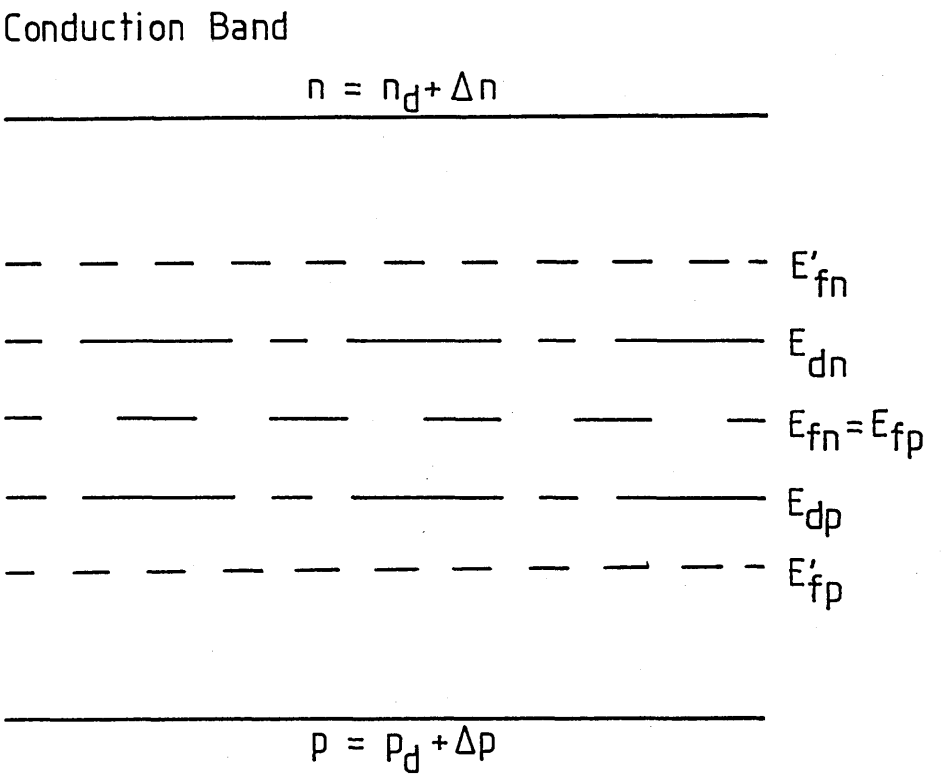

Figure 2.14. Positions in the energy gap of the electron and hole demarcation levels (E_{dn} and E_{dp}) and the quasi - Fermi levels (E'_{fn} and E'_{fp}). The position of the Fermi level with no external excitation is also shown ($E_{fn} = E_{fp}$).

E_{dp} are the positions in the energy gap of the electron and hole demarcation levels respectively. Demarcation levels are illustrated in figure 2.14.

2.3.6 STEADY STATE PHOTOCONDUCTIVITY.

The variation with temperature of the photoconductivity is similar for all amorphous materials, and has the general form shown in figure 2.15. For a constant illumination intensity (and for uniform illumination throughout the specimen) the photocurrent goes through a maximum near the temperature at which it equals the dark current. At higher temperatures the photocurrent increases with 1/T; this is denoted region I. In region II the photocurrent decreases with 1/T, until in region III it gradually levels off.

As an example of the types of analysis performed on this photoconductive response, the models advanced for chalcogenide semiconductors will be examined, (photoconductivity in a-Si will be discussed in Chapter 5). In essence, two fundamental different types of models have been adopted:

(a). The classical type of model with discrete sets of localised states in the energy gap (27-31).

(b). The "C-F-O" or "Mott-C-F-O" approach with energetically distributed localised states in the mobility gap (2,32-37).

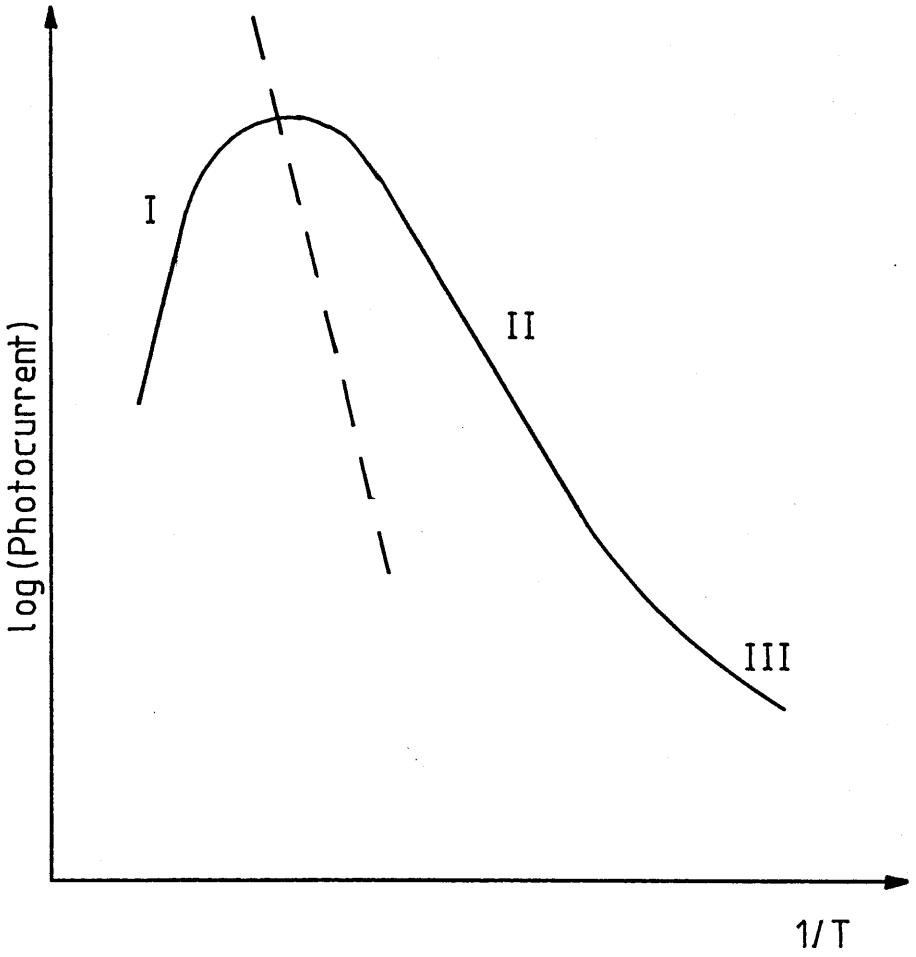

Figure 2.15. Temperature dependence of the photocurrent in most amorphous semiconductors. The broken line represents the dark current.

In analysis type (a), Main (27) proceeded by assuming the presence in the energy gap of the minimum number of sets of localised states necessary to account for the transport data. In materials such as $As_2 Te_3$ and $As_2 Se_3$, the photoconductivity data appeared to require only two sets of localised states in order to account for the observed response. However, it should be noted that this does not rule out the occurrence of other localised states, so long as they would not tend to dominate the photoresponse behaviour.

A two level model, with the appropriate transition paths is shown in figure 2.16. Transitions G and R represent interband generation and recombination respectively, and the other paths represent all possible electron and hole transitions. Some band tailing and states at the Fermi level (effectively pinning it), were also introduced by Main, both having some influence on the charge neutrality condition, but not taking part in the recombination traffic. Other assumptions were that trapping centers are in quasi - equilibrium with the nearest band and lie outwith the appropriate quasi - fermi levels under all experimental conditions; and that <u>where possible</u>, rates which are very small compared to others can be eliminated in determining the equilibrium conditions. Using these assumptions, combined with the charge neutrality condition, and the appropriate transition equation for holes, Main arrived at a solution of the form (for holes):

$$G = \left[2p_d \Delta p + \Delta p^2\right]\left\{C_{ve}\frac{N_p}{p_i} + C_{cp}\left(\frac{N_p}{p_i}\right)^2 + K\left(\frac{N_p}{p_i}\right)^2\right\} \quad - (2.45)$$

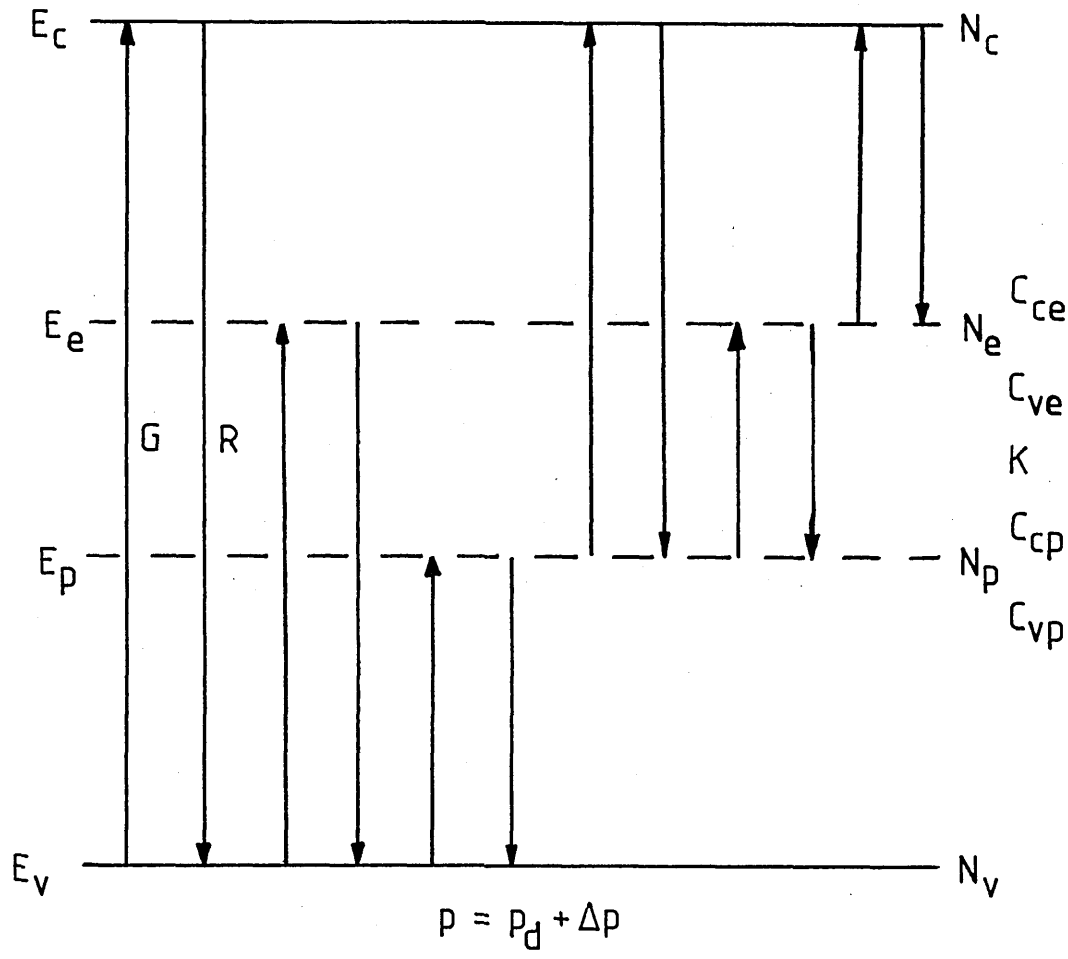

Figure 2.16. A two level model used by Main (27, 28) showing all possible electron and hole transition paths. The capture coefficients are:-

C_{ce} - Capture of a free electron by a trapped hole at E_e.

C_{ve} - Capture of a free hole by a trapped electron at E_e.

C_{cp} - Capture of a free electron by a trapped hole at E_p.

C_{vp} - Capture of a free hole by a trapped electron at E_p.

K - Capture of a trapped electron at E_e by a trapped hole at E_p.

where p_d and Δp are the densities of holes in the dark and due to photoexcitation respectively, p_i and n_i are the effective densities of free holes and electrons which would exist if the Fermi level were coincident with the traps at E_p and E_e respectively, and the other parameters are defined in figure 2.16. This equation can be solved for Δp and clearly there is a small signal case where $\Delta p << p_d$ and $\Delta p \propto G$ (monomolecular regime), and a large signal case where $\Delta p >> p_d$ and $\Delta p \propto G^{\frac{1}{2}}$ (bimolecular regime). The three terms in curly brackets represent firstly, band to localised recombination via electron trapping centers, secondly band to localised recombination via hole trapping centers and thirdly localised to localised recombination via both sets of localised centers.

Equation 2.45 can be solved for each recombination path separately and the solution checked against experimental data. The activation energy of each solution is found to be a combination of two or more of the energies E_c, E_e, E_p and E_v. To determine which solutions are appropriate to the experimental observations, it is necessary to analyse the data carefully and make comparisons with other electrical properties, e.g., dark conductivity, transient photoconductivity, etc. The above analysis, however, can only explain the photoconductivity in regions I and II. Main (27) finds that in region III the photoconductivity has a constant activation energy which is less than in region II (in the case of $As_2 Te_3$), and argues that the trapped hole quasi - Fermi level approaches E_p at low temperature. The expected transition to an unactivated current behaviour at low temperature is not predicted by equation 2.45.

Other analyses which fall into category (a) are those by Arnoldussen el al (29), who interpret the photoconductivity results using three discrete sets of localised levels, and Simmons and Taylor (30,31) who use a two discrete level model similar to that used by Main.

Several variants of the analysis type (b) have been advanced to analyse photoconductivity data on disordered semiconductors. The differences between the variants involve both the extent and the nature of the trapping centers controlling transitions. In most cases, the postulated characteristics are such as to produce local peaks in the occupied trap distribution at two energies, just as would occur in the discrete trap case.

Mott and Davis (2) discuss photoconductivity kinetics using the limited band tail model shown in figure 2.17. The band tail states are taken to be shallow relative to the appropriate Fermi or quasi - Fermi levels, and thus are in equilibrium with the free carrier states beyond the mobility edges. Recombination is assumed to occur via localised to localised transitions between the two tails, bypassing the "bump" at mid - gap, whose states must have a low density or small transition coefficient. Moreover, to ensure that charge neutrality at high excitation levels is determined by the occupancy of the tail states, the gap centers must be assumed to become depopulated by such illumination. Since the occupancy of the tail states will peak close to their tips (unless the energy / density variation is very rapid), the transport properties will be dominated by states within about a kT of the tips. Using effective densities as

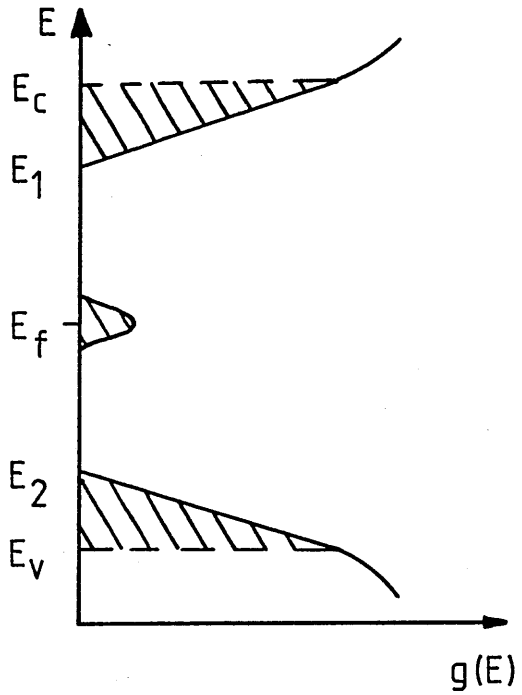

Figure 2.17. Model of Mott and Davis.

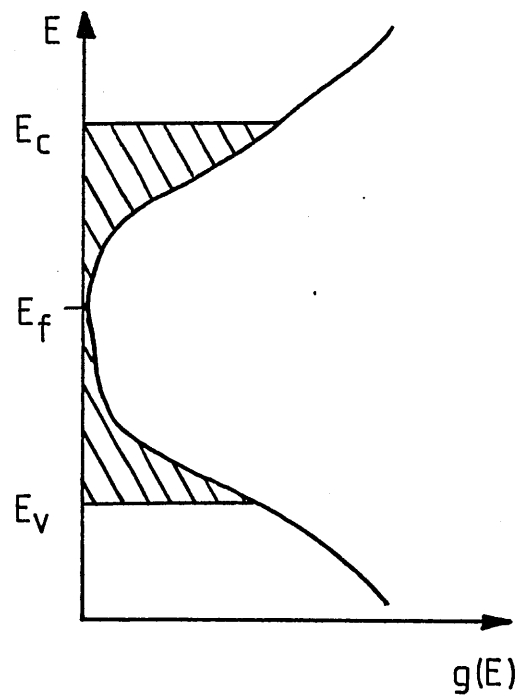

Figure 2.18. C-F-O model.

equivalent to densities of discrete traps situated at the tips of the tails, the analysis clearly becomes closely equivalent to that of Main outlined above, and the conclusions will be similar.

Weiser et al (32) interpret photoconductivity in the disordered alloys $2As_2Te_3.As_2Se_3$ in terms of the C-F-O model, shown in figure 2.18, and localised to localised transitions. According to this model the excess carriers thermalise in the tails of the localised states with decreasing probability as the depth increases. It is assumed that the probability of recombination (via localised transitions) decreases more slowly than the thermalisation probability. Hence, an energy will be reached where the two are equal and below that energy (for electrons) the probability of recombination is greater. Weiser et al (32) call this critical energy the "recombination edge". An important consequence of the model is that the trap occupancy is a maximum at the recombination edge. To obtain agreement between the model and experimental data, however, it is necessary to further assume that the thermalisation probability decreases with energy (for electrons) much more rapidly than seems likely. As a result, the trap occupancy peaks very sharply at the recombination edge. This model is then almost indistinguishable from a discrete - trap - level model, with localised levels situated at energies corresponding to the recombination edge.

Other analysis which fall into category (b) are those by Arnoldussen et al (36) who advanced an analysis similar to Weiser et al (32) above, except localised to localised transitions via intermediate states in mid - gap are assumed to explain the low

temperature results. Also Simmons and Taylor (33-35) who considered only band to localised transitions with no "recombination edge" since the transition coefficients are assumed not to vary rapidly with energy at any point. This means that the peaks in occupation, which are due to the density of states tailing and the fall off in occupancy beyond the trap Quasi - Fermi levels, will move outwards with increasing illumination. As a result, a plot of photoconductivity (Δ p) versus 1/T will be curved, and the intensity relationship intermediate between square root and linear.

2.3.7 TRANSIENT PHOTOCONDUCTIVITY.

Consider a step - function illumination applied to a semiconductor in thermal equilibrium. Then

$$G(t) = \eta F(t) \qquad - \quad (2.46)$$

where η is the quantum efficiency, and G(t) and F(t) are the generation rate of free electron - hole pairs and the photon flux respectively, both being a step function of time.

At times shorter than the trapping time for the shallowest traps

$$\frac{d\Delta n}{dt} \simeq G \qquad - \quad (2.47)$$

and

$$\frac{dI_{ph}}{dt} = e\mu_o E \frac{d\Delta n}{dt} \qquad - \quad (2\cdot48)$$

where Δn is the excess (electron) carrier density, μ_o the free carrier mobility, E the applied electric field and I_{ph} the photocurrent. Short time measurement of this orders have only become possible recently with the introduction of picosecond resolution techniques (38 - 40). Vardeny et al (40), resolved the thermalisation of photogenerated hot - carriers in amorphous Silicon, and observed the trapping of these carriers by states in the mobility gap.

For times longer than a given trapping time, τ_t, and a corresponding trap release time τ_r, but shorter than the trapping time for another (deeper) set of traps and shorter than the recombination time, a quasi - thermal equilibrium will be established between the band states and the traps so that

$$\Delta n + \Delta n_t = Gt \qquad - \quad (2\cdot49)$$

and

$$\frac{\Delta n}{\Delta n_t} = \frac{N_c}{N_t} \exp\left[-\frac{E_c - E_t}{kT}\right] \quad - \quad (2\cdot50)$$

Here, Δn_t is the excess density of trapped electrons in a density of traps N_t, situated at an energy E_t below the conduction band edge. (Note. The above argument assumes that quasi - equilibrium can be established between shallow traps and the band before

quasi - equilibrium is established with deeper traps and the band. The validity of this assumption will be discussed in section 2.5.5). It follows that

$$\frac{dI_{ph}}{dt} = eEG\mu_0 \frac{N_c}{N_t} \exp\left[-\frac{E_c - E_t}{kT}\right] = eEG\mu_d \quad - (2.51)$$

where μ_d is the electron drift mobility. At still longer times, (of the order of the recombination time and longer), excess carriers will be lost due to recombination, and the photocurrent will approach a quasi - equilibrium situation described by steady state photoconductivity kinetics. If the equilibrium photocurrent is still dominated by the same single carrier, its magnitude may be written in the form

$$I_{ph} = eEG\mu_d \tau \quad - \quad (2.52)$$

where $eEG\mu_d$ is the rate of photocurrent rise as given by equation 2.51, and τ is the average carrier trap limited lifetime under steady state illumination. If the magnitude of the drift mobility is the same under conditions of both photocurrent rise (equation 2.45) and steady state photocurrent, then taking the ratio of the rate of rise of the photocurrent, to the steady state photocurrent, yields the trap limited carrier lifetime τ, i.e.

$$\tau = \frac{I_{ph}}{dI_{ph}/dt} \quad - \quad (2.53)$$

Using the above arguments, the expected response of the photocurrent to a step illumination is shown in figure 2.19. Regime (a) is the photocurrent rise before trapping events, regime (b) is the rise after quasi - equilibrium has been established with a set of traps, but before recombination becomes significant, regime (c) is recombination limited growth, and regime (d) follows the establishment of steady state photoconductivity. In theory, the photocurrent rise could be characterised by a number of linear regions corresponding to other discrete trap levels.

In the case where there exists an energetically distributed trap configuration, the photocurrent may reach quasi - equilibrium with specific trap levels at different times after the onset of illumination. Under these circumstances, the photocurrent would rise sublinearly with time. The carrier drift mobility as a function of time could then be found by differentiating the photocurrent rise with respect to time, commencing at the onset of illumination. The differentiation would only be valid for times shorter than the recombination time.

2.3.8 LIFETIMES AND RISE AND DECAY OF PHOTOCURRENT.

In materials containing high densities of traps, each carrier will on average undergo many trapping events before recombination, except at very low temperatures. When the traps are in quasi - thermal equilibrium with the respective bands, rate equations must be written for the whole reservoir of carriers and for all paths.

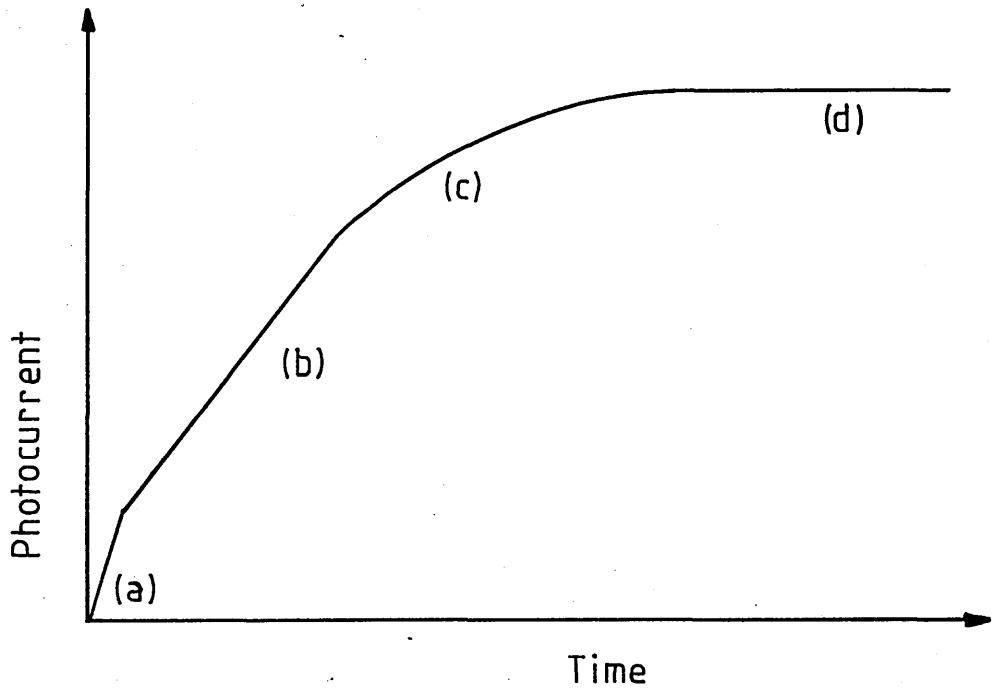

Figure 2.19. Response of the photocurrent to a step function illumination (a) before trapping, (b) after quasi - thermal equilibrium has been established with a set of traps, but before recombination becomes significant, (c) recombination limited growth, (d) establishment of steady state photocurrent.

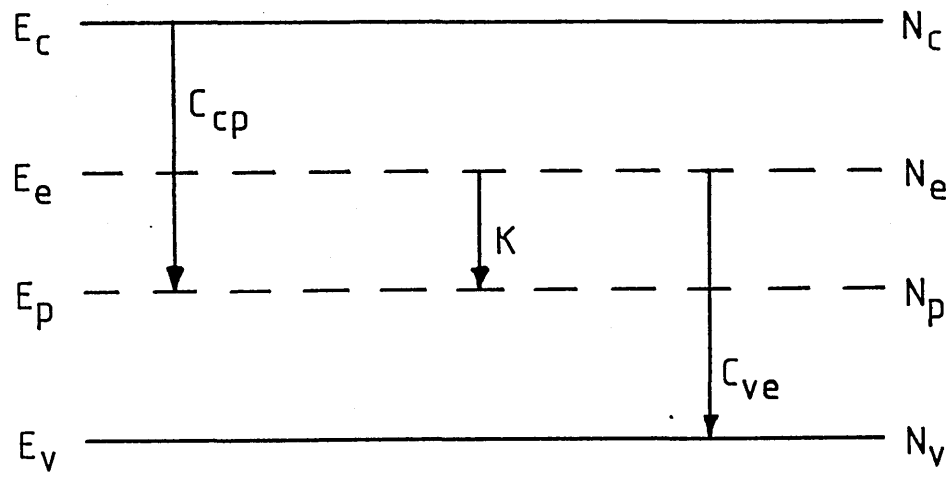

Figure 2.20. Recombination paths for electrons. Trap parameters are shown alongside recombination paths.

Considering the two discrete level model of Main (27) previously discussed, (for electrons)

$$\frac{d}{dt}(\Delta n+\Delta n_t) = G-\left[2n_d\Delta n+\Delta n^2\right]\left\{C_{cp}+C_{ve}\frac{N_e}{n_i}\frac{P_i}{N_p}+K\frac{N_e}{n_i}\right\}\frac{N_e}{n_i} \quad (2.54)$$

describes the rate of change of free and trapped electrons taking part in the conduction process. The right hand side is the generation rate for electrons, free and trapped at E_e, minus the various recombination rates through the paths shown in figure 2.20. In quasi thermal equilibrium

$$\Delta n_t = \frac{N_e}{n_i}\Delta n \gg \Delta n \quad - \quad (2.55)$$

so that

$$\frac{d}{dt}(\Delta n+\Delta n_t) \simeq \frac{N_e}{n_i}\frac{d\Delta n}{dt} \quad - \quad (2.56)$$

Also, the instantaneous electron recombination lifetime, τ_e, can be defined in terms of the instantaneous recombination rate, R_e, and the electron density (free and trapped), i.e.,

$$R_e\tau_e = \Delta n+\Delta n_t \simeq \frac{N_e}{n_i}\Delta n \quad - \quad (2.57)$$

R_e, however, is just the second term on the right hand side of equation 2.54, and solving for τ_e gives

$$\tau_e = \left[2n_d+\Delta n\right]^{-1}\left\{C_{cp}+C_{ve}\frac{N_e}{n_i}\frac{P_i}{N_p}+K\frac{N_e}{n_i}\right\} \quad (2.58)$$

In the monomolecular regime ($2n_d >> \Delta n$), the recombination lifetime is independent of excitation intensity. Equation 2.54 can then be written as

$$\frac{N_e}{n_i}\frac{d\Delta n}{dt} = G - \frac{N_e}{n_i}\frac{\Delta n}{\tau_{em}} \qquad - (2.59)$$

where τ_{em}, is the constant monomolecular recombination time. This equation can be solved (41), e.g., for a step function illumination, and neglecting diffusion

$$\frac{N_e}{n_i}\Delta n = G\tau_{em}\, g(t) \qquad - (2.60)$$

and

$$\frac{dI_{ph}}{dt} = eE\mu_d \tau_{em} G\, g(t) \qquad - (2.61)$$

The function g(t) is given by

$$g(t) = 1 - \exp\left(-\frac{t}{\tau_{em}}\right) \qquad - (2.62a)$$

or

$$g(t) = \exp\left(-\frac{t}{\tau_{em}}\right) \qquad - (2.62b)$$

depending on whether the excitation is switched on or off at t=0, respectively.

Equation 2.59 can be applied in general if τ_{em} is understood to be the instantaneous lifetime, but it is often more useful to write the bimolecular case as

$$\frac{N_e}{n_i}\frac{d\Delta n}{dt} = G - \frac{N_e}{n_i}\Delta n^2 \theta \quad - (2.63)$$

where θ is the term in curly brackets in equation 2.54. Equation 2.63 can be solved, and for the rise

$$\Delta n = \left(\frac{G\theta n_i}{N_e}\right)^{\frac{1}{2}} \tanh\left[t\left(\frac{G\theta N_e}{n_i}\right)^{\frac{1}{2}}\right] \quad - (2.64a)$$

whilst for the decay

$$\Delta n = \left(\frac{G\theta n_i}{N_e}\right)\left[t\left(\frac{G\theta N_e}{n_i}\right) + 1\right] \quad - (2.64b)$$

i.e., the rise curve is a hyperbolic tangent and the decay curve a hyperbola.

2.4 THERMOELECTRIC POWER.

The thermoelectric power, S, (or Seebeck coefficient), is determined by measuring the voltage, dV, developed between two points of a material maintained at a small temperature difference, dT. For an n - type crystalline semiconductor, the thermoelectric power is given by

$$S = \frac{dV}{dT} = -\frac{k}{e}\left[\frac{E_c - E_f}{kT} + A\right] \quad - (2.65)$$

where E_c and E_f are the energies of the conduction band edge and the Fermi level respectively, and AkT is the average energy of the transport electrons, measured with respect to E_c. The value of A depends upon the scattering process existing within the semiconductor and is a constant normally between 2 and 4. If the current is carried by holes, the sign of S is reversed and $E_c - E_f$ is replaced by $E_f - E_v$ in equation 2.65. For ambipolar conduction the thermopower associated with each carrier is weighted according to the contribution each makes to the total current.

In amorphous semiconductors, no major modification to equation 2.65 is required. This is mainly because the transport term, A, makes only a small contribution to S, when $E_c - E_f$ (or $E_f - E_v$) $\gg$ kT. For current carried in extended states, A is expected to be equal to unity (2,42) and E_c (or E_v) refers to the appropriate mobility edge. For current carried in localised states at the band edges, A will again be small and E_c (or E_v) in equation 2.65 is replaced by E_d, where E_d represent the energy of the conduction path through the localised states. If there are several conduction paths acting in parallel, S is determined by a weighted average over the energy difference between E_f and the various current paths through the energy spectrum. The sign of S is therefore a reliable indicator of whether conduction in the material is dominated by electrons or holes (i.e. n - type or p - type).

At the temperature corresponding to a transition in transport from hopping at E_d say, to motion in extended states at E_c, there will be a change in slope of the curve of S versus 1/T. Because the

intercept of the thermopower curve on the S axis at 1/T = 0 remains virtually unchanged, S passes through a transition region between two curves (see figure 2.3). This can be spread over a fairly wide temperature range within which the slope of S versus 1/T has little significance (43).

If the variation of the width of the mobility gap is taken to be linearly dependent on temperature with coefficient δ, (see equation 2.7) then equation 2.65 may be replaced by

$$S = -\frac{k}{e}\left[\frac{(E_c - E_f)_o}{kT} - \frac{\delta}{k} + A\right] \qquad - (2.66)$$

Therefore, a plot of S against 1/T has slope $(E_c - E_f)o$ (as does a plot of ln (σ) versus 1/T, shown by equation 2.7) and the intercept on the S axis at 1/T = 0 yields δ. Thus, thermoelectric power measurements may provide a most direct method of determining the temperature coefficient δ, of the activation energy for conduction.

Analysis of thermopower data becomes less simple when S is small (i.e. S < Ak/e). If this is not because of ambipolar conduction but because $E_c - E_f$ (or $E_f - E_v$) $\simeq$ kT, then the situation approaches that of a metal, with current being carried by electrons with energies within a few kT of the Fermi level. In this case, Mott (2) has suggested that the metallic formula should apply, i.e.

$$S = \frac{\pi^2}{3}\,\frac{k^2 T}{e}\left(\frac{\partial \ln(\sigma)}{\partial E}\right)_{E=E_f} \qquad - (2.67)$$

Under these circumstances, the sign of S depends on whether the density of states in the vicinity of E_f increases or decreases with energy. However, some doubt (2) has been thrown on the applicability of equation 2.67.

2.5 EXPERIMENTAL TECHNIQUES FOR THE MEASUREMENT OF CARRIER MOBILITIES.

In crystalline semiconductors, the most common technique for the measurement of carrier mobilities involves the Hall effect. However, in non - crystalline materials, experimental data are both fragmentary and anomalous (2). Measured Hall mobilities are typically 10^{-1} to 10^{-2} $cm^2 V^{-1} s^{-1}$, and are frequently found to exhibit an anomalous sign reversal with respect to other properties providing information concerning the dominant charge carrier. Thus, although of some theoretical interest, Hall effect measurements are of minimal value in the study of macroscopic transport in amorphous semiconductors.

A second common technique, in the case of crystalline semiconductors, is the procedure developed by Haynes and Shockley (44) in 1949, for the measurement of carrier drift mobilities (see figure 2.21a). In its original form as applied to the examination of specimens of relatively high electrical conductivity, the technique is restricted to the study of minority carrier transport. Excess packets of majority carriers rapidly spread out during transit, so that information regarding their transit time along the specimen is lost. Since this spreading occurs in a time of the order of the dielectric

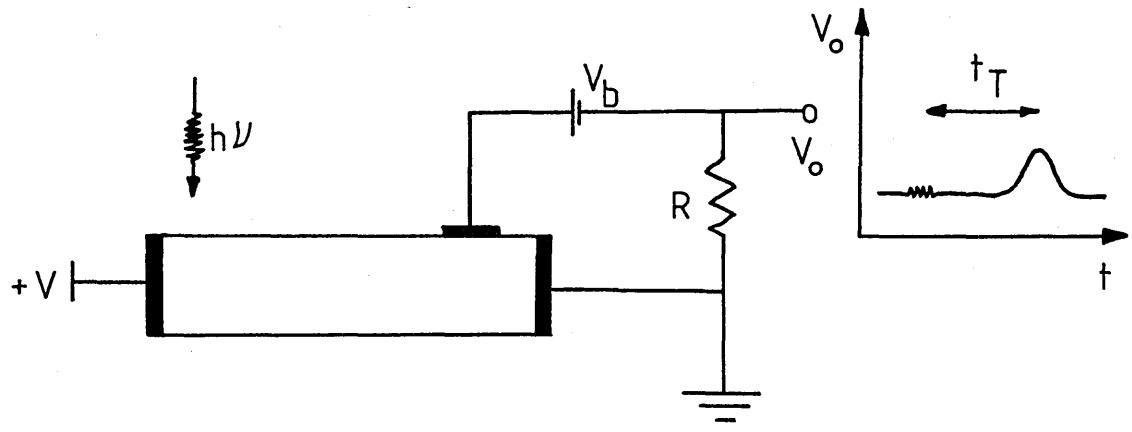

(a)

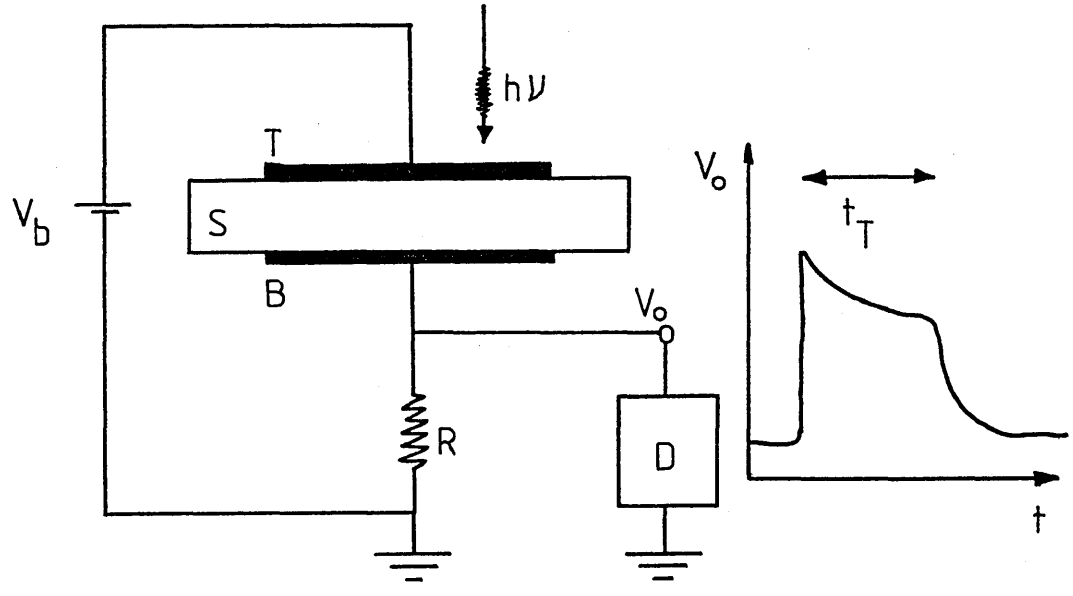

(b)

Figure 2.21. Experimental techniques for the measurement of carrier mobilities.
(a). The Haynes - Shockley technique.
(b). The time of flight technique.

relaxation time, it will take place more slowly in materials of low electrical conductivity, as in the case of most amorphous semiconductors of interest. Against this, amorphous semiconductors are characterised by drift mobilities which are typically much lower than those in crystalline semiconductors, so that transit times must be reduced to acceptable short values if the technique is to be of value.

An experimental method which achieves the above objectives is the "Time of Flight" technique. This will be discussed in detail below.

2.5.1 THE TIME OF FLIGHT TECHNIQUE.

Drift mobility measurements using the time of flight technique have for some time been recognised as a powerful probe of the transport properties of high resistivity, low mobility materials (45). The technique provides a rather direct and straight - forward evaluation of the transport properties of both electrons and holes and has been applied to a wide range of both solid and liquid materials. The basic ideas of the time of flight technique are illustrated schematically in figure 2.21b. A sample of material (S) is sandwiched between two non - injecting contacts (T and B) across which a bias voltage (V_o) is applied. A short pulse of strongly absorbed radiation passes through the top semi - transparent electrode and generates a thin sheet of carrier pairs in a period much shorter than the time required for the carriers to traverse the sample (transit time). The intensity of the radiation must be sufficiently low as to avoid space

charge effects and the response time of the detector (D) fast enough so that detail of the transient response can be resolved. If the dielectric relaxation time is much longer than any subsequent time of observation, then the carrier pairs can be separated and the independent drift of either carrier studied by choice of the appropriate polarity of bias voltage. Apart from a short time immediately after excitation, the current flowing in the resistor (R), will be due to the drift of excess carriers produced by the radiation. This transient current, as measured in the external circuit, may bear a predominant feature associated with the carrier extraction time at the back electrode, which can be analysed in terms of the carrier transit time.

The transit can be monitored in either the integrated or non - integrated mode, depending on the relative magnitude of the transit time, t_T, and the external circuit CR time constant. If $CR \ll t_T$, a rectangular current pulse is observed as in figure 2.22a, whereas if $CR \gg t_T$, its integral, a ramp function as shown in figure 2.22b, is the observed response. In the following discussion, the pulses described will be those for which $CR \ll t_T$, i.e. non - integrated current pulses.

2.5.2 CONVENTIONALLY DISPERSIVE TRANSPORT.

In the ideal case when all the carriers excited into the system previously described survive their journey across the specimen, and the charge maintains its initial sheet distribution, an ideal current

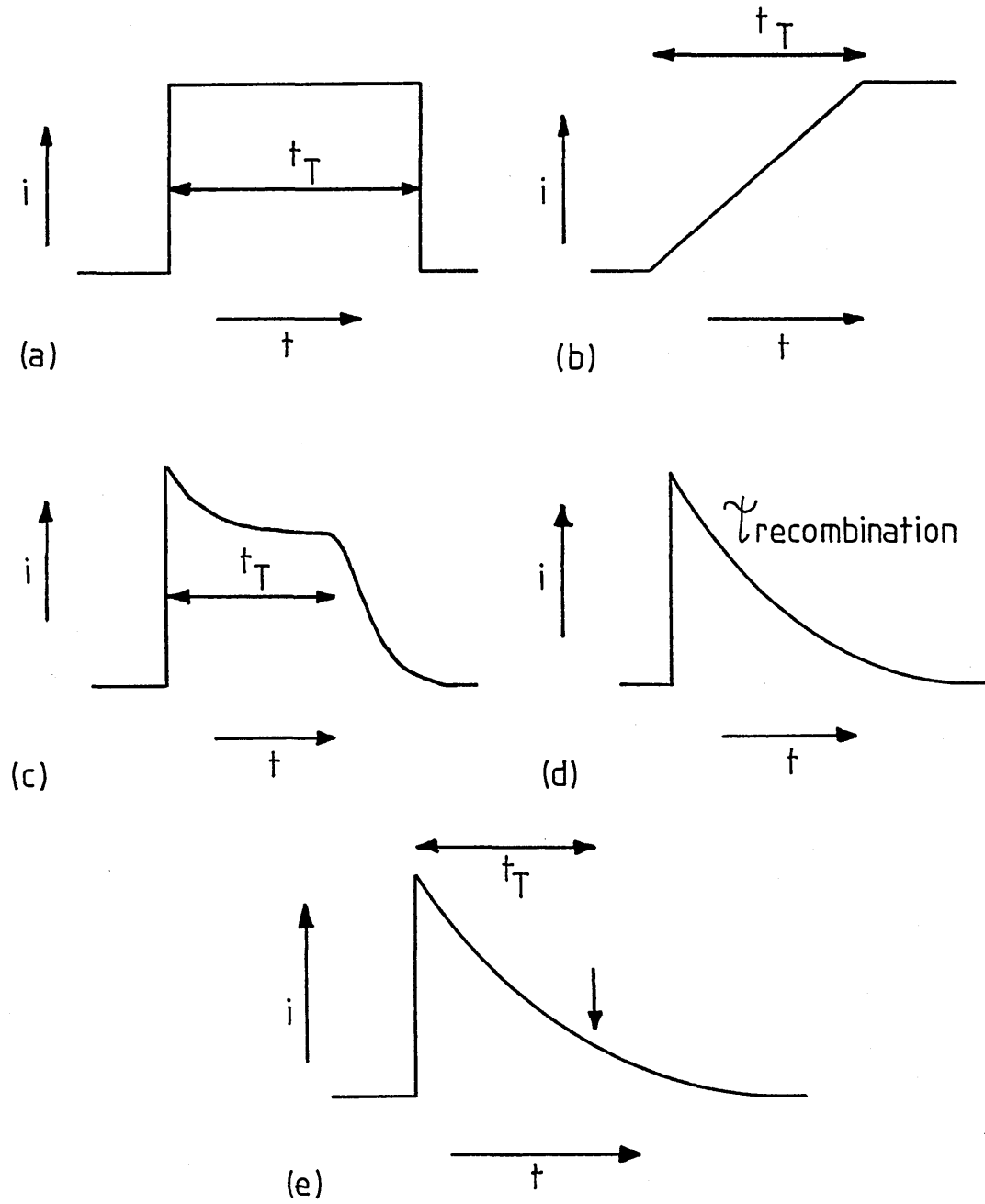

Figure 2.22. Types of transient current pulse expected from a time of flight experiment.
(a). Ideal non - integrated.
(b). Ideal integrated.
(c). Conventionally dispersive.
(d). Recombination limited.
(e). Anomolously dispersive.

pulse as shown in figure 2.22a will be observed. The drift of charge across the sample generates a constant current in the external resistor the duration of which is set by the carrier transit time, t_T. In practice this type of transient is never observed and it is likely that there will be some amount of deep trapping which will reduce the charge sheet as it moves through the sample. Certainly, the charge sheet will statistically broaden as the carriers thermally diffuse out of the sheet resulting in a current pulse which may appear more like that shown in figure 2.22c where the extraction time feature at t_T is now less sharp. Experimentally, it has been observed (46) that the most ideal transients are produced in amorphous selenium around room temperature.

The relative degree of dispersion of the drifting charge packet is of order

$$\frac{\Delta t}{t_T} = \left(\frac{2D}{\mu}\right)^{\frac{1}{2}} (EL)^{-\frac{1}{2}} \qquad - \qquad (2.68)$$

where E is the applied electric field, L the sample thickness, and D, a diffusion coefficient which is related to the carrier mobility, μ, via the Einstein relationship

$$D = \left(\frac{kT}{e}\right)\mu \qquad - \qquad (2.69)$$

Thus, if measurements are performed upon specimens of differing thichnesses, at identical applied electric fields, it is interesting to note that variations in the relative degree of dispersion should be observed, with thicker specimens being characterised by less

dispersive transit pulses.

In most of these conventionally dispersive transients, if the effect of deep trapping is not too severe, it is possible to determine t_T, and a drift mobility can be unambiguously defined by

$$\mu = \frac{L^2}{V_b t_T} \qquad - \quad (2.70)$$

μ can normally be found accurately by measuring the slope of a plot of V_b versus $1/t_T$.

If deep trapping effects predominate, it may not be possible to pick out the transit time from the current transient (see figure 2.22d), rendering the time of flight method ineffective. Young et al (47), however, suggested that by using an interdigital bottom electrode, it may still be possible to observe an extraction feature under conditions of severe trapping. These workers used such an electrode arrangement to observe electron transients in anthracene (47).

2.5.3 THE EFFECT OF TRAPPING.

In the case of a material with a significant concentration of localised states, it is by no means possible to assume that carriers will traverse the specimen in states confined to a single energy. A particular important departure from this limiting situation is that of trap - limited band motion (48). Here, transport of a carrier via extended states is repeatedly interrupted by trapping in localised

states (with subsequent re - emission into extended states after a period spent immobilised). The macroscopic drift mobility, μ_d, for such a carrier is reduced from the value for free carriers, μ_0, by a factor taking into account the proportion of time spent in traps. Under steady state conditions

$$\frac{\mu_d}{\mu_0} = \frac{\tau_t}{\tau_t + \tau_r} \qquad - \qquad (2.71)$$

where τ_t and τ_r are respectively the mean free carrier trapping time, and the mean free carrier release time.

For the simplest case of a single set of localised states, of density N_t, situated at a particular energy E_t, the trap limited drift mobility of carriers moving in extended states is given by (45)

$$\mu_d = \mu_0 \left[1 + \frac{N_t}{N_c} \exp\left(\frac{E_t}{kT} \right) \right]^{-1} \qquad - \qquad (2.72)$$

where N_c is the effective density of extended states. At sufficiently low temperatures, equation 2.72 predicts an exponentially decreasing effective mobility which in principle permits the density of traps, and their depth to be determined from a study of the temperature dependence of μ_d.

Under conditions where localised states are distributed over a range of energy, it is still possible to compute a value for the steady state drift mobility, providing that the total trapped carrier density remains finite under quasi - thermal equilibrium conditions. Then equation 2.72 may be replaced by

$$\mu_d = \mu_0 \frac{\int_{E_c}^{\infty} g(E) f(E) \, dE}{\int_{E_f}^{\infty} g(E) f(E) \, dE} \qquad - \qquad (2.73)$$

where g(E) and f(E) are respectively the density of states and occupation probability at energy E. In principle, equation 2.73 may be applied to any density of states distribution, but in many cases an exact solution cannot be obtained. One particular density of states distribution, for which equation 2.73 may be readily applied and solved, is the linear tail of states model of Mott and Davis (2) (see figure 2.17). In this case a steady state drift mobility is obtained, which in the low temperature approximation (trapped carriers >> free carriers), is of order

$$\mu_d = \mu_0 \left(\frac{\Delta E}{kT}\right) \exp\left(-\frac{\Delta E}{kT}\right) \qquad - \qquad (2.74)$$

where ΔE represents the extent of the linear tail.

An alternative to trap - limited band motion is trap - limited hopping (49,50), where carriers hop between shallow localised states with constant interruption by trapping in deeper localised states. Under these conditions a drift mobility may be derived from equation 2.71 by replacing μ_0 with a hopping mobility appropriate to motion between the shallower localised states, and τ_t and τ_r by trapping and release times associated with the details of the distribution of localised states under consideration.

The discussion in this section so far has assumed that thermal equilibrium exists between electrons (or holes) in extended states and in traps (or between two sets of traps in the case of trap limited hopping). This will not be the case, however, when trap release times are greater than the measured carrier transit time. The condition

that a trap will release a carrier during the passage of a transit pulse is

$$\nu t_p \exp\left(-\frac{E_t}{kT}\right) > 1 \qquad - \qquad (2.75)$$

where t_p is the duration of the pulse and ν is a phonon "attempt to escape" frequency. For deep traps $\tau_r \gg t_T$, and their effect on time of flight pulses will depend upon their lifetime τ_d, with respect to free carriers. If $\tau_d > t_T$, then the presence of deep centers will have little effect. With shorter lifetimes $\tau_d \simeq t_T$, there will be a loss of free carriers during the carrier transit, resulting in a lack of saturation in the charge collected at the back electrode. Under these conditions, it is still possible to determine an extraction time, but it is important to realise that only those traps with a release time less than the transit time are being probed. Finally, if τ_d is appreciable shorter than t_T, all the charge is trapped before it crosses the sample, and the time of flight method can no longer be applied.

2.5.4 ANOMOLOUSLY DISPERSIVE TRANSPORT.

The slight rounding of the transit pulse around t_T in the conventionally dispersive case was attributed to the statistical spread in the arrival times of individual carriers in the charge sheet at the back electrode. In some cases, however, the dispersion of transit pulses was found to be much more than that expected from conventional theory, and in many cases the current transients were

completely featureless as shown in figure 2.22e. Even when a transit time feature could be distinguished, there existed a long tail to the current after the transit time suggesting a considerable spread in the transit time of individual carriers, which was significantly larger than a Gaussian spread. The best documented cases of this type of observation are from measurements performed on a - As_2Se_3 (51-55) and a - Se (56). a - Selenium is of particular interest since the transition from conventional behaviour at room temperature to anomalously dispersive transport can be observed as the sample is cooled to about 190K (56).

Early attempts to analyse dispersive transport (52,53) led Scharfe (52) to describe the phenomenon as involving carriers possessing a range of drift mobilities. However, at that time, the concept was not in itself of great value, since it was difficult to imagine how such a spread of drift velocities could arise in apparently homogeneous materials. Thus, although transit pulses of this anomalous form were observed in the early 1970s, their origin remained a mystery. Even so, a detailed phonomological characterisation of the phenomenon was achieved, primarily as a consequence of various studies by investigators at the Xerox Research Laboratories (57,58). From this work three main properties emerged which were used to characterise anomalously dispersive transport.

(1). "Universality" of transit pulse shape; i.e. transit pulses obtained from measurements upon a given specimen at various values of applied electric field and temperature were suggested to exhibit almost identical degrees of relative dispersion.

(2). The algebraic time dependence of the excess current; i.e. if an anomalously dispersive transit pulse were replotted using logarithmic axis of both current and time, a curve was obtained which appeared essentially as two straight lines of different negative slope separated by a "knee" at a time close to, but not the same as, that taken to be the transit time from a linear plot. The transit pulse was thus characterised by

$$I \propto t^{-(1-\alpha_1)} \qquad (0 < t < t_T) \quad - (2.76a)$$

$$I \propto t^{-(1+\alpha_2)} \qquad (t > t_T) \quad - (2.76b)$$

(3). These algebraic or power law characteristics were further suggested to be inter - related, in the sense that the parameters α_1 and α_2 were identical, i.e.

$$\alpha_1 = \alpha_2 = \alpha \qquad (0 < \alpha < 1) - (2.77)$$

Figure 2.23 displays experimental data for a - As_2Se_3, illustrating both the universality of pulse shape and the occurance of the two regimes.

The first attempt to explain why transit pulses in amorphous semiconductors should exhibit anomalous dispersion, were not made until 1971 when Marshall and Owen (59) and Silver, Dy and Huang (60) examined the possibility that in thin specimens, carriers moving in extended states might experience just a few trapping events (on

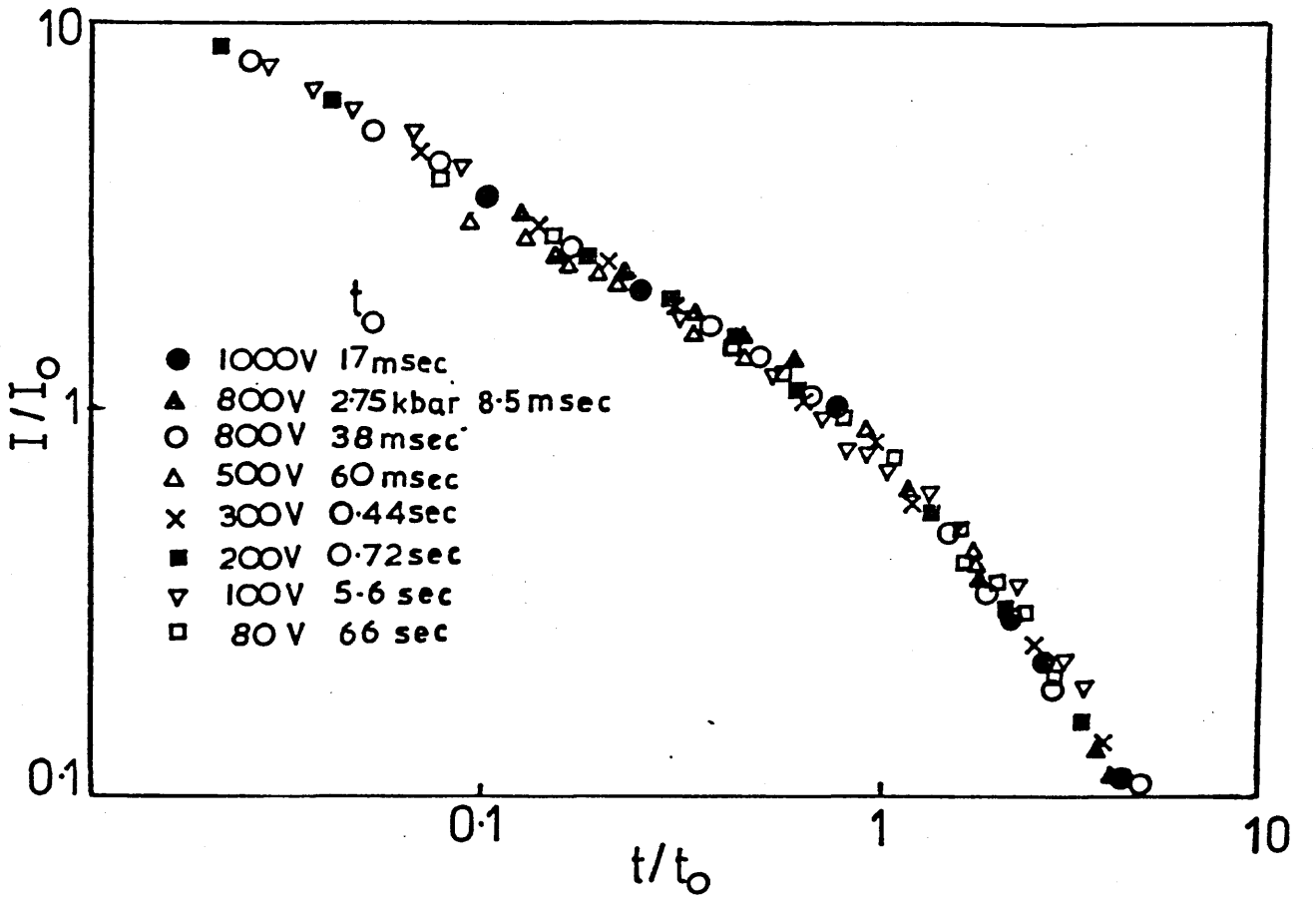

Figure 2.23. Superimpose transient characteristics for hole carriers in amorphous As_2 Se_3 at room temperature, under various values of applied electric field. (After ref. 51).

average) during transit. Thus, whilst some carriers might be trapped several times during transit, others would cross the specimen without localisation, giving a broad spread of individual carrier transit times. However, whilst such a mechanism would yield a considerable degree of dispersion, it was difficult to reconcile it with the apparent characteristic of universality of shape.

A major advance in the understanding of the subject was achieved in 1975 when Scher and Montroll (51) developed a description of anomalously dispersive transport based on a stochastic hopping process. The predictions of the Scher and Montroll (SM) theory, although controversial, have been used to explain possible fundamental mechanism giving rise to anomalously dispersive transport. What follows is a brief summary of the main features of their work.

The situation described by the SM theory is one where there is a wide spread in individual carrier transit times. This is expected to be the case in disordered materials where parameters such as trap depth, hopping distance and energy are likely to vary widely. These parameters in the arguments of exponential functions control the rate of individual transport steps, resulting in the step rate displaying an even greater variation. Even after many trapping events or hops, the event times experienced by individual carriers can be sufficiently different that a marked dispersion in transit time results.

SM approached the problem by treating the carrier motion as a "continuous time random walk" (CTRW) where the mobile charge moves in a random walk, by hopping from one site to another in an array of localised states. The random walk is biased in one direction to

simulate the effect of an applied field. The major conclusion of SM is that the event time distribution function, $\psi(t)$, which is a measure of the probability of a step in the motion occurring at a time, t, after trapping in a particular site, can be approximated by

$$\psi(t) \propto t^{-(1+\alpha)} \qquad - (2.78)$$

where α lies between 0 and 1. One feature of this distribution function is the slow variation of $\psi(t)$ with time, which ensures that over a wide range of time, a carrier has a substantial probability for a jump. This contrasts with the familiar exponential distribution, in which the probability of a jump is governed by a single transition time, τ, as in

$$\psi(t) \propto \exp\left(-\frac{t}{\tau}\right) \qquad - (2.79)$$

A second observation noted by SM was that while the distribution in 2.79 gives rise to conventional Gaussian transport, 2.78 causes the motion of a charge packet to be such that the ratio $\sigma/\langle 1\rangle$ is independent of time. σ is the dispersion of the carrier distribution and $\langle 1\rangle$ its mean position. In contrast, for Gaussian transport $\sigma/\langle 1\rangle \propto t^{-\frac{1}{2}}$. With Gaussian transport, the maximum of the charge distribution moves obviously in time, while for the dispersive, non - Gaussian case, the maximum remains close to its initial position. Some idea of the differing propagation characteristics can be gained from figures 2.24a and b. These diagrams show how the charge distribution develops for both dispersive and non - dispersive

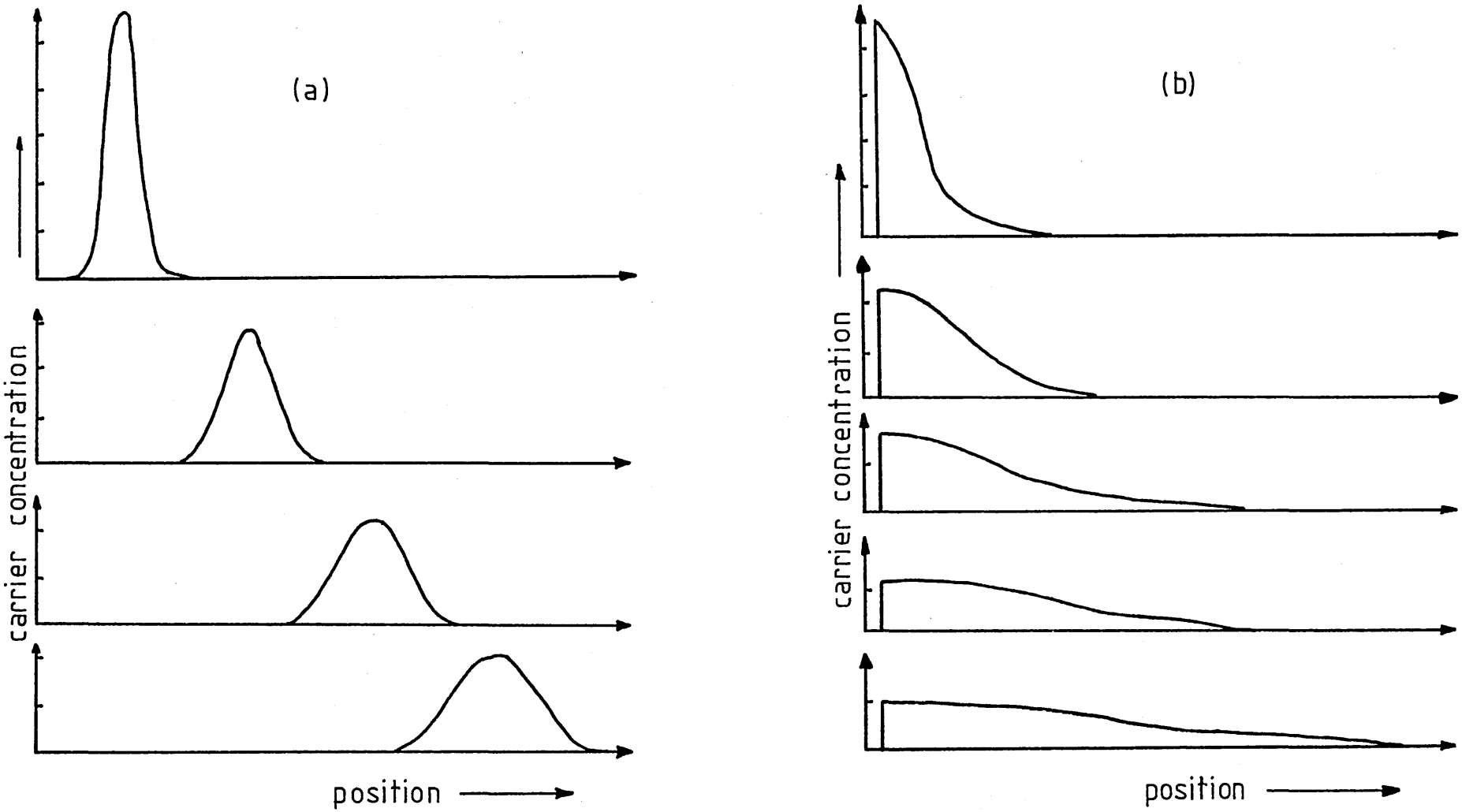

Figure 2.24. The evolution of the distribution of drifting charge carriers in a specimen for the cases in which, (a) $\Psi(t)$ has the "conventional" form, (b) $\Psi(t)$ has the anomolous form. Time increases from the top to the bottom diagram.

transport.

In terms of current flow, SM find that the transient current decays algebraically as

$$I(t) \propto t^{-(1-\alpha)} \qquad - \quad (2.80)$$

for $\langle 1 \rangle \ll L$, where L is the sample thickness. Thus, even in an infinitely thick specimen, the current will decay, though no carriers are extracted at the back electrode. When carriers are extracted, the current falls off faster as

$$I(t) \propto t^{-(1+\alpha)} \qquad - \quad (2.81)$$

Equation 2.81 is expected to apply when $\langle 1 \rangle \gg L$. α is determined by such things as trap depth, hopping distance and energy, and so is a characteristic of a given system.

A current pulse described by equations 2.80 and 2.81 will exhibit the universality experimentally observed, since the shape of the pulse will not alter as the transit time varies. If the pulse is plotted on logarithmic scales, the power law decay will generate two linear regions of different slope, just as in figure 2.23. The time at which the knee on the curve occurs will be a measure of the time at which the fastest carriers reach the back electrode.

SM also deduced that the transit time would be dependent both on electric field, E, and sample thickness, L, in a different way from conventionally dispersive transport. They found that

$$t_T \propto \left(\frac{L}{\bar{l}}\right)^{\frac{1}{\alpha}} \qquad - \quad (2.82)$$

where $\bar{l}$ is the average distance that a carrier moves between each localised site in the direction of the applied field. At low fields, $\bar{l}$ should be proportional to E, resulting in the relationship

$$t_T \propto \left(\frac{L}{E}\right)^{\frac{1}{\alpha}} \qquad - \quad (2.83)$$

Since $\alpha < 1$, equation 2.83 implies that t_T and $1/t_T$ will exhibit superlinear dependencies on sample thickness and field respectively. This also means that the drift mobility defined by equation 2.70 will be both field and thickness dependent.

After publication of the SM theory, much experimental work was carried out in order to test its validity. It was subsequently shown by Pfister (55,56,61), Scher (51) and others that the theory does in fact give a good description of some of the features of dispersive transport. However, deviations from the SM theory do exist. It was shown by Marshall (62) and by Pfister (56) that universality of current pulse shape with temperature is not obtained in the case of hole transport in amorphous Selenium. Additionally, it was noted that whilst transit pulses observed at low temperature may be characterised to a first approximation as involving two power - law regimes, there were detectable deviations from such algebraic behavior within the

experimentally - accessible time range. Moreover, force - fitted values of α, obtained from the transit pulse before and after the transit time were found in general not to be equal to one another (63-67). These deviations from the SM theory lead some workers to look for an alternative description of anomalously dispersive transport. Such a description was obtained in the form of a trap limited band transport mechanism. The basis of this approach is outlined below.

The possibility that anomalously dispersive transport may arise in the case of trap limited band transport became clear from a number of studies published in 1977. Marshall (4,68) and Silver and Cohen (69) explored the situation via Monte Carlo simulation techniques, in which the transport of each carrier through a specimen was modeled using random number procedures to determine each free carrier trapping time and trapped carrier release time. Additionally, Schmidlin (70,71) and Noolandi (72,73) performed theoretical analysis for model systems. It rapidly became clear that all which was required for the generation of anomalous dispersion in the case of this transport mechanism, was for the localised states to be distributed over a sufficient range of energy.

A complete review of the above work is not appropriate here, but it is sufficient to say that in the simulation studies, various distributions of trapping centers have been examined and it was established that in all cases, highly dispersive transit pulses could be generated if the localised states extended (in significant numbers) over more than a few kT.

2.5.5 EXTENSION OF THE TIME OF FLIGHT TECHNIQUE.

In recent years a transient photoconductivity technique has been developed (74) which is thought to be intimately related to the time of flight technique. The new method is concerned with the time dependence of the decay of the photocurrent, following carrier excitation by means of a short pulse of illumination, in a coplanar specimen (see figure 2.25). The technique has become popular since it allows measurements to be performed on very thin films under conditions appropriate to their use in many device applications. It also allows an examination of the photocurrent over several decades of time, without the complication associated with carrier extraction at the back electrode, which exists in the time of flight technique.

Figure 2.26 shows typical experimental results obtained from the transient photoconductivity technique, i.e. the decay of the photocurrent following a flash excitation of excess carriers in a thin film of a - As_2Se_3. In principle the photocurrent decay follows the interaction of initially free carriers with various levels of localised states within the mobility gap. In the absence of recombination effects and with phenomena associated with carrier drift close to the surface of the film, the response shown should correspond to the initial pre - transit "time of flight" pulse, as described by equation 2.80.

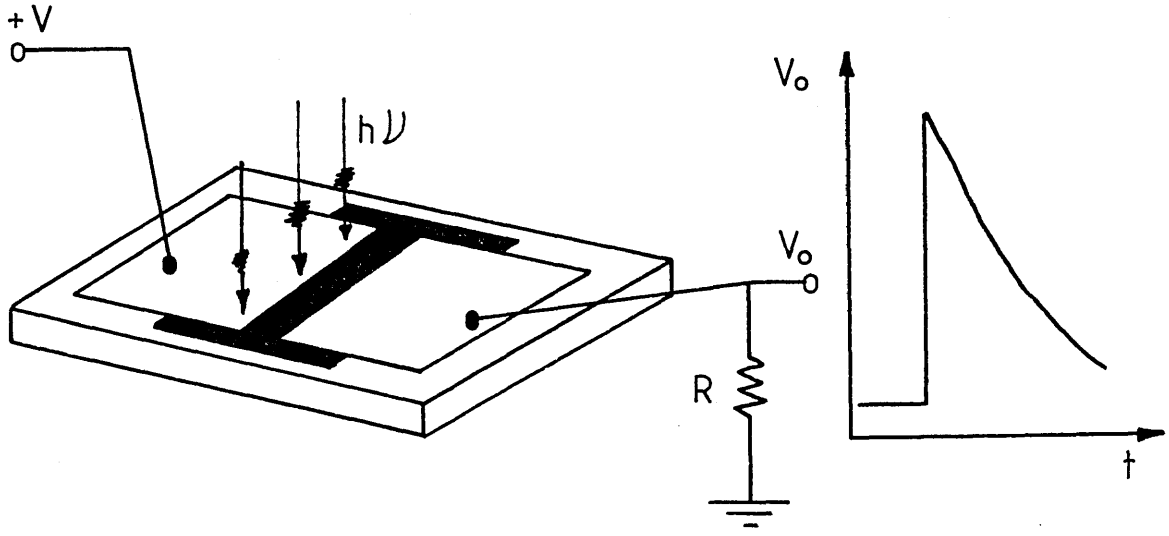

Figure 2.25. The transient photo-decay technique.

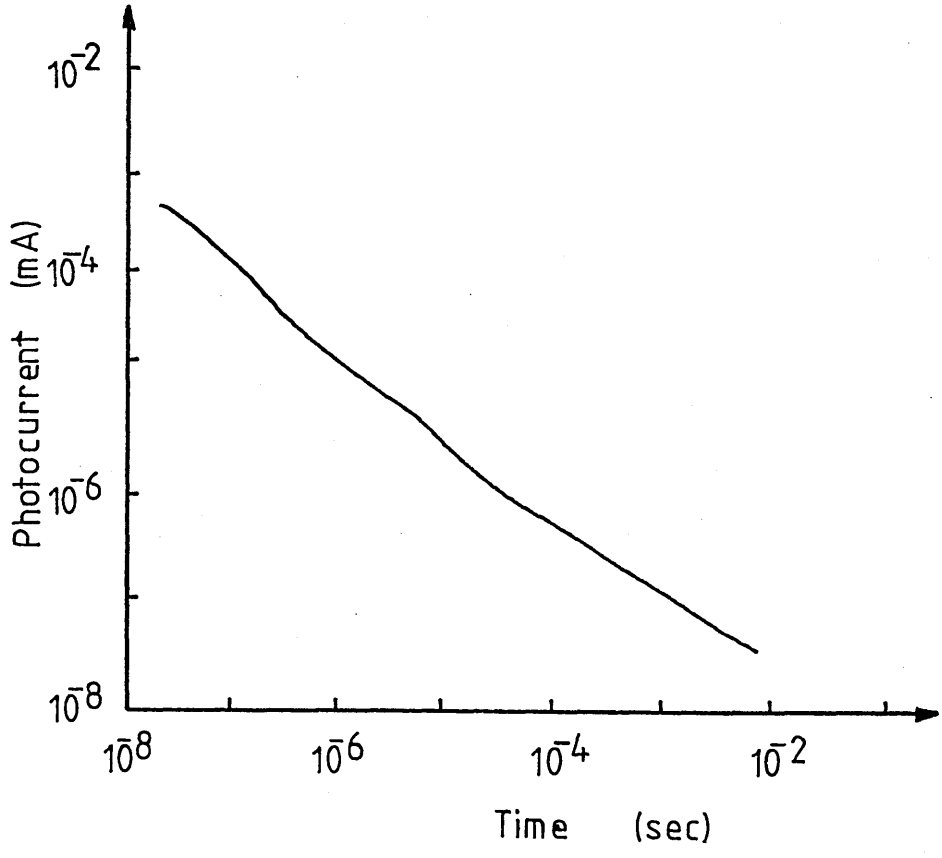

Figure 2.26. Decay of the photocurrent following flash excitation of excess carriers in a thin film of amorphous As_2 Se_3.

Two main types of analysis have been performed on results obtained from the transient photoconductivity technique; those by Tiedje and Rose (75), and Orenstein and Kastner (74) (TROK) and by Michiel, Marshall and Adrianssens (76) (MMA). It is not the intention of the author to give a complete review of the above work here, but a brief description of the important points will be presented.

In the analysis by TROK, the concept of carrier thermalisation was re - introduced. TROK proposed that drifting carriers thermalise to progressively greater depths in the mobility gap, with increasing time after generation. They also introduce a thermalisation energy E_{th}, separating "shallow" from "deep" trapping centers. The occupancy of the two types of centers are envisaged as being determined by radically different considerations. The energy E_{th}, measured relative to the mobility edge E_c, is specified by the criterion that a trap at this depth has a release time constant equal to the total elapse time since the creation of the excess carriers, i.e.

$$t = \nu^{-1} \exp\left(\frac{E_{th}}{kT}\right) \qquad - \quad (2.84)$$

giving

$$E_{th} = kT \ln(\nu t) \qquad - \quad (2.85)$$

where ν is a phonon "attempt to escape" frequency. It is argued that trapping centers with a release energy less than E_{th} have had sufficient time to both trap and release carriers, and thus should be in quasi - thermal equilibrium with extended states. On the other

hand, deeper - lying states are envisaged as being populated purely by recombination kinetics, since insufficient time has elapsed for appreciable carrier release to occur. Thus, under the assumption of an energy - independent capture cross section, such deep traps are seen as containing numbers of excess carriers in linear proportion to their density.

TROK then considered the case of an exponential tail of localised states, extending below the mobility edge. A simplifying assumption was made, namely that all carriers at a depth E, remained localised for a total time exactly equal to the release time constant at that depth, rather than being released over a range of times statistically distributed about this value. TROK proceeded to calculate the expected form of the decay of the photocurrent after an impulse excitation, and found that the photocurrent exhibited a power law decay with time. Since this was identical to the experimentally observed result, this lead many workers (77,78) to assume that the experimental observation of an approximate to power - law decay of the photocurrent, constituted evidence of an exponentially distributed tail of localised states. The conclusions of TROK, however, were put into question by MMA (76). Additionally, the validity of the "thermalisation energy" concept was examined in a more general case by Marshall and Main (79).

At first sight, it seems reasonable to assume that sufficiently - shallow centers are in a state of quasi - thermal equilibrium with extended states, while deeper centers are not. This appears valid because centers with release time constants considerably

shorter than the experimental elapse time have had ample opportunity to trap and release carriers. However, upon further examination, the thermalisation concept becomes more questionable. If there exists a significant number of deeper - lying centers, these serve to "syphon off" free carriers released from shallow traps, throwing the release trapping process out of balance. Thus, the presence of a significant density of deep states is also a condition for the continued decay of the transient photocurrent over an extended time range.

Marshall and Main (79) illustrated this behaviour using a model with three discrete sets of traps, of equal density and capture cross section, situated below the mobility edge. Their results show that (contrary to intuitive thinking) quasi - thermal equilibrium cannot be established between shallow traps and the band, before quasi - thermal equilibrium is established between deeper lying states and the band. This result throws considerable doubt on the work of TROK.

MMA (76) approached the problem by trying to deduce the density of states below the mobility edge, from the shape of the time dependence of the decay of the photocurrent (I(t)), (this is in stark contrast to TROK, who first assumed the form of the density of states then proceeded with the analysis). Starting with I(t), MMA first deduced the form of $\psi(t)$, (where $\psi(t).dt$ is the probability that if a carrier is trapped at t = 0, it will be released during the time interval t to t + dt), finding that $\psi(t)$ and I(t) are interrelated via a Volterra equation of the first kind. Having determined $\psi(t)$, the density of states as a function of energy below the mobility edge (G(E)) was deduced. It was found that $\psi(t)$ and G(E) are related via

a Fredholm equation of the first kind. By solving both the Volterra and the Fredholm equation using a computer technique, MMA were able to deduce the form of the density of states below the mobility edge.

In order to obtain a solution of the Volterra equation, however, it was necessary to determine a full knowledge of I(t), and to obtain a value for the free carrier trapping time constant, τ_t. Unfortunately, such total specification of I(t) is unlikely to be available in the case of amorphous semiconductors, and in practice it is usually necessary to assume values for the photocurrent at t = 0 (Io) and τ_t. MMA find, however, that it is possible to make such approximations to a satisfactory degree, and that errors in the assumed values may not radically affect the computed form of N(E) (80).

MMA applied the technique outlined above to transient photocurrent data generated from a know distribution by Monte Carlo techniques (80). They find that their method is in fact able to reproduce the original density of states profile, with some minor distortions associated with the limitations of the numerical techniques employed for the solution of the Volterra equation. They also observe a blurring of the computed localised state distribution over a range of order $\pm kT$, which is due to the use of a simplifying assumption similar to that described for the TROK analysis.

REFERENCES CHAPTER 2

(1) Fritzsche H., Amorphous and Liquid Semiconductors, ed. J. Tauc, (Plenum, London, 1974), p.221.

(2) Mott N.F., Davis E.A., Electronic Processes in Non - Crystalline Materials. (2nd ed. Clanerdon, Oxford), (1978).

(3) Andriesh A.M., Kolomiets B.T., Soviet Phys. - Solid State 6, 2652, (1965).

(4) Marshall J.M., Phil. Mag. 36, 959, (1977).

(5) Mott N.F., Phil. Mag. 19, 835, (1969).

(6) Mott N.F., J. Non - Cryst. Solids 8 - 10, (1972), 1.

(7) Frenkel J., Phys. Rev. 54, 647, (1938).

(8) Hartke J.L., J. App. Phys., 39, 4871, (1968).

(9) Ieda M. et al., J. Appl. Phys. 42, 3737, (1971).

(10) Shottky N., Spenke E., Wiss. Veroff. Siemens Werke 18, 1, (1939).

(11) Bagley B.G. Solid State Comm. 8, 345, (1970).

(12) Hill R.M., Phil. Mag. 24, 1037, (1971).

(13) Marshall J.M., Millar G.R., Phil. Mag. 27, 1151, (1973).

(14) Cohen M.H., J. Non-Cryst. Solids 4, 326, (1970).

(15) Mott N.F. Phil. Mag. 24, 911, (1971).

(16) Emin D., Electronic and Structural Properties of Amorphous Semiconductors, (Ed. Le Comber P.G., Mort J.), Academic Press, p.261, (1973).

(17) Urbach F., Phys. Rev. B 92, 1324, (1953).

(18) Davis E.A., Electronic and Structural Properties of Amorphous Semiconductors, (Ed. Le Comber P.G., Mort J.), Academic Press, p.425, (1975).

(19) Tauc J., Optical Properties of Solids (ed. Abeles F.) North Holland, Amsterdam, (1970).

(20) Davis E.A., Mott N.F., Phil. Mag. 22, 903, (1970).

(21) Dow J.D., Redfield D., Phys. Rev. Lett. 26, (1971).

(22) Tabac M.D., Warter P.J., Phys. Rev. 173, 899, (1968).

(23) Pai D., Ing S.W., Phys. Rev. 173, 729, (1968).

(24) Hartke J.L., Regensburger P.J., Phys. Rev. 139, A970, (1965).

(25) Davis E.A., Shaw R.F., J. Non-Cryst. Solids 2, 406, (1970).

(26) Knights J.C., Davis E.A., J. Phys. Chem. Sol. 35, 543, (1974).

(27) Main C., Ph.D Thesis, Edinburgh University, (1973).

(28) Main C., Owen A.E., Electronic and Structural Properties of Amorphous Semiconductors, (Ed. Le Comber P.G., Mort J.), Academic Press, p.527, (1973).

(29) Arnoldussen T.C. et al., Phys. Rev. B, 3377, (1974).

(30) Simmons J.G., Taylor G.W., J. Phys. C 7, 3051, (1974).

(31) Taylor G.W., Simmons J.G., J. Phys. C 7, 3067, (1974).

(32) Weiser K. et al. Proc. 10th Int. Conf. on the Phys. of Semicond. (ed. Keller et al), U.S. Atomic Commission, p.667, (1970).

(33) Simmons J.G., Taylor G.W., Phys. Rev. B4, 502, (1971).

(34) Taylor G.W., Simmons J.G., J. Non-Cryst. Sol. 8-10, 940, (1972).

(35) Simmons J.G., Taylor G.W., J. Non-Cryst. Sol. 8-10, 946, (1972).

(36) Arnoldussen et al., J. Appl. Phys. 43, 1798, (1972).

(37) Howard., Tsu., Phys. Rev. B1, 4709, (1970).

(38) Vardeny Z., Tauc J., Phys. Rev. Lett. 46, 18, 1223, (1981).

(39) Vardeny Z. et al, Phys. Rev. Lett. 48, 16, 1132, (1981).

(40) Vardeny Z. et al, Appl. Phys. Lett. 42, 7, 580, (1983).

(41) Petursson J., Ph.D Thesis, Edidburgh University, (1975).

(42) Butcher P.N., Friedmann L., J. Phys. C10, 3803, (1977).

(43) Nagels P., Callaerts R., Denayer M., Proc. 5th Int. Conf. on Amorphous and Liquid Semiconductors, (Ed. Stuke J., Brenig W.) p.867, (1973).

(44) Haynes J.R., Shokley W., Phys. Rev. 75, 691, (1949).

(45) Spear W.E., J. Non-Cryst. Sol. 1, 197, (1969).

(46) Marshall J.M., Owen A.E., Phys. Stat. Sol. A12, 181, (1972).

(47) Young R.H., Mey W., Marchetti A.P., Appl. Phys. Lett. 30, 38, (1977).

(48) Rose A., R.C.A. Rev. 12, 362, (1951).

(49) Street G.B., Gill W.D., Phys. Stat. Sol. 18, 601, (1966).

(50) Gibson D.J., Spear W.E., J. Phys. Chem. Sol. 27, 1917, (1966).

(51) Scher H., Montroll E.W., Phys. Rev. B12, 2455, (1975).

(52) Scharfe M.E., Phys. Rev. B2, 5025, (1970).

(53) Pai D.M., Scharfe M.E., J. Non-Cryst. Sol. 8-10, 752, (1972).

(54) Pfister G., Phys. Rev. Lett. 33, 1474, (1974).

(55) Pfister G., Scher H., Phys. Rev. B15, 2065, (1977).

(56) Pfister G., Phys. Rev. Lett. 36, 271, (1976).

(57) Scharfe M.E., Bull. Am. Phys. Soc. 18, 454, (1973).

(58) Pai D.M., Proc. 5th Int. Conf. on Amorphous and Liquid Semiconductors, (Ed. Stuke J., Brenig W.), p.355, (1973).

(59) Marshall J.M., Owen A.E., Phil. Mag. 24, 1281, (1971).

(60) Silver M., Dy K.S., Huang D.L., Phys. Rev. Lett. 27, 21, (1971).

(61) Pfister G., Proc. 7th Int. Conf. on Amorphous and Liquid Semiconductors, (Ed. Spear W.E.), (1977).

(62) Marshall J.M., Owen A.E., Phys. Stat. Sol. A12, 181, (1972).

(63) Sharp A.C., Marshall J.M., J. Phys. C14, (761), (1981).

(64) Pfister G., Griffith C.H., Phys. Rev. Lett. 40, 659, (1978).

(65) Kolomiets B.T., Lebedev E.A., Kazakova L.P., Sov. Phys. Semicond. 12, 1049, (1978).

(66) Tiedje T. et al, Phys. Rev. Lett. 46, 1425, (1981).

(67) Marshall J.M., Michiel H., Adriaenssens G.J., Phil. Mag. B47, 211, (1983).

(68) Marshall J.M., Proc. 7th Int. Conf. on Amorphous and Liquid Semiconductors, (Ed. Spear W.E.), p.541, (1977).

(69) Silver M., Cohen L., Phys. Rev. B15, 3275, (1977).

(70) Schmidlin F., Phys. Rev. B6, 2362, (1977).

(71) Schmidlin F., Bull. Am. Phys. Soc. 22, 434, (1977).

(72) Noolandi J., Phys. Rev. B16, 4466, (1977).

(73) Noolandi J., Phys. Rev. B16, 4474, (1977).

(74) Orenstein J., Kastner M.A., Phys. Rev. Lett. 46, 1421, (1981).

(75) Tiedje T., Rose A., Solid State comm. 37, 48, (1981).

(76) Marshall J.M., Michiel H., Abrianssens G.J., Phil. Mag. B47, 221, (1983).

(77) Tiedje T. et al, Phys. Rev. Lett., 46, 1425, (1981).

(78) Orenstien J. et al, Phil. Mag. B46, 23, (1982).

(79) Marshall J.M., Main C., Phil. Mag. B47, 5, 471, (1983).

(80) Michiel H., Marshall J.M., Adrianenssens G.J., Phil. Mag. 48, 2, (1983).

(81) Nagles P., Topics in Applied Physics Vol. 36, Amorphous Semiconductors, (Ed. Brodsky M.H.), (1979).

CHAPTER 3

ELECTRONIC PROPERTIES OF AMORPHOUS SILICON.

This chapter presents a brief review of the electronic properties of a - Si which are relevant to the study. Special emphasis is placed on results obtained from films prepared by sputtering. (See Chapter 4 for a description of sputter deposition.)

3.1 MATERIAL PREPARATION AND THE ROLE OF HYDROGEN.

Early studies on the properties of thin films of amorphous tetrahedrally coordinated semiconductors such as Si and Ge, prepared by evaporation or sputtering, showed that these materials possessed a large density of structural defects ranging from single dangling bonds to macroscopic voids. There was a corresponding large density of electronic states in the band gap, and these densities were not appreciably reduced by ultra - high vacuum deposition, high substrate temperature or high temperature annealing. In 1974, however, the group working at Harvard University reported (1) that the deliberate addition of hydrogen to the Argon in the sputtering plasma produced films of a - Ge whose spin density was reduced by many orders of magnitude, and which showed much reduced absorption at low photon energies and much improved photoconductivity. They interpreted these results in terms of a compensation of dangling bonds and other defects by hydrogen, thus simulating the effect of defect removal.

Subsequently, similar behaviour, consistent with the removal of states in the gap by the addition of Hydrogen, were reported by the Harvard group (2) for sputtered films of a - Si.

It is now generally accepted that sputtering in an Argon - Hydrogen atmosphere and glow discharge decomposition of Silane both yield a Silicon - Hydrogen alloy with up to about 30 at. % of Hydrogen. It is also acknowledged that it is the presence of this Hydrogen in the alloy which gives a - Si:H characteristics suitable for many semiconductor device applications.

3.2 ELECTRICAL CONDUCTIVITY.

The magnitude and temperature dependence of the electrical conductivity of a - Si is found to be intimately related to the conditions of material preparation. In particular, it has been shown (2) that the temperature dependence of the conductivity, for a given specimen of a - Si, is controlled to a large extent by its Hydrogen content. This point is illustrated in figure 3.1, which shows a plot of $\ln(\sigma)$ versus $1/T$ for a series of films of sputtered a - Si deposited at a substrate temperature (T_S) of $200^{\circ}C$ and various Hydrogen partial pressures (P_H). The hydrogen partial pressure and the hydrogen content of the films increase from (a) to (f).

In curve (a), an unhydrogenated specimen, the room temperature conductivity is high ($\simeq 10^{-3} (\Omega\ \text{cm})^{-1}$) and the weak temperature dependence of the conductivity cannot be described by any unique activation energy. The addition of 1 at. % Hydrogen to the film is

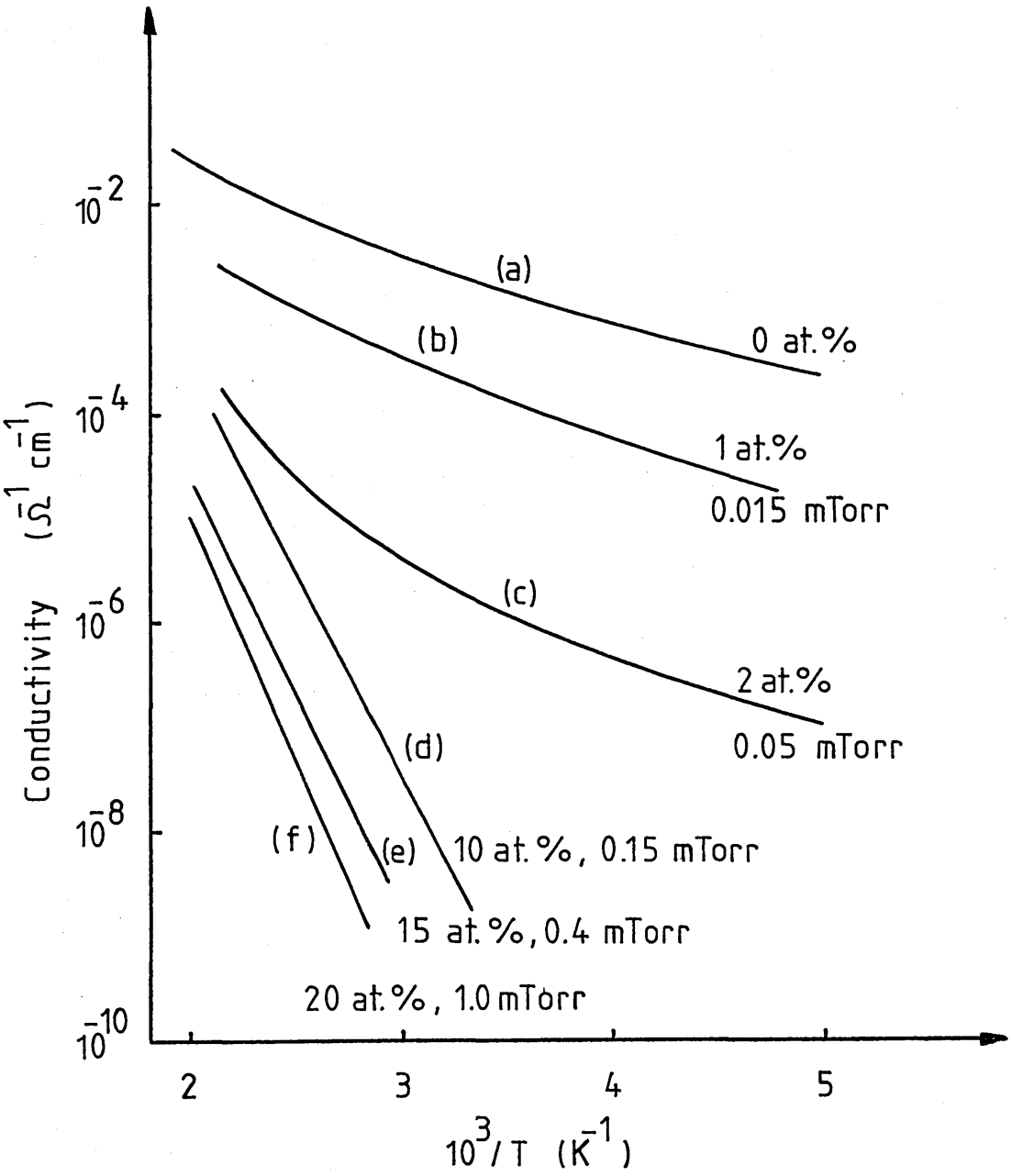

Figure 3.1. Conductivity versus inverse temperature for a-Si:H specimens prepared at T_s=200°C using P_H between 0 and 1 mTorr. Hydrogen content (at. %) and Hydrogen partial pressure in 5 mTorr of Argon are given for each curve. (After ref. 3).

seen to reduce the conductivity at all temperatures, but not change the overall form of the temperature dependence. For a Hydrogen content of 2 at. % the room - temperature conductivity drops by almost three orders of magnitude and there is an indication of activated transport at high temperatures. For 10 at. %, the conductivity has a single activation energy over the entire range of measurement. Further increases in Hydrogen content to 20 at. %, by increasing P_H to 1 mTorr, results in a larger activation energy and a general reduction in the magnitude of the conductivity at all temperatures.

These results are consistent with the effective removal of defect states from the gap, by the introduction of Hydrogen. Anderson and Paul suggest (3) that the introduction of Hydrogen removes states from the gap in a fairly uniform manner, preserving the general shape of the density of states distribution. They describe the conductivity at low P_H as being dominated by carriers hopping close to the Fermi level in a large density of localised states. The reduction in this density of states, with increasing Hydrogen content, is envisaged as reducing the hopping contribution to the conductivity and allowing activated conduction at the mobility edge to dominate (for high enough Hydrogen content or temperature). In the regime where the conductivity is defined by a unique activation energy, the increase in activation energy with Hydrogen content is thought to be due to either an increase in the optical gap with increasing Hydrogen content (see Section 3.3), or to a shift in the position of the Fermi level, from the conduction band towards the gap center, again with increasing Hydrogen content.

The level of substrate temperature during deposition is also found to have a determining influence on the nature of the conductivity obtained from films of a - Si. This is illustrated in figure 3.2, which shows a plot of $\ln(\sigma)$ versus 1/T for a series of films of sputtered a - Si deposited at different substrate temperatures but with no Hydrogen added to the plasma. The figure shows that the temperature dependence of the conductivity for all of these unhydrogenated specimens is weakly activated, with an activation energy which increases with increasing temperature. There is also an underlying trend for the magnitude of the conductivity at all temperatures to decrease, for increasing substrate temperature. Applying the previously mentioned argument of Anderson and Paul (3) to these results, implies that for all of the curves the conductivity is dominated by carriers hopping in a large density of localised states. Increasing the substrate temperature results in a decrease in the magnitude of the density of states in the gap, coupled with a corresponding reduction in the hopping conductivity. Comparing figures 3.1 and 3.2, however, it can be seen that the effect on the form of the conductivity (and hence on the form of the density of states in the gap) of increasing the substrate temperature during deposition, is far less profound than the addition of small amounts of Hydrogen to the films. Never - the - less, the level of substrate temperature during deposition is important for two main reasons. Firstly, high substrate temperatures allow more efficient Hydrogen incorporation into growing films, and secondly, higher substrate temperatures permit greater lattice reorganisation and relaxation during film growth. These two points will be discussed further in

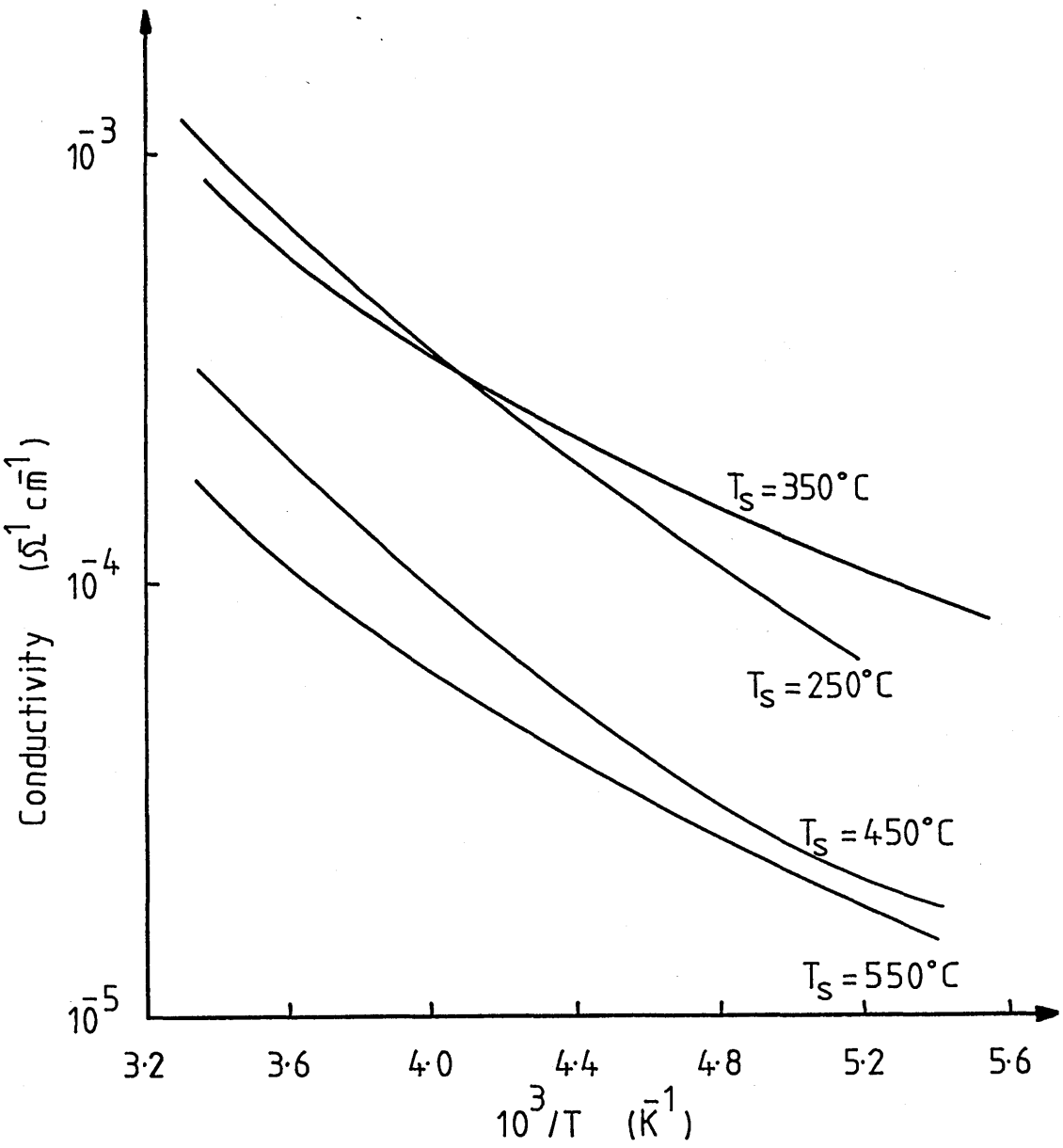

Figure 3.2. Conductivity versus inverse temperature for unhydrogenated specimens of a-Si deposited at several substrate temperatures (T_s). (After ref. 2).

Chapter 4.

3.3 OPTICAL ABSORPTION.

The optical absorption edges for both glow discharge and sputtered films of a - Si:H are very similar (see figure 3.3), and are usually characterised by three distinct regions: (1) At high photon energies, and α approximately greater than 10^4 cm^{-1}, by $\alpha h\nu = Const.(h\nu - Eo)^2$, (2) at intermediate photon energies, roughly $10^2 cm^{-1} < \alpha < 10^4 cm^{-1}$, by an exponential variation of α with $h\nu$, and (3) at low photon energies and optical coefficient, by an optical absorption which is variable and is commonly related to defect and impurity states. There is no sharply defined transition between these three overlapping regions, which were discussed more thoroughly in Section 2.2.

The detailed shape of the optical absorption edge for sputtered films of a - Si is found to be intimately related to the hydrogen content. This is illustrated in figure 3.4, which shows the shift in the optical absorption edge of sputtered a - Si:H, as the Hydrogen partial pressure is increased from 0 to 5 mTorr, at fixed T_S. The initial increase in the optical gap, deduced from these curves at very low values of P_H, strikingly illustrates the effect of Hydrogen in eliminating gap defect states. At high P_H, however, it has been found (4) that both the detailed shape and the position of the absorption edge, obtained from samples prepared under seemingly identical conditions, are somewhat random. This infers that these samples have

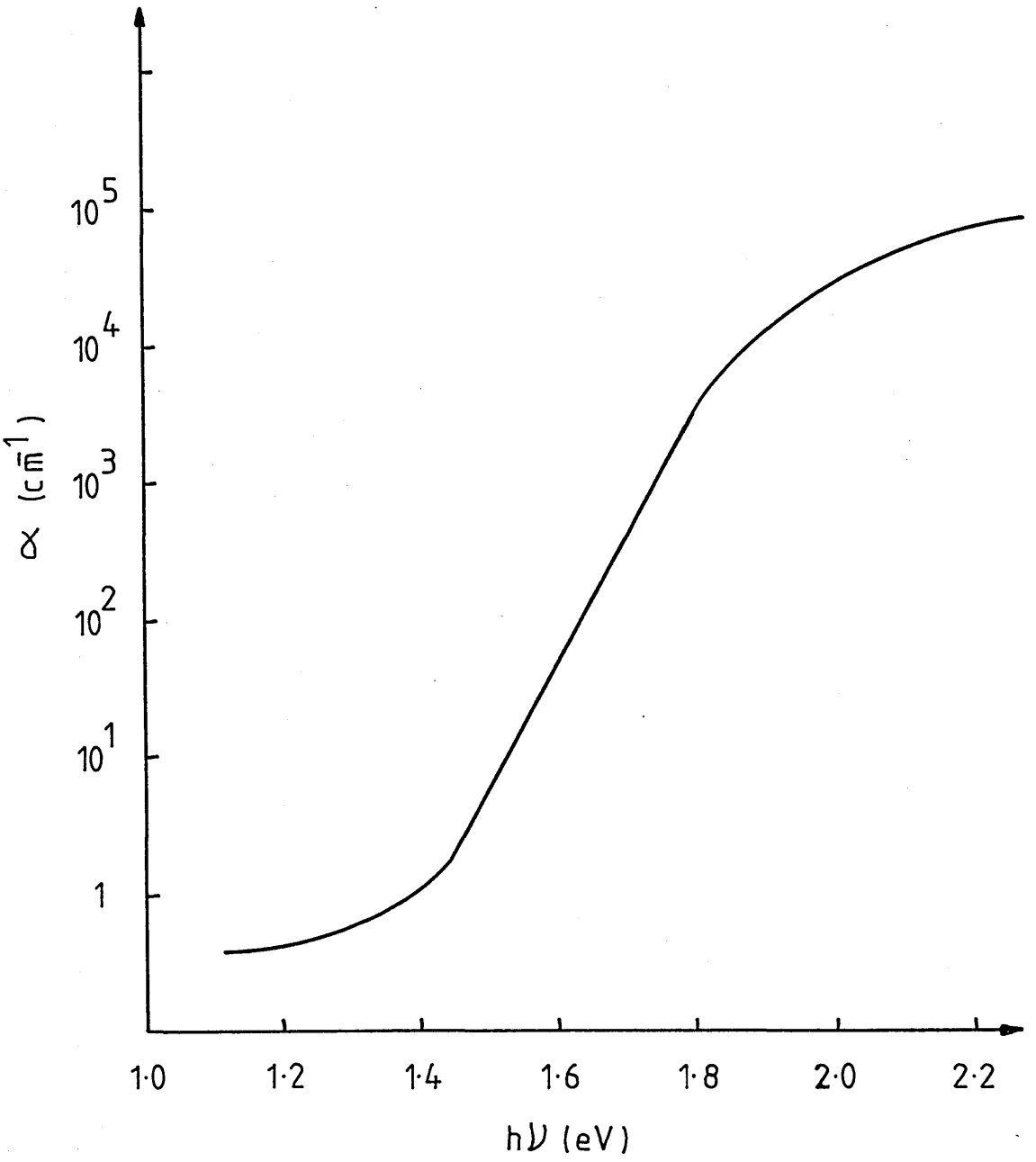

Figire 3.3 Absorption edge spectrum of glow discharge deposited a-Si:H. Results from optical transmission, from collection efficiency and from photoconductivity on the same specimen all agree with the graph shown. (After ref. 4).

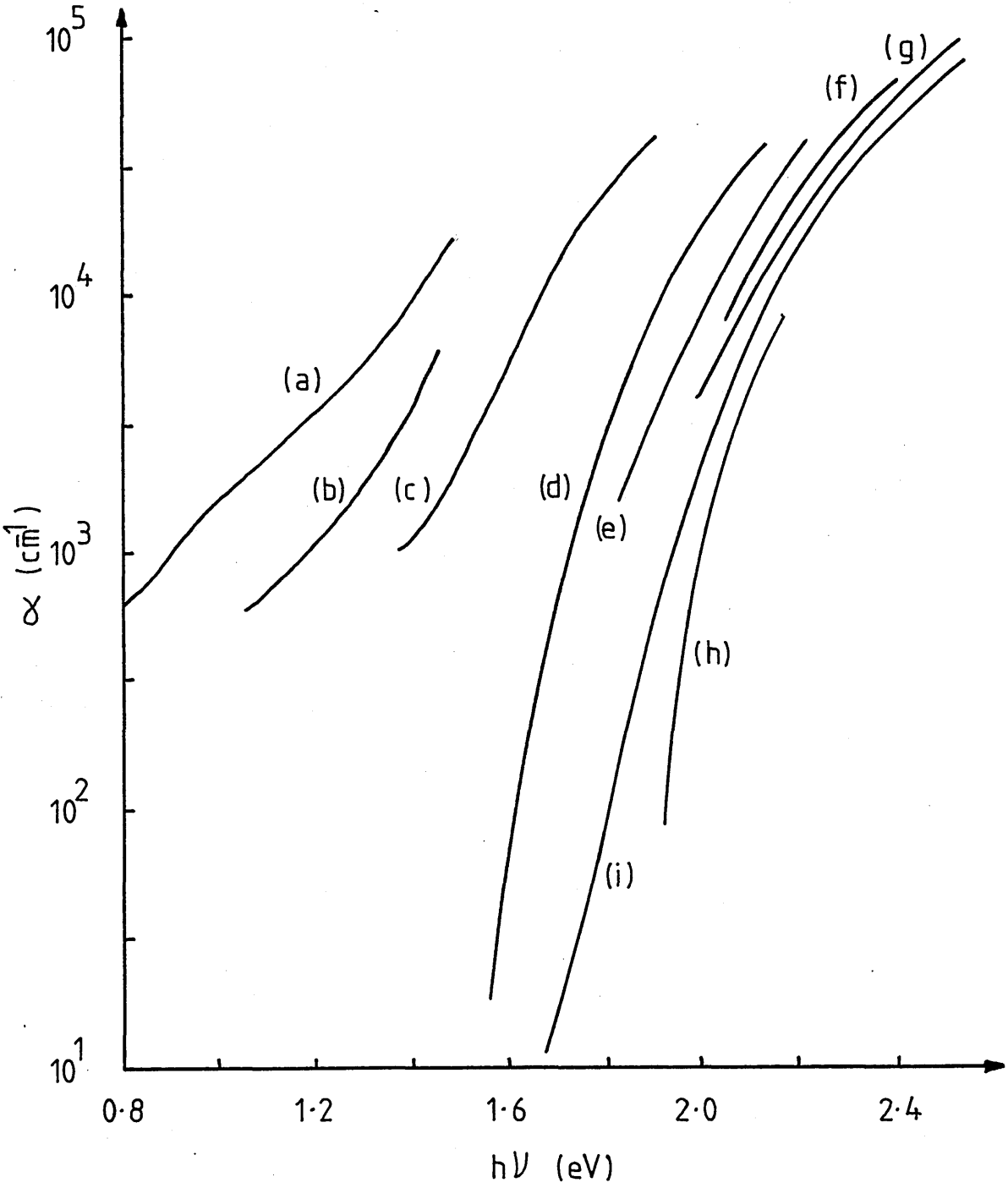

Figure 3.4. Shift of the absorption edge of sputtered a-Si:H as P_H increases from 0 to 5 mTorr, at fixed T_s. The P_H used to prepare each specimen were (in mTorr), (a) 0, (b) 0.05, (c) 0.2, (d) 0.4, (e) 0.8, (f) 1, (g) 2, (h) 3, (i) 5. (After ref. 5).

different band gaps and densities of states at the band edges, and further that these parameters are dependent on the precise sputtering and plasma conditions. Paul and Anderson suggest (4) that it is quite probable that several combinations of the many sputtering parameters lead to films having the same Hydrogen content, but with the Hydrogen being assembled in different Si - H bonding configurations. This in turn leads to different densities of states at the band edges and in the band gap. They also suggest that different sputtering parameters lead to different microstructural heterogenities, which again yield different average properties.

The absorption edge spectra for films of sputtered a - Si:H prepared at different T_S but fixed P_H is shown in figure 3.5. For increasing T_S, the absorption edge is found to first displace to higher photon energies and then reverse. The first effect is thought to be related to the increased relaxation of the lattice at higher T_S and to the more efficient defect compensation by Hydrogen incorporation. The reversal stems from the fact that Hydrogen is not easily incorporated into the network at higher T_S.

The form of the absorption edge of a - Si:H is also found to be altered by the addition of dopant impurities to the films. The absorption edge shifts towards lower photon energies for increasing impurity concentration, the shift being much larger than that expected from the creation of simple impurity energy levels (4). This phenomenon has therefore been attributed to a combination of the creation of new levels from dopant elements which are fully coordinated and to dopant induced defect configurations (4).

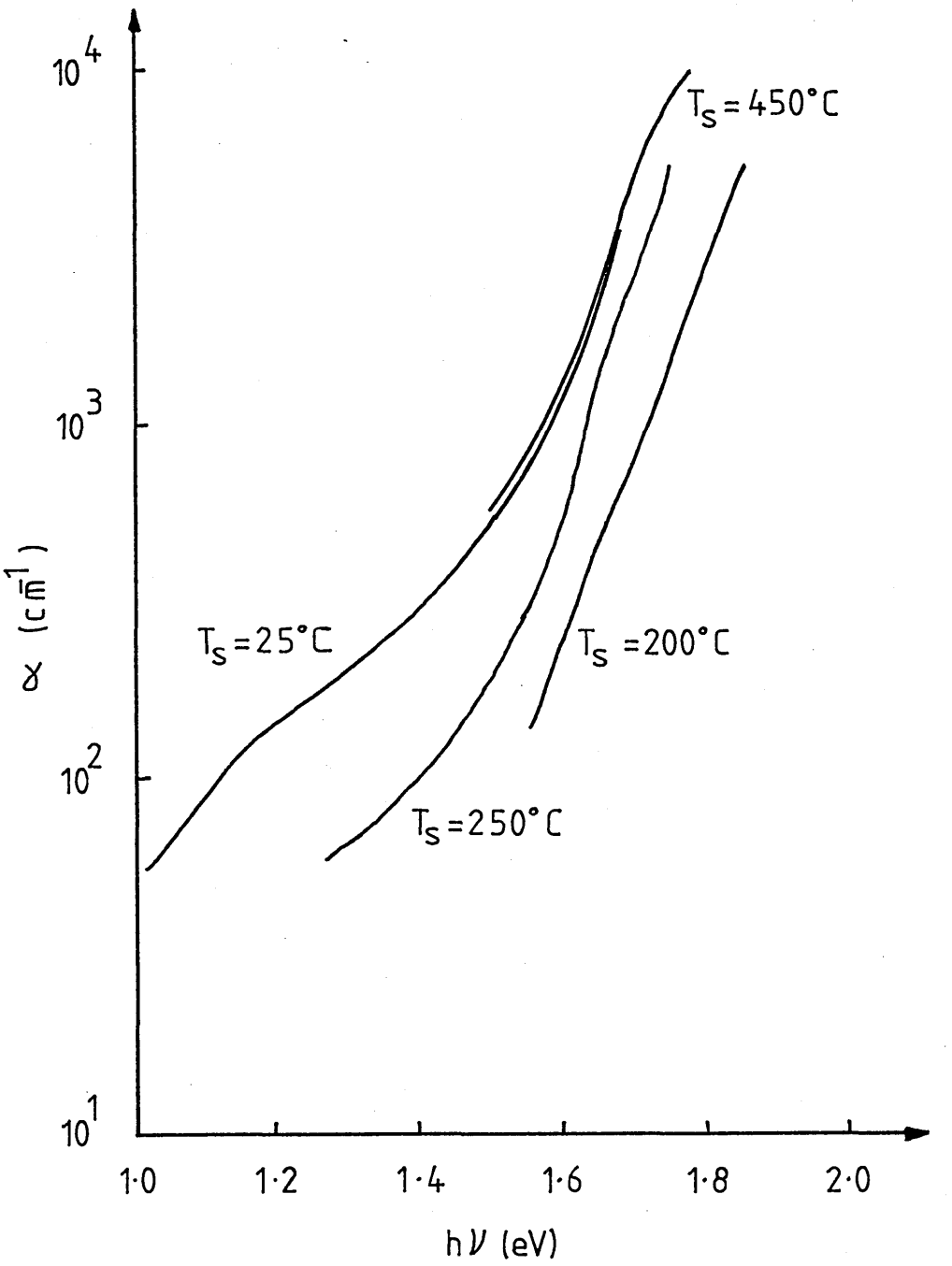

Figure 3.5. Shift of the absorption edge of sputtered a-Si:H with T_s. (After ref. 5).

3.4 PHOTOCONDUCTIVITY.

The forms of the temperature dependence of the photoconductivity obtained from both glow discharge and sputtered films of a - Si:H are very similar, and exhibit the general shape shown in figure 3.6. Most analyses of photoconductivity on a - Si, however, have been performed on results obtained from films produced by the glow discharge process, and the main features of these results will be presented briefly first, before those for sputtered material.

Spear et al proceed (6) by analysing the temperature dependence of the photoconductivity in terms of the discrete trap model of Main and Owen (see section 2.3.6) using the density of states distribution shown in figure 3.7, which was deduced from Field Effect measurements (7). It is suggested that for the case of glow discharge specimens with a low density of gap states, (i.e. films prepared at a high substrate temperature; $\simeq$ 600 K), the localised states in the regions of E_a, E_x and E_y may be predominantly involved in the recombination process. They use the criterion of Main (8,9), (i.e. assuming the presence in the energy gap of the minimum number of levels of localised states necessary to account for the photoconductive data) and proceed to fit the solutions derived by Main for the different regions of the photoconductive response, to the results obtained for a - Si. What follows is a brief review of the conclusions.

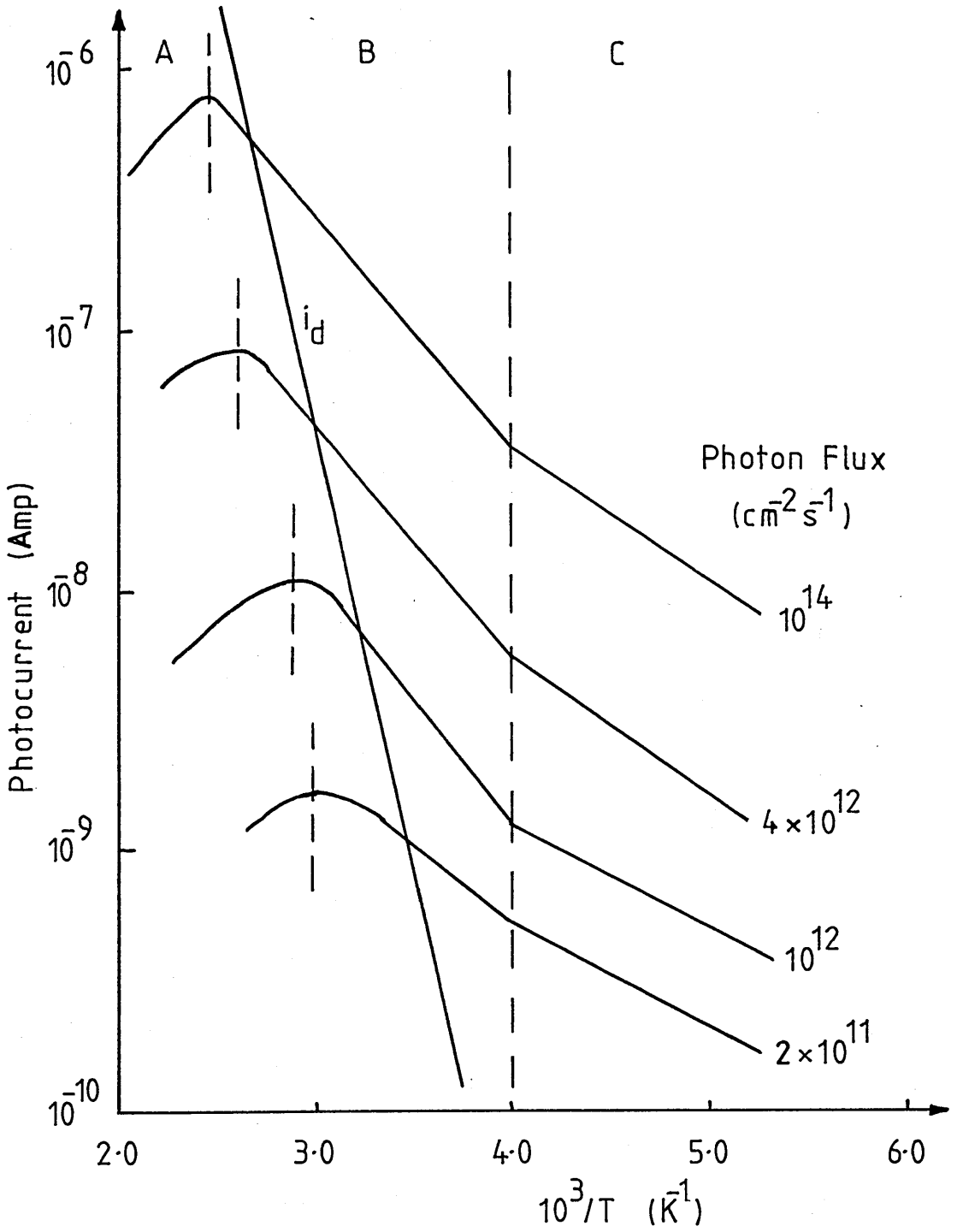

Figure 3.6. Photocurrent in glow discharge deposited a-Si:H versus inverse temperature. Measurements were made at $h\nu$=2 eV at the stated intensities. i_d denotes the dark current. (After ref. 6).

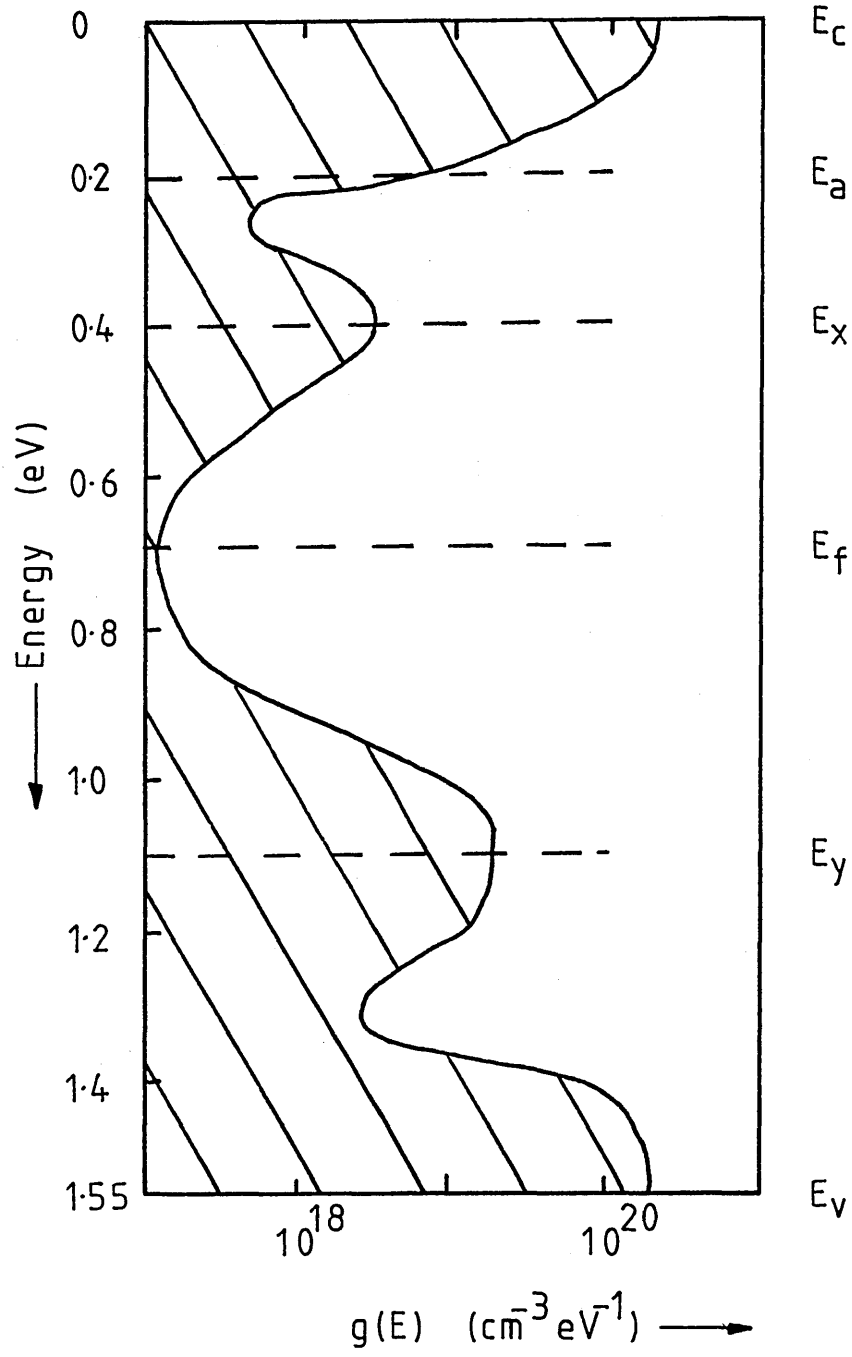

Figure 3.7. Density of states distribution for glow discharge deposited a-Si prepared at a high substrate temperature ($\simeq$ 600K). (After ref. 7).

At temperature above the photoconduction maximum, (region A in figure 3.6), the photocurrent is much less than the dark current and the occupancies of the various states are practically the same as in thermal equilibrium. Recombination from E_a to E_y is found to produce the best fit to the experimental data; this assumption leading to a photoconductivity expression of the form

$$\Delta\sigma = \frac{e f N_c}{K N_y N_a} \mu_c \exp\left[-\frac{(E_f - E_y) - (E_c - E_a)}{kT}\right] \quad (3.1)$$

where f is the generation rate of free electron - hole pairs, μ_c is the electron drift mobility and the other symbols are defined in figures 3.6 and 3.7. This equation yields an activation energy, and linear intensity dependent photocurrent, both of which are in agreement with experimental results.

At temperature just below the photoconduction maximum (region B), recombination between E_a and E_y still provides the best fit to the experimental data, although the microscopic conditions are now basically different from those previously described. The photogenerated density of carriers at E_c (and E_v) is far larger than the density of carriers produced by thermal excitation and the quasi - Fermi levels move apart. States enclosed by the quasi - Fermi levels become depopulated and localised negative and positive charge densities are largely concentrated at E_y and E_a. The fact that states near E_a and E_y become relatively more populated makes the suggested recombination path from E_a to E_y a likely one (this may be an over simplification, however, in view of the probable appreciable density of trapped negative charge near E_x). Using the above assumptions,

Spear et al find the photoconductivity in this region to be of the form

$$\Delta\sigma = e\left(\frac{f}{K}\right)^{\frac{1}{2}} \mu_c \frac{N_c}{N_a} \exp\left[-\frac{E_c - E_a}{kT}\right] \quad - \quad (3.2)$$

where the symbols have their previously defined meanings. This equation again yields an activation energy and intensity dependence both of which agree favorably with experimental results.

The plots of photocurrent versus 1/T shown in figure 3.6 are seen to change gradient from region B to region C. This is interpreted as signifying a change in the predominant transport mechanism from extended state conduction at E_c (region B), to electron hopping at E_a (region C). Under these latter conditions, recombination between E_a and E_y still yield the best fit to the experimental data and the photoconductivity is expected in the form

$$\Delta\sigma = e\left(\frac{f}{K}\right)^{\frac{1}{2}} \mu_h \exp\left(-\frac{W}{kT}\right) \quad - \quad (3.3)$$

where μ_h is a hopping mobility and exp(-W/kT) represents the probability that an electron will surmount a barrier, W, in order to move from one site to another. This equation again effectively describes the experimental results. (It should be noted here that specimens having high gap state densities are likely to have other predominant recombination paths in the gap, which will act in parallel to those considered. The above analyses, therefore, is only specific to those specimens of a - Si prepared under conditions which will yield low gap state densities.)

In support of the above model, Spear et al correlate photoconductivity results with results obtained from drift mobility experiments (10,11). They concluded that drift mobility experiments provide details about the positions of the localised state peaks in the gap, which are in agreement with their positions derived from photoconductivity measurements.

The above interpretation of photoconductivity in glow discharge deposited a - Si is somewhat simplified and such modeling ignores many complications. Furthermore, the approach depends upon the adoption of the density of states distribution established at Dundee University (7) by Field Effect measurements, the validity of which has become controversial over recent years. In order to extend the deduced density of states measurements over as wide an energy range as possible, Field Effect measurements were performed on both n - type and p - type doped material, under the assumption that the effect of doping was simply to provide carriers that shifted the Fermi level. In view of the low doping efficiency for all of the dopant impurities used, and the likelihood that non - doping configurations produce defects in the gap (5), considerable doubt can be thrown on those parts of the density of states distribution derived from doped samples. To add further doubt to the derived density of states distribution, Goodman and Fritzche (12,13) demonstrated that, in practice, the same field effect response could result from several different density of states distributions, thus placing limits on the magnitudes of features that could be appreciated.

A factor which adds further confusion to the interpretation of photoconductivity in a - Si, is the apparent randomness observed in the properties of a - Si, prepared in different laboratories under seemingly identical deposition conditions. Such similarly deposited specimens can exhibit photoconductivity results which vary in some cases by up to four orders of magnitude. This anomaly seriously hinders the development of a universal model for the interpretation of photoconductivity in a - Si. Clearly, there is still much work to be done in this area.

As stated previously, the features of the photoconductivity observed in both glow discharge and sputtered films of a - Si are very similar. Consequently, analyses of the type described above have been carried out on experimental data obtained from sputtered material (14), and as may be expected results and conclusions consistent with those deduced by Spear et al have been obtained. In the case of sputtered material, however, much work has been carried out in order to characterise the photoconductive response of samples in terms of preparation conditions. The main conclusions of this work will be outlined below.

Figure 3.8 shows the variation of the room temperature photoconductivity measured under standard conditions, for sputtered samples of a - Si deposited at the same T_S but with P_H systematically varied. The increase in the photoconductivity as P_H increases from 0 to 1 mTorr is relatively well understood and corresponds to the elimination of dangling bonds and other recombination centers by Hydrogen compensation. For P_H above 1 mTorr, there is much scatter in

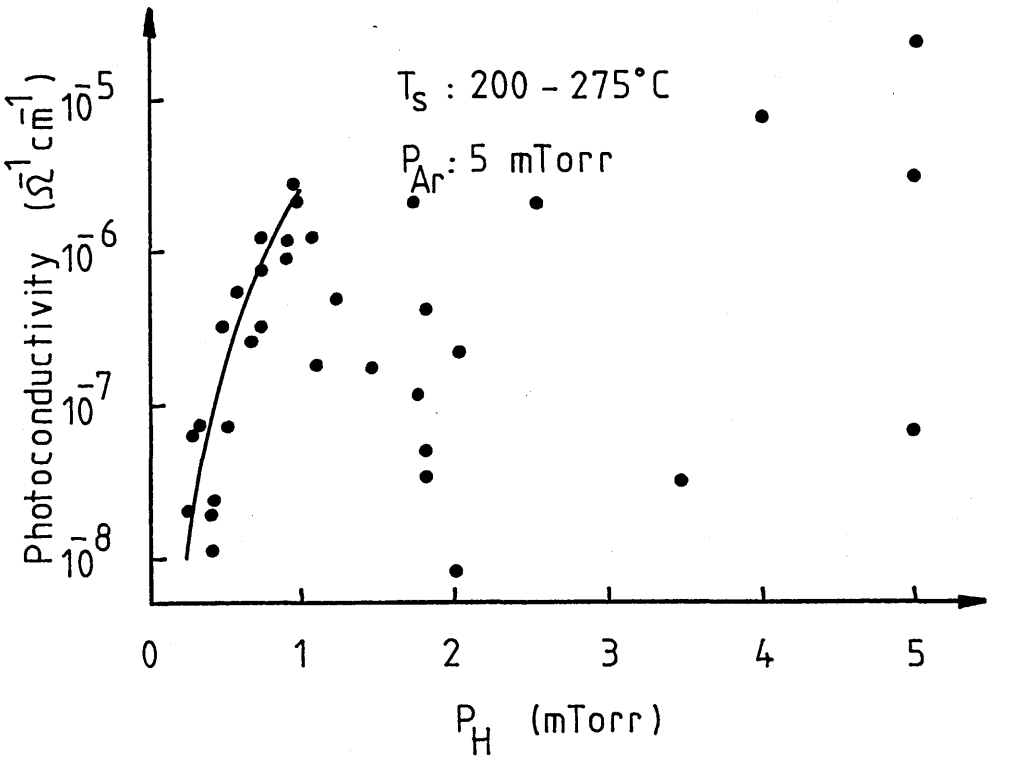

Figure 3.8. Variation of the room temperature photoconductivity, measured under standard conditions, for specimens prepared at the same T_s, but various P_H. (After ref. 4).

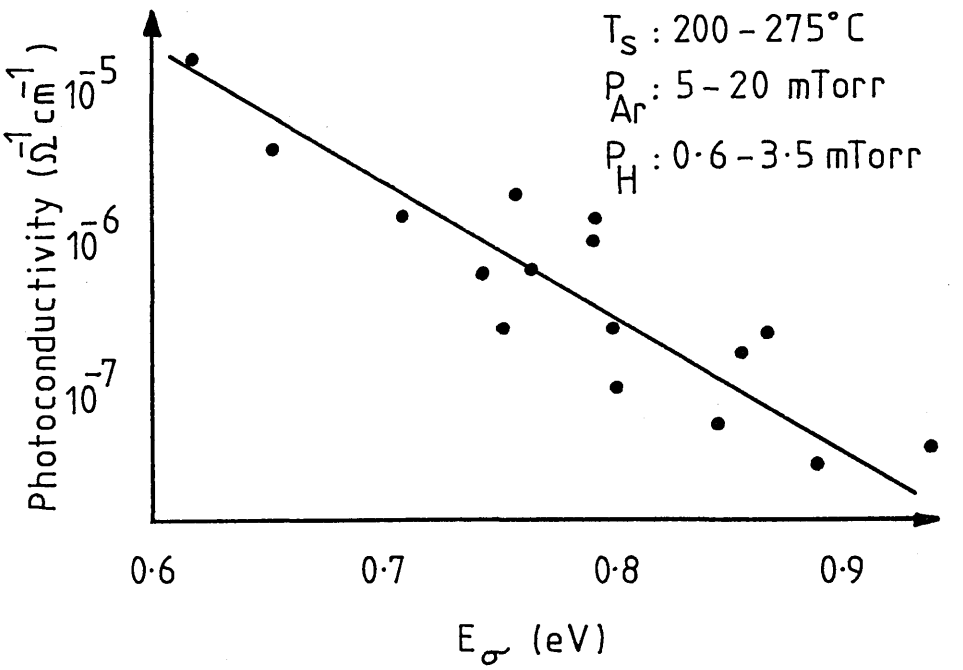

Figure 3.9. Test of correlation between the magnitude of the photoconductivity (Figure 3.8), and the corresponding dark conductivity activation energy. (After ref. 4).

the results, this indicating the intimate relationship between the macroscopic properties of a - Si and the minute details of sputtering parameters during film deposition. Some degree of order in this latter region can be restored, however, if the photoconductivity of each specimen is plotted against its dark conductivity activation energy (E_σ) (see figure 3.9). This plot illustrates an inverse relationship between photoconductivity and E_σ which was first pointed out by Anderson and Spear (15). Anderson and Spear observed results similar to those shown in figure 3.9 in glow discharge deposited a - Si, when the Fermi level was systematically shifted from mid gap towards the conduction band edge by the introduction of Phosphorus doping. The relationship was interpreted as an increased electron lifetime when recombination centers near mid gap were filled, as the Fermi level rose. The same interpretation can be applied to sputtered a - Si, except that for the case of sputtered material, the Fermi level shift is not due to doping, but is a consequence of the random variations in the density of states in the gap, and at the band edges, which in turn depend upon the minute details of sputtering parameters during film deposition.

The effect of varying the substrate temperature on the room temperature photoconductivity of films of a - Si prepared at a constant value of P_H, is fairly well understood (16), and is shown in figure 3.10. The initial increase in the photoconductivity with increasing T_S is consistent with the removal of states in the gap. At high values of T_S, the decrease in photoconductivity with increasing T_S, is again due to the fact that Hydrogen is not easily incorporated into the growing films at high T_S.

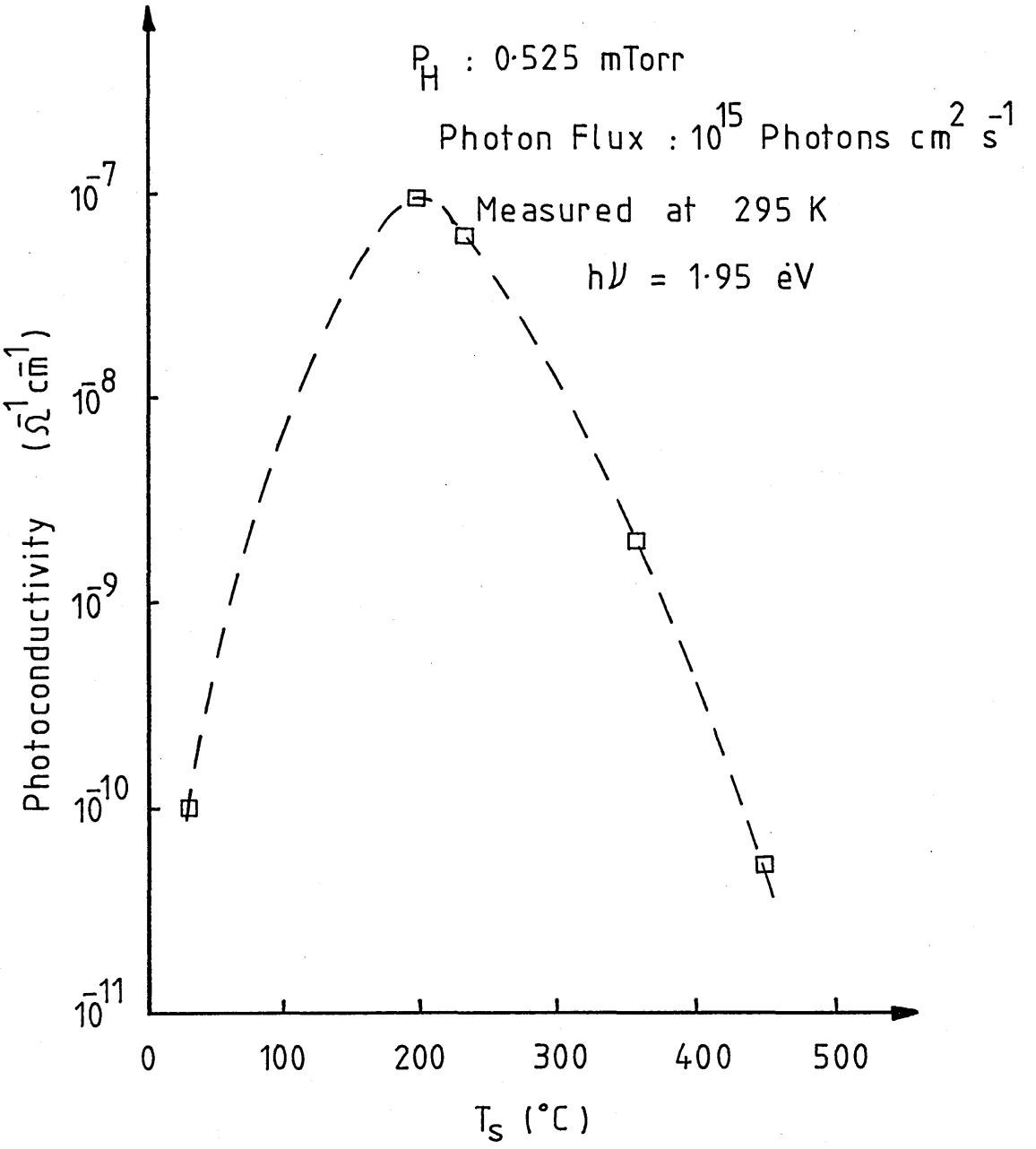

Figure 3.10. Room temperature photoconductivity versus substrate temperature for sputtered a-Si:H.(After ref. 16).

3.5 DRIFT MOBILITY.

The first direct measurement of the electron drift mobility in glow discharge deposited a - Si:H was reported by Le Comber and Spear in 1970 (10), and followed up in 1972 by a more detailed investigation (11) of the same phenomenon. Those workers used a time of flight technique to deduce drift mobilities, (a complete description of which is given in Section 2.5.1) with excess carriers being generated by a pulsed electron beam. The authors observed a well - defined transit time for electrons, even although there existed a substantial dispersive tail to the transit pulse, due to the slow release of charge from traps. They found electron drift mobilities ranging from 10^{-3} $cm^2 V^{-1}s^{-1}$ at 150 K to 10^{-1} $cm^2 V^{-1}s^{-1}$ at 300 K, in a number of samples. No signal was detected for the drift of holes. In subsequent investigations, various authors (17,18,19) observed electron drift mobilities in agreement with the above work. More recent measurements by Tiedje et al (20) on glow discharge a - Si:H, however, have clearly shown that it is possible to obtain either highly dispersive or non - dispersive electron transients, depending on the preparation conditions used. It has been found that films displaying non - dispersive behaviour have higher room temperature mobilities than previously measured (10), the highest reported being 0.8 $cm^2 V^{-1}s^{-1}$. (Even higher room temperature drift mobilities of around 2 to 3 $cm^2 V^{-1}s^{-1}$ have recently been reported (44) for glow discharge deposited a - Si:H.)

In reactively sputtered a - Si:H, electron drift mobilities of the order of 10^{-3} $cm^2 V^{-1} s^{-1}$ at room temperature have been deduced (21) from steady state and transient photoconductivity measurements. It was not until 1980, however, that Tiedje (20) reported the first direct measurement of the electron drift mobility in sputtered a - Si:H, using the time of flight technique. Since then, much work has been directed towards investigating drift mobility phenomena in sputtered a - Si:H, and what follows is a brief review of these studies.

The measurements performed by Tiedje et al (20) on sputtered material, revealed highly dispersive transit pulses at room temperature. Transit times could only be deduced from log - log plots of current as a function of time, and drift mobilities of the order of 5×10^{-2} $cm^2 V^{-1} s^{-1}$ at room temperature were obtained, these being at least an order of magnitude lower than corresponding drift mobility results obtained from glow discharge material. The work of Tiedje et al was followed up by a more extensive study by Kirby and Paul (22,23). They performed time of flight measurements on sputtered films of a - Si:H and observed results which fall into three main categories: (1) Films which exhibit a rapid decrease of the photocurrent, characterising highly dispersive transport; (2) Films which display non - dispersive Gaussian transport, where the mobility is time independent; and (3) Films whose transients display the features of dispersive transport, but where it is not possible to define a transit time on log - log axis of current against time.

In the first of these categories, the results are in broad agreement with those of Tiedje, with a room temperature mobility of 10^{-1} $cm^2 V^{-1} s^{-1}$ being observed. In region (2), however, the room temperature transit pulse is non - dispersive and is similar to those observed in glow discharge material (11). For samples displaying this phenomenon, it is found that a dramatic change occurs in the pulse shape when the temperature is lowered below 290 K (see figure 3.11). Down to 225 K a feature corresponding to carriers reaching the back contact can still be observed on linear axis, but at still lower temperatures a featureless decay is obtained. For temperatures below 225 K, log - log axis of current versus time must be employed in order to deduce the transit time. Transients which fall into category (3), are only observed in specimens having a large density of states at the Fermi level (as measured by the conductance - capacitance technique (24)). Kirby and Paul find the fall off in the photocurrent to be faster in specimens exhibiting a large density of gap states and propose the possible explanation of electrons sinking quickly into traps which lie deep within the gap, never to be re - released into extended states during the experimental time scale.

Kirby and Paul explain the occurrence of the three different categories of results in terms of differing density of state distributions within the gap. They find that lifetime limitations of the propagating carriers restrict the measurement of electron drift mobilities, using the time of flight technique, to films of sputtered a - Si:H which have fewer than $5 \times 10^{17} cm^{-3} eV^{-1}$ states at the Fermi level. For films which display dispersive transport over the complete temperature range, they propose that transport is by a trap limited

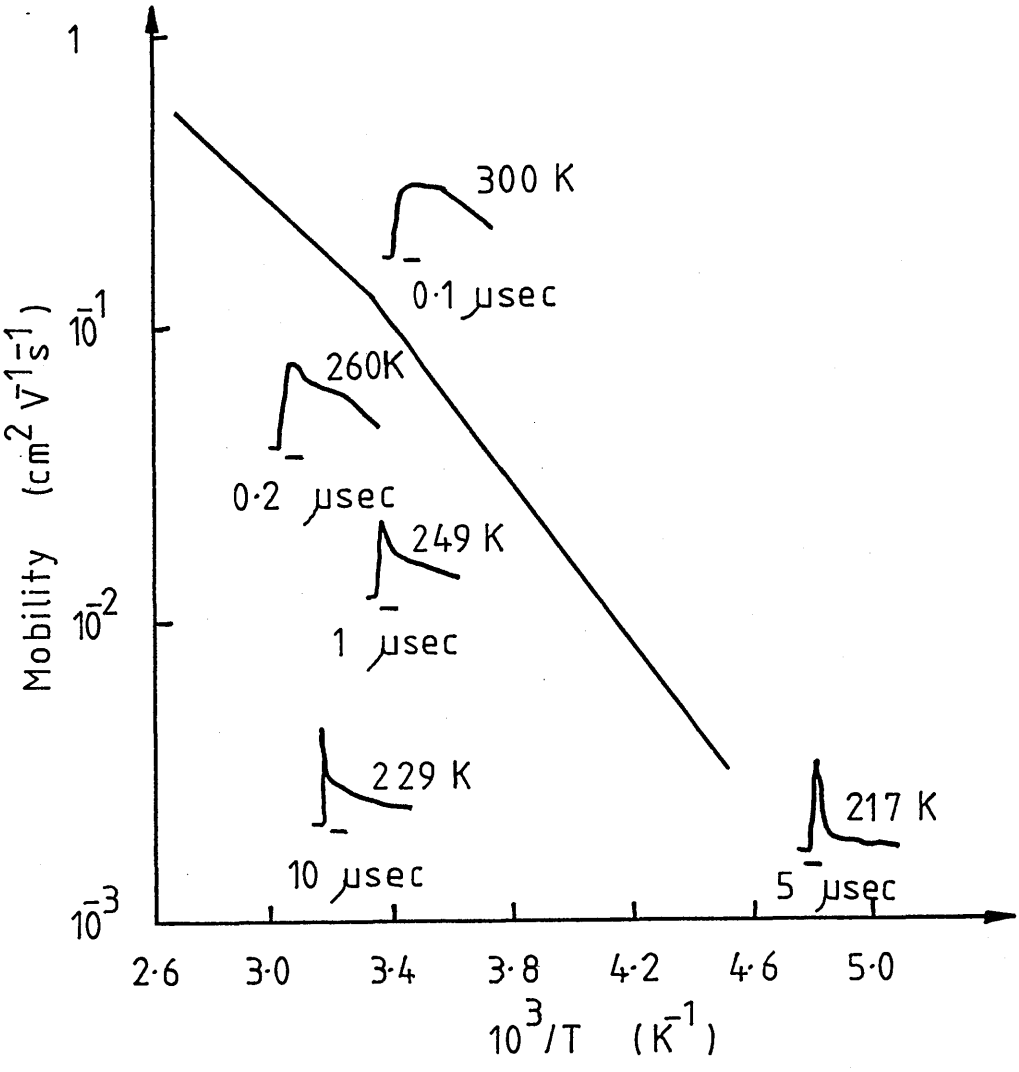

Figure 3.11. Mobility versus inverse temeperature for a specimen displaying non-dispersive transport at high temperatures, and dispersive transport at low temperatures. (After ref. 22).

band motion. This is deduced from the magnitude and activation energy of the mobility and from the temperature dependence of the dispersion parameter. For films which display non - dispersive behaviour, they find a transition to dispersive transport as the temperature is lowered. The transition is not accompanied by any discontinuity in the magnitude or in the activation energy of the mobility, and Kirby and Paul therefore propose that transport in the non - dispersive regime is also by a trap limited band motion. The reasons why similarly deposited specimens exhibit different transport mechanisms it not entirely known, but it is thought to stem from the previously mentioned fact that samples prepared under seemingly identical deposition conditions may contain different densities of states in the band gap and at the band edges. Clearly, there are still many unresolved problems in explaining charge transport phenomena in sputter (and glow discharge) deposited a - Si:H, and this is the subject of continuing and intense research.

3.6 DOPED AMORPHOUS SILICON.

Substitutional doping in crystalline semiconductors has been one of the most important factors in the development of modern Semiconductor Physics and Solid State Electronics. With the growing interest in amorphous semiconductors in the early 1970s, a number of attempts were made to achieve a similar systematic control of the electronic properties of these materials. The work was mainly concentrated upon the tetrahedrally coordinated amorphous semiconductors such as Si and Ge, and techniques such as

co - evaporation (24), flash evaporation (25) and sputtering from a composite (26) or heavily doped target (27) were tried. The results of these experiments were dissapointing and led to the general conclusion that such semiconductors are highly insensitive to doping as compared with corresponding crystalline materials. In 1975, however, Spear and Le Comber were able to show (28,29) that the electronic properties of a - Si, prepared by the glow discharge technique, could be controlled through substitutional doping in a systematic way, and over a remarkably wide range. These workers also gave a qualitative explanation as to why previous attempts at doping, using other methods of film preparation had failed. The conclusions of this work will be briefly reviewed below.

In considering amorphous semiconductors in general, there appear to be two reasons why these materials are insensitive to doping. The first concerns the way in which the impurity atoms are incorporated into the random network. Mott (30) argued that, for instance, a pentavalent impurity atom would be accommodated into the structure in such a way that the additional bond would be satisfied. The evidence (31) suggests, however, that although this may be true under certain circumstances, the picture is somewhat more complex, and it is likely that substitutional doping efficiencies will depend, perhaps quite critically, on the method of film preparation.

The second reason is concerned with the effect of the incorporation of donor or acceptor impurities on the electronic properties of amorphous materials. This is best illustrated by referring to figure 3.12, which represents the density of states

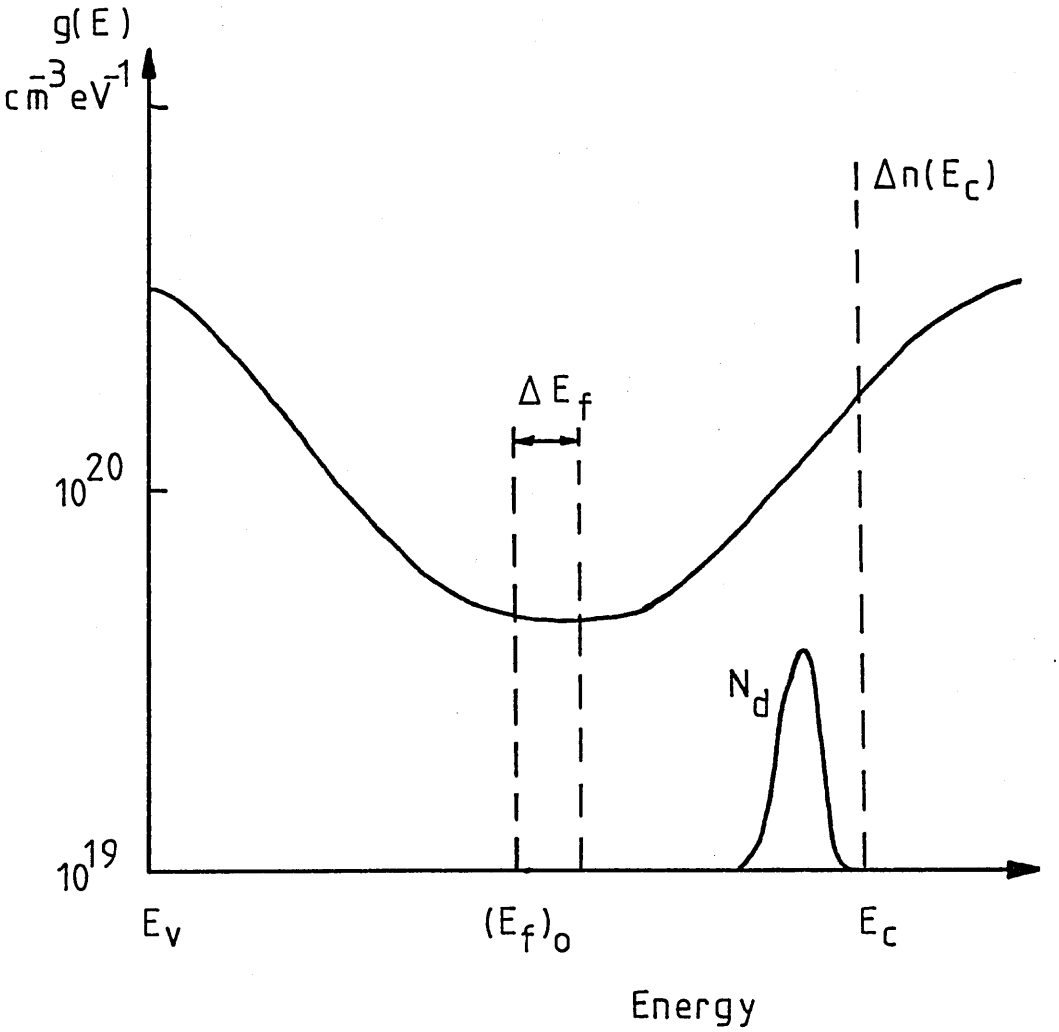

Figure 3.12. Schematic density of states in an amorphous semiconductor. $(E_f)_o$ is the position of the Fermi level in the undoped material and ΔE_f is the Fermi level shift when a band of N_d donors is introduced.

distribution, g(E), in the mobility gap of an imaginary amorphous semiconductor. The Fermi level in the undoped material lies at $(E_f)o$. Now suppose that a band of N_d substitutional donors is introduced. Practically all the excess electrons will condense into empty gap states, displacing the Fermi level towards the conduction band by an amount ΔE_f. The new Fermi level position is determined approximately by

$$N_d \simeq N_d^+ \simeq \int_{(E_f)_o}^{E_c} \frac{g(E)\,dE}{1+\exp\left[\frac{E-E_f}{kT}\right]} + \Delta n(E_c) \qquad (3.4)$$

where $\Delta n(E_c)$ is the increase in the extended state electron density, which in an amorphous semiconductor is negligible in comparison to the first term in equation 3.4. This is basically different from the crystalline case, where $N_d \simeq \Delta n(E_c)$ describes the exhaustion region. Thus in the amorphous case, changes in the electrical properties are brought about primarily by changes in the gap state occupation. For sensitive doping, ΔE_f which is of the order of $N_d/g(E_f)$, should be as large as possible, implying that a low level of gap states is an essential condition. With the above in mind, Spear and Le Comber (28,29) argue that the glow discharge technique provides the most promising approach to doping a - Si, since it produces material having a relatively low density of states in the gap. They also use the above result to explain the insensitive behaviour to doping of evaporated or sputtered material, suggesting that although it may be possible to incorporate quite appreciable densities of donors or acceptors into the material, $g(E_f)$ is too high to allow much change in the Fermi level position, and consequently in the electrical

properties.

The above conclusions, deduced by Spear and Le Comber, were supported by results (28,29) which characterised the dramatic effect of n - type and p - type doping on the electronic transport properties of glow discharge deposited a - Si and a - Ge. Subsequently, similar results were obtained (32,33) by other groups, for Phosphorus doped films prepared by the same technique, which re - enforced the work of Spear and Le Comber. These results will not be presented here, but are cited in the references (i.e. 32,33). In under one year from the initial publication of the paper on doping by Spear and Le Comber (28), doping studies on a - Si were extended to materials prepared by other means of deposition (34,35,36,37). Results which are of particular interest to this investigation are those obtained from materials prepared by r.f. sputtering, and these will be reviewed below.

The first successful attempt at preparing doped specimens of a - Si and a - Ge by r.f. sputtering was made by Paul et al (37) in 1976. These workers argued that in order for controlled doping of a - Si and a - Ge, it is essential to prepare the material under conditions that will yield a minimum density of defect states in the gap. In the case of sputtered a - Si, this implies that the Hydrogen and Argon partial pressure, the target and substrate geometry, the substrate bias and the r.f. power should all be optimised (4) to achieve this aim. Paul et al performed depositions under such optimum conditions and found that the simultaneous removal of gap defect states by Hydrogen incorporation, and the introduction of donor or

acceptor states due to Phosphorus or Boron, produced material in which the electronic transport properties could be systematically varied. They proposed that this method of deposition provided a viable alternative to the glow discharge technique. In recent years, the range of n - type dopants used has been increased to include almost all of the suitable elements (38), and these studies have shown that the conductivity, and where measured the thermoelectric power, is relatively independent of the method of film deposition, the type of dopant used, and its method of incorporation.

Figure 3.13 shows the temperature dependence of the conductivity for a series of Phosphorus doped films of sputtered a - Si:H, where the dopant gas partial pressure is systematically varied from 0 to 10^{-5} Torr. The pressure of only 2×10^{-7} Torr of Phosphine has a dramatic effect on the room temperature conductivity of the material, increasing it by about four orders of magnitude. For the highest partial pressure used, the room temperature conductivity is increased by almost seven orders of magnitude to 10 Ω^{-1} cm^{-1}. Accompanying this increase in the conductivity is a systematic reduction in the slope of the Arrhenius plot.

The above data can be explained in terms of a two level transport model (34,38,39,40). At high temperatures, the Arrhenius plot is singly activated and is interpreted as electron motion at the conduction band mobility edge. In the lower temperature region, transport is envisaged as hopping in a Phosphorus donor band, the density of which increases with increasing Phosphine partial pressure. In the high temperature region the conductivity is given by

$$\sigma = \sigma_0 \exp\left[-\frac{E_c - E_f}{kT}\right] \qquad - \qquad (3.5)$$

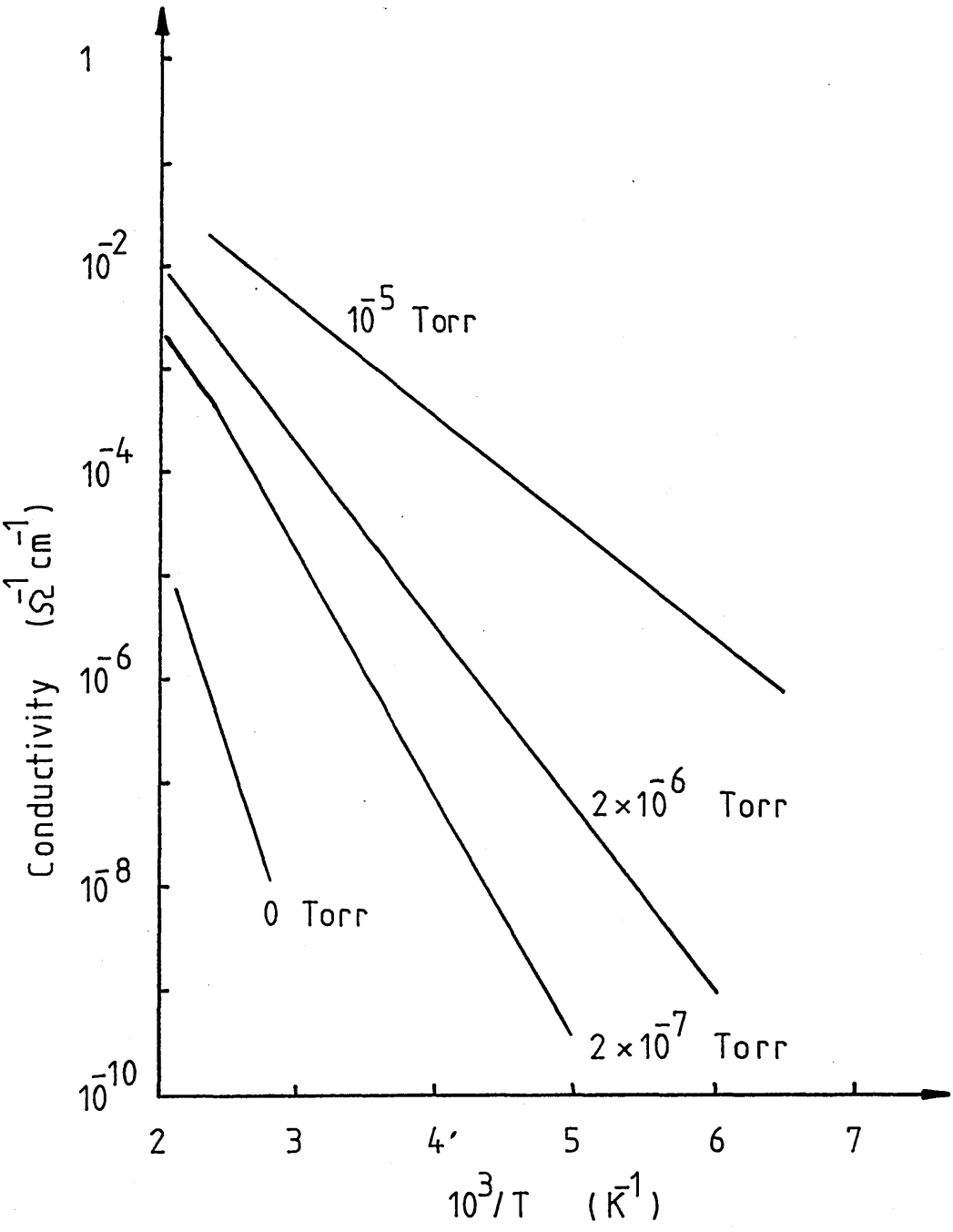

Figure 3.13. Conductivity versus inverse temperature for a series of Phosphorus doped specimens of a-Si:H. Each curve is labelled with the Phosphine partial pressure in the sputtering gas. (After ref. 38).

where σ_0 and $(E_c - E_f)$ are the conductivity pre - exponential and activation energy respectively. Figure 3.14 shows the values of σ_0 and $(E_c - E_f)$ deduced from figure 3.13 at high temperatures, plotted as a function of Phosphine partial pressure. The decrease in $(E_c - E_f)$ with increasing Phosphine pressure is not unexpected. Assuming that with increasing Phosphine pressure there is a corresponding increase in the density of fourfold coordinated Phosphorus atoms in the films, then it is possible to interpret the conductivity data in terms of a shift in the position of the Fermi level, from the gap center towards the conduction band edge, with increasing Phosphorus content, and an unchanged transport mechanism of extended state conduction. In such a model, however, the prefactor σ_0 should be the same for each film, but as show in figure 3.14(b) this is not the case. Jones et al (41) attempted to account for this anomaly in the value of σ_0 in terms of a coefficient γ, which describes the dependence of the Fermi level position upon temperature. In order to explain the data, they find that γ must increase with increasing film Phosphorus content. Equation 3.5 can therefore be replaced by

$$\sigma = \sigma_0 \exp\left(\frac{\gamma}{k}\right) \exp\left[-\frac{E_c - E_f}{kT}\right] \qquad (3.6)$$

where $\sigma_0 \exp\left(\frac{\gamma}{k}\right)$ becomes the new effective prefactor. Thus, to account for the observed decrease in σ_0 from 5×10^3 to $10\ \Omega^{-1}\,cm^{-1}$ (in figure 3.13), γ must increase from 0 to approximately 5×10^{-4} eV K^{-1}.

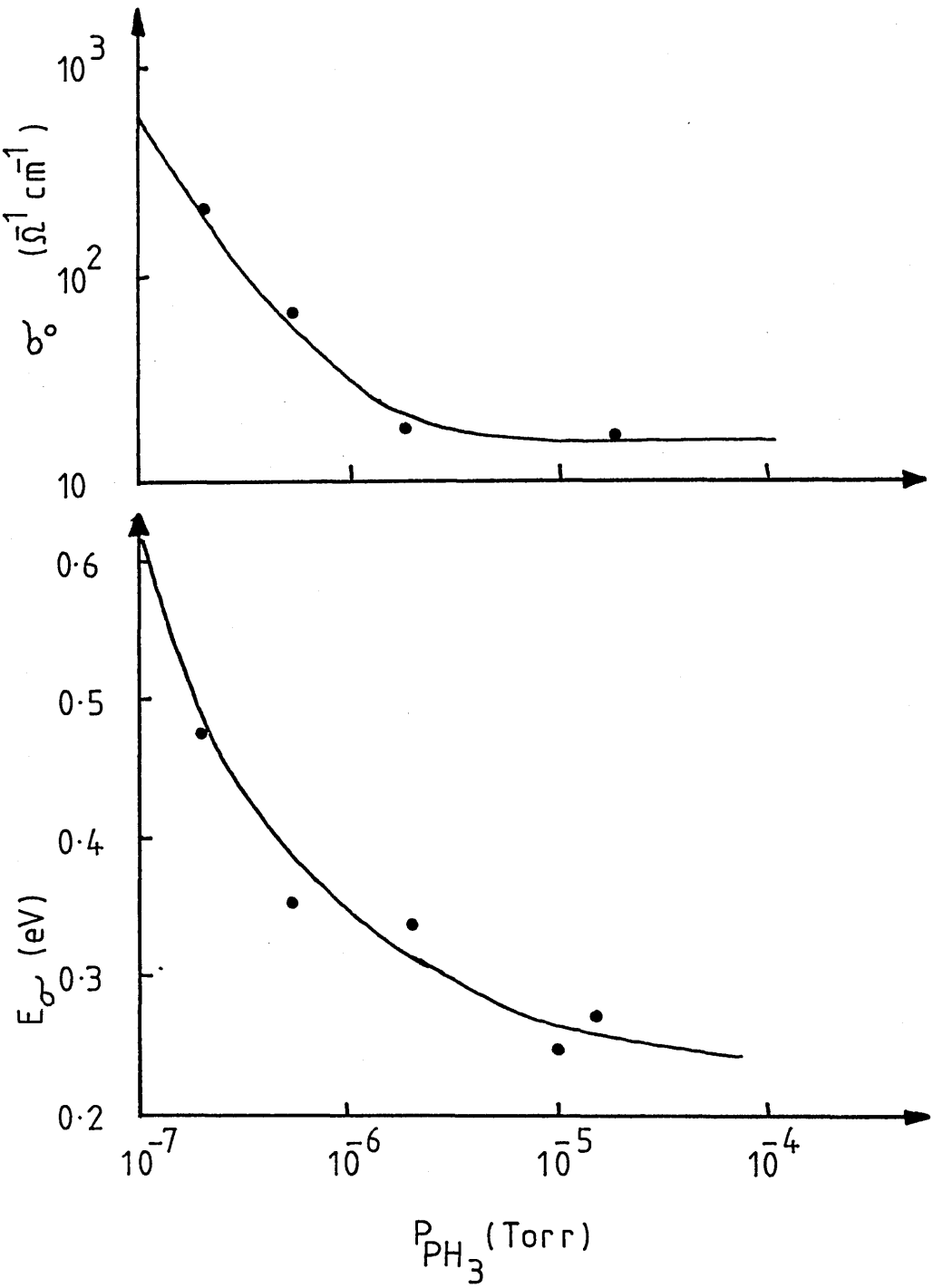

Figure 3.14. Plots of σ_o and E_σ versus Phosphine partial pressure for doped specimens of a-Si:H. (After ref. 38).

In a substantial number of studies (38), conductivity data have been obtained from Phosphorus doped films of a - Si:H, which when plotted as a function of reciprocal temperature display "kinks" at high temperature (above about 400 K). These kinks have been explained in terms of discontinuous changes in the temperature coefficient γ, described above (42), and in terms of transitions between transport paths (34,38,40,43). These data, although worth mentioning here, are not directly relevant to the study and will not be discussed further.

3.7 CONCLUSION.

The review of the electronic transport properties of amorphous Silicon presented in this chapter is by no means exhaustive. It does, however, lay down foundations which will assist in interpreting results obtained in this study. For a more extensive review of the properties of sputtered films of a - Si in general, the author refers the reader to the articles and publications cited (i.e. 3,4,38).

REFERENCES CHAPTER 3

(1) Lewis A.J. et al, Int. Conf. on Tetrahedrally Bonded a - Semi., AIP Conf. Proc. 20 ,27, (1974).

(2) Anderson D.A., Moustakas T., Paul W., Proc. 7th Int. Conf. on Amorphous and Liquid Semiconductors, (Ed. Spear W.E.), (1977).

(3) Anderson D.A., Paul W., Phil. Mag. B44, 2, (1981).

(4) Paul W., Anderson D.A., Solar Energy Materials 5, 229, (1981).

(5) Freeman E.C., Paul W., Phys. Rev. B20, 716, (1979).

(6) Spear W.E., Loveland R.J., Al-Sharbaty A., J. Non-Cryst. Sol. 13, 55, (1974).

(7) Madan A., LeComber P.G., Spear W.E., J. Non - Cryst. Sol. 20, 239, (1976).

(8) Main C., Ph.D Thesis, Edinburgh University, (1973).

(9) Main C., Owen A.E., Electronic and Structural Properties of Amorphous Semiconductors, (Ed. Le Comber P.G., Mort J.), Academic Press, p.527, (1973).

(10) LeComber P.G., Spear W.E., Phys. Rev. Lett. 25, 509, (1970).

(11) LeComber P.G., Madan A., Spear W.E., J. Non - Cryst. Sol. 11, 219, (1972).

(12) Goodman N.B., Fritche H., Ozaki H., J. Non - Cryst. Sol. 35 - 36, 599, (1980).

(13) Goodman N.B., Fritzche H., Phil. Mag. B42, 149, (1980).

(14) Kim G.I. et al, Japanese J. Appl. Phys. 19, 95, (1980).

(15) Anderson D.A., Spear W.E., Phil. Mag. 36, 695, (1977).

(16) Moustakas T.D., Anderson D.A., Paul W., Solid State Comm.

23, 155, (1977).

(17) Moore A., Appl. Phys. Lett. 31, 762, (1977).

(18) Fuhs W., Milleville M., Stuke J., Phys. Stat. Sol. B89, 495, (1978).

(19) Allan D., LeComber P.G., Spear W.E., Proc. 7th Int. Conf. on Amorphous and Liquid Semiconductors, (Ed. Spear W.E.), p.323, (1977).

(20) Tiedje T. et al., Appl. Phys. Lett. 36, 8, (1979).

(21) Kirby P.B., Paul W., Ray S., Tauc J., Solid State Comm. 42, 7, 533, (1982).

(22) Kirby P.B., Paul W., Phys. Rev. B25, 8, 5373, (1982).

(23) Viktrovitche P., Moddel J., J. Appl. Phys. 51, 4847, (1980).

(24) Vass R.W., Meininger M.A., Anderson R.M., J. Appl. Phys. 45, 843, (1974).

(25) Luby S., Thin Solid Films 8, 333, (1971).

(26) Messier R., Sarhar A.K., Roy R., Mater. Res. Bull. 9, 157, (1974).

(27) Hauser J.J., Solid State Comm. 13, 1415, (1973).

(28) Spear W.E., LeComber P.G., Solid State Comm. 17, 1193, (1975).

(29) Spear W.E., LeComber P.G., Phil. Mag. 33, 935, (1976).

(30) Mott N.F., J. Non - Cryst. Sol. 8 - 10, 1, (1972).

(31) Spear W.E., Advances in Physics, 26, 6, 811, (1977).

(32) Beyer W., Medeisis A., Mell H., Commun. Phys. 2, 121, (1977).

(33) Beyer W., Mell H., Overhof H., Proc. 7th Int. Conf. on Amorphous and Liquid Semiconductors, (Ed. Spear W.E.), p.328, (1977).

(34) Van Dong N., Hai T.Q., Phys. Stat. Sol. (b), 88, 555, (1978).

(35) Beyer W., Barna A., Wagner H., Appl. Phys. Lett. 35, 539,

(1979).

(36) Taniguchi M., Hiros M., Osaka Y., J. Cryst. Growth, 45, 126, (1978).

(37) Paul W., Lewis A.J., Connell G.A.N., Moustakas T.D., Solid State Comm. 20, 969, (1976).

(38) See References in: Anderson D.A., Paul W., Phil. Mag. B45, 1, (1982).

(39) LeComber P.G., Jones D.I., Spear W.E., Phil. Mag. B36, 1173, (1977).

(40) Jan Z.S., Kang J.H., Knights J.C., J. Electron. Mater 8, 47, (1979).

(41) Jones D.I., LeComber P.G., Spear W.E., Phil. Mag. B36, 541, (1977).

(42) Overhof H., Beyer W., J. Non - Cryst. Sol. 35 - 36, 375, (1980).

(43) Ast D.G., Brodsky M.H., Phil. Mag. B641, 273, (1980).

(44) Marshall J.M., Street R.A., Thompson M.J., Phys. Rev. B29, 4, 2331, (1983).

CHAPTER 4

SAMPLE PREPARATION

4.1 INTRODUCTION

In this study two classes of materials were prepared, namely the Chalcogen amorphous Selenium (a - Se) and the tetrahedrally bonded semiconductor amorphous Silicon (a - Si).

Measurements performed on a - Se were limited to the "Time of Flight" experiment and were primarily used for characterising the equipment developed for detecting and for analysing "Time of Flight" data. a - Se was ideal for this purpose since measurements obtained could be compared with the large body of published data characterising a - Se in terms of the "Time of Flight" experiment. Only one technique was used for preparing a - Se, namely quenching from the melt, that being discussed in this chapter.

The bulk of the work carried out in this project comprised of measurements performed on a - Si. The main techniques available for preparing thin films of a - Si, with particular emphasis on r.f. sputtering, will be reviewed. Finally, the system used and the methods employed for depositing both doped and undoped a - Si will be described.

4.2 AMORPHOUS SELENIUM

Specimens of vitreous Selenium of thickness in the 20 - 80 micron range were prepared by quenching from the melt (1). Thin mica plates approximately 5 cm by 8 cm were preheated to around 700 Kelvin in a bunsen flame. A small pellet of 99.999% pure Selenium was sandwiched between the hot plates and pressure immediately applied. The material became molten and quickly flowed into a wide thin layer between the mica sheets. Being of very low thermal capacity, the structure quickly cooled to room temperature causing the material to quench rapidly from the molten phase. Once cooled, the mica sheets could be peeled away leaving a large sample of glass with high quality surfaces. It was generally observed that surface impurities which had collected on the Selenium pellet flowed to the edges of the film during preparation and these parts of the film could be discarded.

From such layers, specimens 10 mm by 10 mm were produced by dicing the film using a scalpel. Gold or Aluminium electrodes were evaporated onto each side of the film using an in-contact mask to produce the electrode configuration shown in figure 4.1.

4.3 AMORPHOUS SILICON - GENERAL PREPARATION TECHNIQUES.

Various processes are available for depositing a - Si, the most important and commonly used being r.f. sputtering and glow discharge decomposition. Other methods such as vacuum evaporation (2), electrolytic deposition (3), ion beam bombardment (4), and chemical

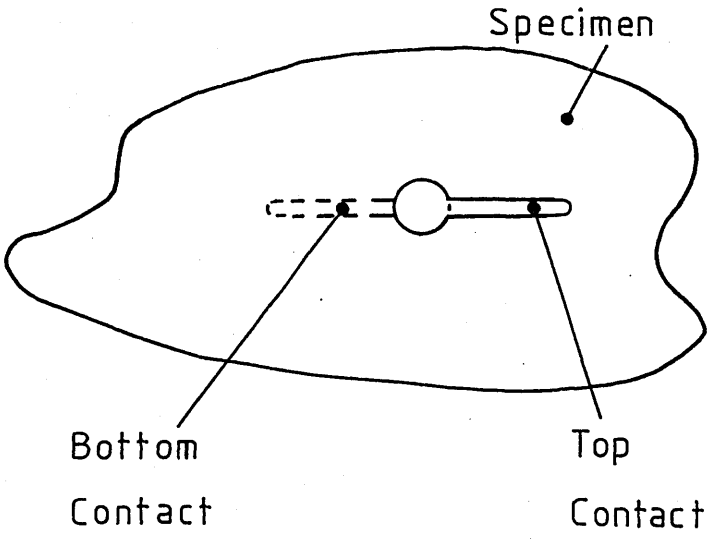

Figure 4.1. Sandwich cell electrode configuration.

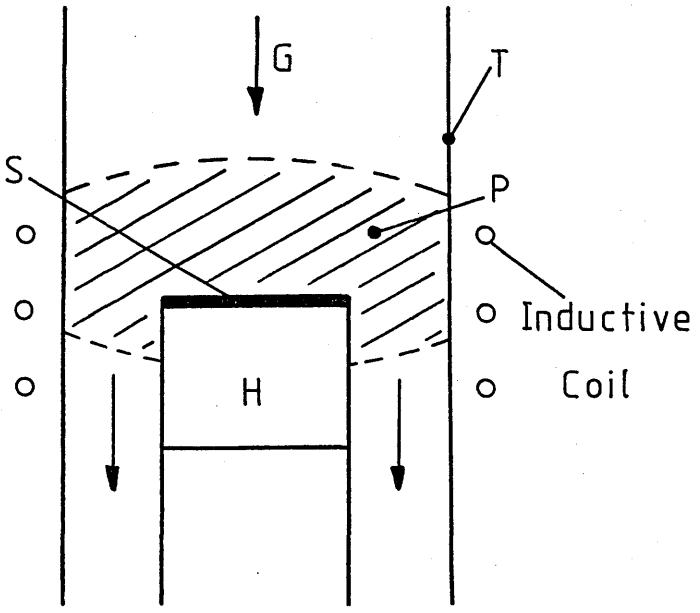

Figure 4.2. Elements of an inductively coupled glow discharge system.

vapour deposition (5) exist, but these fall outwith the scope of this study.

4.3.1 GLOW DISCHARGE DECOMPOSITION.

Figure 4.2 illustrates the basic experimental configuration for an inductively coupled gas-phase decomposition of a material. The gas, G, flows through the quartz reaction tube, T, past the substrate, S, which is held on a pedestal, H. The plasma, P, is maintained by inductively (or capacitively) coupling r.f. power into the plasma gas.

It has been known for many years that if Silane gas ($Si H_4$) at low pressure is passed through a glow discharge system, the deposition of amorphous Silicon takes place (6). Undoped specimens can be prepared by passing pure Silane through the system, while doped specimens can be deposited by mixing small amounts of dopant gases such as Phosphine ($P H_3$) or Diborane ($B_2 H_6$) with the Silane. The properties of the films deposited, however, depend critically upon the details of the apparatus and upon preparation conditions. Parameters such as substrate temperature and position, gas pressure and flow rate, and r.f. power are all important.

A significant point about the preparation of a - Si by the glow discharge technique, is that the plasma is in contact with the specimen surface during deposition. This feature is of great importance since complex surface reactions take place during growth, involving electrons and positive ion fragments such as Si-H, $Si-H_2$ and $Si-H_3$. The experimental control of these surface reactions to obtain

well-defined and reproducible electronic specimen properties remains a major problem of the technique. As a result, there can be pronounced differences between samples produced in different laboratories under seemingly identical deposition conditions, and this has lead to complications of comparison and understanding.

4.3.2 R.F. SPUTTER DEPOSITION.

The elements of an r.f. sputter deposition system are shown in figure 4.3. An r.f. discharge is set up between the target to be deposited and the substrate electrode. Ions with energies ranging from a few tenths to several hundred electron volts are accelerated by a field, from the plasma into the target causing atoms or groups of atoms to be knocked out of the target and collected on the substrate. The target is normally a prefabricated polycrystalline or compressed powder disc and Argon is the most commonly used gas for supporting the discharge. Deposition rates depend on factors such as Argon pressure, target size, electrode separation, r.f. power, etc., but normally deposition rates of around 0.5 microns per hour can be achieved. As in the case of glow discharge decomposition, the properties of a - Si prepared by sputtering are determined by complex interatomic surface reactions which are difficult to control; this again leading to marked differences between samples produced in various laboratories under seemingly identical deposition conditions. In general, however, it has been observed (7) that films deposited using the r.f. sputtering technique, have structural and electrical properties which are very similar to films deposited in a high vacuum evaporator.

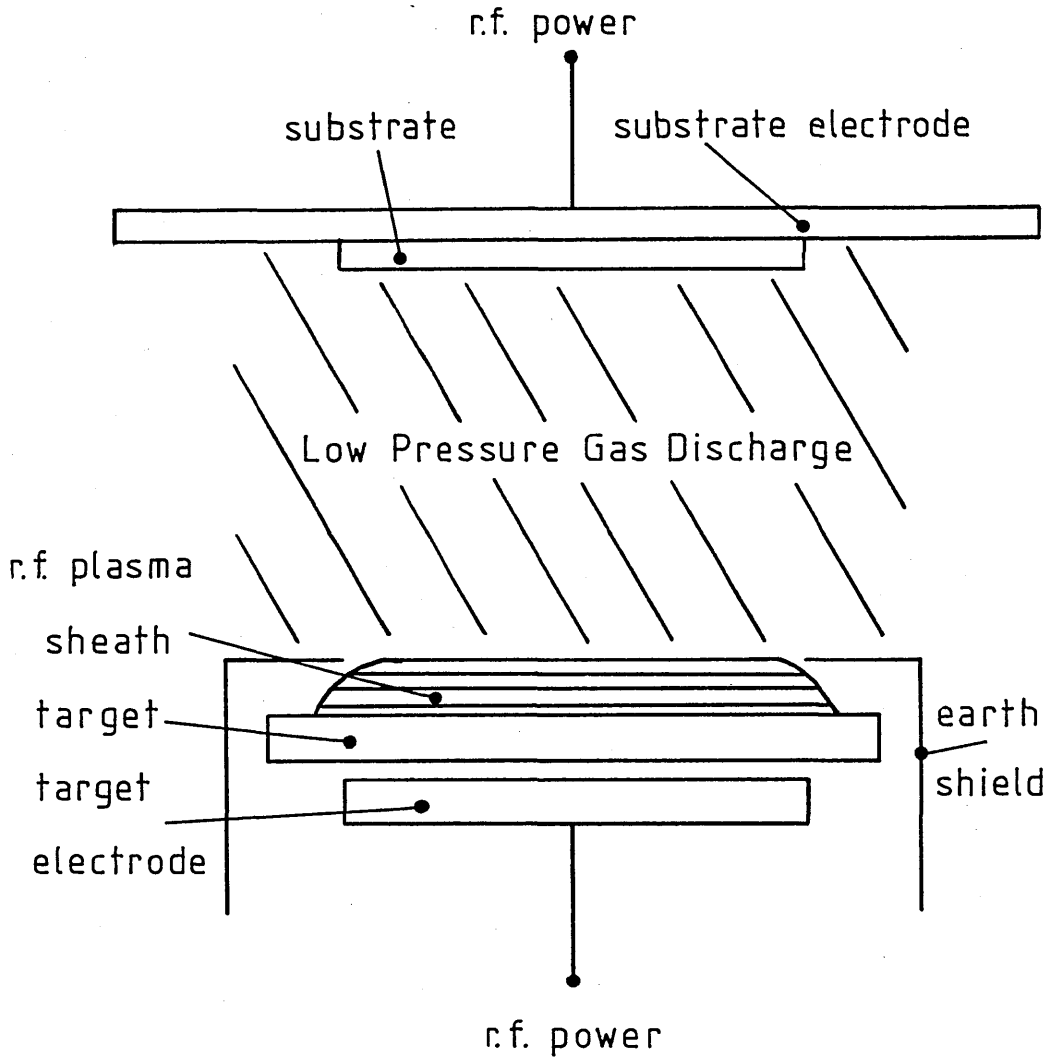

Figure 4.3. Elements of an r.f. bias sputter deposition system.

Sometimes a reactive gas can be introduced in "reactive sputtering", to combine with the target material in the plasma resulting in the deposition of a compound on the substrate. This is the case when depositing Hydrogenated amorphous Silicon (a - Si:H), where Hydrogen gas is introduced into the chamber along with the Argon gas. The Hydrogen is bonded with the Silicon both in the plasma and on the substrate resulting in the deposition of a Silicon - Hydrogen alloy. It has been reported by Anderson et al (8), Connell et al (9), and others, that the electrical, optical and structural properties of such sputtered a - Si:H films differ significantly from those of both sputtered films without the introduction of Hydrogen and evaporated films. In fact it has been observed (9) that sputtered films of a - Si:H have properties more akin to material deposited by the glow discharge decomposition of Silane, as described in the previous section.

Doping of sputtered a - Si:H can be achieved by sputtering from a degenerately doped crystalline target, by co - sputtering from a Silicon target with a small percentage of dopant material placed on its surface, or by introducing dopant gases into the chamber in the gas phase.

4.4 FACTORS AFFECTING FILM PROPERTIES IN R.F. SPUTTER DEPOSITION

In the previous section it was stated that interactions between the plasma and the specimen surface were very difficult to control in both sputter and glow discharge systems. In a sputter system, however, there are additional complications due to the interactions of the plasma with the target material. Because these interactions are so numerous and are interrelated, it is impossible to separate them completely. However, an attempt is made below to describe the most important substrate, plasma and target reactions that bear on the properties of deposited films.

4.4.1 TARGET - SUBSTRATE INTERACTIONS.

The most fundamental parameter of a sputtering process is the "sputtering yield", defined as the number of atoms ejected from a target surface per incident photon. The sputtering yield determines the erosion rate of the target material, and largely, (but not entirely) the deposition rate of sputtered films. The yield itself is determined by the incident energy of bombarding ions, having a lower limit set by the heat of sublimation of the target material. Atoms removed from the target are mainly neutral although both positive and negative ions can be liberated.

Since sputtering targets are held at high negative potentials, after bombardment secondary electrons are accelerated away from the target surface with an initial energy equal to the target potential. These electrons help to sustain the plasma by the ionisation of neutral sputtering gas atoms, which in turn bombard the target and release more secondary electrons in an avalanche process. Many of the secondary electrons are thermalised by collisions in the gas, but even at high pressures, a substantial number can retain full target potential until impact with the substrate. Such substrate bombardment may produce structural deformation in deposited films, causing an increase in the density of defect states.

Other particles such as secondary ions and reflected incident particles, and irradiation such as photons and X - rays are liberated from the target. All of these represent possible sources of substrate bombardment and deformation during film growth.

4.4.2 SUBSTRATE BIAS AND POWER.

In a bias - sputtering system, the substrate and target electrodes are simultaneously supplied with r.f. power. This causes etching of material from both the substrate and the target, and for net growth of material on the substrate the rate of deposition must be greater than the etch rate. It has been suggested (10,11), that materials with improved properties can be produced using this technique.

Supplying power to the substrate induces a negative potential on its surface due to the difference in mobility of electrons and ions. As the r.f. power is increased, the induced potential increases causing greater bombardment of the substrate by Argon, Hydrogen and Silicon - Hydrogen ions. Allison (10) has suggested that such bombardment could be instrumental in the production of higher quality films for three main reasons. Firstly, interactions of bombarding ions with loosely bound and impurity species could selectively remove these from the film surface. This could result in the production of purer films, since the growing surface is kept free from reactive contaminant gases. Secondly, enhanced diffusion of surface atoms due to momentum transfer could improve the morphology of the film and prevent void and cluster formation. Thirdly, bombardment of the film with Hydrogen ions could improve the level of saturation of dangling bonds. The amount of bombardment received by a growing film, however, is critical, and if excessive power is delivered to the substrate the quality of the deposited film may decline due to the creation of bombardment - induced defects states. Indeed, a compromise must be struck between bombardment damage and bombardment enhancement.

4.4.3 SUBSTRATE TEMPERATURE.

Figure 3.10 shows the effect of varying the substrate temperature on the room temperature photoconductivity of sputtered Hydrogenated amorphous Silicon prepared at an Argon partial pressure of 5 mTorr (16). The initial increase in photoconductivity with increasing substrate temperature is consistent with the removal of defect states

from the gap and is believed to be the result of two effects. Firstly, some network reorganisation and relaxation can take place at higher temperatures; Secondly, the probability of Hydrogen atoms migrating on the growing surface, to sites were they can compensate incipant dangling bonds, increases with temperature. Figure 3.10, however, depicts the photoconductivity going through a maximum between about 200°C and 300°C. This has been shown to be (8,16) the result of the increased likelihood at higher temperatures that Hydrogen will be unable to bond into the Silicon network. As a result, the Hydrogen content of the film will decrease; this being coupled with a corresponding increase in the density of defect states.

4.4.4 INERT GAS DILUTION.

Recent results (15) have suggested that the bombardment of growing films by dilutent gas atoms plays a major role in determining the density of defect states. Higher pressures result in more gas collisions which moderate the kinetic energy of the species that hit the substrate, resulting is less film damage. This suggestion is supported by figure 4.4 which shows the Argon content of a - Si films increasing with decreasing Argon pressure, all other things being equal.

Knights et al (14), have shown that dilutent gas incorporation into films during deposition can result in the production of voids and microcracks, leading to inferior properties. The type of gas used to support the discharge has also been found to be critical, and films

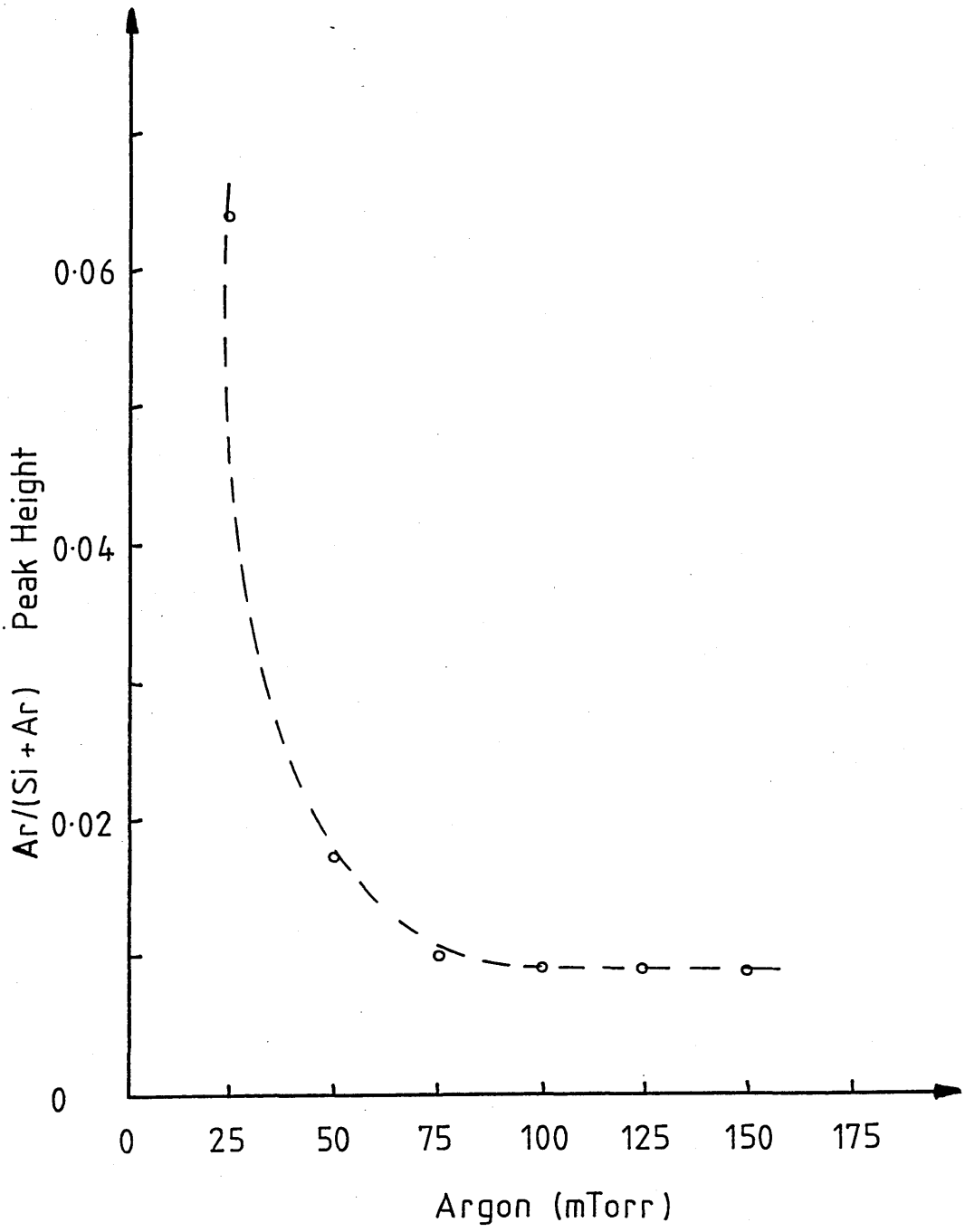

Figure 4.4. Influence of Argon gas pressure on the Argon content of a-Si:H films prepared under identical conditions of r.f. power, substrate - target spacing and substrate temperature. Argon content estimated from the ratio of the Ar - to - Si peak height in electron beam excited X - ray fluorescence spectrum. (After ref. 15).

with different electronic, structural and optical properties can be produced using different dilutent gases. The general trend is that the quality of deposited films increase with decreasing atomic mass of the dilutent gas.

4.5 DUNDEE "MOBS" SPUTTER HARDWARE.

All amorphous Silicon films were deposited using the NORDICO Bias Sputtering system shown in figure 4.5. The chamber was evacuated using a 20 cm oil diffusion pump backed by a suitable mechanical rotary pump. Gases were admitted into the chamber using either needle valves or automatic mass flow equipment. The gas flow rate was adjusted in order to maintain a constant pressure within the chamber. Three 10 cm diameter targets could be accommodated by the system, the target chosen for deposition being rotated underneath the substrate. The substrates were held in contact with a 19 cm diameter Copper plate which could be heated electrically, or cooled by water or liquid Nitrogen. The main features of the unit are described below.

4.5.1 TARGET AND SUBSTRATE.

The sputter target used for depositing a - Si was an 8 cm diameter polycrystalline disc of electronic grade Silicon, bonded with conductive epoxy to a stainless steel backing plate. The plate was screwed into a water cooled target holder, the complete arrangement shown in figure 4.6, being partially shrouded by a stainless steel

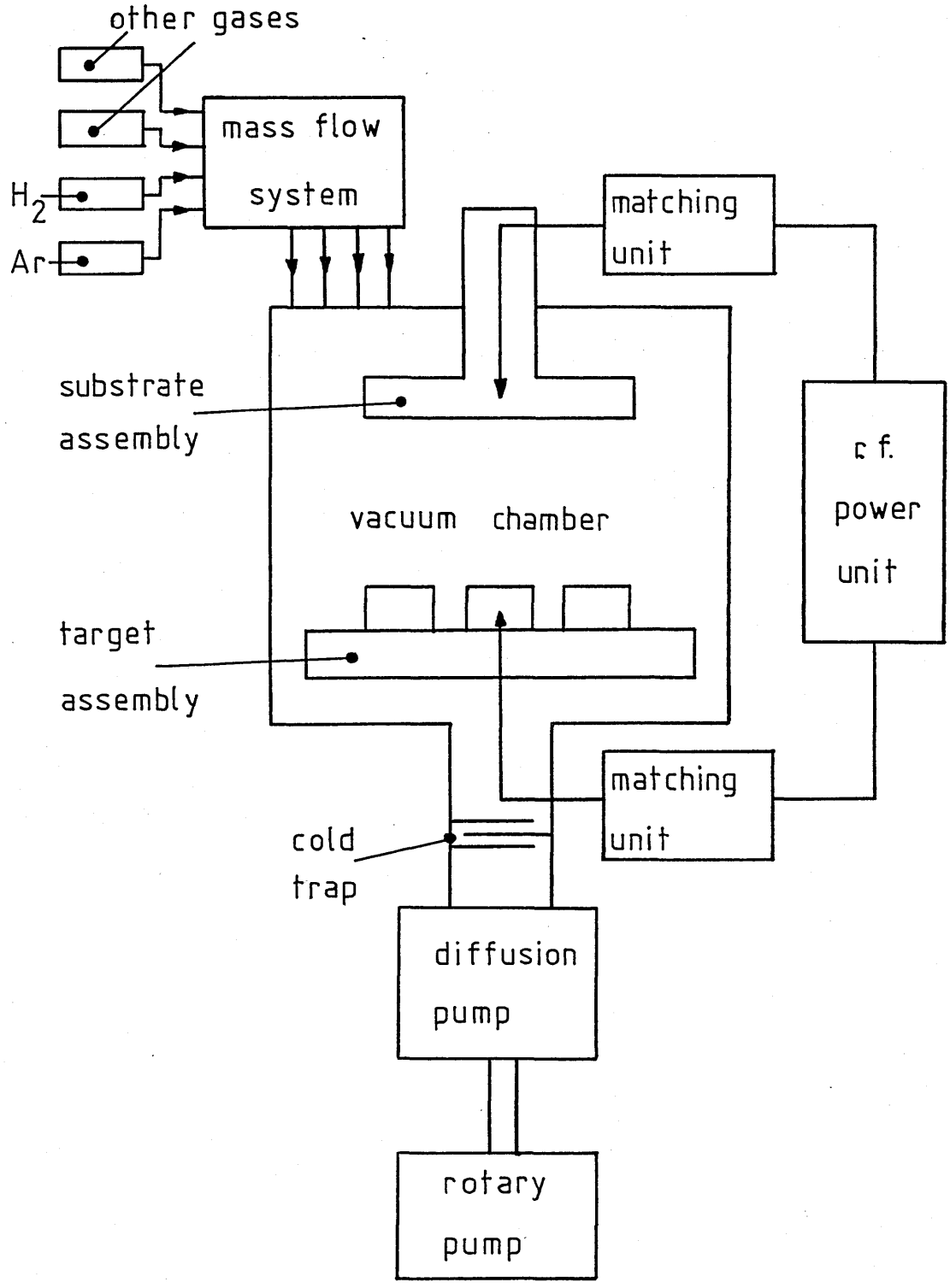

Figure 4.5. Schematic diagram of Nordico bias sputter deposition system.

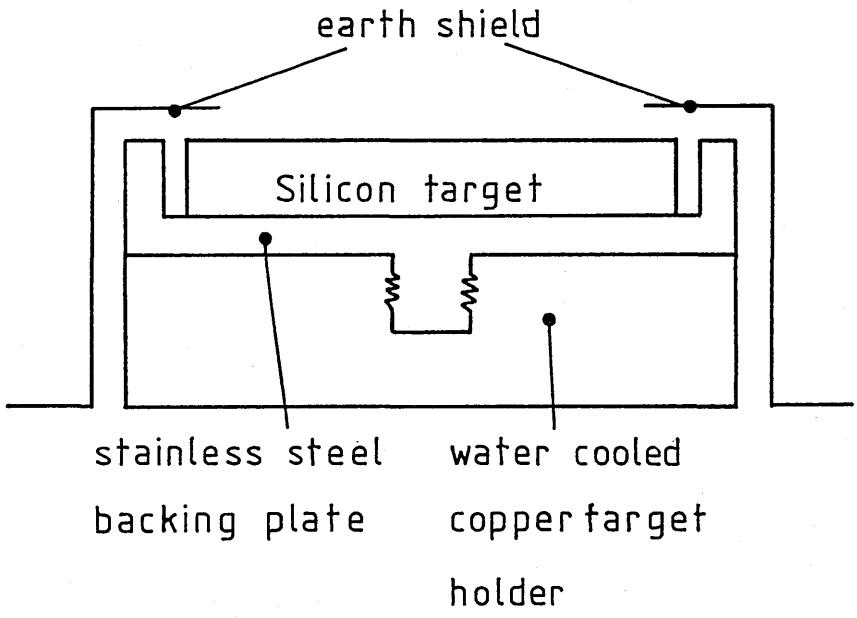

Figure 4.6. Details of Silicon target assembly.

earthing shield. The purpose of the earthing shield was to prevent stainless steel at the edges of the Silicon target from being sputtered.

It was found that the position of the earthing shield with respect to the target had a major influence on the negative bias voltage induced on the target surface during deposition. This was due to the target - to - earth capacitance being affected by small changes in the target geometry. In order to counter such undesirable variations between depositions, a jig was constructed which accurately located the earthing shield in the same position each time it was fitted.

Eight Corning 7059 glass substrates could be loaded into the sputtering system for each deposition, the substrates being held in good thermal contact with a Copper plate by a shaped brass holder. To facilitate substrate and mask positioning, the plate was demountable from the system. Inside the chamber, the Copper plate was located directly above the target and was maintained in good thermal contact with a 1.5 kW electric heater element by a large Copper o - ring. The substrate plate could be heated to a maximum temperature of 650^{o}C. The heater element was supplied, through a suitable isolation transformer, from a 6 Amp 240 Volt variac, the temperature of the Copper plate being monitored via a Copper - Constantan thermocouple. The temperature of the plate was calibrated against the variac output voltage, the calibration graph being shown in figure 4.7.

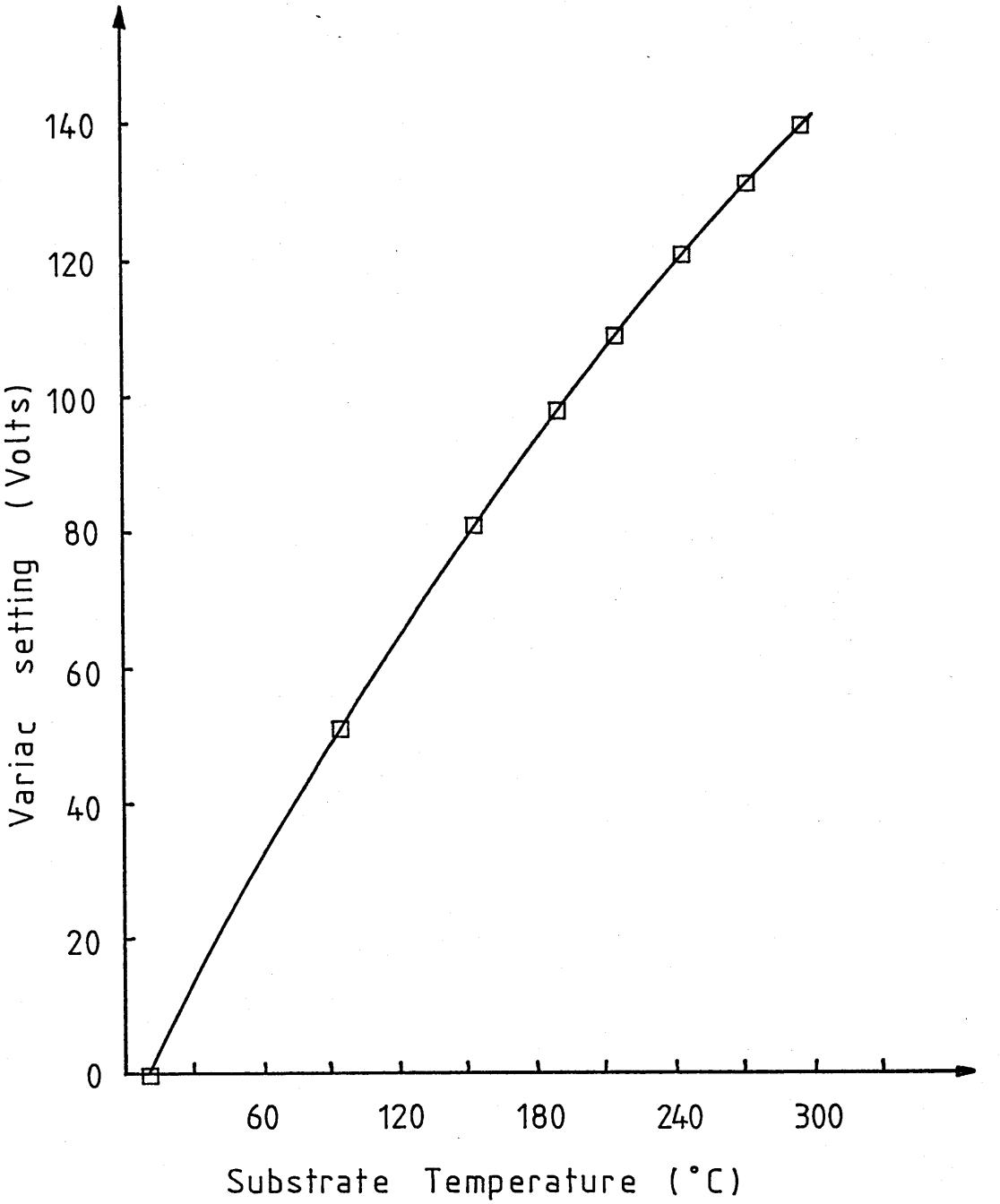

Figure 4.7. Calibration graph of variac output voltage versus Copper substrate - plate temperature.

The target - substrate separation employed during deposition has been shown to have a determining influence on the electronic properties of films produced. Oguz et al (12), found that optimum film properties (i.e. films which, among other things, displayed the largest room temperature photoconductivity), are obtained at a separation of around 3 to 4 cm. In the Nordico system employed in this study, it was possible to vary the target - substrate separation over the range 5 to 25 cm. After some preliminary film depositions, it was decided to fix the target - substrate separation at 5 cm throughout the duration of the project. This was the minimum target - substrate separation that could be achieved using the Nordico system.

4.5.2 GAS CONTROL AND VACUUM SYSTEM.

As already mentioned, gases were removed from the sputtering chamber using a 20 cm oil diffusion pump, backed by a mechanical rotary pump. A maze - type water cooled trap was situated above the diffusion pump to prevent backstreaming of oil into the chamber and above that a pneumatically controlled baffle plate, which was used to control the rate at which gases were removed from the chamber. Preceding a deposition run, the background pressure in the chamber was reduced to between 10^{-5} and 10^{-6} Torr. No mass-spectrometry equipment was available to analyse the residual gases, but Nitrogen and water vapour were found to be the principal impurities in a similar system (15).

During the term of this project the sputtering system was upgraded and as a result two methods of admitting gases into the chamber were employed. The first method involved the use of needle valves to control the flow of both Hydrogen and Argon gas. After the chamber had been pumped down to its background level, the Hydrogen valve was opened and the desired Hydrogen partial pressure set up by adjusting the needle valve setting. Once this pressure had stabilised, the Hydrogen valve was closed, the Argon valve was opened and the required Argon partial pressure set up using its controlling needle valve. Once this pressure had stabilised both needle valves were opened and the chamber pressure allowed to settle. Usually, the chamber pressure settled at a value that was close to the sum of the individual partial pressures.

The above procedure had a number of severe limitations. Firstly, the only time that the chamber partial pressures were known was during initial setting up. Once the deposition had commenced, only the total chamber pressure could be monitored. Secondly, during a sputtering run (which in most cases had a duration of about 48 hours), the needle valves required adjustment in order to counter variations in the chamber pressure. It was found that the best method of adjustment was to increase or decrease both needle valves by the same amount. Using such a method, however, gave no guarantee that the required partial pressures would be maintained at their initial setting, and it was likely that partial pressures would progressively drift as the run proceeded. Thirdly, variations in the gas line pressure could cause a further source of both chamber and partial pressure drift.

As might be expected, by using such unreliable procedures for controlling the gas flow rates, the electronic and optical properties of deposited films, produced from different runs under seemingly identical conditions, varied in some cases by up to four orders of magnitude. In an attempt to remedy this problem, automatic mass flow equipment was obtained for the system, (MKS Baratron type 260 modular mass flow control system). The equipment operated by adjusting the mass flow rates of gases entering the chamber in order to maintain a preset pressure. Flow rates were adjusted by applying three term control to the difference signal between a setpoint pressure and the chamber pressure, the chamber pressure being monitored via an MKS Baratron type 261 manometer. Up to four gases could be controlled simultaneously, their ratio of flow being kept constant by the controller.

Although this equipment did not allow control over the absolute chamber partial pressures, it was capable of maintaining a fixed ratio between the flow rates of individual gases. This was a significant improvement over the needle valve arrangement and provided a suitable means for standardising film properties against gas flow rates.

4.5.3 R.F. POWER GENERATOR.

R.F. power was delivered to the sputter electrodes using a crystal controlled generator operating at a frequency of 13.56 MHz. The generator had an output impedance of 50 Ohms and was capable of delivering 1.25 kW at 5 Amps. In order to deliver power to the

sputtering discharge the generator had to be impedance - matched to the electrode assembly.

The equivalent circuit of an electrode is shown in figure 4.8, where C_s is the capacitance of the electrode to ground (mostly due to the presence of the ground shield), C_t is the capacitance of the target and C_b is a d.c. blocking capacitor. R_p and L_p are respectively the resistance and inductance of the plasma discharge. The impedance of the electrode system was in general not equal to 50 Ohms and under such conditions the gross impedance mismatch caused practically all the r.f. power to be reflected back to the generator, with very little power being available for sputtering. To overcome this problem, the target and substrate electrodes were fitted with matching units shown in figure 4.9, which transformed the electrode impedance to a value close to 50 Ohms.

Three methods of sputtering were possible using the NORDICO system, namely sputter deposition, sputter etching and bias sputtering (see figure 4.10). Bias sputtering required the use of a power splitter to apportion the generated power between the substrate and the target electrode. The splitter used was capable of operating over a continuous range from 1:1 to 20:1, (i.e. power to target : power to substrate).

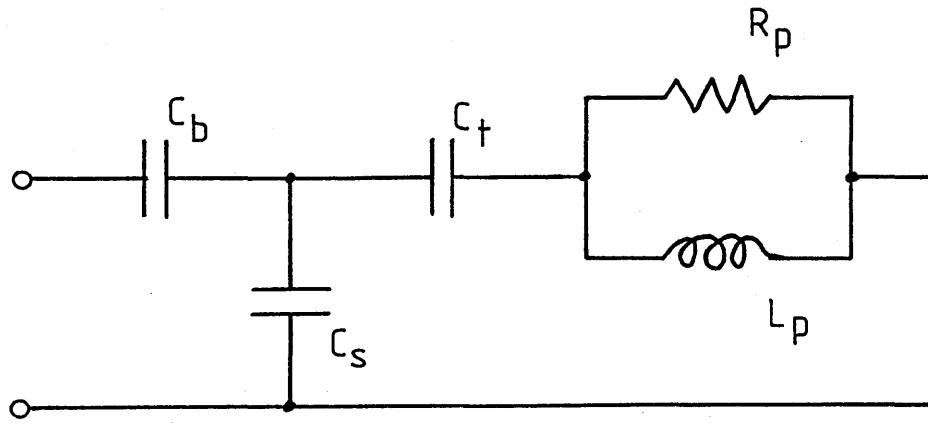

Figure 4.8. Equivalent r.f. circuit for sputter electrode and plasma discharge.

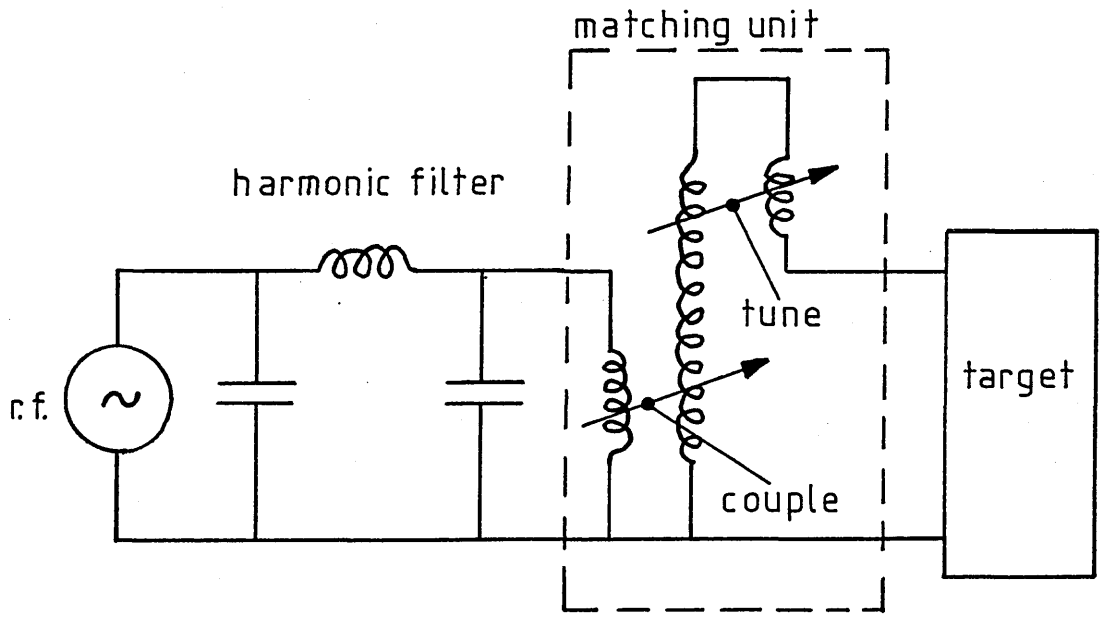

Figure 4.9. Matching unit used to transform the electrode impedance to a value close to 50 Ohms. The harmonic filter used in the system is also shown.

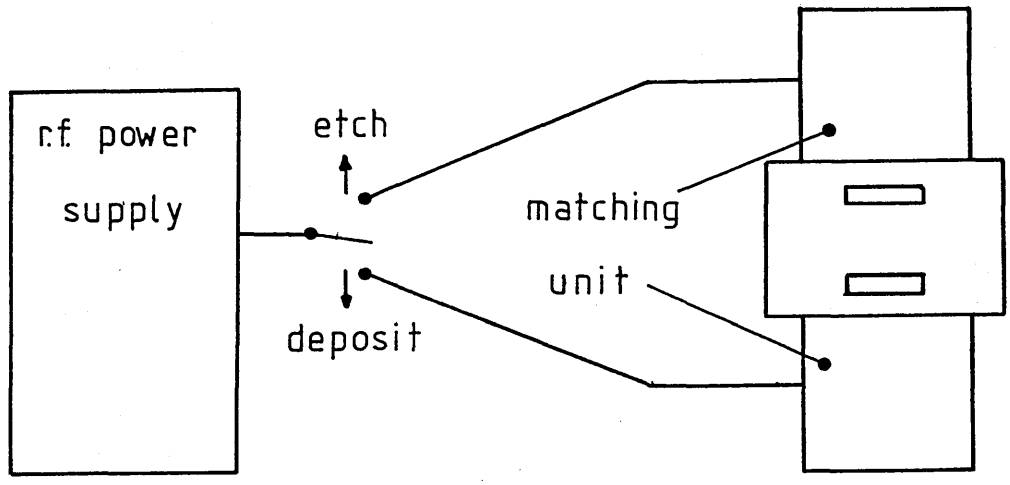

sputter deposition & sputter etch

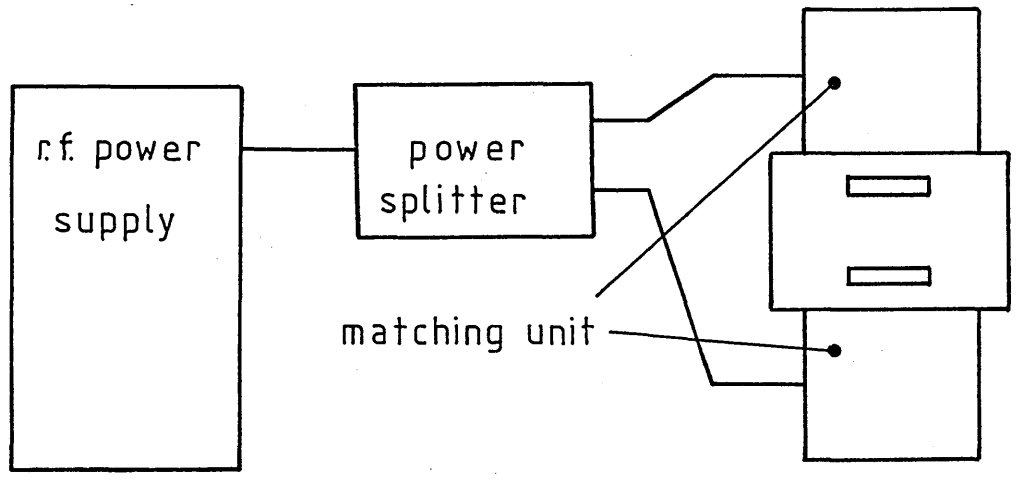

bias sputtering

Figure 4.10. Methods of sputtering available using the Nordico system.

4.6 DEPOSITION OF DOPED AND UNDOPED a - Si:H.

Two types of specimen configuration were employed, namely co - planar gap cells and sandwich cells. The co - planar geometry shown in figure 4.11 was realised by evaporating Gold or Aluminium through a mask which held a thin stretched wire across the surface of the substrate. The cell was completed by sputtering a - Si onto the electrodes. In some cases, the a - Si was deposited onto the substrates first, followed by the electrodes, (this variation having no effect on the measured film properties). The sandwich cell geometry used is shown in figure 4.1 and consists of an a - Si film sandwiched between a Molybdenum bottom contact and an Aluminium top contact. The Molybdenum was r.f. sputtered prior to the a - Si deposition, the Aluminium being deposited onto the a - Si to complete the cell. Both metals were deposited through a suitably shaped in - contact mask. In order to perform optical absorption measurements, a - Si films were deposited onto substrates having no electrodes fitted.

Doped and undoped a - Si were deposited using the same polycrystalline Silicon target. The undoped material was deposited directly from the Silicon target, while the doped material was deposited by co - sputtering the Silicon with a small percentage of dopant material distributed evenly over the target surface. Antimony shot was used for n - type doping and Aluminium wire for p - type. The dopant concentration in the films was controlled by varying the amount of dopant material placed on the target.

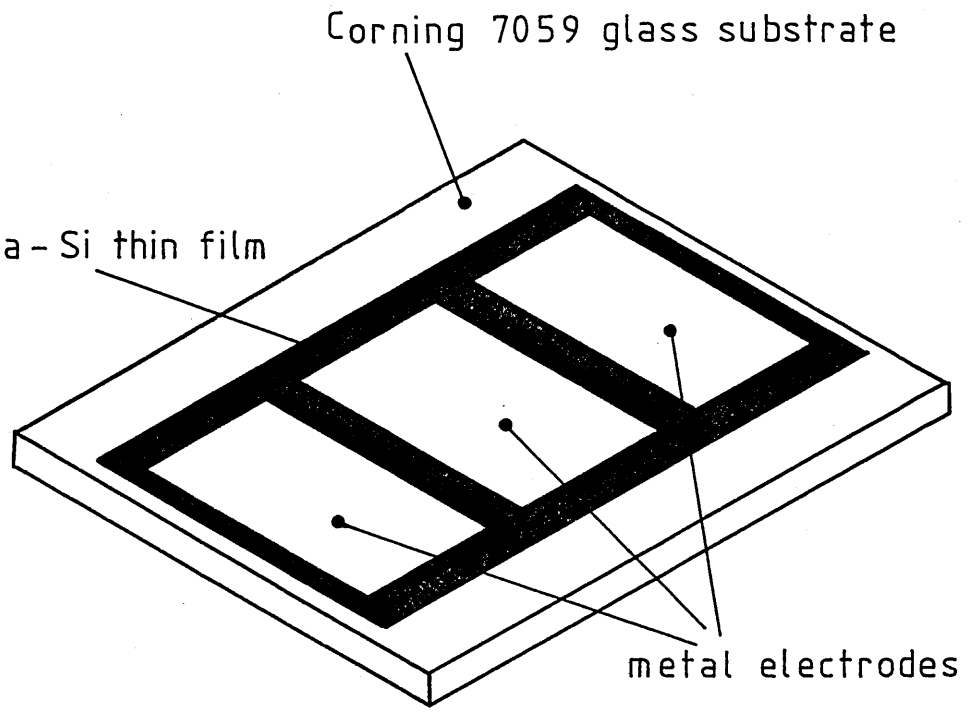

Figure 4.11. Co-planar specimen geometry.

The deposition conditions employed for preparing both doped and undoped a - Si were identical and were standardised to achieve consistent film properties. Hydrogen and Argon partial pressures of 4 mTorr and 11 mTorr respectively were used, the method of establishing and maintaining these pressures being described in section 4.5.2. The temperature of the Copper substrate plate was maintained at 270^{o} C during deposition, this temperature being monitored via a Copper - Constantan thermocouple connected to the Copper substrate plate. No direct measurement of the glass substrate surface temperature was made during film growth. 100 Watts of r.f. power were supplied to the target electrode, the reflected power being minimised by adjusting the impedance of the matching unit. No power was supplied to the substrate electrode which was allowed to "float". Under these conditions a d.c. bias voltage in the range 900 to 1100 Volts was established between the target surface and earth potential.

Before commencing the deposition of material onto the substrate, the target was presputtered for around six hours. This was achieved by rotating a shutter between the target and the substrate. Presputtering facilitated the removal of absorbed impurities (particularly Oxygen), from the surface of the target and from walls and fixtures within the chamber. Material deposition commenced upon the removal of the shutter and in general, accumulation rates of approximately 0.15 microns per hour were obtained on the substrate.

REFERENCES CHAPTER 4

(1) Marshall J.M., Ph.D Thesis, Edinburgh University (1970)

(2) Tauc J., Grigorovici R., Vancu A., Phys. Stat. Sol. 15, 627, (1968). [For Example.]

(3) Szekely G., J. Electrochem. Soc. 98, 318, (1951). [For Example.]

(4) Ceasar G.P. et al, J. De Physique C4, 10, 42, p.627, (1981). [For Example].

(5) Hirose M., J. De Physique C4, 10, 42, p.705, (1981). [For Example].

(6) Sterling H.F., Swann R.C.G., Solid State Electronics, 8, 653, (1965).

(7) Spear W.E., Le Comber P.G., in Photoconductivity and Related Phenonina, (Eds. Mort J., Pai D.M.), (1976).

(8) Anderson D.A. et al, Proc. 7th Int. Conf. on Amorphous and Liquid Semiconductors, (Ed. Spear W.E.), (1977).

(9) Connell G.A.N., Pawlik J.R., Phys. Rev. B13, 787, (1975).

(10) Allison J. et al, Proc. Photo. Solar Energy Conf., Cannes, France, p.820, (1980).

(11) Thompson M.J. et al, I.P. Proc. Int. Conf. Photovoltaic Solar Energy, Lux, p.231, (1977).

(12) Oguz S. et al, J. De Physique C4, 10,42, p.679, (1981).

(13) Paulik J.R., Paul W., Proc. 7th Int. Conf. on Amorphous and Liquid Semiconductors, (Ed. Spear W.E.), (1977).

(14) Knights J.C. et al, Appl. Phys. Lett. 38, 5, 331, (1978).

(15) Pawlewicz W.T., J. Appl. Phys. 49, 11, 5595, (1978).

(16) Moustakas T.D. et al, Solid State Comm. 23, 155, (1977).

CHAPTER 5

EXPERIMENTAL APPARATUS.

In this chapter the equipment developed and used for performing Time of Flight, Dark d.c. Conductivity, Steady State and Transient Photoconductivity and Optical Adsorption measurements will be discussed.

5.1 INTRODUCTION.

In order to perform the experiments listed above over a wide range of temperature, (boiling liquid Nitrogen temperature (77K) to about 500K) it was necessary to house the material to be studied inside an evacuated container so that it did not "ice - up" when lowered in temperature or react with the constituents of air when raised in temperature. Consequently, a vacuum chamber with associated pumps was the first requirement of an experimental rig.

Secondly, due to the differing experimental requirements of the techniques used, the rig developed had to be capable of easy modification in order to accommodate all the experiments listed above, (excluding optical absorption which was carried out on separate apparatus).

At the onset of the project it was envisaged that drift mobility measurements performed using the Time of Flight technique would form the core of the experimental work to be undertaken. Consequently, the

rig developed was constructed round the requirements of a Time of Flight experiment.

To facilitate a description of the complete system, the equipment necessary for the Time of Flight experiment will be discussed first, followed by an outline of the modifications performed to the rig in order to accommodate the other experiments.

5.2 REQUIREMENTS OF THE TIME OF FLIGHT EXPERIMENT.

The practical requirements for the determination of drift mobilities by the Time of Flight technique have been discussed in Chapter 2. Essentially, a thin layer of charge carriers must be generated under the top electrode in a suitably shaped specimen, the drift of these carriers being monitored by some external detector. Thus, having decided to attempt such a measurement the form of the excitation source must be selected and the general requirements of the specimen examined.

In most applications, the means of carrier generation is immaterial and the experimenter is free to choose either light sources, such as spark gaps, lasers, light emitting diodes, or highly ionising radiation such as X - rays, nuclear radiation, or an electron beam source. Since the production of short pulses of nuclear radiation is relatively difficult, and seems to offer no significant advantage over its alternatives, this technique was not pursued in the present study. The use of light pulses offers the advantage that no complex vacuum system is necessary. However, the spectral output of

the source must be matched with the energy gap of the material under investigation; that is, the photon absorption length must be shorter then the thickness of the sample, but yet not so short that a significant number of carriers can be lost due to diffusion to the surface. Thus, whilst light beams may be suitable for materials having high optical absorption in the visible region, more transparent wide band gap materials might be difficult to examine.

The first material studied in this project was amorphous Selenium having an optical gap of approximately 2.2 eV, followed by undoped amorphous Silicon having an optical gap of approximately 1.7 eV. In order for these materials to meet the requirements of the Time of Flight experiment when using photon pulses, it was clear that excitation with radiation at the blue end of the visible spectrum (>2.8 eV) would be required. At that time, no equipment was available in this laboratory for producing such pulsed radiation and this approach was not pursued. However, as the project developed, a pulsed Nitrogen laser which operated in the near ultra - violet range became available. Furthermore, results from optical absorption had shown that doping amorphous Silicon "n" or "p" type reduced the optical gap. Both of these factors made the use of light pulses a much more realistic proposition and laser ionisation was in fact used to illuminate amorphous Silicon in the latter part of the project.

Finally, ionisation could be produced using an electron gun. A pulsed electron gun is an extremely versatile tool when used in the Time of Flight experiment and offers a number of advantages over other ionisation sources. By altering the electron beam energy the

penetration depth can be altered, which ensures absorption in a thin layer just under the top contact of the specimen. The excitation is uniform over the contact area and arrangements can be made for an advanced trigger signal so that pulsed bias fields can be used to reduce sample heating and polarisation effects. The major disadvantage of this technique lies in its relative complexity, since the use of a specialised electron gun and its associated equipment is required. However, the properties of the materials to be studied in the initial stages of the project were suitable for excitation by an electron beam, and this form was adopted.

5.3 DRIFT MOBILITY MEASUREMENTS USING AN ELECTRON GUN.

The fundamental elements of the drift mobility measurement equipment are shown schematically in figure 5.1 and were based on the equipment developed by Spear (1). Specimens in the form of thin films with appropriate electrodes were mounted in a specimen holder which allowed the specimen temperature to be varied over a wide range. The holder assembly was situated inside an electron gun, the pulsed operation of which was controlled by the gun electronics. Overall control of the experiment was provided by a number of interconnected pulse generators, which provided triggering for the gun electronics, the pulsed bias field and the detection network. The detection network consisted either of a storage oscilloscope, or a transient analyser linked through a microcomputer to the College's main frame computer. The main elements of the measurement equipment will be described in detail below.

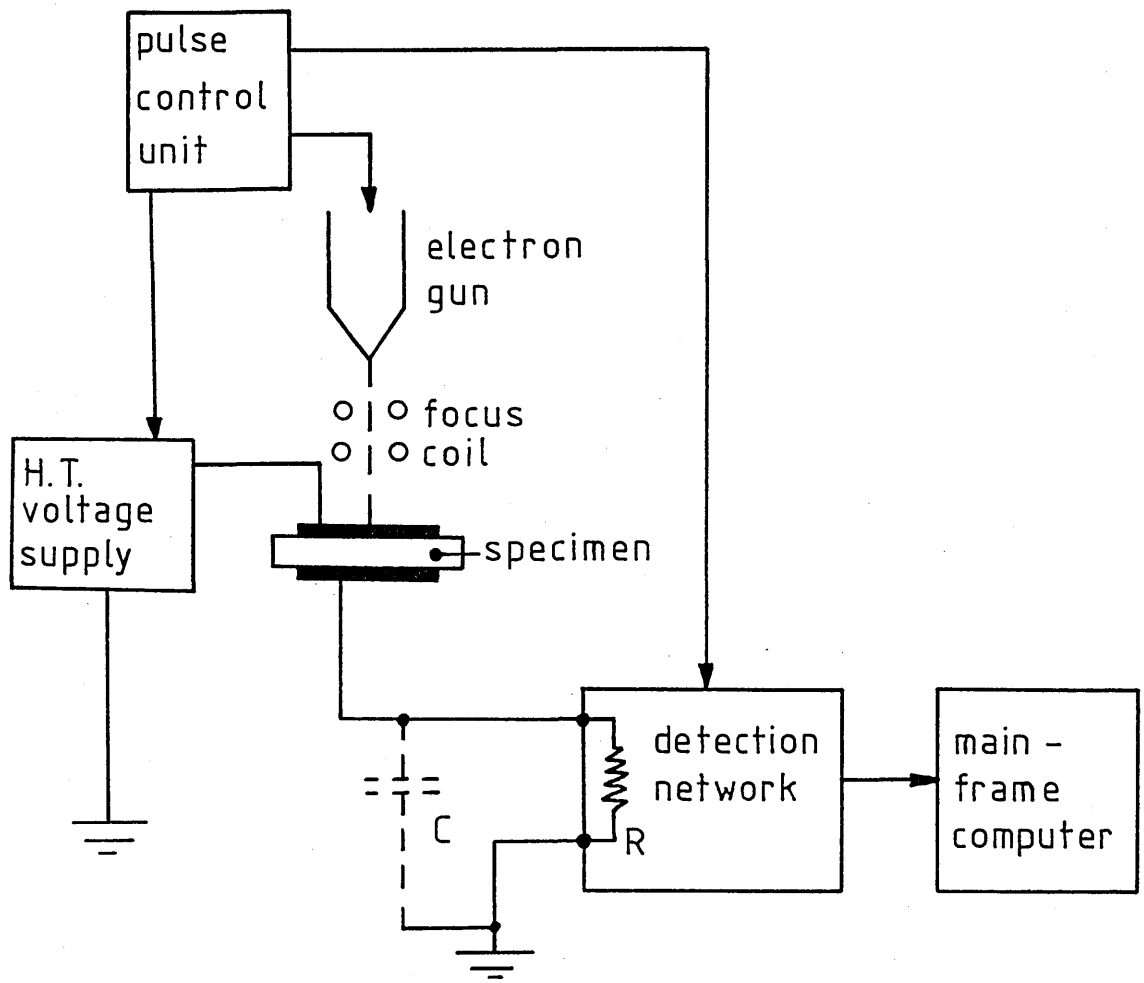

Figure 5.1. Schematic diagram of drift mobility measurement equipment used in this study.

5.3.1 SPECIMEN HOLDER.

The specimen holder employed for this work is shown in figure 5.2. The holder permits the specimen temperature to be continuously varied over the range 100K to 500K. The specimen, on its substrate, was held in position on a shaped brass block by a smear of either Silicone grease or silver paint, depending upon the temperature range to be investigated. The block was secured to a brass bobbin, non - inductively wound with Constantan wire to form a heating coil. Using tubular washers as spacers, the bobbin assembly was secured to a copper bar by means of three 3 B.A. screws with the small gap between the bobbin and the bar providing a path of low thermal conductance between the two. The copper bar was partially shrouded by a stainless steel tube, and a brass plate soldered to the outside of the stainless steel tube permitted the holder assembly to be connected to the specimen chamber of the electron gun. By submersing the end of the copper bar in a bath of liquid Nitrogen, the temperature of the brass block could be reduced, whilst the low thermal conductance of the stainless steel tube minimised cooling of the outer electron gun chamber.

Seven vacuum - sealed b.n.c. terminal connectors were mounted on the brass plate, to provide current for the heating coil, to make contact with the specimen and for connecting to the temperature sensor. Two specimen leads were directed from these terminals to the specimen by coiling the leads a number of times round the copper rod, then feeding them through the center of the heater bobbin. Thin wires

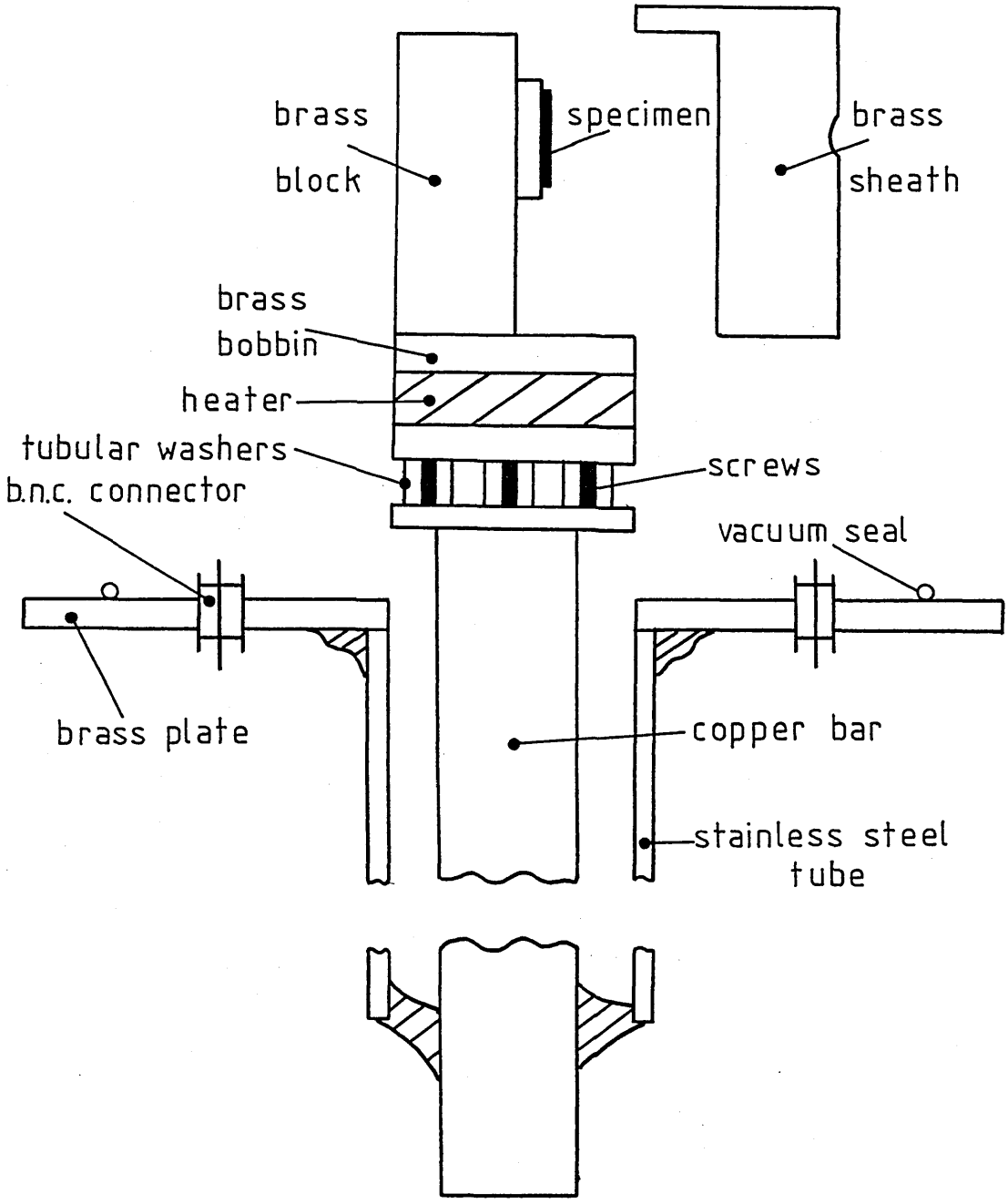

Figure 5.2. Specimen holder.

were attached between the ends of the leads and the specimen using a silver paint suspension. By this method, a path of very low thermal conductance was ensured between the specimen and the external leads.

The specimen temperature was controlled using an Oxford Instruments three term controller (type DTC-2). The controller was connector to the heater coil and to a small Platinum resistance thermometer element mounted inside the brass block. The controller allowed the specimen temperature to be controlled over the range 100K to 300K with an accuracy of $\pm$0.1 Kelvin. For temperatures between 300K and 500K the specimen temperature was monitored via the Platinum resistance thermometer linked to a Comark digital thermometer (type 5000). In this latter configuration the heater current was controlled manually via a 30 Volt, 1 Amp d.c. power supply.

Thermal and electrical shielding of the specimen were provided by a brass sheath. The electron beam passed through a small hole in the sheath.

5.3.2 ELECTRON GUN.

The electron gun construction and its electrical configuration are shown in figure 5.3. The cathode was a directly - heated Tungsten wire, powered from an audio amplifier driven through a high tension (H.T.) isolation transformer. The lateral and vertical position of the filament, with respect to the modulation grid, were easily adjustable, allowing the filament to be correctly positioned in the immersion field of the grid system. The cathode was held in the "off"

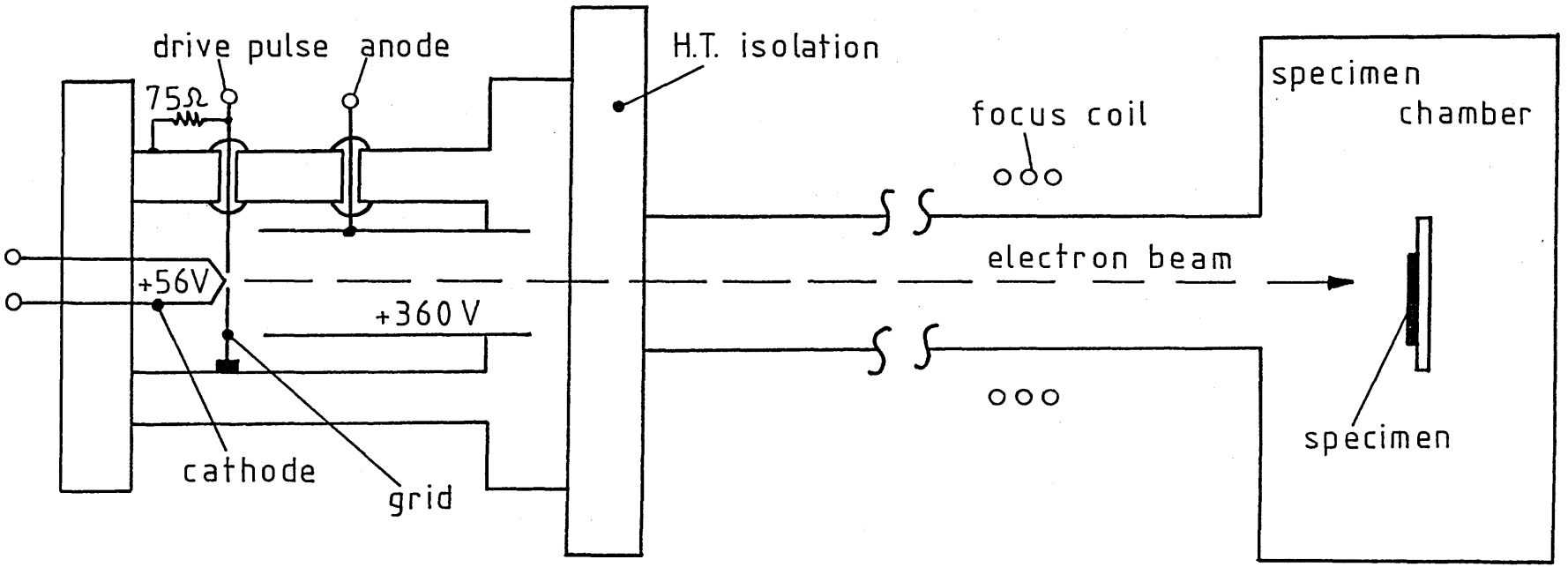

Figure 5.3. Electron gun configuration.

state by a fixed positive bias of +56 Volts relative to the casing of the H.T. section of the gun. The modulation grid was driven via a feed - through in the side of the gun, with a 75Ω resistor connected between the grid and the case to provide correct termination of the drive pulse. Due to the presence of this resistor, the grid was normally at the casing potential, so that its negative bias with respect to the cathode held the gun in the "off" state. A sufficiently large positive pulse on the grid served to switch the electron beam on. The anode electrode was held at a potential of about +350 Volts with respect to the cathode and served to stabilise the operation of the gun. The electron beam was focused by means of an adjustable magnetic coil, which also allowed control of the beam position relative to the specimen.

5.3.3 GUN ELECTRONICS.

The electron gun electronics can be divided into two sections; the high tension (H.T.) electronics and the low tension (L.T.) electronics. The H.T. electronics were mounted on an insulated board, housed within a shielded metal box. The H.T. electronics and the L.T. electronics were electrically isolated by means of suitably rated transformers and capacitors. A diagram of the equipment is shown in figure 5.4.

The electron gun accelerating potential was supplied by a Brandenburg 695P high voltage generator, which was adjustable in the range 4 to 15 kV. This adjustment provided a suitable means for

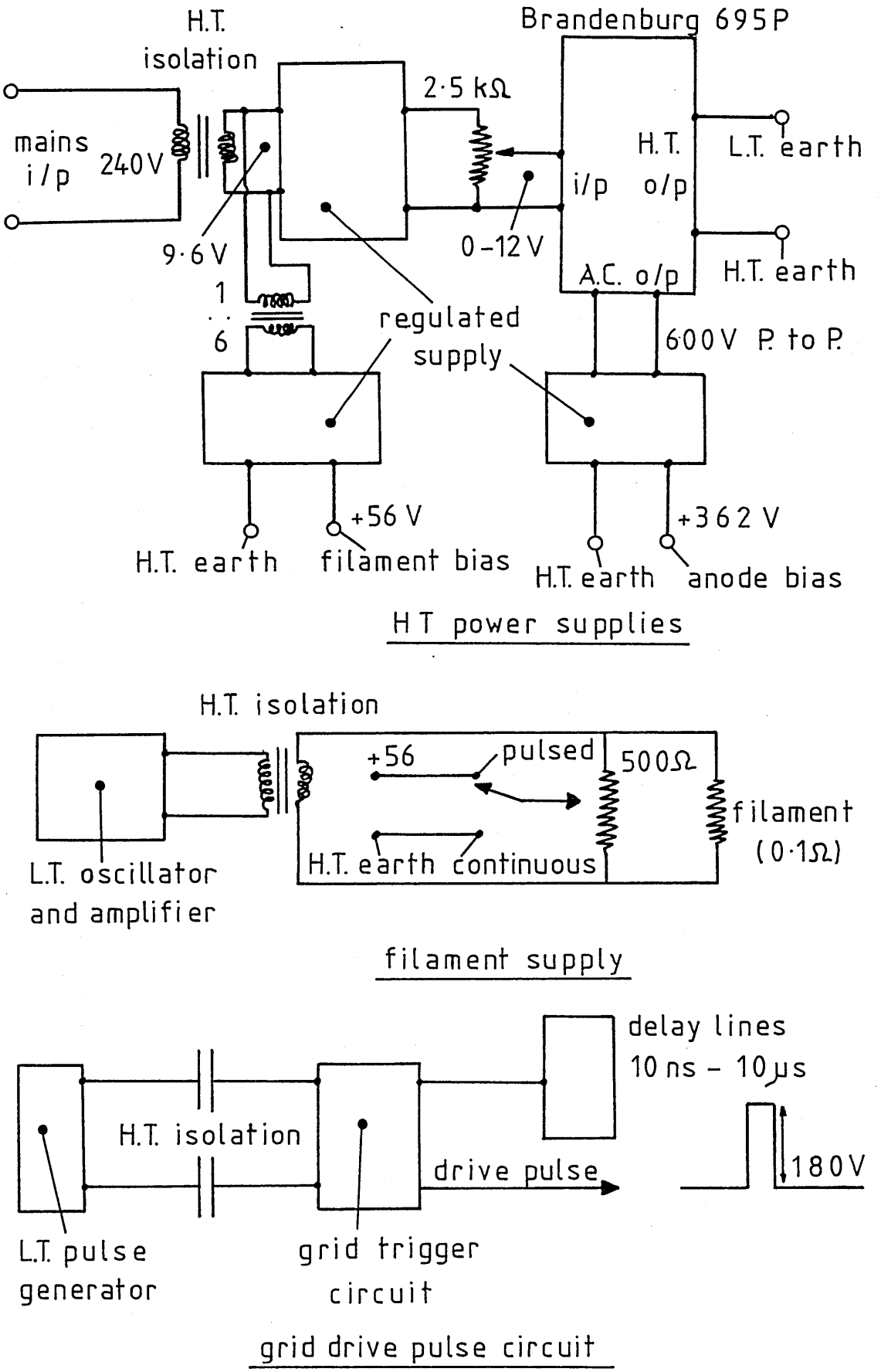

Figure 5.4. Electron gun electronics.

altering the electron beam penetration depth. The +56 Volt filament bias potential was derived from the circuitry powering the Brandenburg. From a secondary 600 Volt peak to peak Brandenburg output, the +360 Volt anode potential was obtained. An ILP - HY50 audio amplifier driven through an H.T. isolation transformer was used to power the filament. The audio amplifier was excited by the Wien Bridge oscillator shown in figure 5.5, operating at a frequency of 12 kHz. The intensity of the electron beam could be varied by altering the temperature of the filament, this being achieved by controlling the amplitude of the signal injected into the HY - 50 amplifier using a suitable potentiometer.

The format of the electron beam, either pulsed or continuous, was controlled by means of a 500Ω resistor connected in parallel with the filament wire. This resistor had a "tap" available at its mid point, which was switchable between the +56 Volt filament potential and H.T. earth. With H.T. earth connected to the tap the gun was biased "on", and provided a continuous electron beam. This setting was used for accurately focusing the electron beam onto the top contact of the specimen. With the +56 Volt potential connected to the tap, the gun was biased "off", and could only be activated by the application of a suitable voltage pulse, (larger than +56 Volts), to the grid. This drive pulse was provided by means of the gun trigger circuit which was driven from an L.T. pulse generator through a small H.T. capacitor.

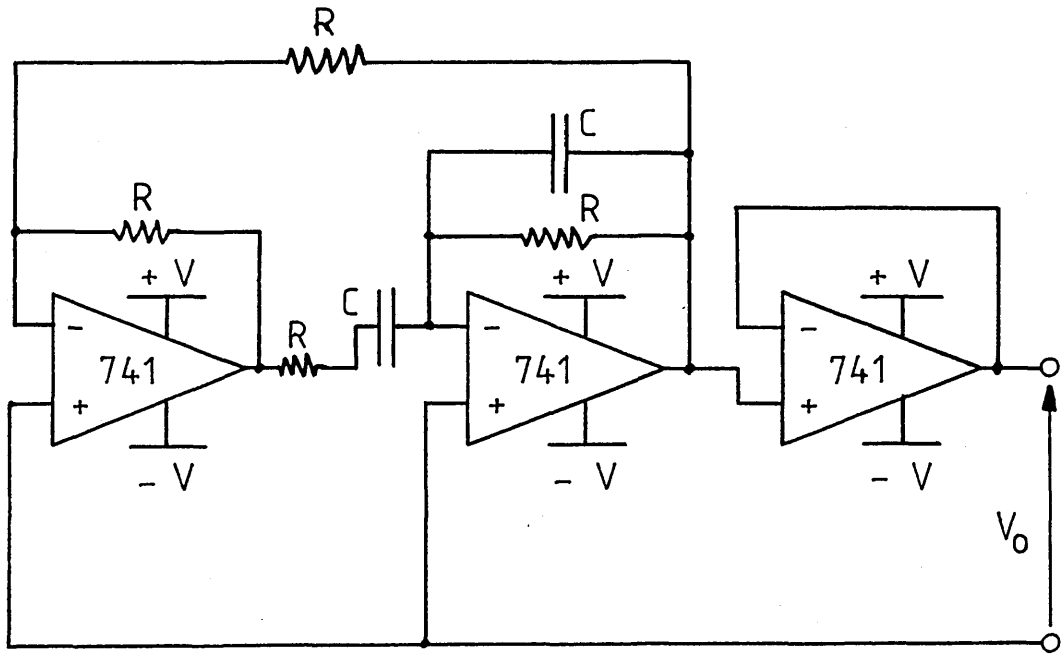

R = 1 kΩ C = 10 nF V = 15 V f = 12 kHz

Figure 5.5. Wien Bridge oscillator.

During the development of the equipment, two methods for generating the gun drive pulse were investigated, these being circuits based on the avalanche transistor, figure 5.6, and the thyristor, figure 5.7. A length of delay line, (either coaxial or lumped), was charged through a 330 kΩ resistor from the +350 Volt anode potential. The output of the trigger circuit was terminated in a 75Ω resistor which was connected between the grid of the electron gun and H.T. earth. By careful impedance matching, (a line impedance of 75Ω was used for all the pulse circuitry), it was possible to minimise the distortion and reflection of fast pulses in the system. By supplying a drive pulse to the active element of the trigger circuit, the delay line was discharged to H.T. earth, supplying the necessary pulse to the grid of the electron gun. The duration of the pulse was determined by the length of the delay line, which gave approximately 10 ns per meter. The minimum pulse duration was set by the turn on time of the active device. A "turn on" time of approximately 60 ns could be achieved with the thyristor while the avalanche transistor could "turn on" in less than 10 ns.

The avalanche transistors used were found to be incapable of handling pulses of duration longer than about 100 ns, due to internal heating at the device junctions. The thyristors on the other hand could withstand a much larger average current. It was therefore decided to use the thyristor circuit for generating drive pulses of duration longer than 100 ns and the avalanche transistor circuit for producing pulses shorter than 100 ns.

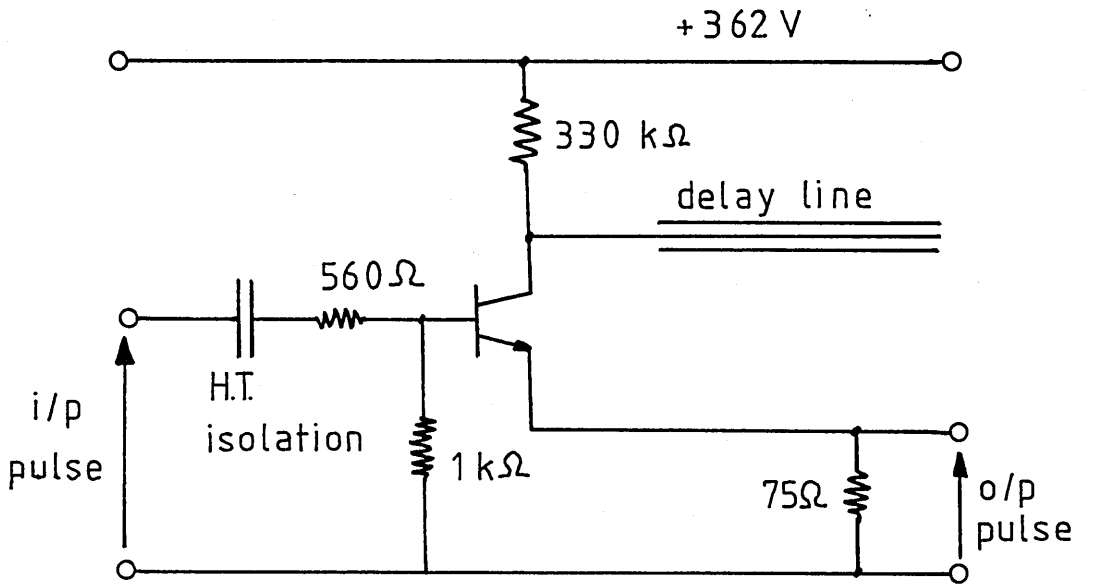

Figure 5.6. Avalanche transistor circuit.

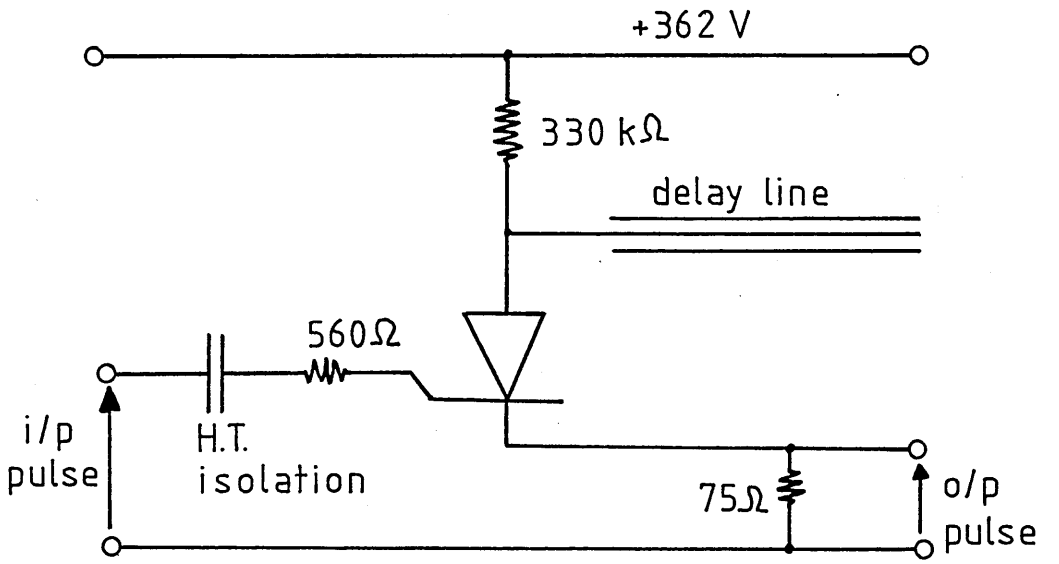

Figure 5.7. Thyristor circuit.

5.3.4 DETECTION EQUIPMENT

The equipment used for detecting "Time of Flight" pulses was controlled by means of three pulse generators, and is shown schematically in figure 5.8. The time relationship between the applied field, the electron bombardment and the detection network trigger pulses is shown in figure 5.9. The purpose of the pulsed field is to minimise the effect of space charge accumulation, and Joule heating within the specimen.

The simplest method of detecting transit pulses involved the use of a storage oscilloscope connected to the bottom contact of the specimen. Generally, the specimen and lead capacitance ($\simeq$100 pF) combined with the input resistance of the oscilloscope (1 MΩ) provided a circuit time constant which was sufficiently long to effect integration of the current pulse. Such integrated current pulses provided a satisfactory means of measuring the transit time when the carrier transport was conventionally dispersive (see figure 5.10), but with the onset of anomalous dispersion, a non - integrated current pulse was desirable in order to obtain the transit time. Furthermore, if a detailed analysis of the shape of the transit pulse was to be carried out, this could only be achieved by studying the non - integrated current pulse.

In order to obtain such non - integrated current pulses, the time constant of the detection network had to be reduced. Since only a marginal reduction in the capacitance could be obtained by shortening cable lengths etc., a significant reduction in the circuit time

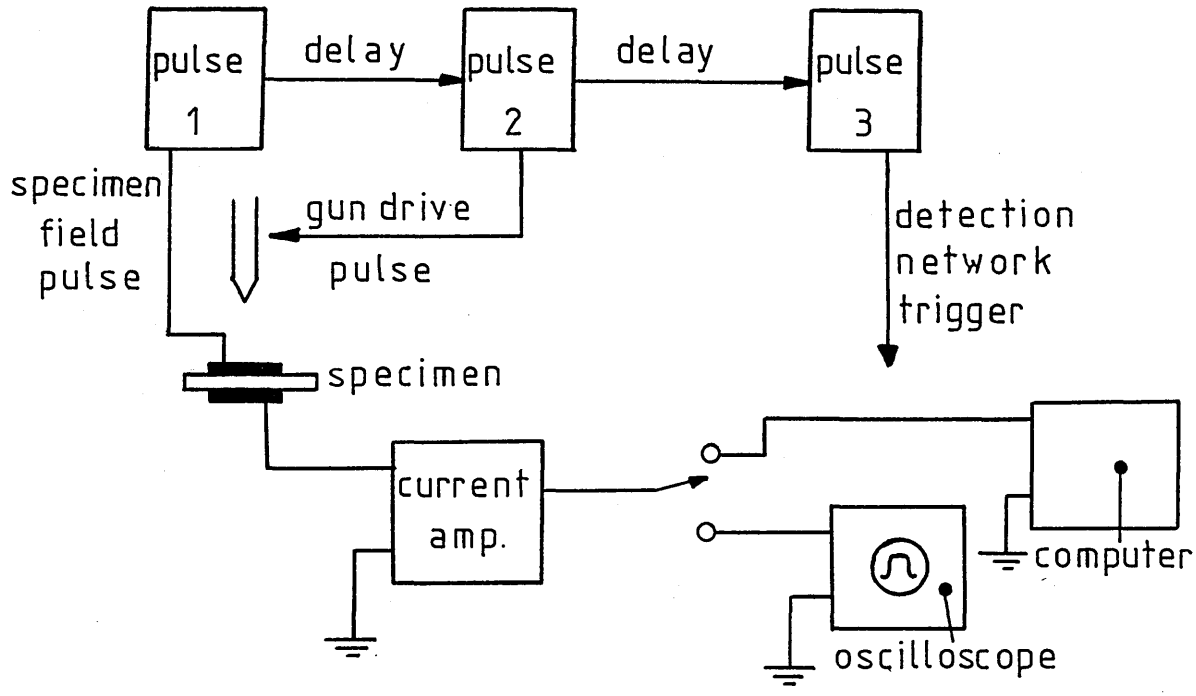

Figure 5.8. Detection network.

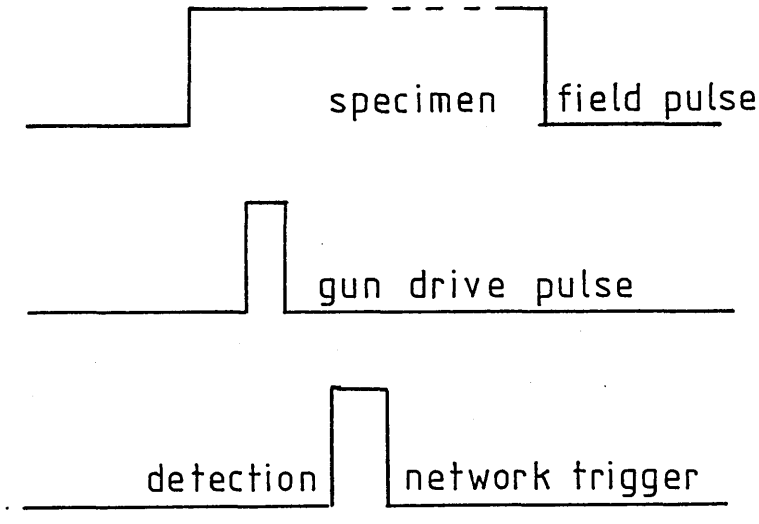

Figure 5.9. Time relationship between the detection network circuit pulses.

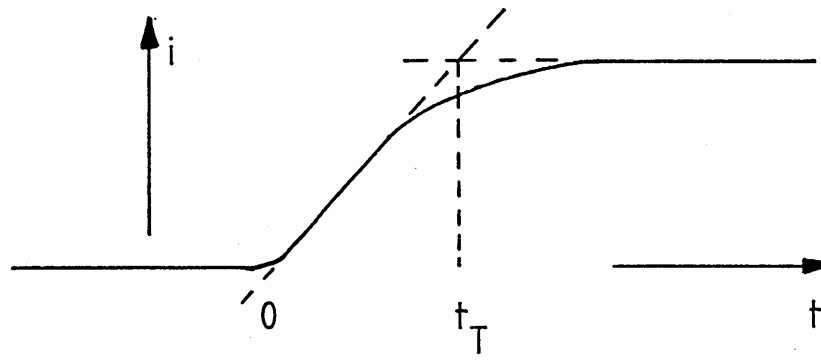

Figure 5.10. Determination of transit time from integrated current pulse.

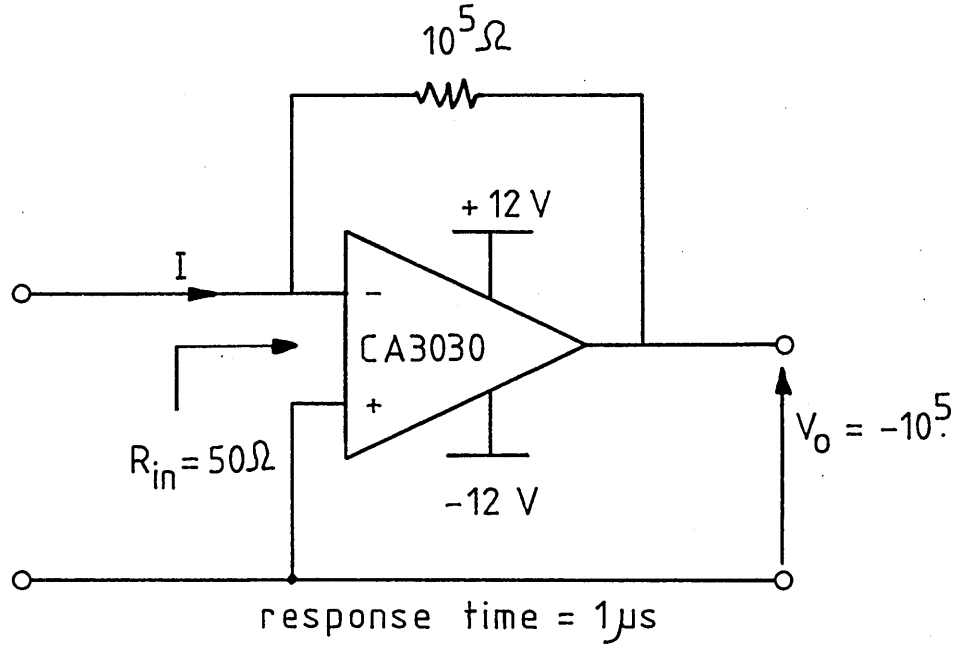

Figure 5.11. Current amplifier.

constant was only obtainable by reducing the effective input resistance of the detection network. This could be achieved in one of two ways. Firstly, the input of the detection network could be shunted by a small value voltage sampling resistor (less than 1 MΩ). Alternatively, a pre - amplifier with a very low input resistance (current amplifier) could be inserted in place of the sampling resistor. Provided that the amplifier used had a sufficiently wide frequency response, the latter choice was much more desirable. Using a shunt resistor reduced the input resistance of the detection network but also resulted in a reduction of the signal amplitude and a degradation of the signal - to - noise ratio. Using a current amplifier, large signals could be obtained which were suitable for analysis. The current amplifier shown in figure 5.11 was employed.

5.4 COMPUTER ANALYSIS OF PULSE SHAPE.

It has been suggested in many publications over recent years (1-5) that a detailed analysis of the shape of the current pulse obtained from the Time of Flight experiment can yield useful information about the distribution of localised states in the mobility gap of amorphous semiconductors. Consequently, one of the aims of this project was to build a system, using a digital computer, to analyse experimental data obtained from the Time of Flight experiment. A block diagram of the system constructed is shown in figure 5.12, and its constituent parts are discussed below.

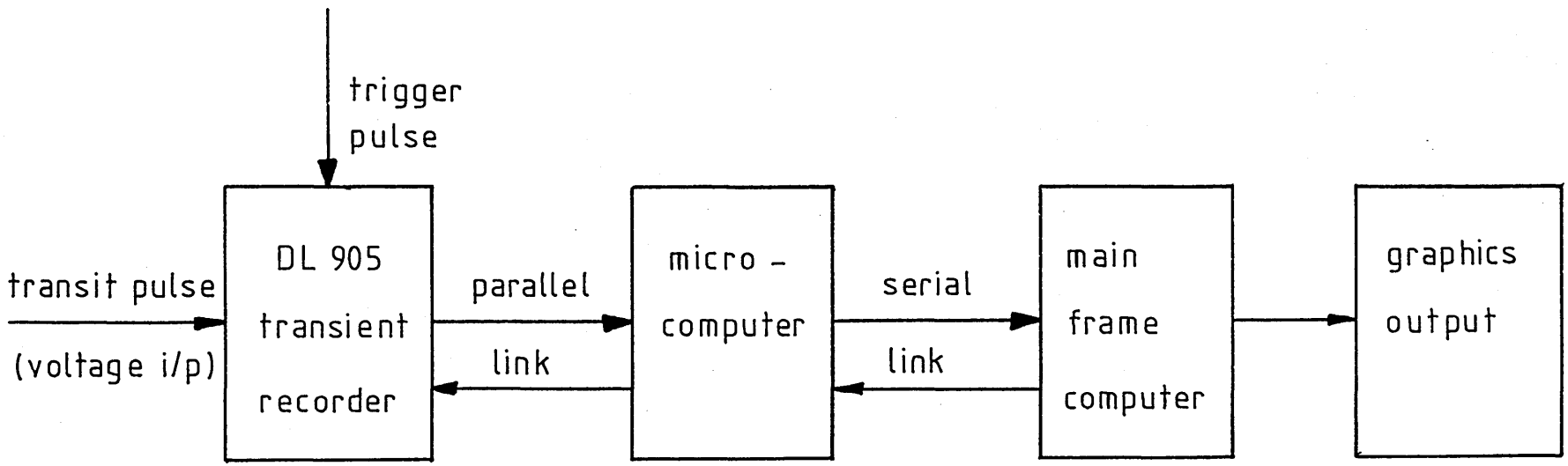

Figure 5.12. Microcomputer controlled transit pulse analysis system.

5.4.1 THE DATALAB DL905 TRANSIENT RECORDER.

The Datalab DL905 transient recorder (DL905) is an instrument capable of storing a waveform in digital form, in 1024, 8 bit words. Information can be clocked into the recorder's memory at rates up to 5 MHz. Therefore, consecutive samples of a waveform can be taken at time intervals ranging upwards from 200 ns. Once stored, this data may be transferred from the DL905 to other instruments via a variety of pre - selected interfaces. In the system designed, digital information in parallel form was transferred to a microcomputer under "Handshake" control.

When computer analysis of a current pulse was required, the output of the current amplifier was switched to the input of the DL905. The DL905 has signal input characteristics similar to those of an oscilloscope (i.e. input resistance 1 MΩ, input capacitance 48 pF).

5.4.2 THE NASCOM II MICROCOMPUTER.

The College's Dec - System - 20 (Dec - 20) main frame computer is capable of displaying and analysing transit pulses obtained from the Time of Flight experiment. However, in order to use these facilities, transit pulses in the form of digital data had to be transferred from the DL905 to the Dec - 20. No suitable interface between the DL905 and the Dec - 20 could be obtained commercially, so it was necessary for one to be designed and constructed. The interface developed was

based on the Nascom II Microcomputer (Nascom), and once completed had many useful facilities.

In order to interface between the DL905 and the Dec - 20, three basic functions were required of the Nascom.

(1). The Nascom had to "make contact" with, and "talk" to the Dec - 20 in a manner similar to that employed by a standard video display unit (V.D.U.). This was necessary in order to set the Dec - 20 into a state suitable for accepting data from the Nascom.

(2). The Nascom had to be capable of loading data from memory of the DL905, into its own resident memory.

(3). The Nascom had to be capable of transferring the contents of its memory, into an opened data file in memory of the Dec - 20.

The procedures used to accomplish the above tasks will be described below.

(1). The standard V.D.U. terminal at Dundee College operates as follows: when a key is depressed on the keyboard, the symbol selected is constructed in ASC II code and transmitted down an RS 232 interface to the Dec - 20. In acknowledgment of reception of this transmitted character, an identical character is sent by the Dec - 20, to the V.D.U., along the RS 232 interface, this reflected character appearing on the V.D.U. screen. If the transmitted character is not recognised by the Dec - 20, a default symbol is returned. In order to

communicate with the Dec - 20, the Nascom had to mimic the above operations. This was achieved using the Nascom's resident RS 232 interface controlled by the machine code program listed in Appendix I. The operation of this V.D.U. mimic program is illustrated by the flow diagram shown in figure 5.13.

(2). The interface between the Nascom and the DL905 (shown in figure 5.14) transmitted data via an 8 - bit (1 word) parallel channel under the direction of four control lines. The Nascom communication was via a Parallel Input - Output chip (P.I.O.) which was an integral part of the micro - computer. The P.I.O was programmed into a configuration having the required number of input and output lines necessary for the transfer task.

To initiate data transfer, the DL905 interface board was activated by setting the DIGITAL OUTPUT ENABLE line high. The DIGITAL OUTPUT REQUEST line was also set high to activate the clock pulses within the interface board of the DL905. In order to obtain data from the DL905 the WORD REQUEST line was pulsed high for a time not less than 200 ns. On this command, data from memory of the recorder was latched onto the 8 - bit parallel data lines. Once this data had stabilised (after a time of about 100 ns) the DATA READY line was set high by the DL905 to indicate to the receiving device that data was available for transfer. After the data had been read, in this case by the Nascom, the WORD REQUEST line was again pulsed high. This reset the DATA READY line low, and allowed the next word of data from the memory of the recorder to be latched onto the data lines. This information was again read by the Nascom once the DATA READY line had

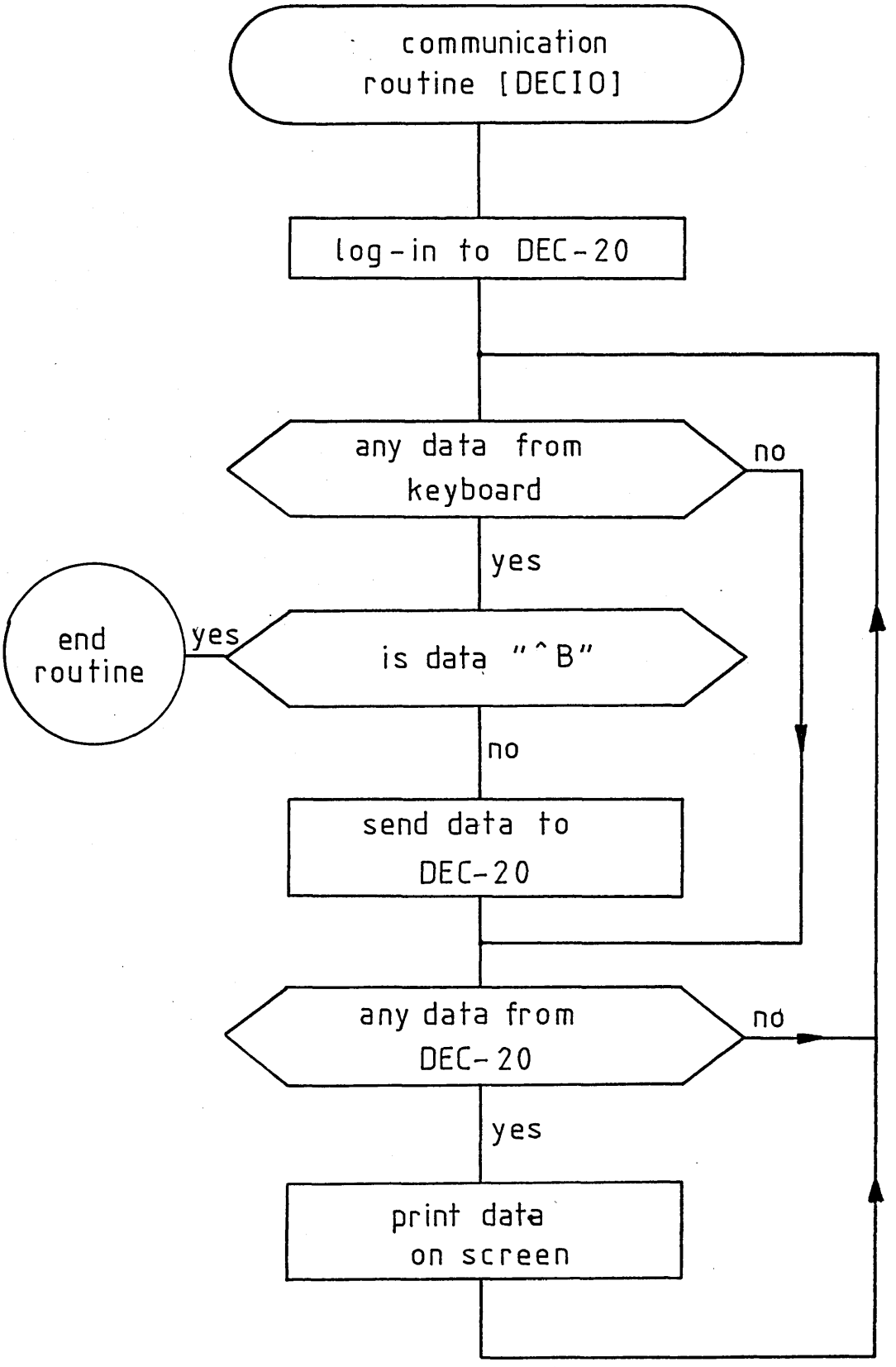

Figure 5.13. Operation of V.D.U. mimic program.

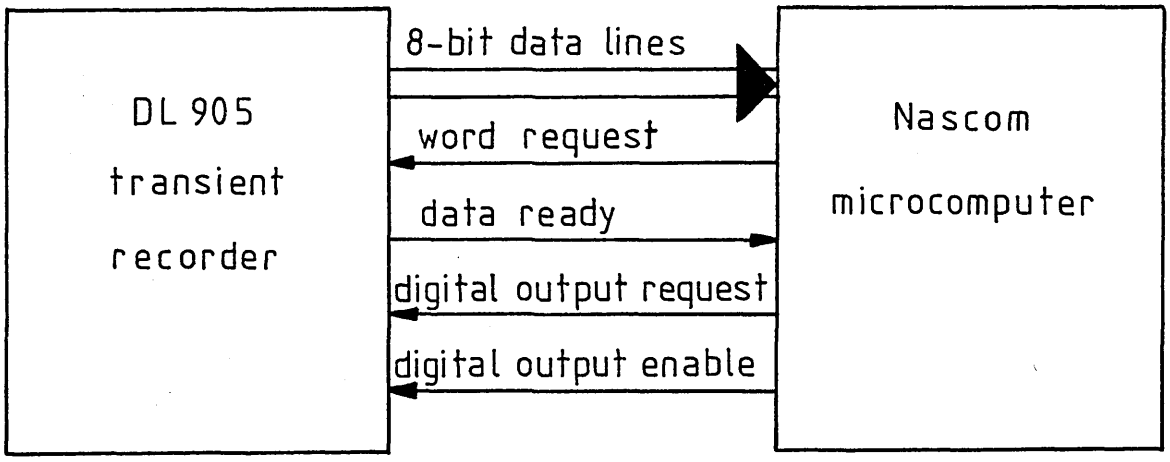

Figure 5.14. DL905 - Nascom interface lines.

gone high. The process was repeated until the complete memory of the DL905 (1024 words) had been transferred to the Nascom.

The software used to control this data transfer is shown in Appendix I, and the operation of the program is illustrated in the flow chart shown in figure 5.15.

(3). The final task of the Nascom was to transfer the information received from the DL905, to a data file within the Dec - 20. As previously mentioned, the interface between a V.D.U. (or Nascom) and the Dec - 20 operates by transmitting and receiving characters in serial ASC II code. The data stored in Nascom, however, was in 8 - bit binary form, and required conversion into Asc II code prior to transmission. This was achieved in a two step process. Firstly, the binary code was converted into two hexadecimal characters, and secondly, the hexadecimal characters were converted into Asc II code. (For example, the 8 - bit binary code 10101001 would be converted into the hexadecimal code C9, the two hexadecimal characters C and 9 being converted into the ASC II codes 43 and 39 respectively. Finally these ASC II codes would be sent to the RS 232 interface for transmission to the Dec - 20).

The Dec -20 had to be suitably programmed in order to accept data sent by the Nascom. Furthermore, the software operating in the Dec - 20 had to run in unison with the software operating in the Nascom. This was essential in order to synchronise the data transfer. Before the relevant programs are discussed, the data format adopted for the transfer operation will be described.

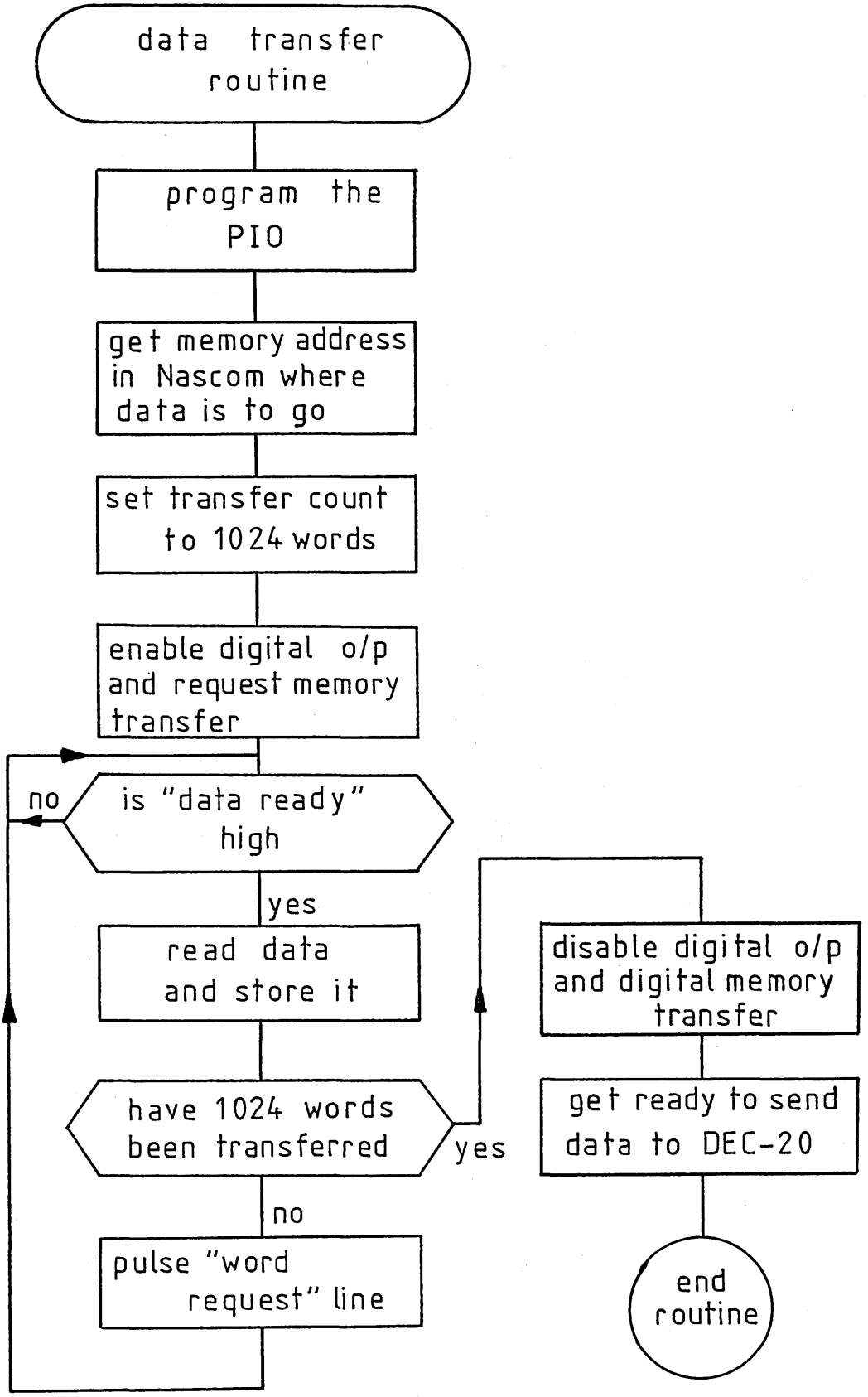

Figure 5.15. DL905 - Nascom data transfer routine.

The data format adopted was that developed by the Intel company, namely "Standard Intel Format". Shown below are representative data configured in that format. It should be noted that all the symbols are in hexadecimal notation.

:10100000112233445566778899AABBCCDDEEFF3B

The first character is a colon indicating the start of a line. The next two symbols (10) indicate the number of memory locations that are represented in the line of information (in this case sixteen). The next four characters specify the location in memory where the first data word has been obtained from (in this case memory location 1000 Hex.). The next two characters are used as a buffer and have no numerical significance. The following sixteen pairs of characters are the contents of the memory locations commencing at the previously specified address. The final two symbols are a checksum. The checksum is generated by adding together, in hexadecimal form, all the information present in the line (excluding the checksum). The total of this addition (neglecting overflow) is transmitted at the end of the data line and provides a means of checking the validity of the transmitted data.

The flow diagram shown in figure 5.16 illustrates the operation of the programs developed both for the Nascom and for the Dec - 20. Inspection of these flow diagrams reveals that both programs are interlinked and run together, performing one overall task. The "locking" of the programs is achieved by sending suitable control characters between the Nascom and the Dec - 20. Listings of the

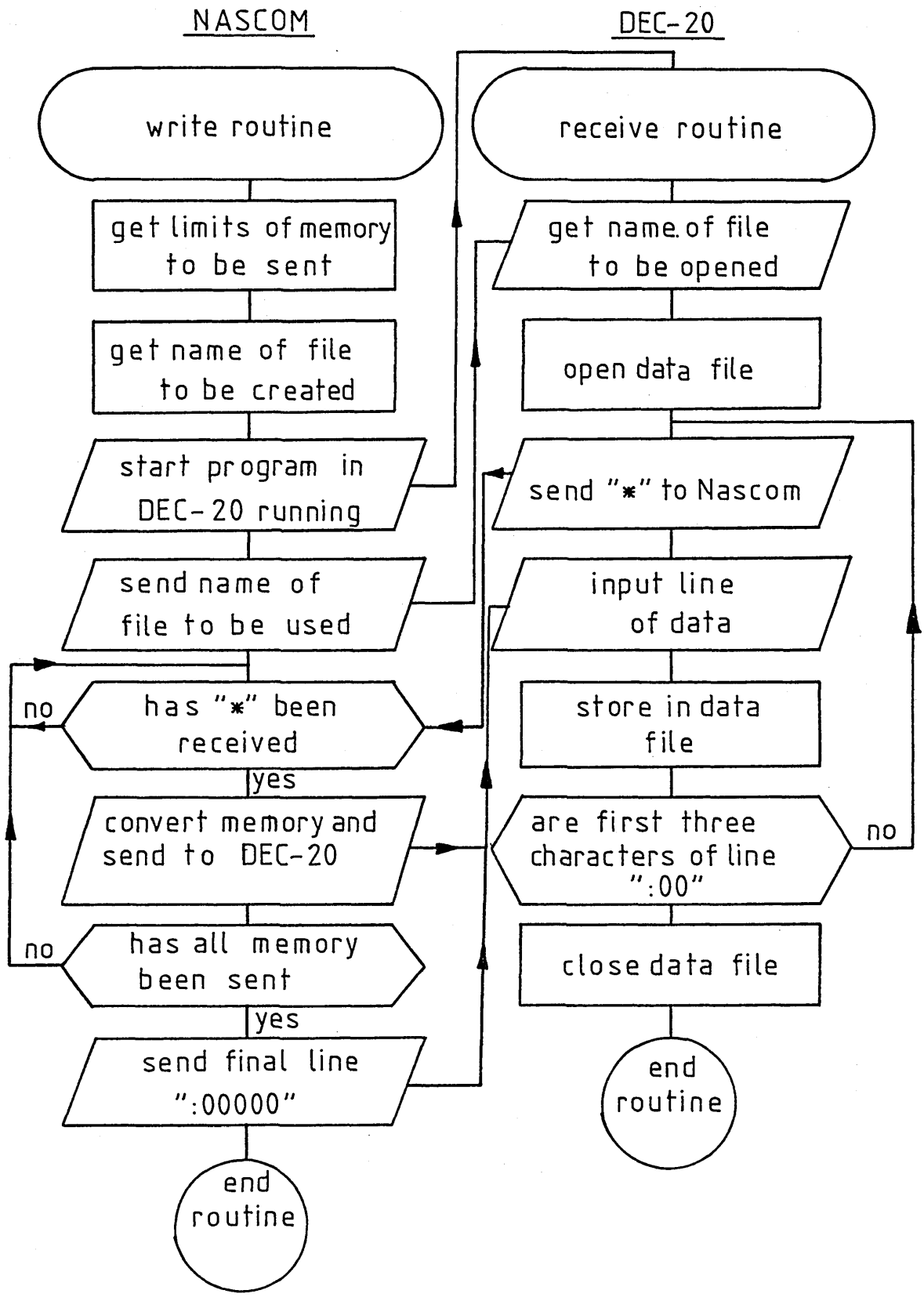

Figure 5.16. Nascon - Dec System 20 data transfer routine.

Nascom and the Dec - 20 software are given in Appendix I and Appendix II respectively.

5.4.3 THE DEC - 20 ANALYSIS ROUTINES.

At this stage in the development of the computer analysis system, there exists a data file, configured in standard Intel format, in memory of the Dec - 20. The remaining requirements of the Dec - 20 can be split into two sections. Firstly, the data file in Intel format must be converted from hexadecimal form into a list of decimal numbers suitable for use in a standard Fortran program. Secondly, these data must be plotted both on linear axes of signal amplitude versus time, and on logarithmic axes of log (signal amplitude) versus log (time).

Consider firstly the task of converting the data file in Intel format into a list of decimal numbers. This was achieved using the program listed in Appendix III. The program operates by interrogating the hexadecimal data file line by line. It strips the leader information from the start of the line (i.e the colon, start of line address and buffer) and from the end of the line (i.e. the checksum). The program selects the remaining data in pairs of hexadecimal numbers converting them into decimal numbers. The decimal numbers are entered sequentially into a newly created data file, the process being repeated until all the information has been converted and stored.

The required graphs were plotted using the Fortran program listed in Appendix IV. This program calls upon the facilities of a "GHOST" graphics package resident on the Dec - 20. The program operation is outlined below.

Firstly, information from the data file of decimal numbers is entered into arrays defined within the program. Secondly, the starting point of the transit pulse within the data, and the correct base line value is automatically determined. This information is essential in order to correctly define the logarithmic graph. Finally, the data are arranged on both linear and logarithmic axes and plotted on a high resolution drum plotter.

5.4.4 CONCLUSIONS.

Throughout the duration of this project, the computer analysis system has been extensively tested and upgraded. It has proven versatile and become invaluable for recording transient waveforms obtained from a number of experimental techniques (especially waveforms produced from the transient photoconductivity experiment). At present, the system is available on three Nascom micro - computers and is in regular use by research workers studying in this laboratory.

The system was used to collect Time of Flight data from thin films of amorphous Arsenic Selenide and these results have been published (6).

5.5 STEADY STATE AND TRANSIENT PHOTOCONDUCTIVITY.

The basic requirement of a photoconductivity experiment, steady state or transient, is to observe the change in conductivity when a specimen is illuminated with photons. The equipment necessary for performing these experiments will be described in this section.

5.5.1 THE LIGHT SOURCE.

There are a number of different methods for producing photons such as electric filaments, lasers, light emitting diodes (l.e.d.), gas discharge lamps, etc., but before a source was chosen for this project a number of factors had to be considered. Firstly, since a transient experiment was envisaged, the source chosen had to be capable of continual pulsing, on and off, with mark and space times related to the transient time constants of the semiconductors under investigation. For complete versatility this implies that the source should be capable of generating photons in a form ranging from very short pulses at one extreme, to a steady flow at the other extreme.

Secondly, in order to successfully perform a transient photoconductivity experiment, it was necessary to ensure that the response of the specimen under investigation was not distorted by transient electrical signals associated with the illumination source. This problem could be avoided by making sure that rise and fall times related to turning on and off the illumination source, were considerably shorter than rise and fall times associated with the

growth and relaxation of the semiconductor photoconductive signal.

Thirdly, it was necessary to have control over the intensity of illumination generated by the source. This was essential in order to determine the dependence of the sample photoconductivity upon illumination intensity.

Finally, the photon energy of the illumination source had to be matched to the energy gap of the material under investigation. If a photon energy much less than the energy gap was used, only a small percentage of the incident light would be absorbed (mainly involving localised states in amorphous semiconductors) and the resulting photoconductive signal would be very small. Conversely, using a photon energy much greater than the energy gap would result in all the photons being absorbed in a thin layer close to the illuminated surface. Such a beam might produce a large photoconductive signal, but its interpretation may be complicated by the fact that only a small percentage of the specimen had been illuminated. Such a problem becomes acute when the absorption depth of illumination is comparable to the depth to which states exist in a semiconductor due to surface deformation. Under these conditions, the illumination would not probe the bulk properties of the semiconductor, but the photoconductive signal produced would reflect the photoresponse of the surface layer.

Under normal conditions it is necessary to avoid the extreme situations mentioned above, and in general the specimen should be illuminated with photons of energy somewhere between these limits.

In practice, in order to facilitate ease of detection and analysis, it is advantageous to maximise the amplitude of the photoconductive current generated in a given sample. This can best be achieved by optimising two important parameters. Firstly, the photon energy of the source should be adjusted so that electron - hole pairs are created with a quantum efficiency close to unity. This condition can normally be achieved by illuminating the specimen with photons of energy slightly greater than that of the specimen energy gap (although in some materials the quantum efficiency does not approach unity until the photon energy is about 0.5 eV above that of the energy gap: see section 2.3.2). Secondly, the amount of light lost due to transmission through the semiconductor should be reduced to an acceptable level. In doing this however, care must be taken not to approach the conditions mentioned previously, where all the light is absorbed close to the specimen surface.

The materials to be investigated in this study were alloys based on a - Si:H, which, depending upon preparation conditions and dopant levels, had optical gaps of around 1.7 eV. A light source was therefore required having a photon energy greater than 1.7 eV. It was found that high power light emitting diodes were the best suited source for the type of work to be carried out. This was mainly due to the fact that the l.e.d.s used were small and versatile, had fast response times, and were easily mounted into the experimental rig.

5.5.1.1. HIGH POWER LIGHT EMITTING DIODES.

Two light emitting diodes were chosen for use both in steady - state and in transient photoconductivity measurements. The diodes were manufactured by the STANLEY ELECTRIC COMPANY, the ESPY5501 model emitting in the yellow region of the visible spectrum, and the 591519G model emitting in the red region. The relevant manufacturers' specifications for the diodes are given in table 5.1.

5.5.2 SPECIMEN ILLUMINATION.

Photons were transmitted to the specimen using a 9 mm diameter light pipe consisting of a bundle of optical fiber strands bonded together in resin. The light emitting diode was mounted in a holder outside the vacuum environmental chamber, the fiber - optic pipe serving as a vacuum seal between the diode and the sample. To maximise the light reaching the specimen, the diode was butted against one end of the light pipe, the other end being positioned about 1 mm from the specimen. Care was taken not to allow the light pipe to make contact with the specimen since under this condition the pipe could act as a heat sink for the specimen causing errors in temperature measurements. The experimental set - up used is shown schematically in figure 5.17.

Diode	ESPY 5501	59151G
Forward current (mA)	20	20
Typical intensity at 20 mA (mcd)	160	500
Peak wavelength (nm)	550	660
Spectral line half width (nm)	30	30

Table 5.1. Relevant diode specifications.

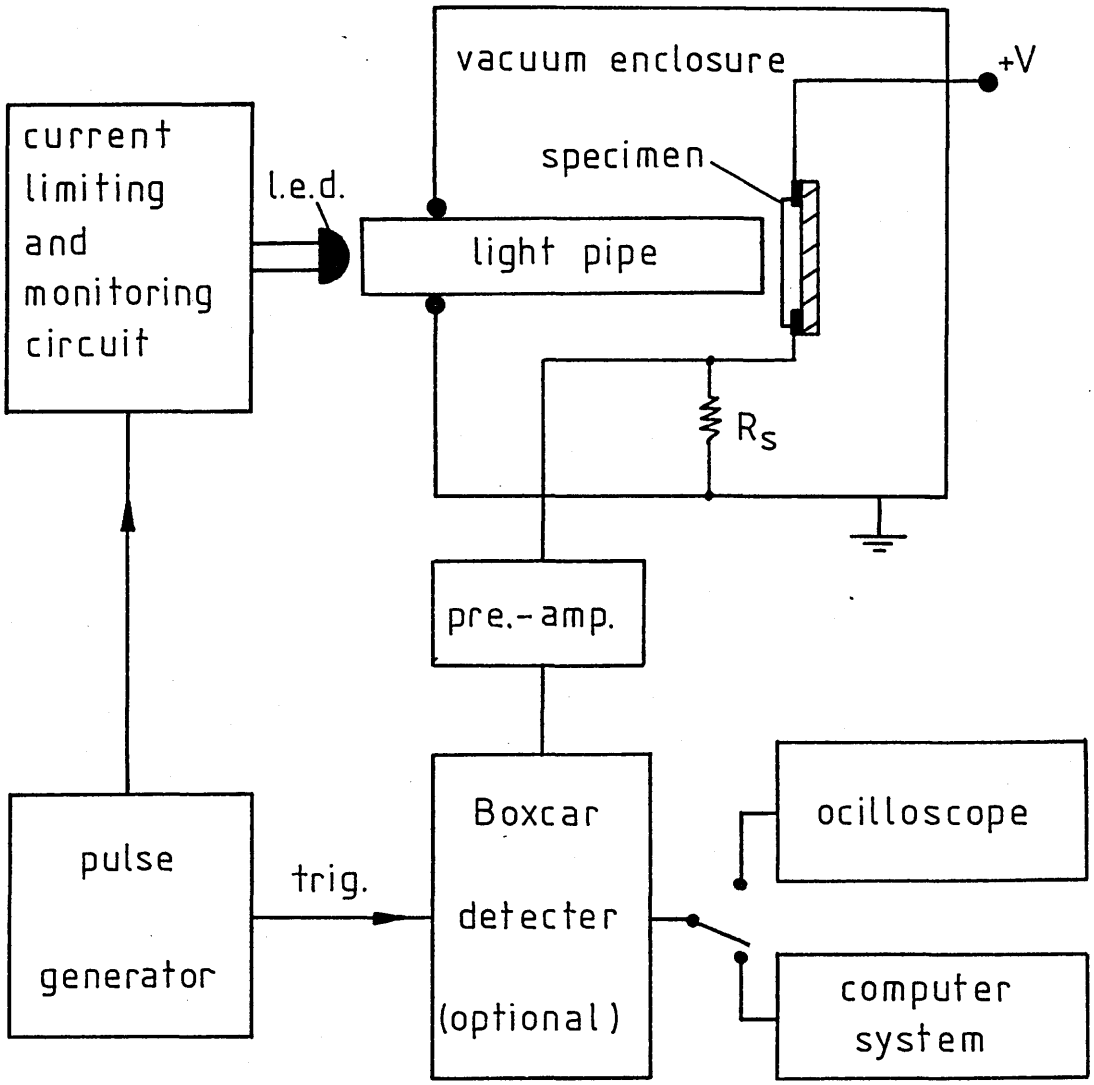

Figure 5.17. Experimental set - up for the measurement of photoconductivity.

5.5.3 ILLUMINATION SOURCE CALIBRATION.

The flux output of the diode - light - pipe assembly, as a function of diode forward current, was required in units of photons cm^{-2} s^{-1}. Figure 5.18 shows the circuit used to monitor the diode forward current under both test and operational conditions. A digital voltmeter (D.V.M.) measured the voltage developed across a precision 2.12 Ω resistor. The variable voltage source could be either pulsed or continuous and the series resistor R_S limited the forward current of the diode to its maximum rating.

The output from the light pipe was monitored using a Hewlet - Packard 5082 - 4207 Silicon pin photodiode, connected in the configuration shown in figure 5.19. The response time of the photodiode was less than 1 ns and the operational amplifier (OP-37; Precision Monolithics incorporated) had rise and fall times less than 3 ns. The overall response time of the photo - detector circuit was less than 10 ns.

The spectral response of the photodiode extends over the wavelength range 400 nm to 1100 nm and is shown in figure 5.20. The maximum flux responsivity occurs at 770 nm and is 0.5 μA per μW. The active surface area of the diode is 8×10^{-3} cm^2 this leading to a maximum power sensitivity of 4×10^{-3} A $W^{-1} cm^{-2}$. Translating this into the required units of photon flux density required a knowledge of the photon energy at the wavelength used. This is given by

$$E = \frac{hc}{\lambda} \qquad (5.1)$$

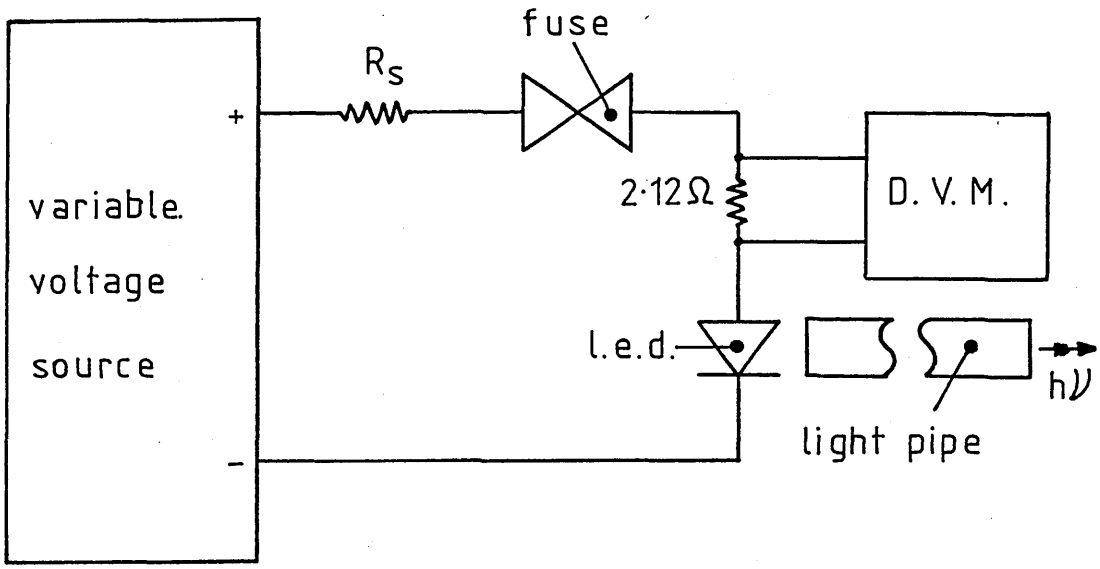

Figure 5.18. L.e.d. current monitoring circuit.

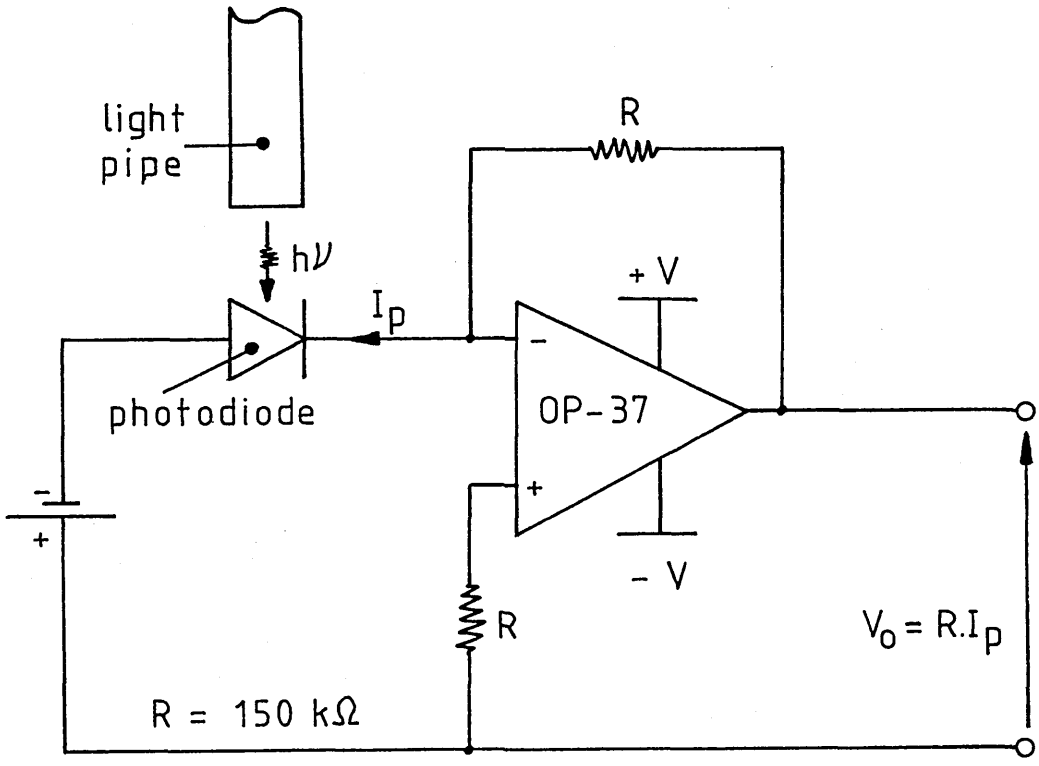

Figure 5.19. Photon flux measurement circuit.

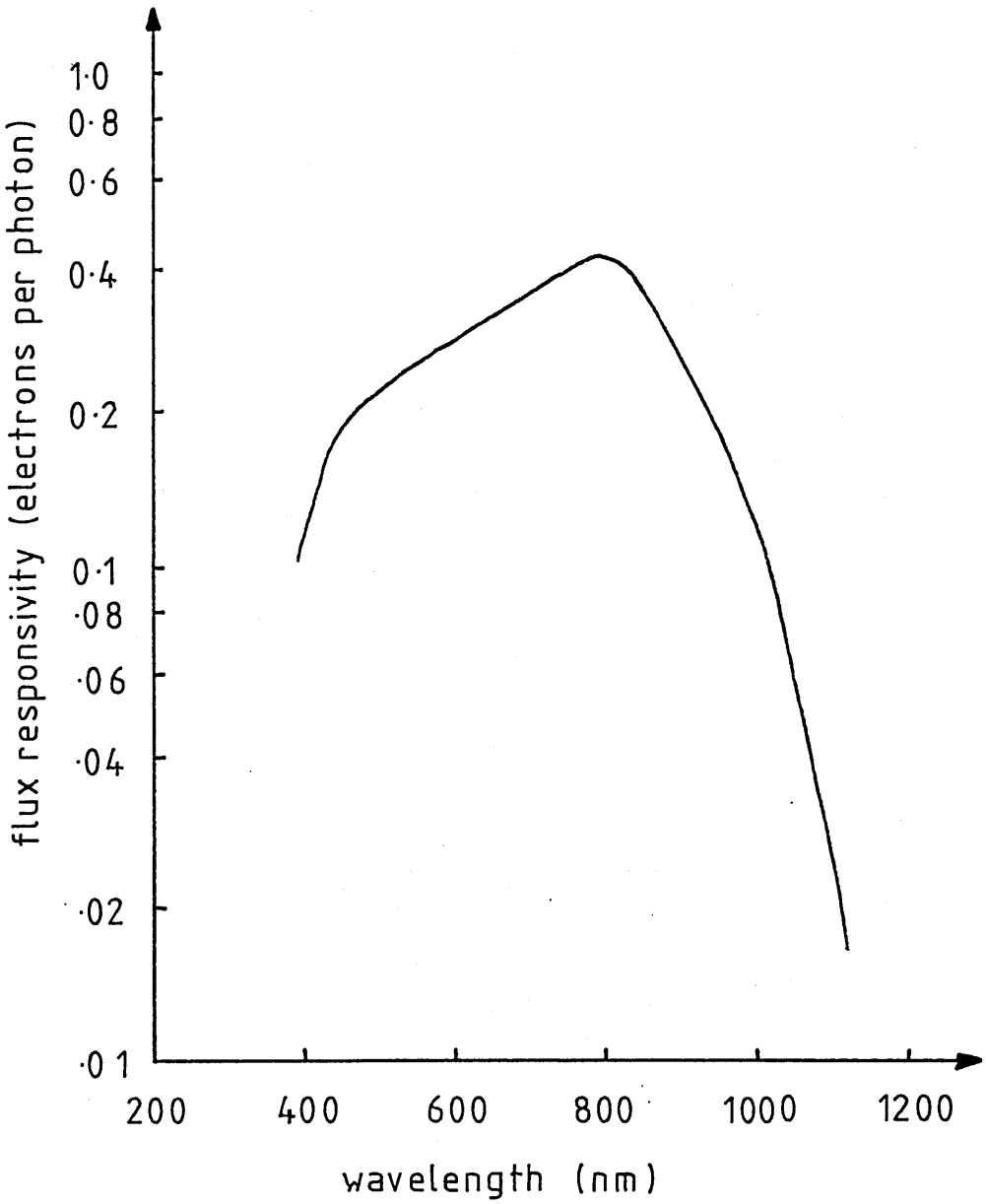

Figure 5.20. Spectral response of the Hewlet - Packard 5082 - 4207 Silicon pin photodiode.

and using the appropriate units

$$E = \frac{1.99 \times 10^{-16}}{\lambda(nm)} \quad \text{Joules} \quad - \quad (5.2)$$

Combining equation 5.2 with the power density sensitivity of the photodiode, and with the magnitude of the output voltage developed from the photo - detector circuit (figure 5.19) results in the relationship:

$$F = 4.2 \times 10^{12} \frac{V_o \lambda(nm)}{R(\mu A \mu W^{-1})} \quad \text{photons } cm^{-2} s^{-1} - (5.3)$$

where R is the flux responsivity of the photo - diode at the wavelength used (see figure 5.20).

Figures 5.21 and 5.22 show the calibration curves obtained for the red and for the yellow light emitting diodes respectively, when operating under steady state conditions. At all times during calibration and subsequent use the diodes were held in a fixed position against the fiber - optic light pipe, and the calibration curves shown refer to the photon output from the end of the light pipe. It can be seen that a wide range (10^{11} to 10^{17} photons cm^{-2} s^{-1}) of photon flux density was available, which could be easily controlled and monitored.

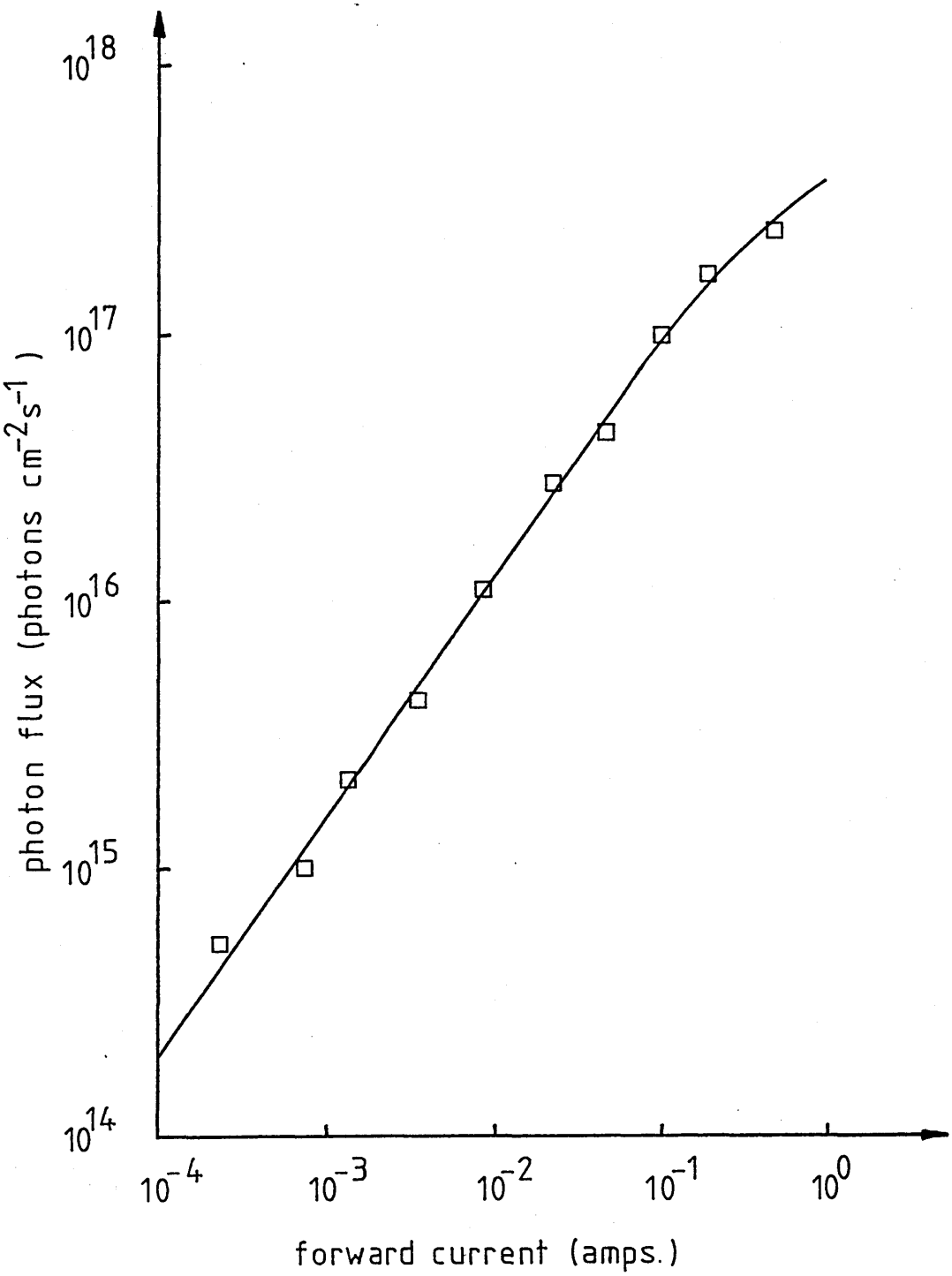

Figure 5.21. Photon flux output from light pipe versus diode forward current for the red l.e.d. (59151G).

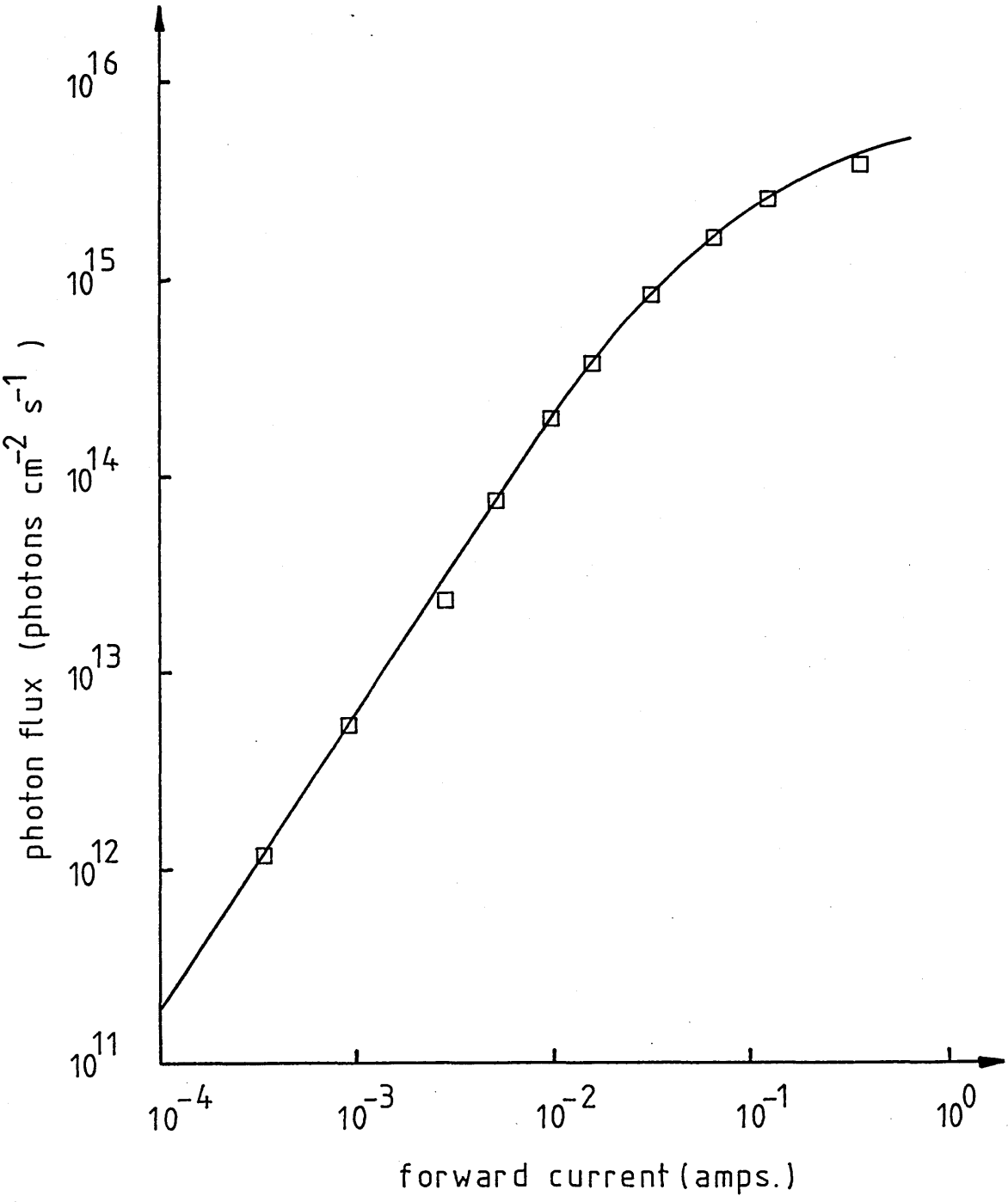

Figure 5.22. Photon flux output from light pipe versus diode forward current for the yellow l.e.d. (ESPY 5501).

5.5.4 STEADY STATE PHOTOCONDUCTIVITY.

Three methods (two d.c and one a.c.) were used to measure the steady state photocurrent, the choice depending upon the level of "background" dark current. The first d.c. method was used when the dark current was small compared to the photocurrent. A d.c. voltage source supplied a constant field to the specimen and the total current under steady state illumination was measured using a Keithley 610C electrometer. The photocurrent was obtained by making a small correction for the known dark current. i.e.

$$I_P = I_T - I_D \qquad - \qquad (5.4)$$

where I_P is the photocurrent, I_T is the total measured current under photoexcitation, and I_D is the known dark current.

The second d.c. method was used when the photocurrent was small compared to the dark current. The method employed a TEKTRONIX 7632A oscilloscope fitted with a 7A22 differential amplifier. The specimen current was fed into the non - inverting input of the amplifier (1 MΩ input resistance), the dark current being "backed off" by applying a suitable voltage to the inverting input. So long as the specimen resistance was large compared to the input resistance of the amplifier the photocurrent could be obtained using the relationship:

$$I_P = \frac{V}{10^6} \quad \text{Amps.} \qquad (5.5)$$

where V is the voltage developed across the amplifier input.

The a.c. method was used when the dark current produced a voltage across the amplifier input too large for "backing off". Under these conditions pulsed illumination was used. The pulse width was adjusted to allow the photocurrent to reach its steady state value. The total specimen current was sampled using a 1 MΩ resistor, the voltage developed across this resistor being fed into the input amplifier of an oscilloscope, through a blocking capacitor. The capacitor value was chosen so that insignificant "droop" occurred while the specimen current reached its steady value during the pulse "on" time. The d.c. voltage due to the dark current was blocked by the capacitor.

5.5.5. TRANSIENT PHOTOCONDUCTIVITY.

Information can be obtained from a transient photoconductivity experiment by investigating the shape of the photocurrent versus time waveform produced by pulsing the illumination source on then off. In order to accurately reproduce the photoconductive response of the specimen, it was necessary to ensure that the rise and fall times of the photocurrent were not distorted by the response time of the detection circuitry.

The simplest method employed for observing the photocurrent response was to allow the current to flow through the 1 MΩ input resistance of the Tektronix oscilloscope amplifier previously mentioned. Under these circumstances the circuit response time was

found to be about 100μs. This was due to the 1 MΩ amplifier input resistance, shunted by a capacitance of approximately 100 pF due to the capacitance of the sample, the co - axial signal cable and the amplifier input.

At room temperature and below, the materials investigated in this study generally had photocurrent rise and fall times of the order of tens of milliseconds, permitting the use of the simple detection method mentioned above. However, when investigating samples with high dopant levels, or when performing measurements above room temperature, it was found that the photocurrent rise and fall times became comparable with the response time of the detection network. Under these conditions it was necessary to use a technique to reduce the circuit time constant. The method chosen employed the use of the F.E.T. bootstrap pre - amplifier, shown in figure 5.23.

The measured characteristics of the pre - amplifier were a gain of 0.98, input and output resistances of approximately 11MΩ and 50Ω respectively, and an overall response time of 10 ns. A reduction in the detection circuit response time was obtained using this pre - amplifier by minimising the shunt capacitance (C_S) across the sampling resistor (R_S). This was achieved by mounting the pre - amplifier close to the specimen, hence reducing the input stray capacitance to about 10 pF. This resulted in an overall circuit response time of approximately 10μs when a 1 MΩ sampling resistor was used.

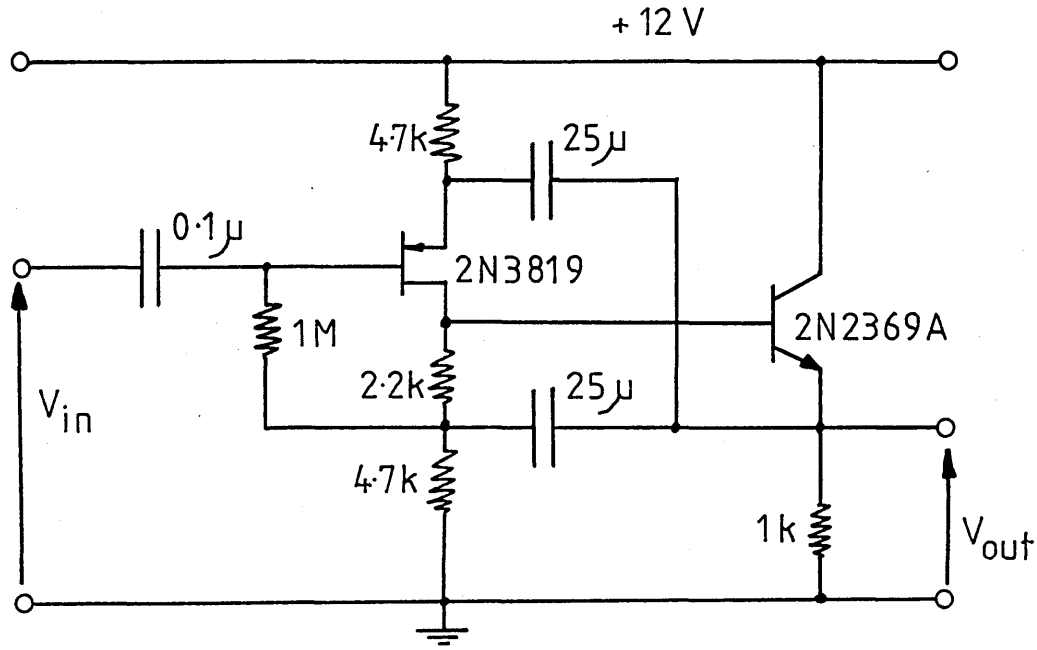

resistance in Ohms

capacitance in Farads

Figure 5.23. F.E.T. bootstrap pre-amplifier.

Voltage gain = 0.98

Input resistance = 11 MΩ

Output resistance = 50Ω

Response time = 10 ns

Under all measurement conditions, the circuit response time was at worst three times shorter than the photoconductive response time of the specimen. However, if necessary, the circuit response time could have been reduced further by reducing the size of the sampling resistor R_S. This was generally avoided since reducing R_S had an adverse effect on the signal to noise ratio and the signal amplitude at the output.

5.6 OPTICAL ABSORPTION.

Optical transmission measurements were performed on thin film specimens mounted in the sample holder of a PYE UNICAM spectrphotometer, (type SP6, model 250). The instrument was calibrated over the wavelength range 400 nm to 950 nm making it suitable for studying the materials used in this project. Light from the monochromator slit was focused on the detector both with and without the specimen in its path, and from the measured light intensities the absorption co - efficient of the film was calculated. The light intensity I, transmitted through a specimen of thickness t, is given by the expression (neglecting reflections and interference)

$$I = I_o \exp(-\alpha t) \qquad - \qquad (5.6)$$

where I_o is the incident light intensity, and α is the absorption co - efficient of the film material. By measuring both I and Io, for a film of known thickness, it was possible to calculate α from the above relationship. Attempts were made to account for the effects of reflections and interference, these being discussed in Chapter 6.

REFERENCES CHAPTER 5

(1) Spear W.E., J. Non-Cryst. Sol. 1, 197, (1969).

(2) Marshall J.M., Phil. Mag. 36, 4 , 956, (1977).

(3) Marshall J.M., Phys. Stat. Sol. A12, 181, (1972).

(4) Pfister G., Phys. Rev. Lett. 36, 5 , 271, (1976).

(5) Pfister G., Scher H., Proc. 7th Int. Conf. on Amorphous and Liquid Semiconductors, (Ed. Spear W.E.), p.197, (1977).

(6) Sharp A.C., Marshall J.M., Fortuna H.S., J. De Physique C4, 10, 42, p.159, (1981).

CHAPTER 6

EXPERIMENTAL RESULTS AND DISCUSSION.

This Chapter presents and discusses experimental results obtained during the investigation. The Chapter is divided into three main sections. Section A presents results obtained from thin films of amorphous Selenium. These results are primarily used for characterising the "Time of Flight" apparatus developed during the study. Section B presents results for both unhydrogenated and Hydrogenated films of a - Si. These results are used in order to characterise the deposition conditions employed in the Nordico sputtering system, in terms of the electronic transport properties of the material prepared. Section C presents results for both Antimony and Aluminium doped films of a - Si:H.

SECTION A.

6.1 AMORPHOUS SELENIUM - RESULTS.

Specimens of a - Se were prepared from the melt and formed into thin sandwich cell structures (see Section 4.2). The Time of Flight experiment was carried out on these samples over the temperature range 130K to 300K.

Figure 6.1 illustrates a typical transit pulse obtained at temperatures above about 190 K. In this temperature region transient current pulses were found to be conventionally dispersive and the carrier transit time could be determined from the current trace displayed on linear axes of current as a function of time. For such conventionally dispersive transport the carrier transit time is normally defined as "the time at which the transient current falls to 50 % of its quasi - thermal equilibrium value". This transit time is marked $t_{50\%}$ in figure 6.1, and the physical significance of this fiduciary mark is that it denotes the time at which 50 % of the excess drifting carriers have been extracted from the specimen by the back electrode. An alternative definition of the transit time is "the time at which the transient current pulse first begins to decrease from its quasi - thermal equilibrium value". The transit time defined in this manner is marked t_{τ} in figure 6.1, and the physical significance of this fiduciary mark is that it denotes the time at which the first few percent of drifting excess carriers reach the back electrode. Both of the above definitions of the transit time are valid, and both lead to the same temperature dependence of the mobility. However, for reasons which will be outlined below the latter definition of the transit time will be employed.

At temperatures below about 190 K, the amount of dispersion in the carrier transit pulse rapidly increases, leading to the observation of current pulses typical of that shown in figure 6.2(a). This figure displays an anomalously high degree of transit pulse dispersion and no visible "break" in the current pulse, associated with carriers reaching the back electrode, can be observed. Closer

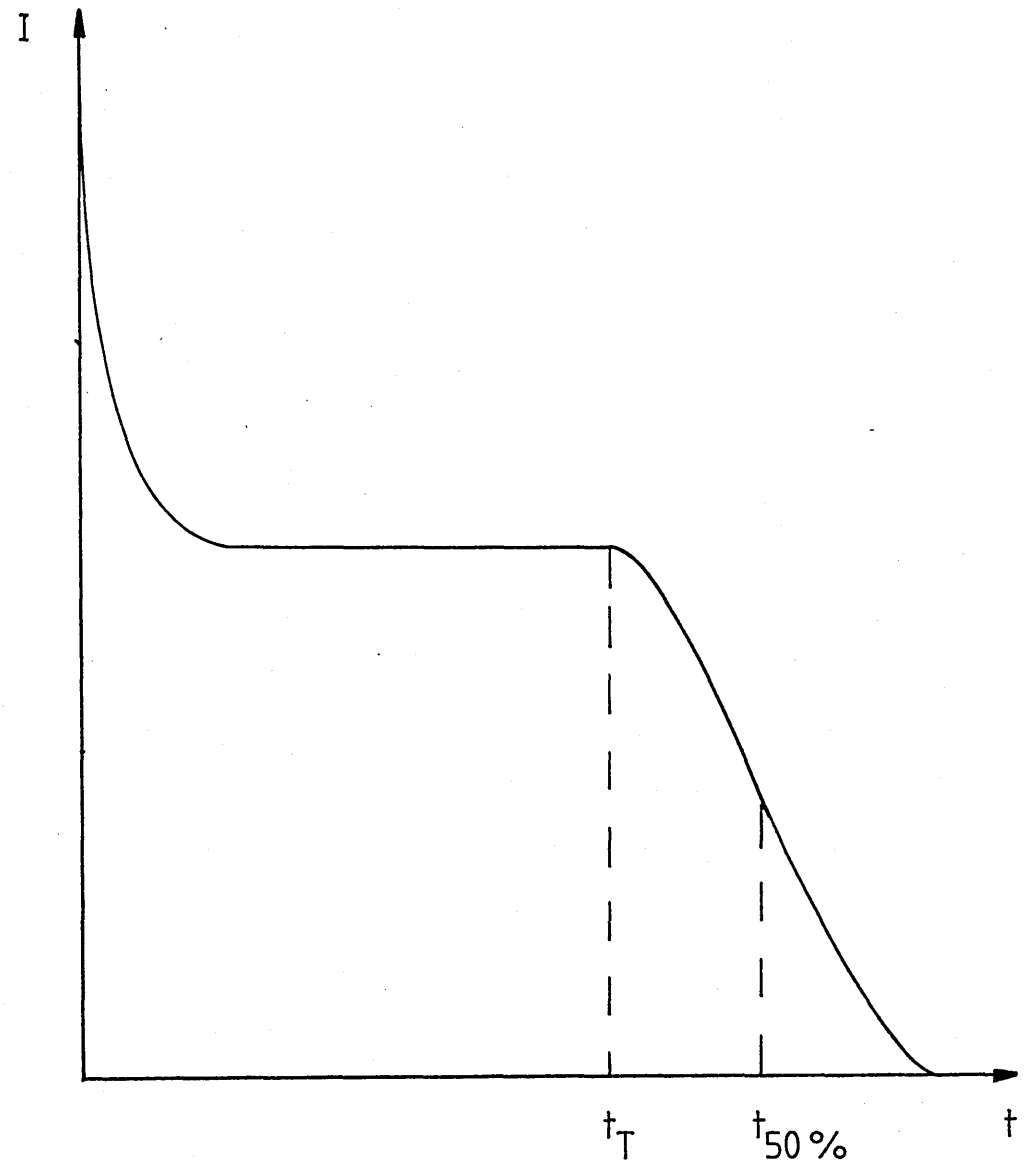

Figure 6.1. Typical high temperature hole transit pulse for a-Se. t_T and $t_{50\%}$ are defined in the text.

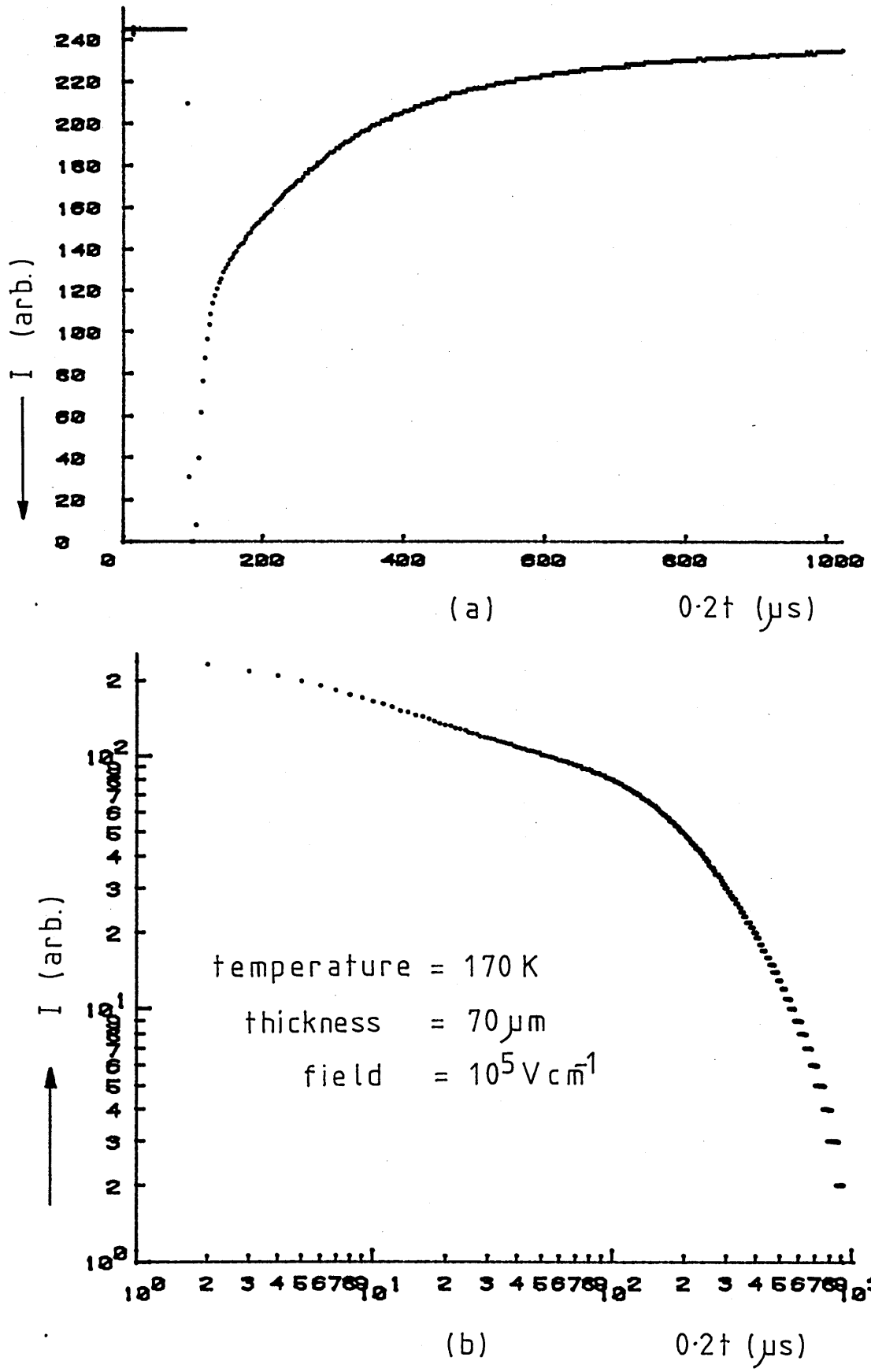

Figure 6.2. Typical low temperature hole transit pulse for a-Se displayed on (a) linear axes and (b) logarithmic axes of current and time.

examination of such current pulses, however, has suggested (see section 2.5 for a fuller description) that re - plotting with logarithmic axes of current and time (figure 6.2(b)) establishes the presence of two approximately linear regions, for times shorter than and longer than the position of the "knee" (discontinuity in gradient) in the transit pulse. Obviously, the large amount of dispersion implies that the transit time of individual carriers will be greatly spread, but the position of the "knee" can be analysed in terms of the transit time of the fastest few percent of drifting carriers. Thus, in order to maintain a consistent definition of the transit time throughout the complete temperature range investigated the above definition of the transit time must be employed for both conventionally and anomalously dispersive transport.

Figure 6.3 shows an Arrhenius plot of the hole drift mobility in a - Se for a specimen of thickness 70 microns at an applied electric field of 10^5 V cm^{-1} . Figure 6.4 illustrates typical current pulse shapes observed at a number of temperatures and fields. The features of the Arrhenius plot are qualitatively similar to those observed by Pfister (1). Below about 250K the mobility falls off exponentially with inverse temperature with an activation energy of E_a = 0.28 eV. At high temperatures the mobility appears to approach saturation in the neighborhood of the glass transition temperature at approximately 300K.

Figure 6.5 shows the values of the dispersion parameter, α , as determined from the initial slope of the log(i) - log(t) graph, as a function of temperature. The values of α calculated from the final

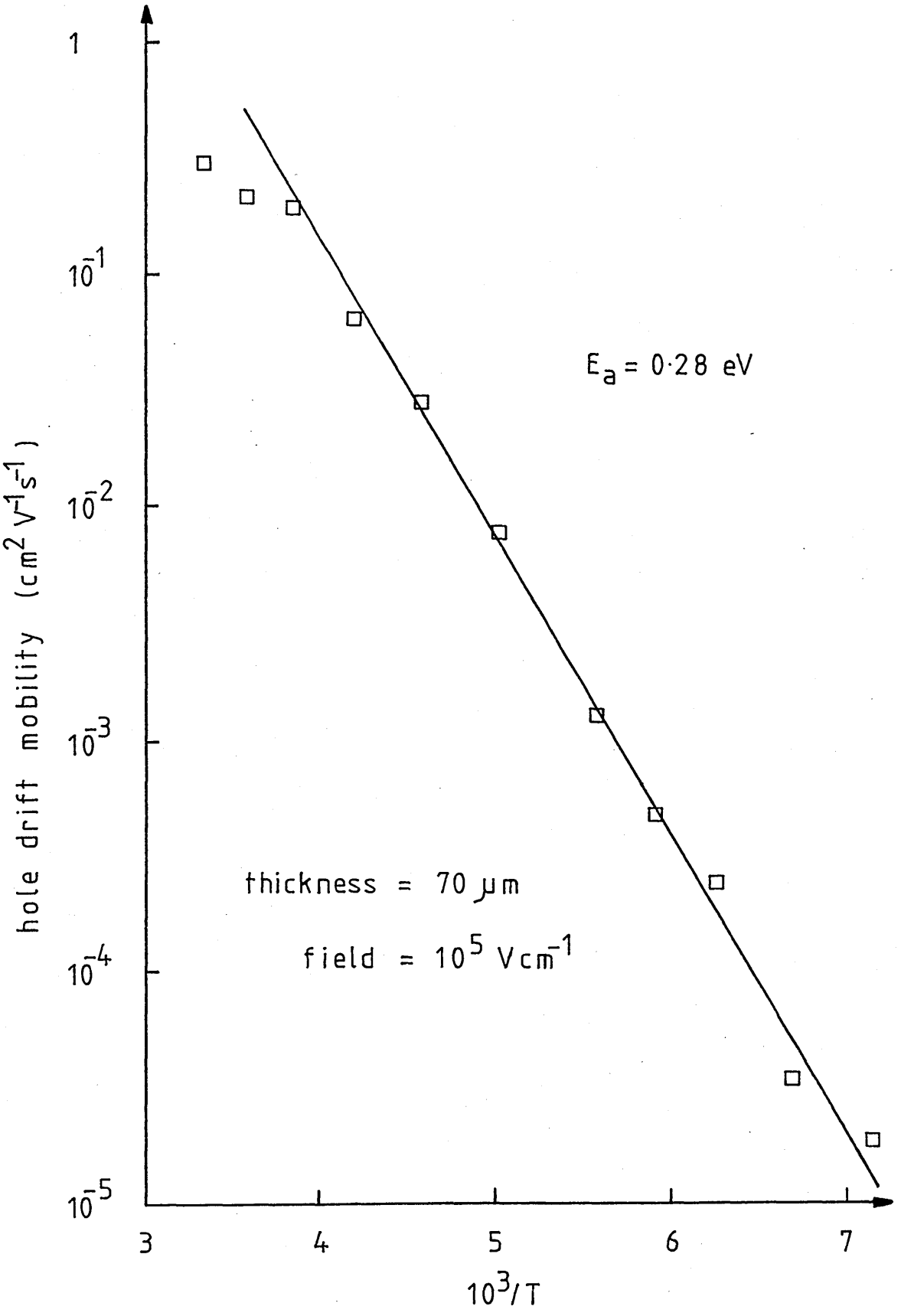

Figure 6.3. Arrhenius plot of the hole drift mobility for a-Se.

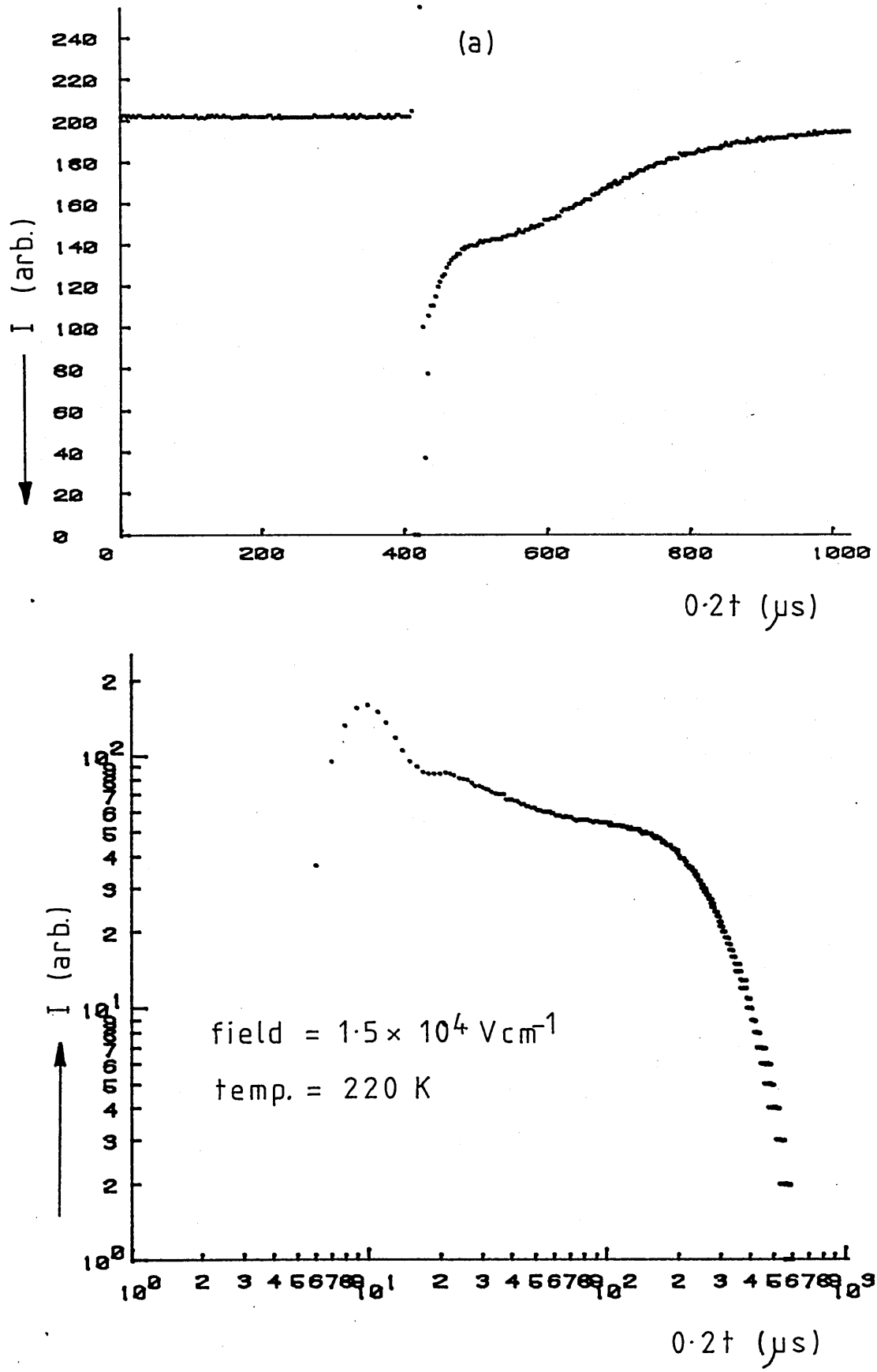

Figure 6.4. Typical hole transit pulse shapes for a-Se observed at a number of temperatures and fields. The specimen thichness is 70 microns.

see over...

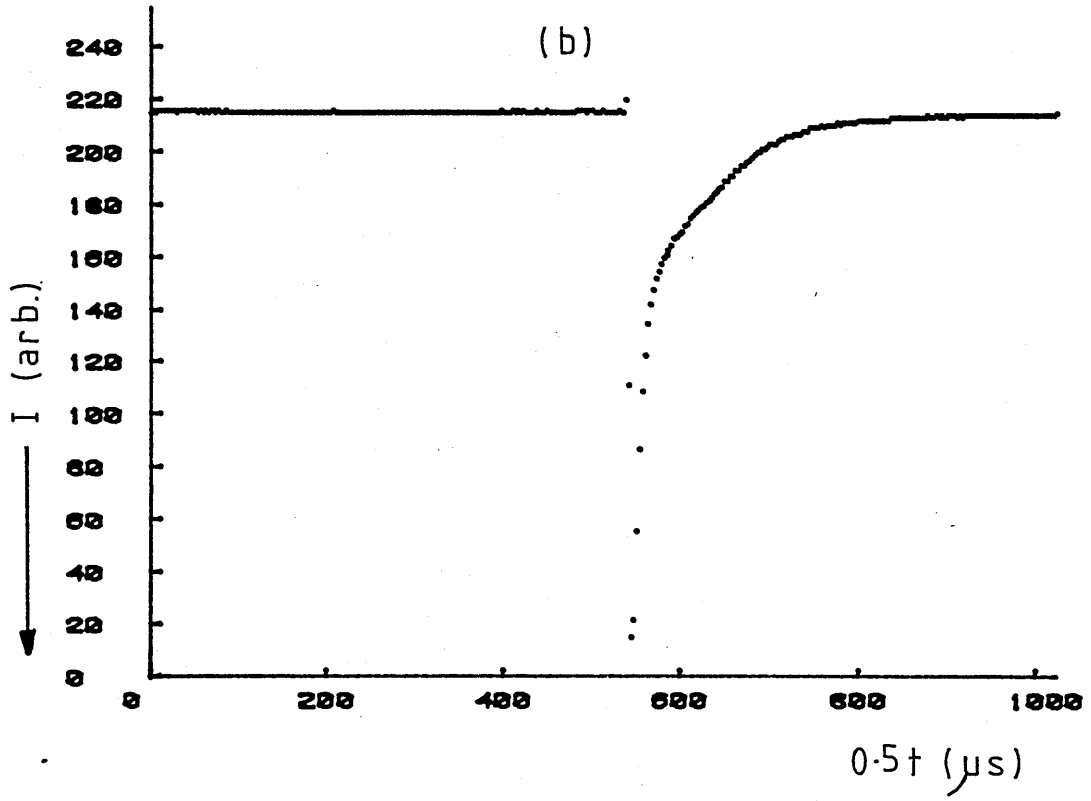
(b)
I (arb.)
240
220
200
180
160
140
120
100
80
60
40
20
0
0
200
400
600
800
1000
0·5t (μs)

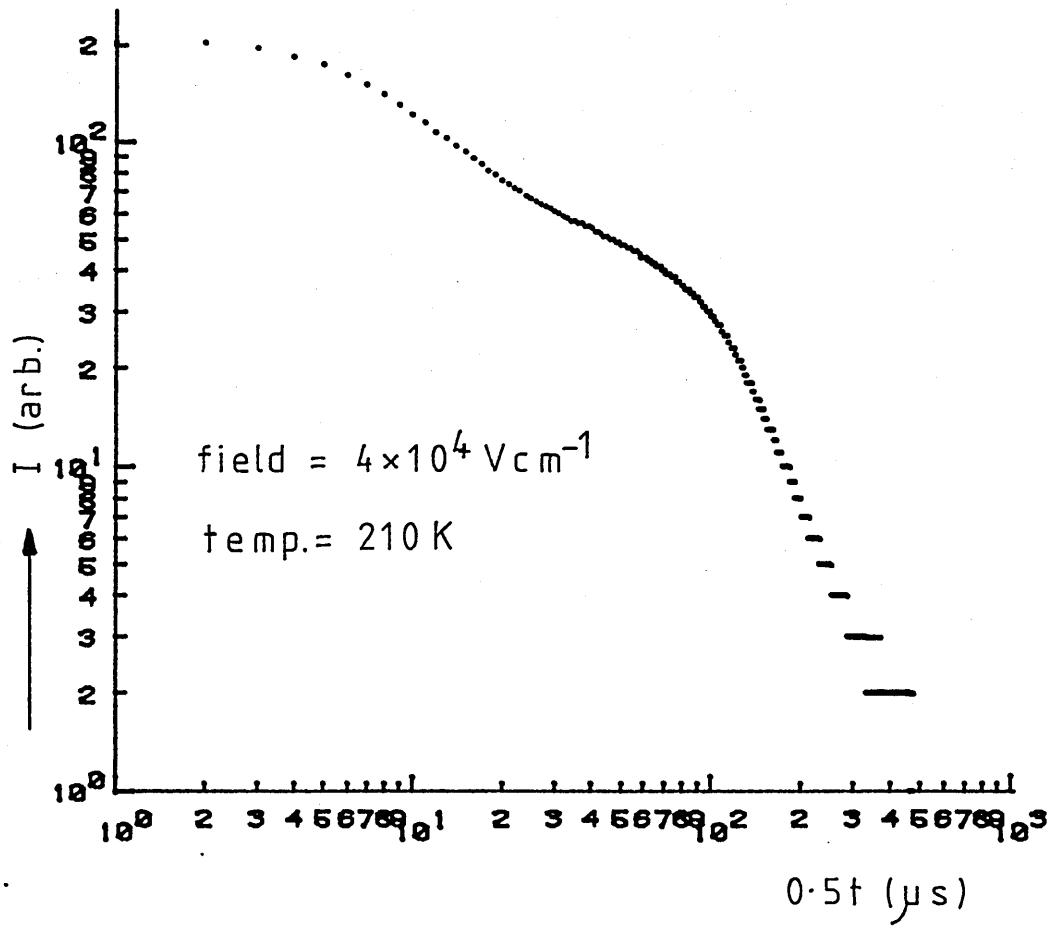
I (arb.)
field = 4×10⁴ V c m⁻¹
temp.= 210 K
0·5t (μs)

see over...

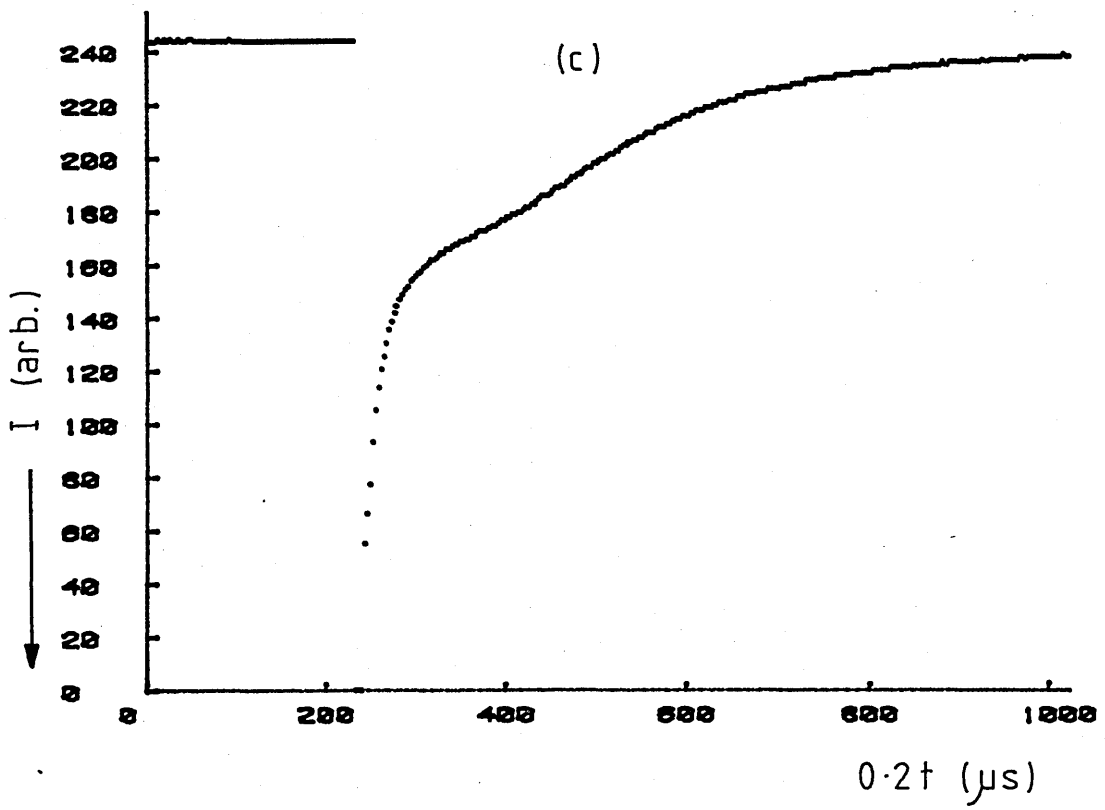
(c)
I (arb.)
0
20
40
60
80
100
120
140
160
180
200
220
240
0
200
400
600
800
1000
0·2t (μs)

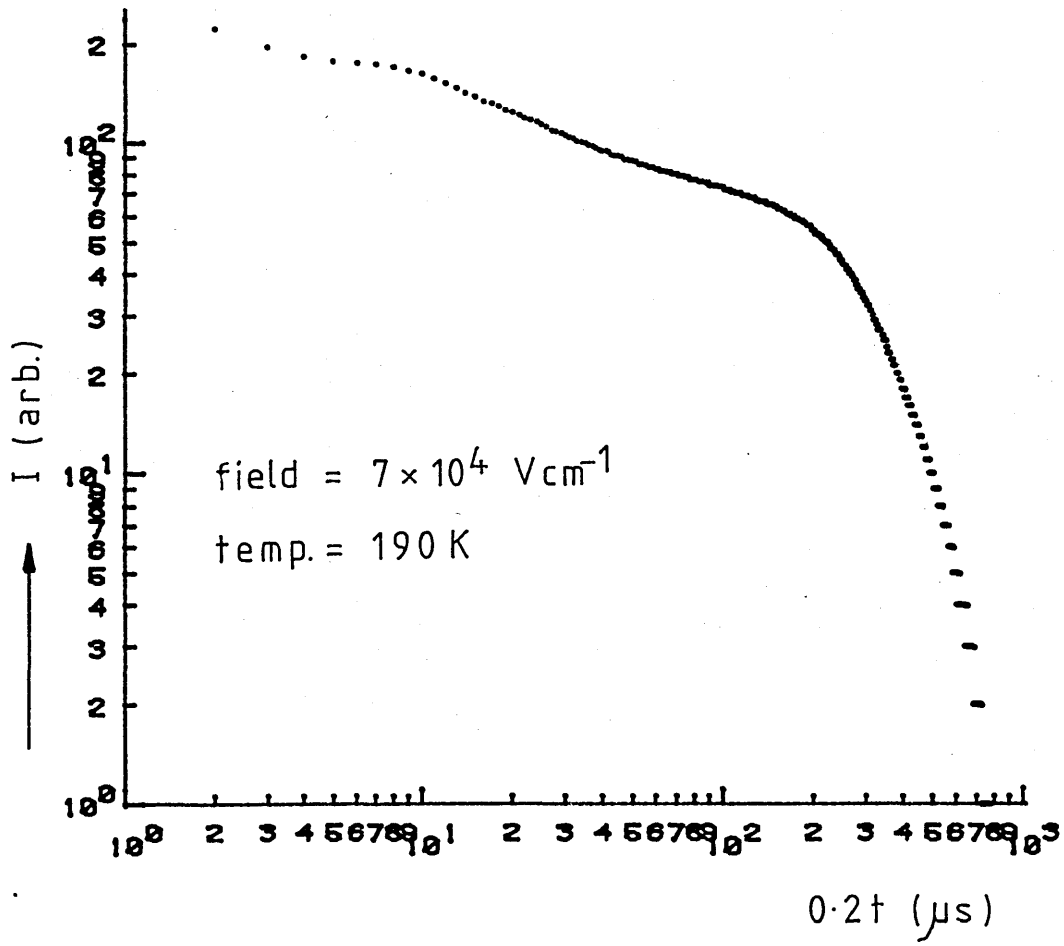
I (arb.)
field = 7 × 10⁴ Vcm⁻¹
temp. = 190 K
0·2t (μs)

see over...

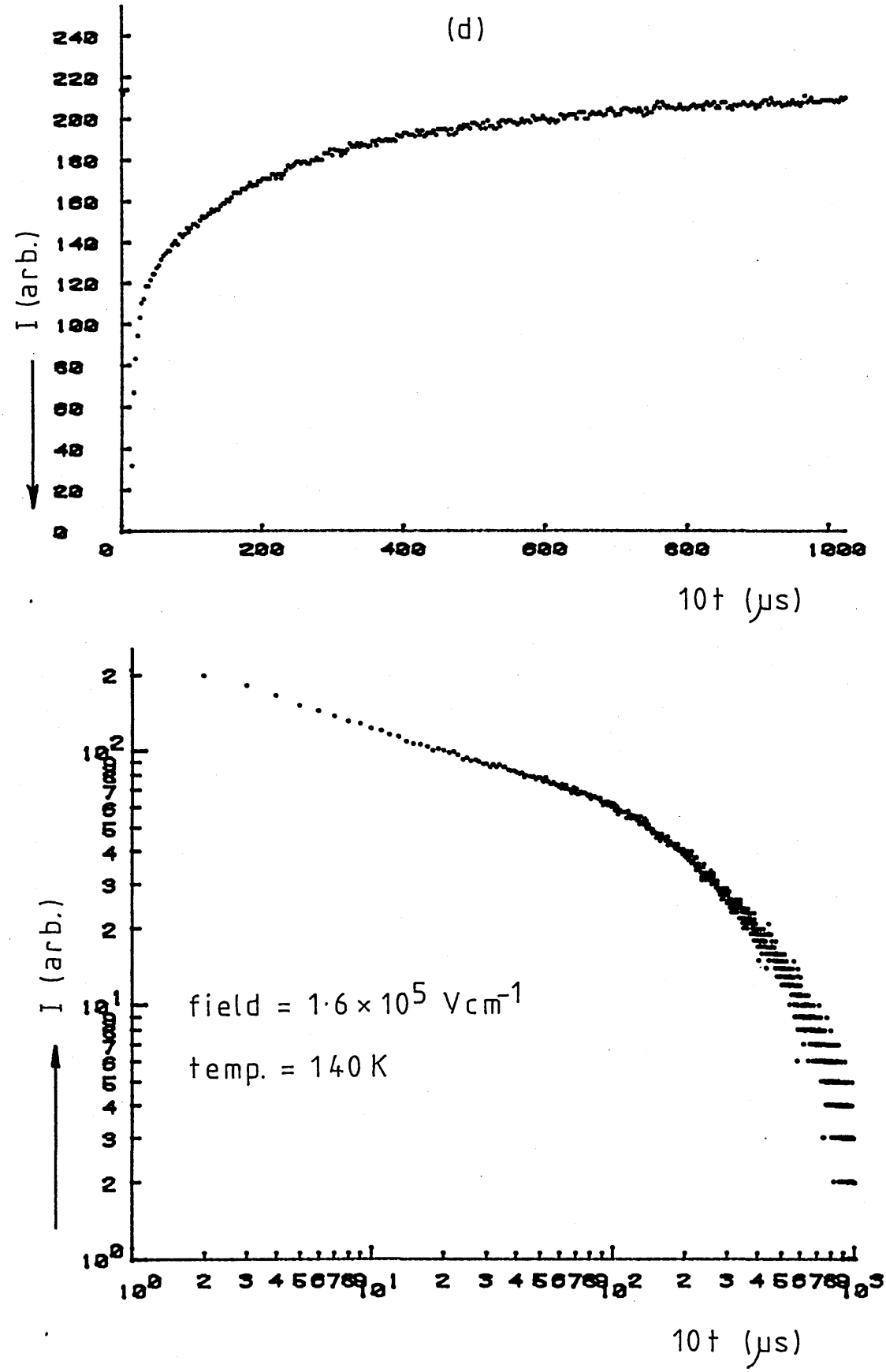
(d)
I (arb.)
240
220
200
180
160
140
120
100
80
60
40
20
0
0
200
400
600
800
1000
10 t (μs)
I (arb.)
field = 1·6 × 10^5 V cm^-1
temp. = 140 K
10 t (μs)

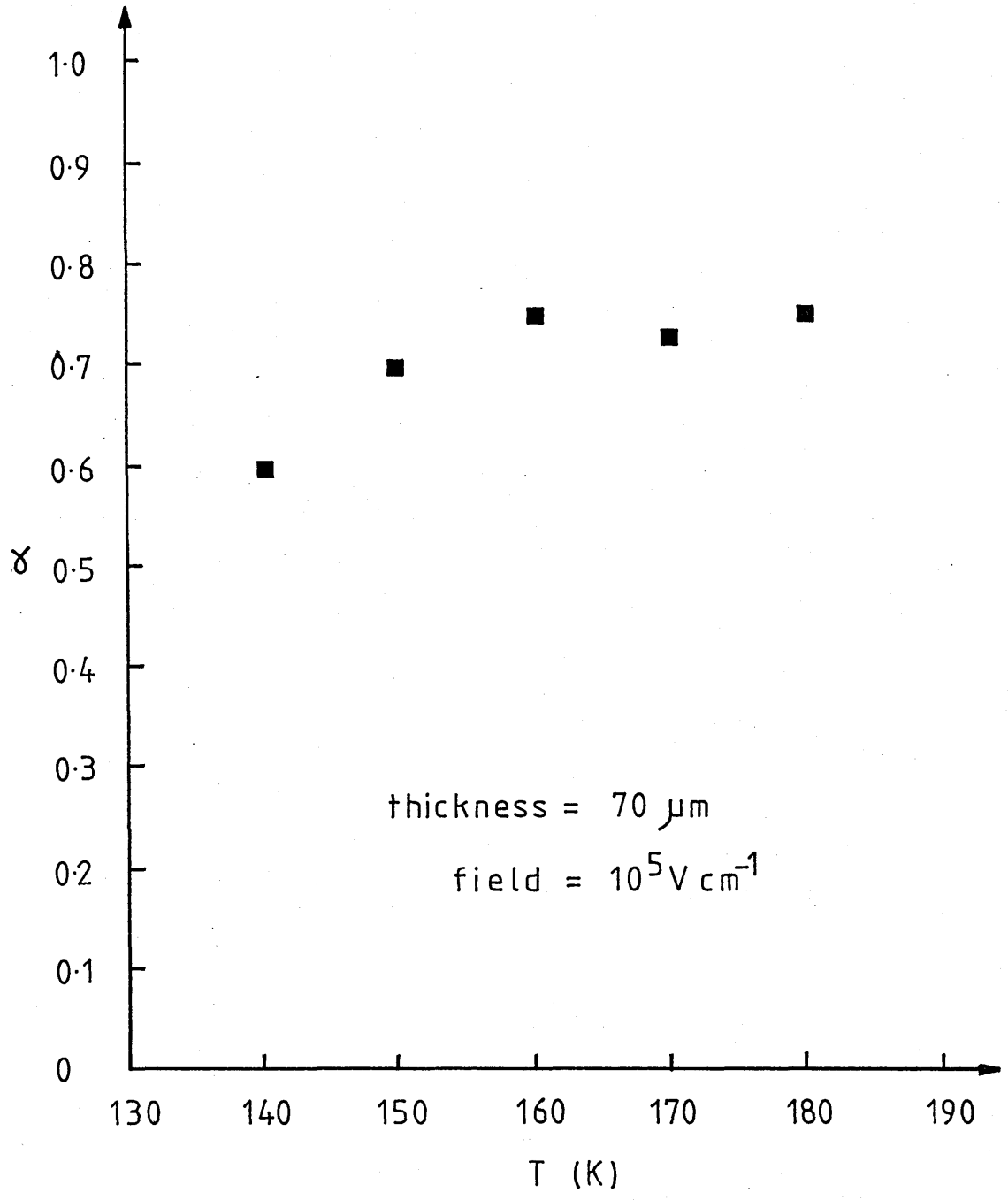

Figure 6.5. Temperature dependence of the dispersion parameter for a-Se determined from the initial part of the hole transient current pulse.

slope were found to be very sensitive to the choice of current baseline, and consequently very difficult to measure within an acceptable degree of accuracy. Inspection of figure 6.5 shows that at temperature below about 190K, α lies between 0 and 1.

6.2 DISCUSSION.

The thermally activated behavior of the carrier drift mobility in a - Se has been attributed to a mechanism in which charge flow occurs in extended states with frequent interruption by trapping in localised levels situated energetically close to the transport states (2). Pfister (1), on the other hand, has suggested that carrier transport occurs via a hopping process. In either case, it has been established that as the temperature is decreased below about 190K, there exists a change in the statistical nature of the carrier propagation, from a Gaussian to a stochastic process. The shift in propagation statistics, however, is not accompanied by any discontinuity in the slope of the Arrhenius plot of the hole drift mobility in a - Se and this has lead to the suggestion that the same basic mechanism of carrier transport prevails over the entire temperature range investigated. The question to be answered, however, is "what is the transport mechanism"?

As already stated, the details of the Arrhenius plots for both the evaporated and the quenched material are similar. This has lead to the general conclusion that the transport mechanism which exists in both materials is the same. In practice, there are three competing

transport mechanisms which could account for the observed plots, namely; isoenergetic hopping in a particular level of localised states, trap limited hopping between two levels of localised states and trap limited band transport. If a hopping mechanism were to exist, an experimentally measured drift mobility of about 10^{-2} $cm^2 V^{-1} s^{-1}$ is not expected to be exceeded. In the specimens of a - Se investigated in this study, however, the highest drift mobility recorded was 3×10^{-1} $cm^2 V^{-1} s^{-1}$ at 300 K, while Pfister (1) observed a similar value at this temperature. It thus seems unlikely that the observed Arrhenius plot results from a hopping process, and it is concluded that a trap limited band transport mechanism is the most likely to occur.

On the assumption of such a transport mechanism, it is possible to explain why differing degrees of transit pulse dispersion are obtained from the same material, but prepared using different methods of film deposition. Figure 6.6 shows the dispersion parameters obtained by Pfister and Scher (3) for thin films of evaporated a - Se, as a function of temperature. Superimposed on this graph are the α - values obtained in this study for vitreous films of the same material. Although relatively few data points exist for the vitreous material, it can be seen that at any given temperature, the vitreous material displays consistently less transit pulse dispersion than does the evaporated material. In this study, it is proposed that this difference in the degree of transit pulse dispersion displayed between the two materials is a direct consequence of the differing details of the mobility controlling localised states. It is further argued, that in a - Se, there is a direct relationship between the details of the

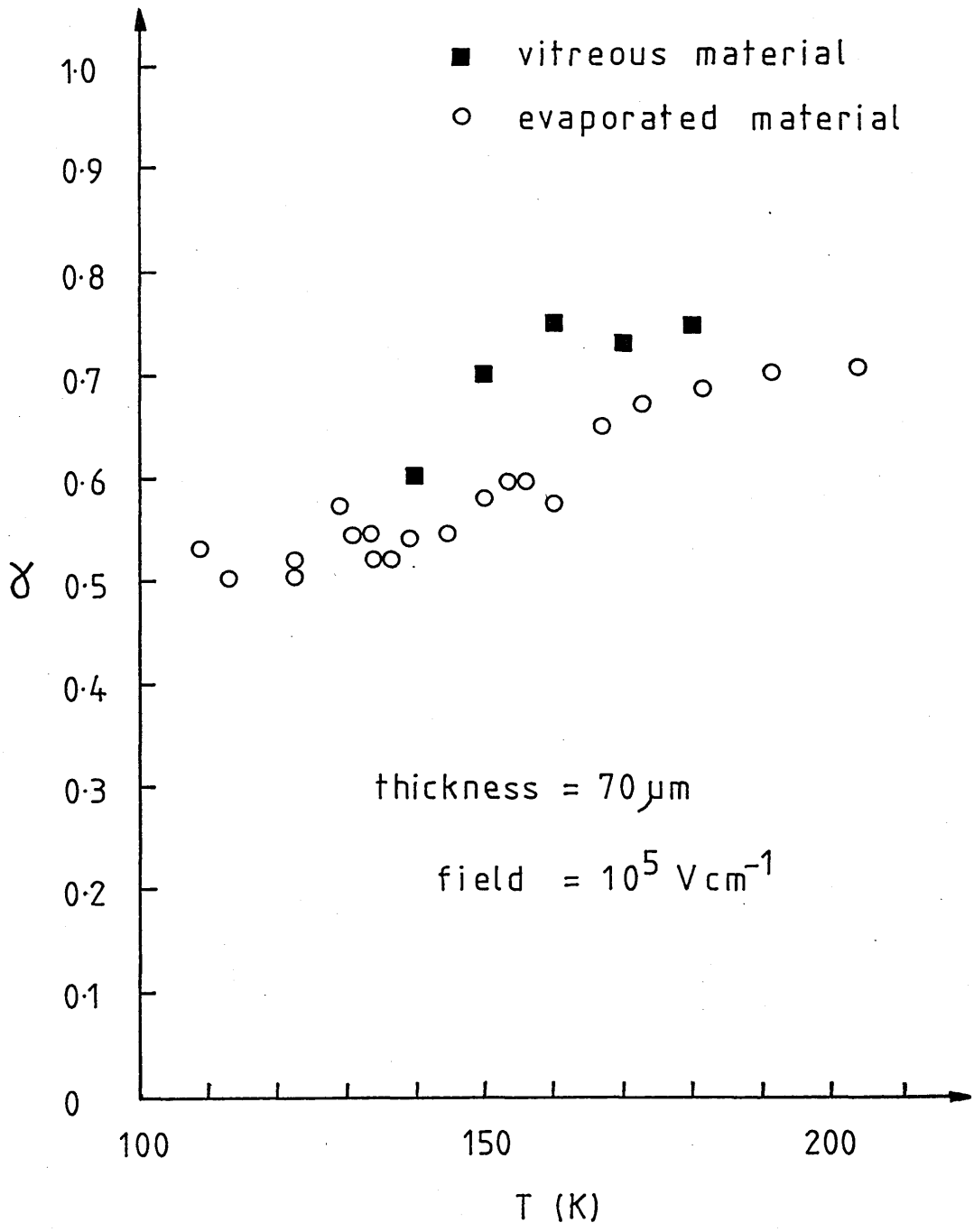

Figure 6.6. Temperature dependence of the dispersion parameter for a-Se obtained from this study (■) and from Pfister and Scher (○). (After ref. 3).

localised states distribution and the method of film preparation.

The evaporated films used in the study by Pfister (1,3) were prepared by open boat evaporation onto substrates held at a temperature of approximately 320K. In such a process the film is "built up" by the accumulation of layers of atoms onto the substrate; these atoms assuming their final lattice position within a brief period after making contact with the film surface. Once deposited, the atoms are unable to adjust their position in order to satisfy any unpaired bonds. The vitreous films used in this study, on the other hand, were prepared by quenching the material rapidly from the melt. As the material cools from the molten phase, there is a limited period of time during which the atoms can adjust their position in an attempt to satisfy their bonding requirements. It is proposed that these differences in the deposition conditions will lead to a greater number of defect sites, coupled with a greater disorder in the site position in the evaporated material, as compared to the quenched material.

Marshall (4) has shown that (all other things being equal) a broader energy distribution of the mobility controlling defect states will result in correspondingly more dispersion in the transient current pulse, if a trap limited band transport mechanism is assumed. It has also been established by Marshall and Sharp (5), that hopping between localised states which are energetically spread out, does not give rise to highly dispersive transport, except at times considerable shorter than those observed under experimental conditions. It therefore seems consistent to assume that carrier transport in a - Se is by a trap limited band motion and that the higher degree of transit

pulse dispersion observed in the evaporated material is a direct consequence of the broader energy distribution of the mobility controlling localised states in that material.

A quantitative estimate of the energy spread of the mobility controlling localised states in each material can be obtained by fitting the "Time of Flight" data generated for each material, to the trap limited band transport computer model developed by Marshall (4). In this model, the mobility controlling localised states take the form of a Gaussian shaped packet situated above the valence band, or below the conduction band, as the case may be, and the energy spread of the packet, ΔE, is quoted as the separation in energy between the two half magnitude points of the distribution. Using this model Marshall (4) generates a series of transit pulse shapes for various values of $B = \Delta E/kT$. By comparing the transit pulse shapes obtained experimentally, and the transit pulse shapes generated by the computer model, an estimate of the factor B can be deduced for the material under consideration. Finally, with a knowledge of the temperature at which the experimental transit pulse was recorded, an estimate of the energy spread of the mobility controlling localised states, ΔE, can be made. Carrying out such a procedure it is found that in the case of the vitreous material the mobility controlling defect sites are spread over an energy range of 0.05 eV, while for the evaporated material the spread is 0.06 eV. The difference in energy spread between these two distributions (0.01 eV) is of the order of kT at about 120K implying that the disorder temperature T_c in the evaporated material is about 120 K larger than that existing in the vitreous material.

6.3 CONCLUSIONS.

As stated previously, the primary nature of this work was to characterise the operation of the "Time of Flight" equipment developed during this study. It has, however, been possible to use the results obtained from a - Se in a constructive manner. It has been suggested that the electronic structure of amorphous chalcogenide semiconductors may be influenced to a measurable degree by the method of film preparation.

It is interesting to note here, that measurements which are in agreement with those presented above, have recently been published for a - As_2Se_3 by Sharp and Marshall (6). These workers observed that evaporated a - As_2Se_3 displayed consistently more transit pulse dispersion than did the quenched material over the investigated temperature range of 260K to 360K.

SECTION B

6.4 UNDOPED AMORPHOUS SILICON - RESULTS

Specimens of a - Si were prepared by sputtering from a polycrystalline Silicon target, and formed into either coplanar or sandwich cell structures (see section 4.6). A number of experimental measurement techniques were applied to these samples over the temperature range 100K to 500K.

6.4.1 DARK D.C. CONDUCTIVITY.

Dark d.c. conductivity measurements were performed on specimens of a - Si:H which were housed in a light tight evacuated chamber in a darkened room. The steady state current flowing through the specimen was monitored using a Keithley 610C solid state electrometer, which could detect currents down to 10^{-15} amps. The electrometer was always switched on 24 hours before any measurements were taken, to ensure stability of operation over many hours. After changes in temperature or applied electric field, the current flowing in the specimen took several minutes to stabilise. To ensure that this did not introduce a systematic error into the measurements, the current was monitored at regular intervals until no increase or decrease was found to occur. Measurements were performed on both sandwich and coplanar cell specimens and no systematic difference could be detected between results obtained from the two sample geometries. Any actual geometric dependence of the conductivity,

however, may have been obscured by wide specimen to specimen variations observed in the conductivity.

Figure 6.7 shows an Arrhenius plot of the conductivity, for three of the specimens of a - Si investigated. Curves (a) and (b) are data obtained from films prepared using a Hydrogen partial pressure of 4 mTorr, and curve (c) is from an unhydrogenated specimen. The three plots shown in figure 6.7 illustrate broadly three categories into which fall all of the Hydrogenated and unhydrogenated films of a - Si investigated in this study.

The unhydrogenated material (curve (c)) displays two distinct regions. In the high temperature region, the conductivity is singly activated with an activation energy $E_a = 0.36$ eV, while in the low temperature region the conductivity plot curves continuously towards lower effective activation energies with decreasing temperature. These characteristics are typical of the conductivity data obtained from all of the unhydrogenated specimens.

Conductivity data obtained from the Hydrogenated material displayed features which in general were unpredictable. The results did fall into the two main categories, however, and these are depicted by curves (a) and (b) in figure 6.7. At high temperatures all of the hydrogenated material displayed a conductivity Arrhenius plot which was singly activated, although the magnitude of the activation energy varied widely from specimen to specimen. In some of the a - Si:H studied, this unique activation energy extended throughout the complete range of measurement (curve (a)), while in others, a low temperature region existed where the Arrhenius plot curved continuously towards lower effective activation

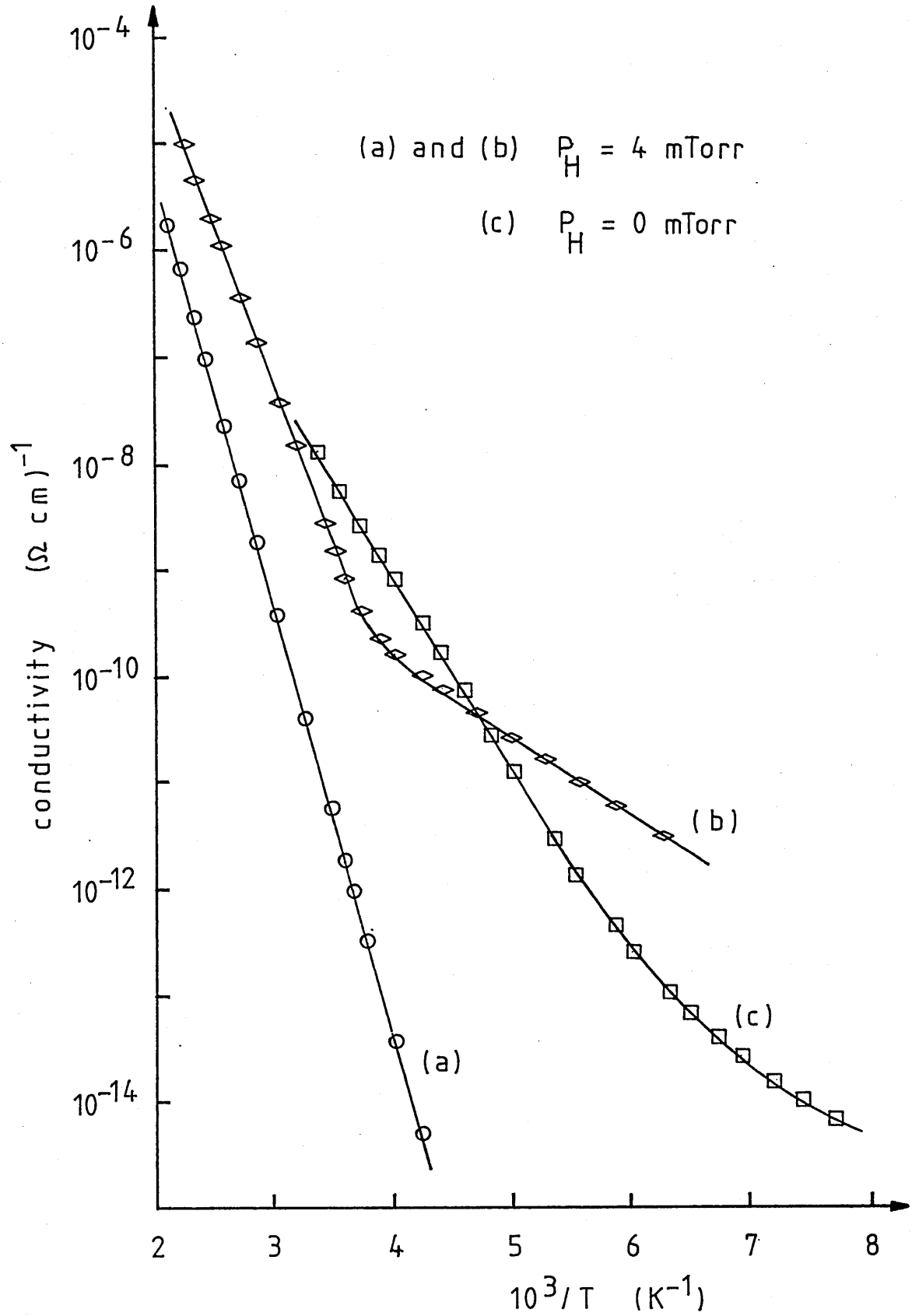

Figure 6.7. Arrhenius plot of the conductivity for three specimens of a-Si. The three curves illustrate three categories into which fall all of the conductivity data obtained from specimens of a-Si investigated in this study.

energies with decreasing temperatures (curve (b)). It was not possible to pre-determine which category a given specimen would fall into, and for those specimens which did display curvature, it was found that the temperature at which this region commenced was widely spread. An attempt was made to correlate low temperature conductivity data with optical absorption measurements taken at low photon energies (see section 6.5.4), but no link between these data could be established.

Figure 6.8 shows plots of E_σ and σ_o (as determined from the high temperature region of the conductivity data), as a function of P_H for all of the undoped specimens of a - Si investigated in this study. The σ_o results are determined from the intercept on the $\ln(\sigma)$ axes at T = 0 K. The substrate temperature and Argon partial pressure used during the deposition of these films were approximately 270^{o}C and 11 mTorr respectively. Although there is wide scatter in both the E_σ and σ_o results, there does appear to be an underlying trend in both plots, this trend being indicated by the solid lines. The lines are not meant to be quantitative in any manner, but are included only to illustrate the underlying trends.

The σ_o results appear to display most scatter at around P_H = 4 mTorr. For both lower and higher values of P_H, σ_o follows fairly closely the trend indicated by the solid line. The E_σ results, on the other hand, do not display significantly more scatter at any particular value of P_H.

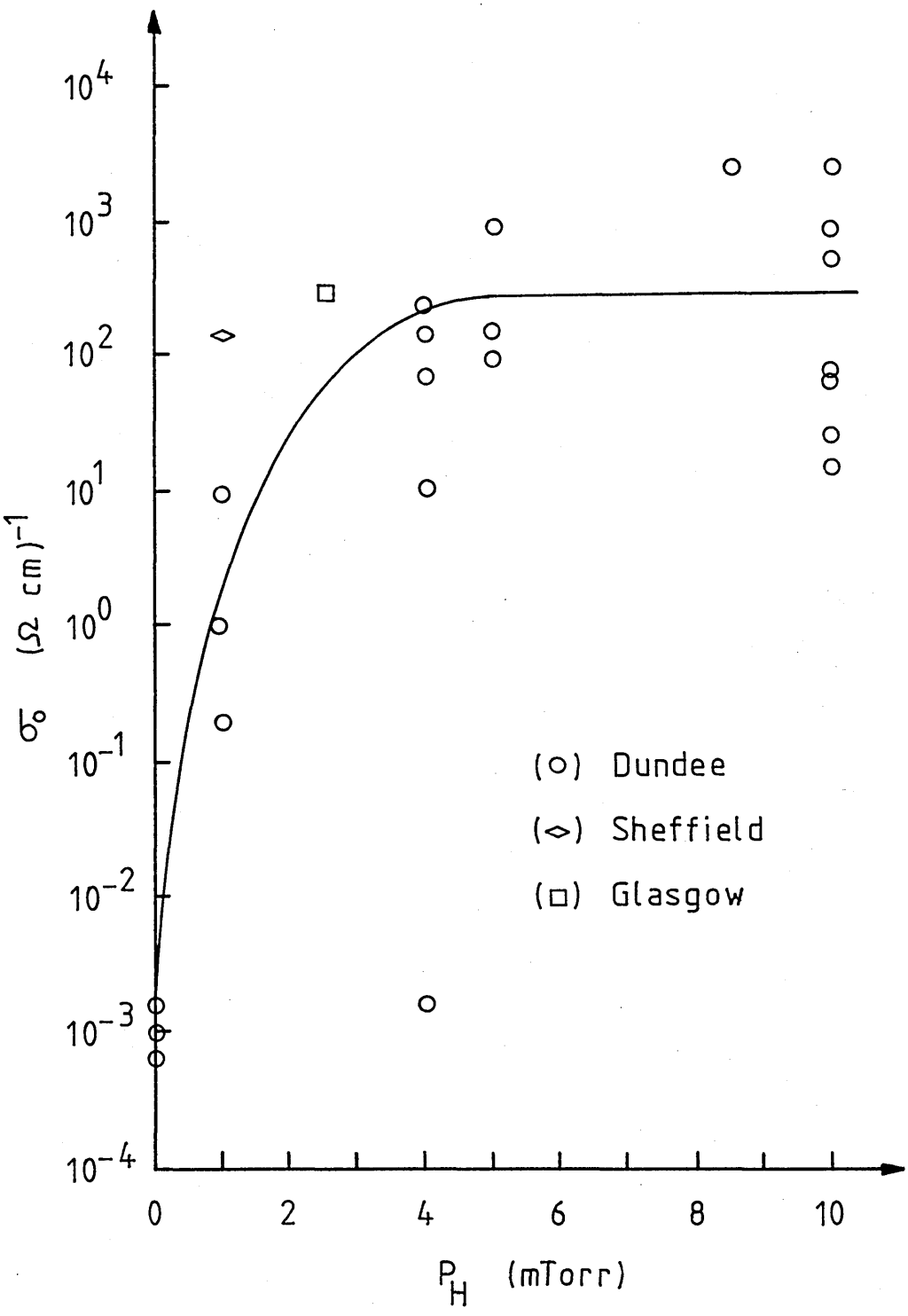

Figure 6.8(a). Conductivity pre-exponential as a function of Hydrogen partial pressure.

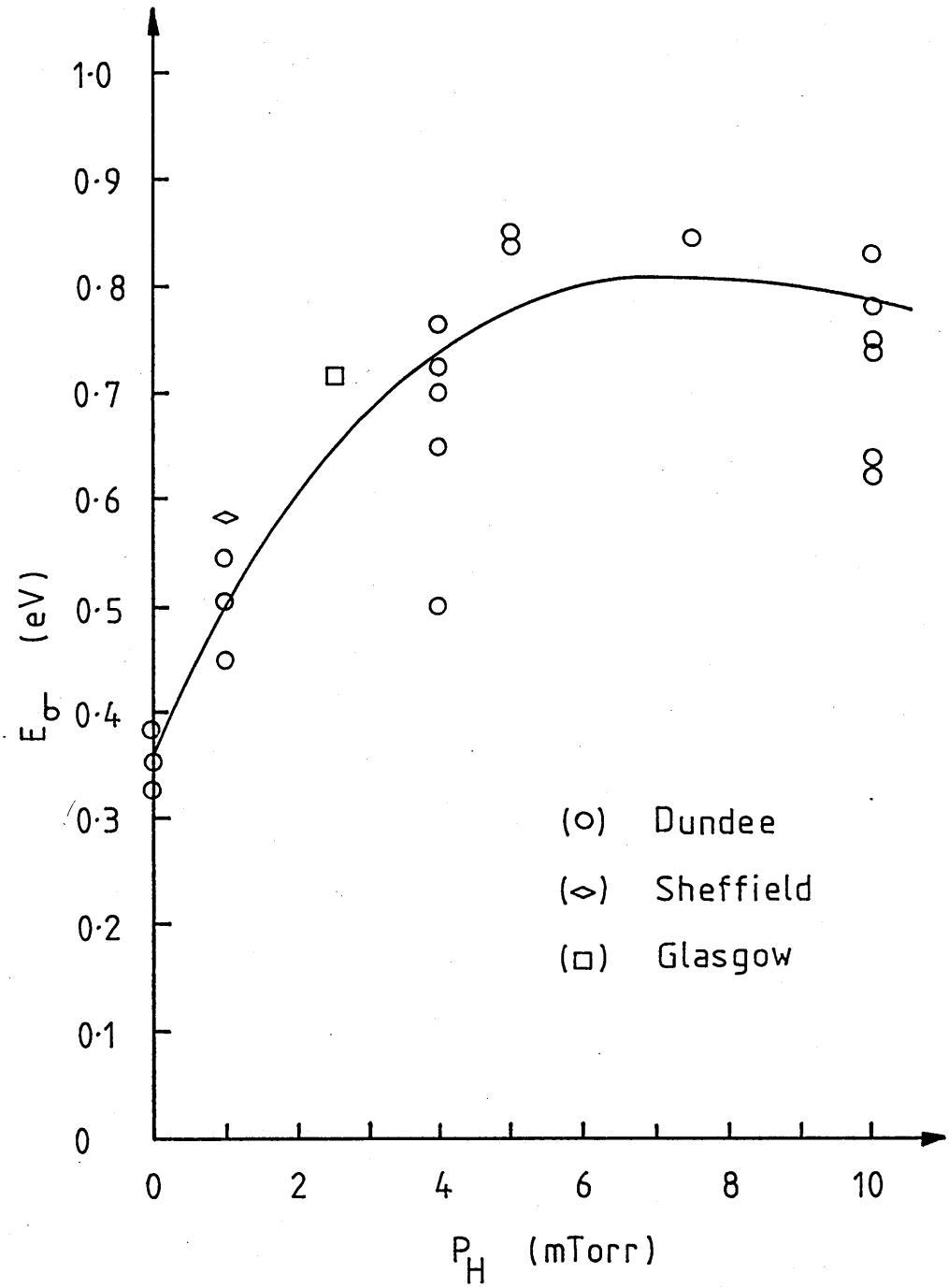

Figure 6.8(b). Dark conductivity activation energy as a function of Hydrogen partial pressure.

For comparison with the material prepared in this laboratory, figure 6.8 also shows conductivity data collected from specimens obtained from Sheffield University (Dr. J. Allison) and from Glasgow University (Dr. A. Long). Both these specimens were prepared using a Nordico sputtering system similar to the equipment used in this study. It can be seen from figure 6.8, that within the experimental scatter, these two externally prepared specimens yield data in agreement with the general trends illustrated.

Note. The values of σ_0 shown in figure 6.8(a) can be adjusted by the factor $\exp(\gamma/\theta k)$ in order to account for temperature dilation of the optical gap. Θ is the ratio of the optical gap to the conductivity activation energy, i.e. $\Theta = E_0/E_\sigma$, and for undoped amorphous Silicon $\gamma \simeq 10^{-5}$ eV K^{-1} (14). Using this value leads to a maximum correction in σ_0 of about 10 %. Clearly, this correction is relatively small and will be ignored in the following discussion.

6.4.1.1 DISCUSSION.

For the unhydrogenated material, σ_0 lies in the range 10^{-4} to 10^{-3} $(\Omega\,\text{cm})^{-1}$. Since for extended state conduction, σ_0 is expected to be greater than about 10^{2} $(\Omega\,\text{cm})^{-1}$, it can be inferred that conduction in the unhydrogenated material is via a hopping mechanism. This fact is not unexpected since a large density of states in the gap is likely to exist in films prepared in a plasma consisting only of Argon gas. From the E_σ data it can be concluded that hopping in the unhydrogenated material takes place at an energy which is about 0.3 to 0.4 eV above the Fermi

level. From these data, however, no information can be obtained about the position of the Fermi level in the gap or about the magnitude of the hopping energy.

Figure 6.8 shows that as a result of the addition of small amounts of Hydrogen to the plasma, there is a sharp increase in σ_o, coupled with a corresponding increase in E_σ. For P_H greater than about 1 mTorr most specimens yield a conductivity pre - exponential which lies in the range 10^1 to 10^3 $(\Omega\,cm)^{-1}$. This range suggests that carrier transport occurs within extended states rather than by a process of hopping between localised centres within the mobility gap. The scatter in the E_σ results in this region, however, implies that the position of the Fermi level in the gap is critically dependent upon the details of film growth. This fact is consistent with the review presented in Chapter 3, which suggests that the details of the density of states in the gap, and at the band edges, are intimately related to the minute conditions of film deposition. Since the position of the Fermi level will depend upon the overall shape of the density of states distribution, the scatter in the E_σ results is not unexpected. A further explanation for the experimental scatter observed in both the σ_o and the E_σ results can be put forward in particular for the material prepared in this laboratory: i.e. The sputtering system used for depositing a - Si:H was also used for depositing a wide range of other materials including Arsenic based compounds and metals such as Aluminium and Antimony. Residues of these elements in the chamber may have contaminated the "pure" a - Si:H films being grown, leading to the wide and spurious scatter in the experimental results.

Although the experimental scatter makes it difficult to be certain, it can be seen from figure 6.8 that at high values of P_H, the magnitude of σ_0 levels off at a value between 10^2 and 10^3 $(\Omega cm)^{-1}$, while E_σ shows signs of decreasing with further increases in P_H. These results (both the scatter and the general trend), are consistent with results presented by Anderson and Paul (7). They suggest (7) that a decrease in both E_σ and σ_0 might be expected at high values of P_H, since excess amounts of Hydrogen could create defects in deposited films, by one of two methods: (i) By occupying a site in the network which could have been a viable site for a Silicon atom, hence terminating the network at that point and forcing it to grow round the Hydrogen atom as best it can; or (ii) By forming multiply bonded Si - H_x complexes which force the network to depart from a regular random, fully coordinated tetrahedral arrangement. Anderson and Paul suggest that these processes may create films of a - Si:H which consist of two phases, one phase being formed from an almost fully coordinated tetrahedral arrangement of atoms, the other phase from a complex arrangement of Si - H_x atoms. Although no direct evidence is obtained in this study to endorse this two phase model, the results presented here are in general agreement with those which led Anderson and Paul to postulate such a model.

In summary, the conductivity data presented here are in general agreement with the following hypotheses:

(a). Hopping conductivity takes place in the unhydrogenated material.

(b). Extended state conductivity takes place in most of the Hydrogenated material investigated (1 mTorr $< P_H <$ 10 mTorr).

(c). There is an initial sharp decrease in the density of defect states in the gap with the introduction of Hydrogen to the plasma, this trend continuing for P_H values up to about 5 to 8 mTorr.

(d). The large experimental scatter in the conductivity data obtained from specimen to specimen may be due to (i) variations in deposition conditions, and (ii) contamination by impurities.

6.4.2 TIME OF FLIGHT.

Time of Flight experiments were carried out on specimens of a - Si:H using the electron gun system described in Chapter 5. All specimens were deposited onto Corning 7059 glass substrates held at a temperature of approximately 270°C. Prior to deposition, the substrates were fitted with sputtered Molybdenum bottom electrodes; after the deposition of the a - Si:H, 2 - 6 microns thick, the sandwich cell structure was completed by either sputtering or evaporating an Aluminium top contact. This electrode configuration has been found to be suitable for studying both the hole and the electron drift mobility in a - Si:H, using the time of flight technique (15).

All the specimens investigated exhibited transient current pulses having a duration approximately equal to that of the excitation pulse width ($\simeq$ 20 ns). The transient pulses were not distorted by the response time of the detector circuit, which, under matched conditions, had a rise time of a few nanoseconds. Measurements were performed over the temperature range 140 K to 500 K for each specimen and it was found that

no significant change in the pulse duration or pulse shape occurred. The electric field applied to the specimen was also varied. It was found that the pulse amplitude scaled approximately linearly with field strength while the pulse duration was unaffected. Measurements were also attempted using a pulsed Nitrogen laser as an excitation source, but no significant change in the results was observed.

Note. It has recently been brought to the attention of the author (16) that the Nitrogen laser may not be a suitable excitation source for performing time of flight measurements on a - Si:H. The precise reason for the phenomenon is not fully understood, but it is thought to originate from the fact that the intense ultra - violet laser light may create excess charge in a narrow region close to the specimen surface, this charge quickly recombining, possibly in a large density of surface states.

6.4.2.1 DISCUSSION.

The origin of the fast transient current pulse is not precisely known, but it is thought to originate from one of two sources. Firstly, the pulse could be due to the drift of excess carriers through the film in times shorter than, or of the order of, 20 ns. It is possible to ascertain whether the "transit time" is shorter than 20 ns by reducing the bombardment pulse width, but this was not possible with the equipment available. Secondly, the observed transient pulse could be due to the rapid trapping of excess carriers as they are injected into the semiconductor, involving states which act as recombination centres.

Considering the former case first, with "transit times" of the order of 20 ns, it is possible that the carriers have insufficient time to interact with traps, and it is therefore the free carrier mobility that is being observed. Under these circumstances, the trapping time of centres situated below the mobility edge must be longer than the observed transit time; the carriers not "seeing" any traps or recombination centres during their transit of the sample. Typical experimental conditions for the observation of such fast current pulses are a specimen thickness of 6 microns and an applied electric field of 5×10^{4} V cm^{-1}. These conditions lead to an assumed free electron drift mobility of about 1 $cm^{2} V^{-1} s^{-1}$, a value which is comparable with free electron drift mobility data presented in the literature (24,25) for various specimens of sputtered a - Si:H. If, however, the free carrier recombination lifetime is to be greater than 20 ns, then a $\mu\tau$ product in excess of 2×10^{-8} $cm^{2} V^{-1}$ is required. This condition compares favorably with measured room temperature electron $\mu\tau$ products in glow discharge deposited a - Si:H (18) of approximately 10^{-7} $cm^{2} V^{-1}$, ($\mu\tau$ products in sputtered a - Si:H, however, are found to be (10) critically dependent on preparation conditions). A further implication of the above interpretation is that the lifetime of free carriers, with respect to shallow traps, must be greater than 20 ns. Assuming a typical shallow trap density of about 10^{19} cm^{-3} implies a room temperature capture cross section of around 10^{-18} cm^{2}. This value is smaller than typical band tail capture cross sections in undoped a - Si:H (18) by about two orders of magnitude. This implies that for the material prepared in this laboratory, there may be a relatively small density of shallow traps associated with the conduction band tail states ($\simeq 10^{17}$ cm^{-3}).

The second possible explanation for the observed fast transient current pulse (i.e. carrier recombination) yields conditions which are in direct contrast with those presented above. If "severe" trapping is to exist, then the trapping time of free carriers, with respect to recombination centres, must be shorter than the duration of the current pulse (20 ns). A second implication of this explanation is that the centres concerned must be "deep", preventing the thermal release of carriers back into extended states to recontribute to the conduction.

In order to determine which of the above two mechanisms is occurring, it was concluded that information must first be obtained about the free carrier lifetime, using an independent experimental technique. Both transient and steady state photoconductivity measurements were performed in order to extract this information.

Note. It was found that both steady state and transient photoconductivity results (and most other results obtained from a - Si:H), varied widely from specimen to specimen. This fact is consistent with the trends presented in both this report and in the literature, and as it can be appreciated, this makes it very difficult to compare results obtained from different specimens. As a result, it was decided to choose one particular specimen (the one which displayed the "best" characteristics), carry out a number of experimental measurements on it, and use these results to form the core of the analyses. In order to present a complete picture of the data collected, where appropriate, graphs and tables will be presented in an attempt to demonstrate the experimental scatter.

6.4.3 TRANSIENT PHOTOCONDUCTIVITY.

Transient photoconductivity (TP) measurements were performed on specimens of a - Si:H using the l.e.d. - light pipe arrangement discussed in Chapter 5. Results were obtained over as wide a temperature range as possible.

Using the TP technique it has been possible to determine the carrier drift mobility and the carrier lifetime. The carrier lifetime was deduced from steady state photoconductivity measurements coupled with both the rise and fall times of the transient photoconductivity. In order to obtain the carrier mobility, it was first necessary to estimate the quantum efficiency and the reflection / transmission loss for the films under investigation. Quantum efficiency experiments were attempted using the charge collection technique, but due to the small signal levels obtained, these experiments provided ambiguous results. It was possible to estimate from the results, however, that the quantum efficiency of a - Si:H at a photon flux of 5×10^{16} photons $cm^{-2} s^{-1}$ and an applied electric field of 3×10^{3} V cm^{-1} was greater than about 0.1. Similar results were obtained for photon energies of both 1.9 and 2.2 eV. In order to verify the validity of this result, a literature survey was carried out. It was found that the best documented measurements of quantum efficiency on a - Si:H had been performed by Mort and Knights (8). They found that (depending on preparation conditions), the zero field quantum efficiency of a - Si:H lies in the range 0.44 to 0.55. Due to the wide experimental error in the results obtained in this study, it was decided to use a value of 0.5 for the quantum efficiency. Loss of incident photons due to

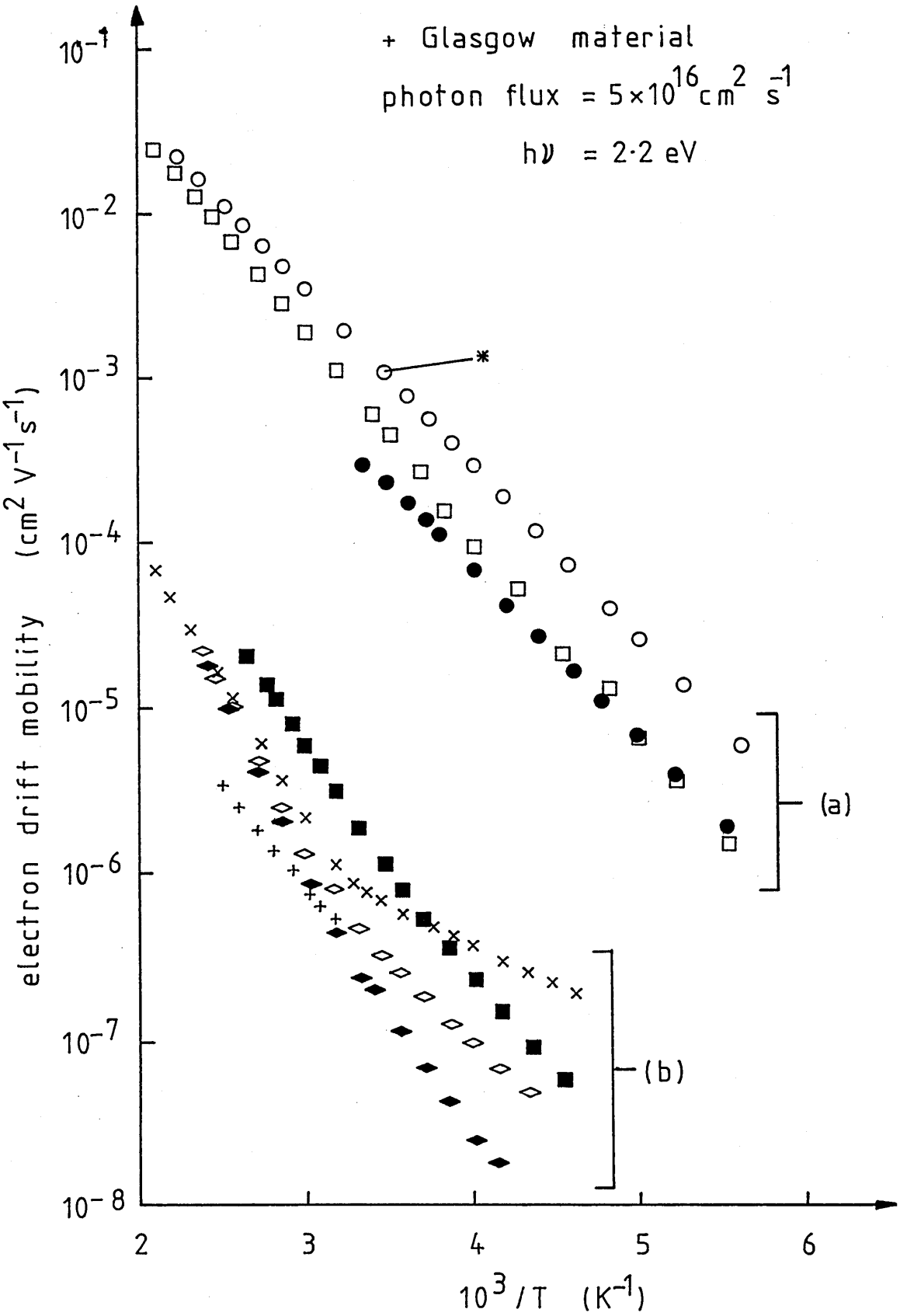

Figure 6.9. Arrhenius plot of the electron drift mobility for all of the specimens of a-Si:H investigated.

transmission was found to be negligible for all of the films investigated. The reflectance, R, of the air - a - Si:H boundary was calculated using the relationship

$$R = \left[\frac{n_s - n_a}{n_s + n_a} \right]^2 \qquad - \quad (6.1)$$

where n_a and n_s are the refractive index of air and the a - Si:H film respectively. Using $n_a \simeq 1$ and $n_s \simeq 3$ (13) it was established that approximately 25 % of the incident photons were lost due to reflection.

Figure 6.9 shows plots of the carrier drift mobility (as deduced from the initial rate of rise of the TP - see equation 2.51) versus inverse temperature for all of the specimens investigated. It can be seen that the data obtained from material prepared in this laboratory fall into two main categories; (a) A room temperature drift mobility of 10^{-3} to 10^{-4} $cm^2 V^{-1} s^{-1}$ and a mobility activation energy of 0.20 to 0.24 eV, and (b) A room temperature drift mobility of 10^{-6} to 10^{-7} $cm^2 V^{-1} s^{-1}$ and a mobility activation energy of 0.30 to 0.42 eV. In category (a), each of the curves is singly activated, while in category (b) some of the curves display an effective mobility activation energy which decreases with decreasing temperature. Table 6.1 shows values of the mobility pre - exponential ($\mathcal{N}'$) and the mobility activation energy ($E_{\mathcal{N}}$) for all of the specimens investigated. Both $\mathcal{N}'$ and $E_{\mathcal{N}}$ were obtained from the high temperature linear portion of the plot where curvature in the low temperature region was present. For completeness, table 6.1 also shows the dark conductivity activation energy and pre - exponential, for all of the specimens considered.

Specimen	E_μ (eV)	μ' ($cm^2\ V^{-1}s^{-1}$)	$\tau_{R.T.}$ (s)	E_σ (eV)	σ_o $(\Omega\ cm)^{-1}$
(a) ○ *	0.21	5	1.5×10^{-2}	0.7	120
(a) ●	0.20	0.9	7×10^{-3}	0.74	80
(a) □	0.24	8	2.5×10^{-2}	0.72	200
(b) ■	0.30	0.5	5×10^{-3}	0.50	1
(b) ◇	0.40	2	1.4×10^{-2}	0.78	860
(b) ◆	0.42	3	7×10^{-2}	0.83	1500
(b) ×	0.32	0.5	2.5×10^{-4}	0.85	2500
+	0.26	0.008	7×10^{-4}	0.72	200

Table 6.1.

Electronic transport data deduced for each of the specimens shown in figures 6.9 and 6.10. Specimen + was obtained from Glasgow University.

Figure 6.10 shows plots of the trap - limited carrier lifetime (photoconductivity decay time) versus inverse temperature for all of the specimens investigated. The data in this case do not fall into the categories (a) and (b) mentioned above. In fact, the specimen which displays the shortest room temperature decay time, and the specimen which displays the longest room temperature decay time both have mobility data which belong to category (b) in figure 6.9.

In general, (excluding the Glasgow material), the curves shown in figure 6.10 exhibit two temperature regimes. At high temperatures all of the curves are thermally activated with an increasing trap - limited lifetime with decreasing temperature. In the low temperature region some curves display an almost temperature independent trap - limited lifetime, while others display thermally activated behaviour where the trap - limited lifetime decreases with decreasing temperature. The room temperature trap - limited lifetime varies from specimen to specimen over the range 3×10^{-2} sec to 2×10^{-4} sec. The former value is remarkably long for a disordered semiconductor, but is consistent with results obtained by others. Mort et al (8) studied non - geminate recombination of photogenerated carriers in undoped a - Si:H and found trap - limited recombination lifetimes greater than 10^{-2} sec at room temperature.

Note. Due to the unsuitability of the electrode configuration, no steady state or transient photoconductivity measurements could be performed using the Sheffield material.

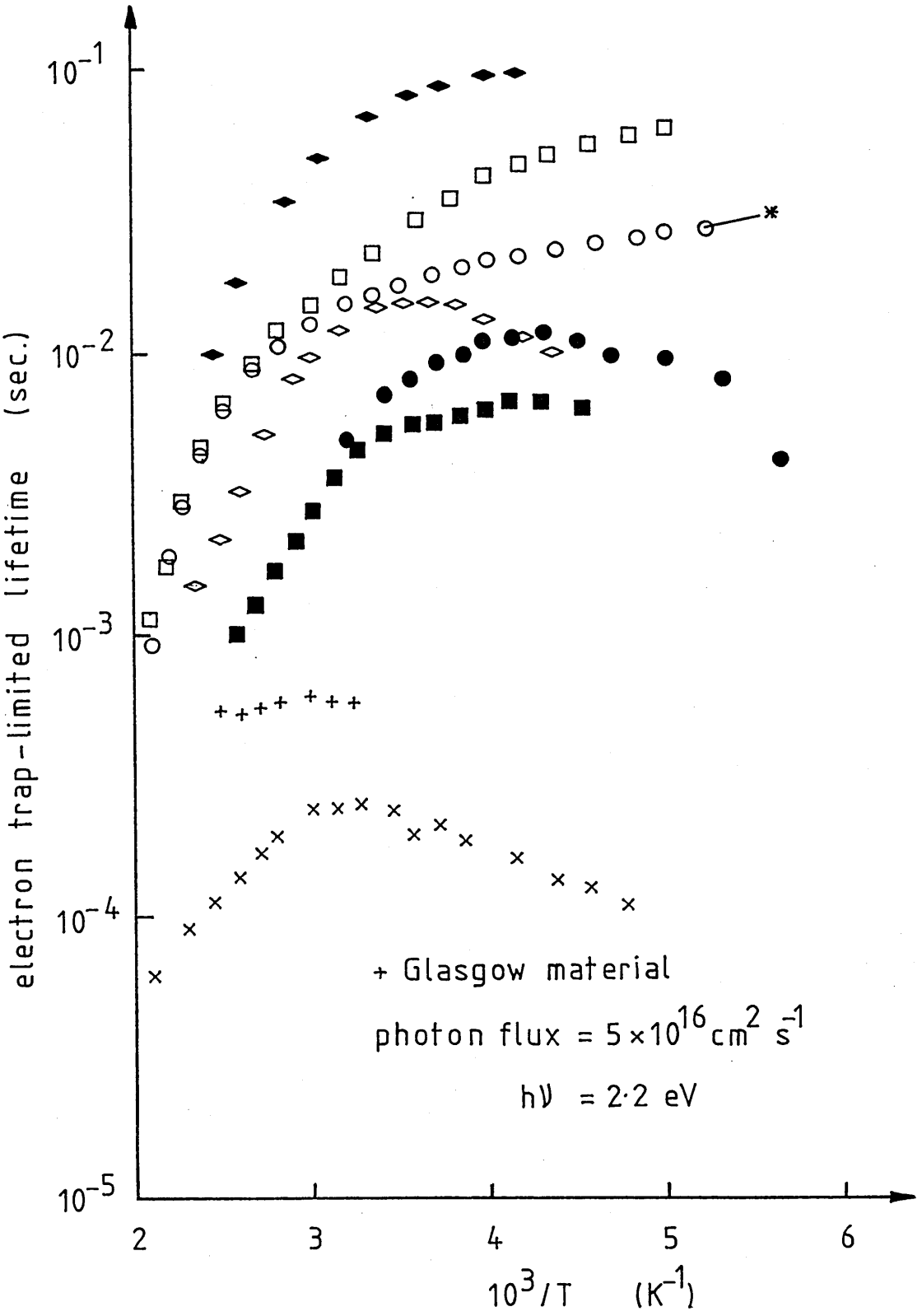

Figure 6.10. Arrhenius plot of the trap limited carrier lifetime for all of the specimens of a-Si:H investigated.

6.4.3.1 DISCUSSION.

The specimen marked with the asterisk in figures 6.9 and 6.10 will be discussed in detail first. This will be followed by an interpretation of the specimen to specimen experimental scatter exhibited by the results.

Before embarking on a detailed analysis of the transient photoconductivity data, it is necessary to first consider the type of carrier controlling the charge transport. As previously mentioned, the carrier sign cannot be determined from transient rise measurements alone, but must be deduced from other information. Thermoelectric power measurements were attempted in order to obtain the sign of the dominant carrier. The results of these experiments were severely distorted by electrical noise, but it was possible to obtain some tentative measurements at very high temperatures (> 150^{o}C). The general conclusion of these measurements was that the dominant carrier (at high temperatures) was electrons. This conclusion is consistent with reports in the literature (9) on the dominant charge carrier in sputtered a - Si:H.

The activated form of the mobility over the temperature range investigated can arise from either a trap controlled band mechanism, or from thermally activated hopping of carriers between localised sites. The hopping process is likely to take one of two forms: either hopping between localised levels situated at a particular energy in the mobility gap, leading to a mobility of the form (see equation 1.8)

$$\mu_h = \text{const.} \exp\left(-\frac{W}{kT}\right) \qquad - \qquad (6.2)$$

where W is a hopping energy and the value of the constant is not expected to appreciably exceed 10^{-2} cm^2 $V^{-1}s^{-1}$; or a trap controlled hopping mechanism producing a mobility of the form (see section 2.5.3)

$$\mu = \mu_h \left[1 + \frac{N_{t2}}{N_{t1}} \exp\left(\frac{E_{t1} - E_{t2}}{kT} \right) \right]^{-1} \quad - \quad (6.3)$$

where μ_h is a hopping mobility, N_{t1} is the trap density at energy E_{t1}, and N_{t2} is the trap density at energy E_{t2}. From curve fitting, the mobility data yield a pre - exponential of 5 cm^2 $V^{-1}s^{-1}$, indicating that the hopping mechanism described by equation 6.2 is unlikely to occur. It is not possible to deduce whether the trap controlled hopping mechanism described by equation 6.3 is consistent with the experimental data, without first obtaining further information about the proposed trap densities N_{t1} and N_{t2}, or by raising the specimen temperature to a level where mobilities substantially greater than 10^{-2} cm^2 $V^{-1}s^{-1}$ can be measured. (It is interesting to note that figure 6.9 shows two specimens where the measured drift mobility is slightly greater than 10^{-2} cm^2 $V^{-1}s^{-1}$ and still rising with increasing temperature, without any sign of saturation).

The exact form of the drift mobility resulting from a trap controlled band mechanism depends upon the energetic distribution of localised states (see section 2.5.3). For a well defined set of traps of density N_t situated at an energy E_t below the mobility edge the mobility is expected in the form

$$\mu = \mu_0 \left[1 + \frac{N_t}{N_c} \exp\left(\frac{E_t}{kT} \right) \right]^{-1} \quad - \quad (6.4)$$

Alternative models which consider the existence of a tail of localised states at the band edge lead to results which in general are similar to those obtained from a linear band tail of depth ΔE, i.e.

$$\mu = \mu_0 \left(\frac{\Delta E}{kT}\right) \exp\left(-\frac{\Delta E}{kT}\right) \qquad - \qquad (6.5)$$

Interpreting the mobility data using equation 6.4 yields a value of 5 $cm^2 V^{-1}s^{-1}$ for the term $\mu_0 N_c/N_t$. Assuming $\mu_0 \simeq 1$ $cm^2 V^{-1}s^{-1}$ (from time of flight data) and $N_c \simeq 10^{20}$ cm^{-3}, implies a discrete trap density of magnitude $N_t \simeq 10^{19}$ cm^{-3} situated at an energy of 0.21 eV below the conduction band mobility edge. This very large trap density throws considerable doubt on the interpretation of these transport data using a model consisting of a single discrete set of traps. A more satisfactory fit to the experimental data can be achieved using the linear band tail model described by equation 6.5. Figure 6.11 shows the mobility data of figure 6.9, re - plotted on axes of $kT\mu$ versus inverse temperature. The plot provides a pre - exponential $\mu_0 \Delta E = 0.33$ $cm^2 V^{-1}s^{-1}$ eV and an activation energy $\Delta E = 0.23$ eV. Combining these data yields a free carrier mobility of $\mu_0 = 1.4$ $cm^2 V^{-1}s^{-1}$. This value of μ_0 is consistent with mobility data deduced from the time of flight experiment reported previously, and with data presented in the literature (17). It is thus concluded that band transport combined with carrier interaction with a limited band tail is more likely to occur as opposed to carrier interaction with a single discrete set of states.

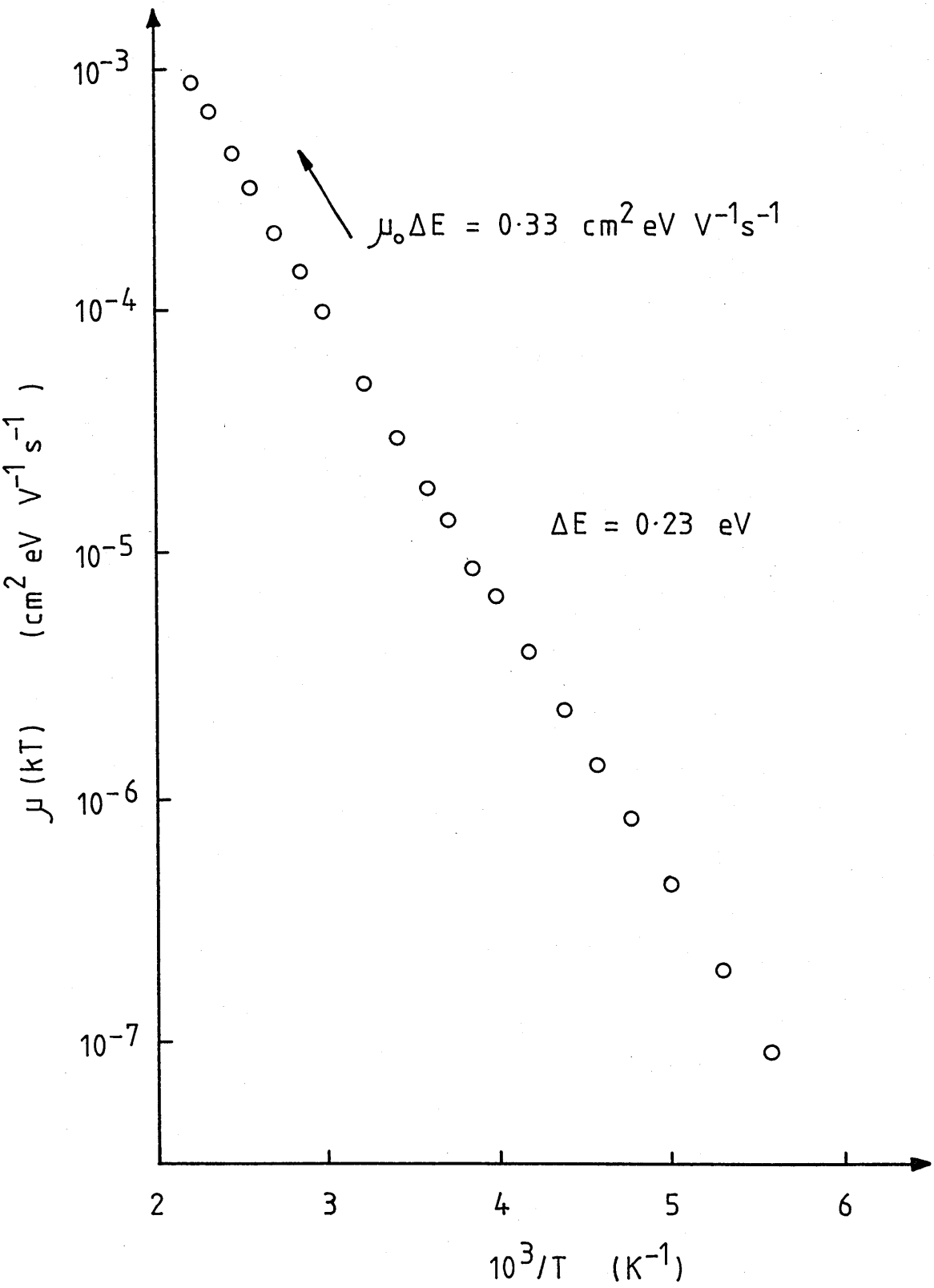

Figure 6.11. Plot of μ(kT) versus inverse temperature for the specimen marked with the asterisk in figure 6.9.

Differentiation must now be made between the existence of a trap - limited hopping mechanism and a trap - limited band transport mechanism. This can be achieved by considering the time of flight data presented previously, and will be discussed below.

Results of the transient photoconductivity experiments have shown that at room temperature, the carrier drift mobility and the trap - limited carrier lifetime of a - Si:H (for specimen *) are of order 2×10^{-3} $cm^2 V^{-1} s^{-1}$ and 1.5×10^{-2} sec respectively. Assuming an extended state free mobility of 1 $cm^2 V^{-1} s^{-1}$ implies a free carrier recombination time of order 30 μs. This recombination time is considerably longer (more than 3 orders of magnitude) than the duration of the 20 ns current pulse observed in the time of flight experiment implying that in the time of flight experiment, the current pulses observed are in fact due to the fast drift of excess carriers through the film, and not due to the loss of injected charge by trapping followed by recombination. On this assumption it is possible to deduce useful information about the temperature dependence of the mobility observed in the transient photoconductivity experiment.

Transit pulses of duration 20 ns were obtained from specimens 10 microns thick, under applied voltages of between 10 and 30 Volts. Assuming these current pulses to be genuine "time of flight" pulses associated with the drift of charge through the specimen, allows a drift mobility of order 1 $cm^2 V^{-1} s^{-1}$ to be derived. The magnitude of this drift mobility is substantially greater than that expected for a hopping process, implying the existence of a band transport mechanism.

The following conclusions can thus be drawn from the above argument:

(1). Transport in r.f. sputtered a - Si:H prepared in this laboratory is controlled by a trap - limited band transport mechanism.

(2). The mechanism predicts carriers (concluded from other evidence to be electrons) moving at the mobility edge but experiencing trapping and thermal release events in a tail of localised states which extends to an energy of 0.23 eV below the conduction band mobility edge.

(3). The experimental data provides a satisfactory fit to a linear band tail model. However, due to the similarity in results obtained from a number of distributions of band tail states it is not possible, with the data available, to uniquely define the "shape" of the limited band tail.

Although the above conclusions are consistent with results obtained from the transient photoconductivity experiment, at first sight they do not appear to be in complete accord with the time of flight data presented previously. Results of the time of flight experiment (in conjunction with lifetime measurements) have suggested that carriers move through extended states, without being slowed down by shallow trapping events. In contrast, the transient photoconductivity experiment has indicated that the electron drift mobility is controlled by interactions with a tail of localised states. The different experimental techniques therefore yield conflicting information about the details of charge transport. This anomaly can tentatively be explained by considering the inherent differences between the two experimental techniques. In the time of flight experiment, the carriers generated by the flash

illumination must traverse the specimen in times shorter than both the trapping time and the recombination time. This explanation has been shown to be the most likely and was discussed in full in section 6.4.2.1. On completion of a transit, carriers cannot be re - injected due to the existence of a "blocking" top electrode. In the transient photoconductivity experiment, however, there are no blocking electrodes and carriers can continually be re - injected until they recombine. Using the deduced $\mu\tau$ product of 30×10^{-6} cm^2 V^{-1} and the experimentally applied electric field of 3×10^3 V cm^{-1}, an electron $\mu\tau E$ range of approximately 900 microns can be established. With an inter - electrode separation of 300 microns it can be seen that, on average, an electron will traverse the specimen three times before recombination. It can thus be argued that in the transient photoconductivity experiment carriers are in transit for a much longer time, (compared with the time of flight experiment), and are thus able to interact with the trapping centres. The distribution of traps will thus be revealed by a transient photoconductivity experiment, but not by a time of flight experiment.

A further argument not considered so far, is that in each of the specimen configurations there may be an appreciable density of surface states. In the co - planar specimens it is likely that the carriers will diffuse to the surface a number of times during their (multiple) transit and will therefore interact with the surface states. In sandwich cell specimens, however, the surface states will not have such an appreciable effect, since the carriers will only encounter these states at the start and at the end of their transit. If the specimen is relatively thick, the effect of the surface states will be small.

The specimen to specimen experimental scatter exhibited by both the mobility and the lifetime data of a - Si:H (figures 6.9 and 6.10) will now be discussed. The discussion will initially be restricted to data obtained from material prepared in this laboratory. Data obtained from specimens of a - Si:H prepared at Glasgow University differ in detail and will be discussed at the end of this section.

From table 6.1 it can be seen that the mobility pre - exponential (μ') varies over the range 0.5 to 8 $cm^2 V^{-1} s^{-1}$. This spread is over about one order of magnitude suggesting that transport in all of the specimens is probably controlled by the same basic mechanism, namely trap controlled band transport. The mobility activation energy (E_μ), on the other hand, assumes a value which lies in two distinct ranges, namely; range (a), E_μ = 0.20 to 0.24 eV and range (b), E_μ = 0.30 to 0.42 eV. None of the mobility data exhibit a high temperature activation energy which lies between these two ranges.

These data suggest that the carrier drift mobility may be controlled by two distinct sets of localised states within the mobility gap. The first set corresponds to mobility data giving an activation energy in range (a), these states probably existing as a limited band tail which extends to an energy of between 0.20 and 0.24 eV below the mobility edge. The second set corresponds to mobility data giving an activation energy in range (b), these states probably existing as a fairly discrete set, situated at an energy of 0.30 to 0.42 eV below the mobility edge. The postulated density of states distribution for the material prepared in this laboratory is thus illustrated schematically in figure 6.12.

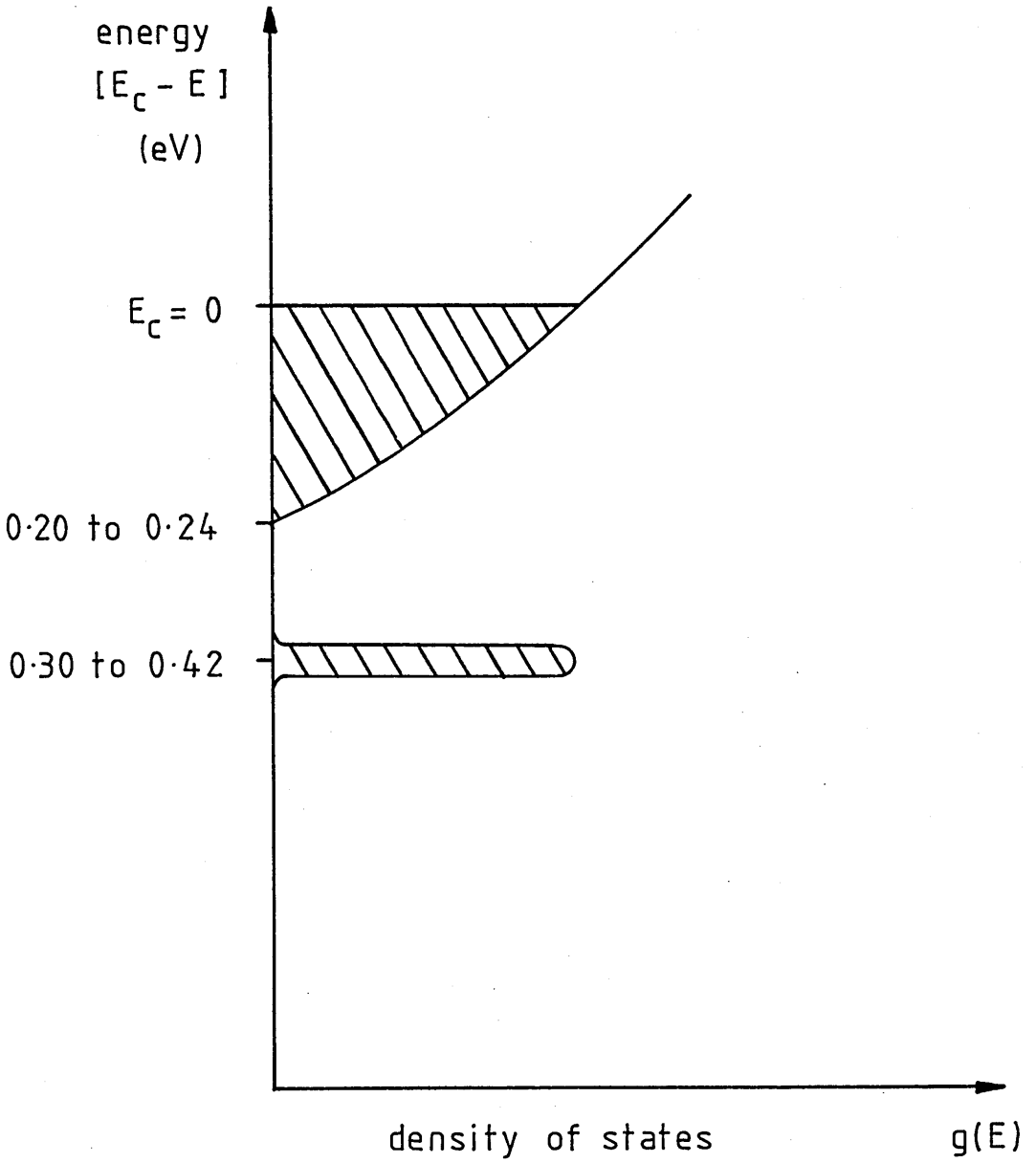

Figure 6.12. Schematic representation of the proposed "general" density of states distribution for the a-Si:H prepared in this laboratory. The discrete state density may vary considerably in magnitude.

It is proposed that all of the specimens deposited will possess the distribution of tail states. The density of discrete states, however, may vary considerably in magnitude from specimen to specimen. In those specimens where the discrete trap density is negligably small, the transport will be dominated by interactions with the tail states, leading to mobility data belonging to range (a). In those specimens where the discrete trap density is considerable, these states will dominate the transport, producing mobility data corresponding to range (b). Mobility data in range (a) are singly activated over the complete temperature range investigated, suggesting that the tail states dominate the transport over the complete temperature range. Mobility data in range (b), however, are not singly activated over the complete temperature span. A possible two - stage explanation can be put forward for this phenomenon. Firstly, at high temperature the mobility is controlled by interactions with the discrete trap density, leading to a well defined mobility activation energy. Secondly, at low temperatures, the dominant transport path may shift from a trap limited band transport mechanism to a hopping mechanism. The exact details of the hopping transport will be determined by the most energetically favorable path through the localised states, which may be one of, or a combination of the following: (i) hopping through the tail states, (ii) hopping between the discrete states and, (iii) trap limited hopping between the tail states and the discrete states.

The question that must now be answered is "why does the density of states distribution vary so considerably from specimen to specimen?" This question can tentatively be answered as follows.

Firstly, as discussed in Chapter 3, it has been found that the density of states distribution throughout the mobility gap of a - Si:H is influenced to a considerable extent by the minute details of film deposition. It is thus proposed that the depth of the tail states (and the density of discrete states) will be influenced by the degree of disorder introduced into the lattice during film growth; this in turn being related to the deposition conditions. Secondly, it has recently been established by X - ray studies (see Sections 6.5.1 and 6.8.1) that there can be a considerable density of impurity atoms in the material prepared in this laboratory. These impurities, which have appeared in concentrations of up to 3 at. %, are principally Arsenic and Selenium. It is most likely that these elements have entered the a - Si:H lattice during film deposition, since Arsenic Tri - Selenide is a commonly deposited substance within the sputtering chamber. It is proposed that these impurity atoms may have a determining influence on the density of defect states below the mobility edge and hence be instrumental in producing the proposed discrete trap density. Further, since the amount of Arsenic and Selenium in the sputtering chamber prior to any deposition will be unpredictable, it is suggested that this fact may, to a large extent, account for the randomness observed in the electronic transport properties obtained from different specimens deposited under seemingly identical conditions in this laboratory.

As a footnote it is worth pointing out that it has been established by compositional analyses of sputtered films of a - Si:H, that after certain impurities (e.g. Arsenic and Selenium) have been introduced into the sputtering chamber, many hours of sputtering must be completed before these impurity atoms can no longer be detected in the deposited films.

It is therefore suggested that in order to produce a material which displays more consistent characteristics from specimen to specimen a completely "clean" deposition system must be employed.

Considering now the experimental scatter exhibited by the trap limited lifetime data, it can be seen from figures 6.9 and 6.10 that no correlation appears to exist between the mobility and the lifetime data. This fact can easily be explained if it is assumed that the carrier mobility is controlled by states close to the mobility edge while the carrier trap limited lifetime is controlled both by such states and by states elsewhere in the energy gap, (recombination centres). With the above in mind, it is proposed that from specimen to specimen, random changes in the minute conditions of film deposition, together with random concentrations of impurity atoms in the films, will affect the density of recombination centres, and the density of states just below the mobility edge, by differing amounts. These unpredictable variations in the density of states distribution will in turn lead to the lack of correlation between the mobility and the lifetime data. One thing is clear, however, that being that in order to produce films with good photoconductive properties, both the carrier lifetime and the carrier mobility should be maximised. Therefore, it must be established which parts of the density of states distribution control the mobility and which parts control the lifetime, and what film preparation conditions are required in order to optimise these distributions so that optimum film characteristics may be achieved. This is one possible avenue along which this investigation may be extended.

Turning now to the material prepared at Glasgow University it can be seen from table 6.1 that this film yields a mobility pre - exponential of $\mu' = 8 \times 10^{-3}$ cm^2 V^{-1}s^{-1} and a high temperature mobility activation energy of 0.26 eV. This value of μ' is not consistent with band transport motion suggesting that carrier conduction in this film is via a hopping mechanism. From figure 6.10 it can be seen that carrier lifetimes in the Glasgow material are comparable with the shortest lifetime values obtained from material prepared in this laboratory.

In conclusion it appears that the particular Glasgow specimen supplied has a relatively large density of states within the mobility gap, suggesting that this material is of inferior quality in terms of photoconductive properties. This fact is born out by steady state photoconductivity measurements which are presented in the following section.

6.4.4 STEADY STATE PHOTOCONDUCTIVITY.

Steady state photoconductivity (SSP) measurements were performed on specimens of a - Si:H using the same l.e.d. - light pipe arrangement as was used for transient photoconductivity measurements. In SSP measurements, the l.e.d. was supplied with a constant current from a variable voltage supply. Measurements were carried out over as wide a temperature range as possible.

Figure 6.13 shows plots of the steady state photocurrent versus inverse temperature for six of the specimens of a - Si:H studied in the previous section. All of the curves shown are qualitatively similar and can be phenomenologically characterised as follows:

(a). The photocurrent displays a maximum at a point where the dark current and the photocurrent are approximately equal.

(b). At temperatures above the maximum, the photocurrent decreases with increasing temperature. This is denoted as region (A).

(c). At temperatures below the maximum, the photocurrent decreases with decreasing temperature and in most cases a unique activation energy (E_{Ph}) can be defined. This is denoted as region (B). (In one particular case (specimen x) no unique activation energy could be defined since the photocurrent displayed continuous curvature towards lower effective activation energies with decreasing temperature.)

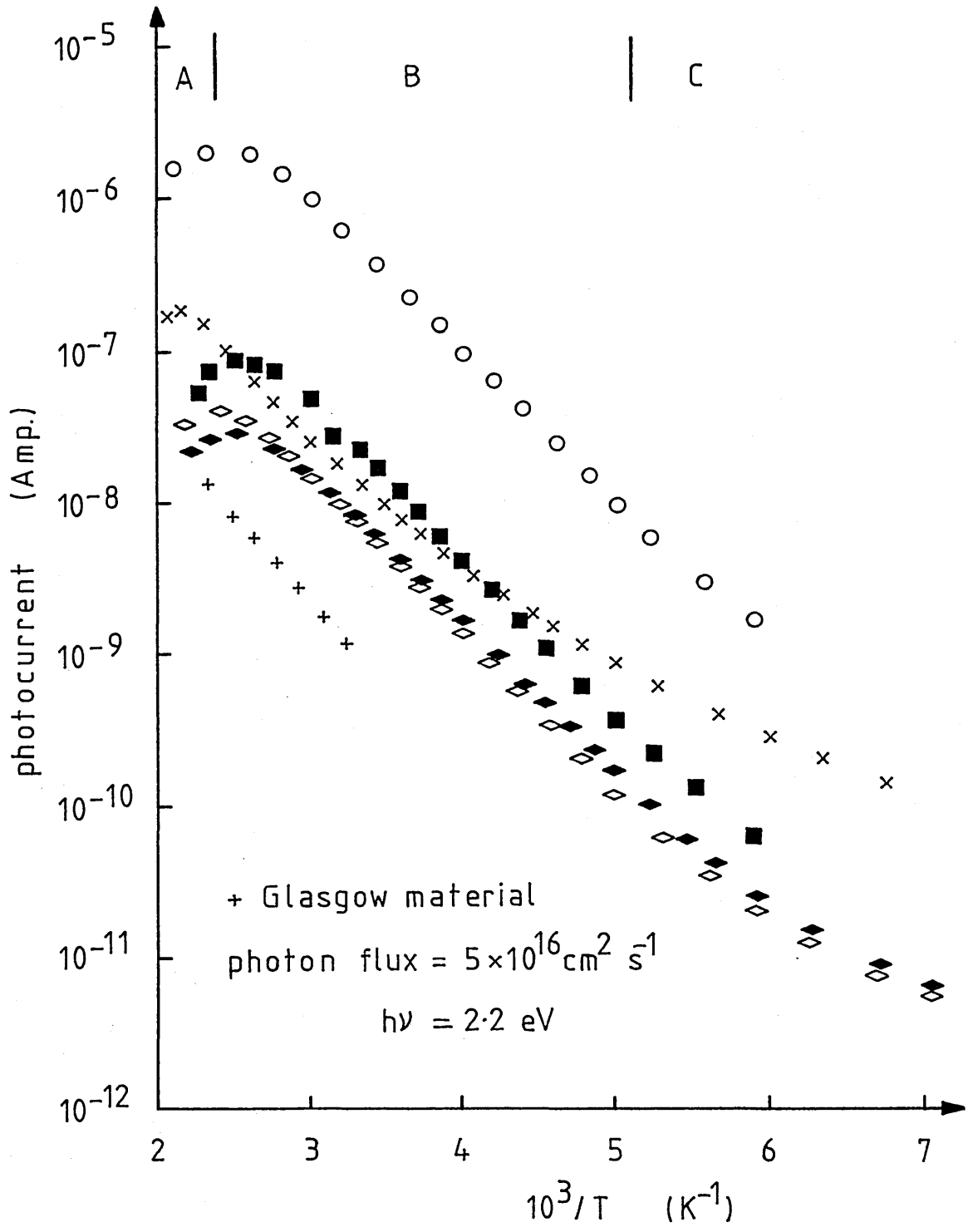

Figure 6.13. Steady state photocurrent versus inverse temperature for six of the specimens of a-Si:H studied in section 6.4.3.

(d). At very low temperatures the photocurrent plots depart from singly activated behavior and tend to "flatten off", displaying an effective activation energy which decreases with decreasing temperature. This is denoted as region (C).

Figure 6.14 shows the relationship between the steady state photocurrent and the incident photon flux density for specimen ■, under conditions of constant temperature. The curve for 420 K shows clearly the transition from a linear (monomolecular) to a "square root" (bimolecular) photocurrent - photon flux dependence, with increasing photon flux density. Such a transition also occurs at other temperatures but is experimentally less accessible (see for example the 340 K curve). In the bimolecular region the photocurrent - intensity index is slightly higher than square root, being approximately 0.66. Figure 6.14 shows also the dark current flowing in the specimen at 420 K. It can be seen that the linear to "square root" transition occurs roughly at a point where the photocurrent and the dark current are equal. Thus, returning to figure 6.13, it can be established that (for specimen ■) at temperatures below the photocurrent maximum a sub - linear relationship exists between the photocurrent and the photon flux density, while at temperatures above the photocurrent maximum a linear relationship characterises the photocurrent - photon flux dependence.

By means of a comparison, table 6.2 shows the activation energies deduced from both the steady state photocurrent (figure 6.13) and the drift mobility (figure 6.9) data, in the temperature region below the photocurrent maximum (Region B), for all of the specimens investigated. The data in this table can, to a first approximation, be divided into

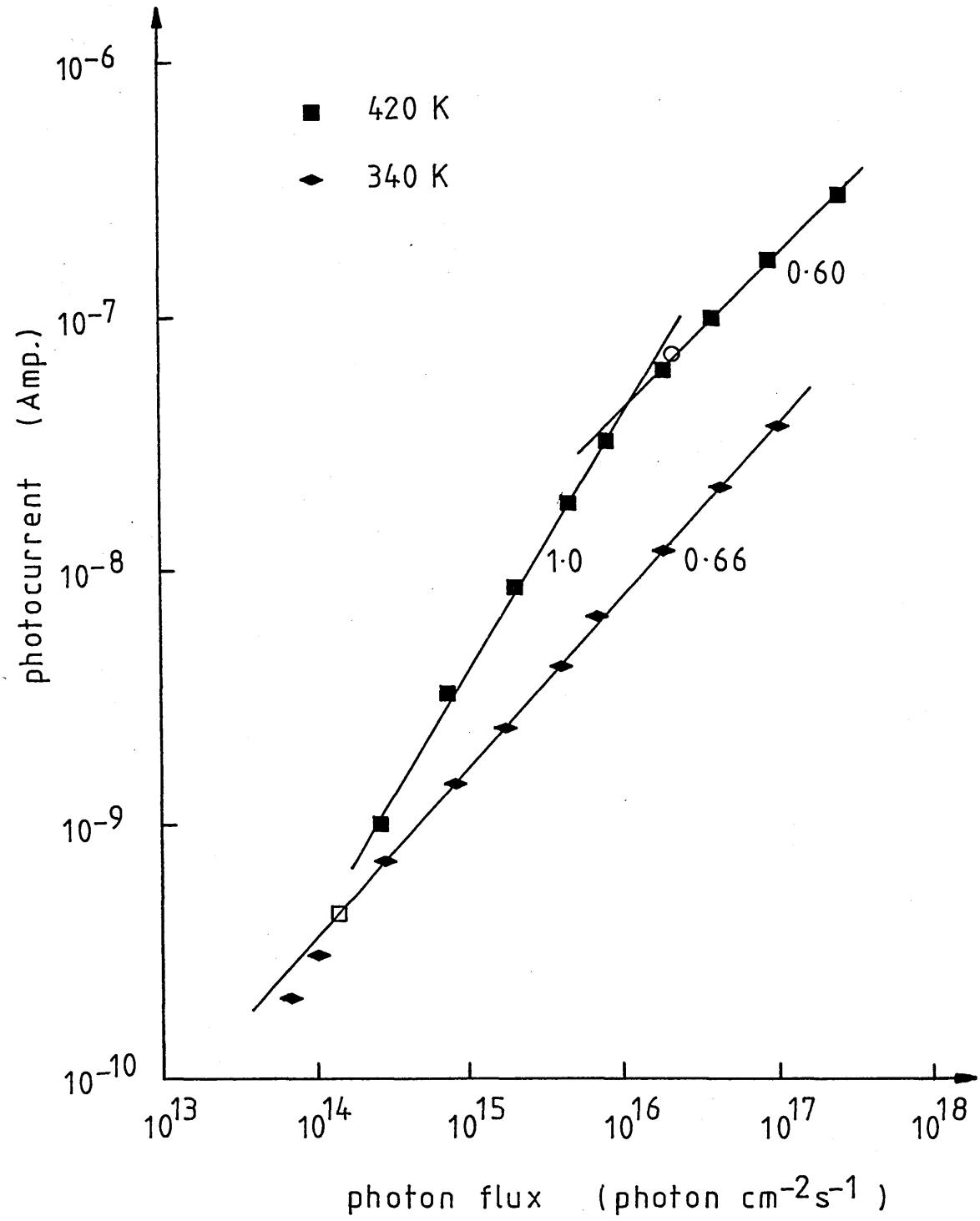

Figure 6.14. Steady state photocurrent versus photon flux for specimen ■ , at the temperatures shown. ○ and □ show the dark current flowing at 420K and 340K respectively. The slope of each line is indicated in the figure.

Specimen	E_{μ} (eV)	E_{ph} (eV)
○	0.21	0.20
■	0.30	0.22
◇	0.40	0.21
◆	0.42	0.20
×	0.32	curved
+	0.26	0.23

Table 6.2.

A comparison of the activation energies deduced from steady state photocurrent data in temperature range B (figure 6.13), and from drift mobility data (figure 6.9).

three main categories, namely; (i) Specimens in which $E_{\mathcal{N}}$ and E_{ph} are approximately equal (○ , +), (ii) Specimens in which E_{ph} is considerable less than $E_{\mathcal{N}}$ (■ ,◇ ,◆), and (iii) Specimens in which the drift mobility is singly activated but where the steady state photocurrent displays no unique activation energy (×).

Note. For all of the specimens studied, too few data points could be obtained at high temperature in order to define an activation energy from the photocurrent plots at temperatures above the photocurrent maximum (Region A).

6.4.4.1 DISCUSSION.

It is immediately evident from figure 6.13, that as with other measurements on sputtered a - Si:H, the photoconductivity measured under standard conditions varies widely from specimen to specimen. It is also clear from the complexity of the curves shown, that no single process of transport and / or recombination is likely to universally characterise the photoconductivity in all of the specimens studied. In section 6.4.3, however, it was shown that transient photoconductivity data could be interpreted using the density of states distribution illustrated in figure 6.12. Thus, in order to be consistent, the steady state photocurrent data presented here will also be analysed in terms of the same density of states distribution. The discussion will be divided into two main sections. Firstly, after some preliminary simplifying assumptions have been made, a photoconductivity analyses will be performed based on the density of states distribution shown in figure

6.12. Using the results of this analyses, the general features of the photocurrent plots of figure 6.13 will be interpreted. Secondly, both the steady state photoconductivity data presented in this section, and the transient photoconductivity data presented in section 6.4.3 will be analysed for each of the three broad categories of specimens outlined in the previous section.

The following simplifying assumptions will be made:

(a). In the steady state, the excess occupation of the band tail states will be dominated by carriers which are trapped within the bottom few kT of the tail. Thus, the tail state distribution will be replaced by a single, discrete set of traps, situated at an energy equal to that of the bottom of the tail. The magnitude of the discrete state density will be equal to the effective density of states within the bottom few kT of the tail.

(b). The Fermi level under thermal equilibrium conditions will be "pinned" close to mid - gap possibly by a density of defect states which do not take part in the recombination traffic.

(c). A density of recombination centres will exist between the dark Fermi level and the valence band mobility edge.(Spear et al (11) found such recombination centres to exist in glow discharge deposited material).

(d). Under all conditions of illumination and temperature the quasi - Fermi levels will be several kT away from all trap and

recombination centres.

Applying these simplifying assumptions to the distribution of figure 6.12 leads to the density of states distribution which is illustrated schematically in figure 6.15.

From transient photoconductivity measurements, it was deduced that both sets of traps (i.e. N_1 and N_2) may exist in all of the sputtered material prepared in this laboratory. It was further proposed that the density, N_2, may be variable in magnitude, its size being directly related to the level of impurity atoms within the film and to the condition of film deposition. In the steady state, however, it is proposed that the excess occupation of level 2 may be considerably greater than that of level 1. If band to localised recombination is then invoked (i.e. E_c to E_3 as illustrated in figure 6.15) a satisfactory fit to the experimental data can be obtained, as illustrated below.

Evidence from transient photoconductivity and dark conductivity experiments has shown that, in the temperature region of interest (Region B), conduction is dominated by electrons in extended states at E_c. Thus, extrapolating this conclusion to steady state photoconductivity (σ_{ph}) measurements yields

$$\sigma_{ph} = n_c e \mu_c \qquad - \quad (6.6)$$

where μ_c is the electron mobility in extended states at E_c, e is the electronic charge and n_c is the density of electrons in the conduction band. Now, under steady state conditions, the majority of the

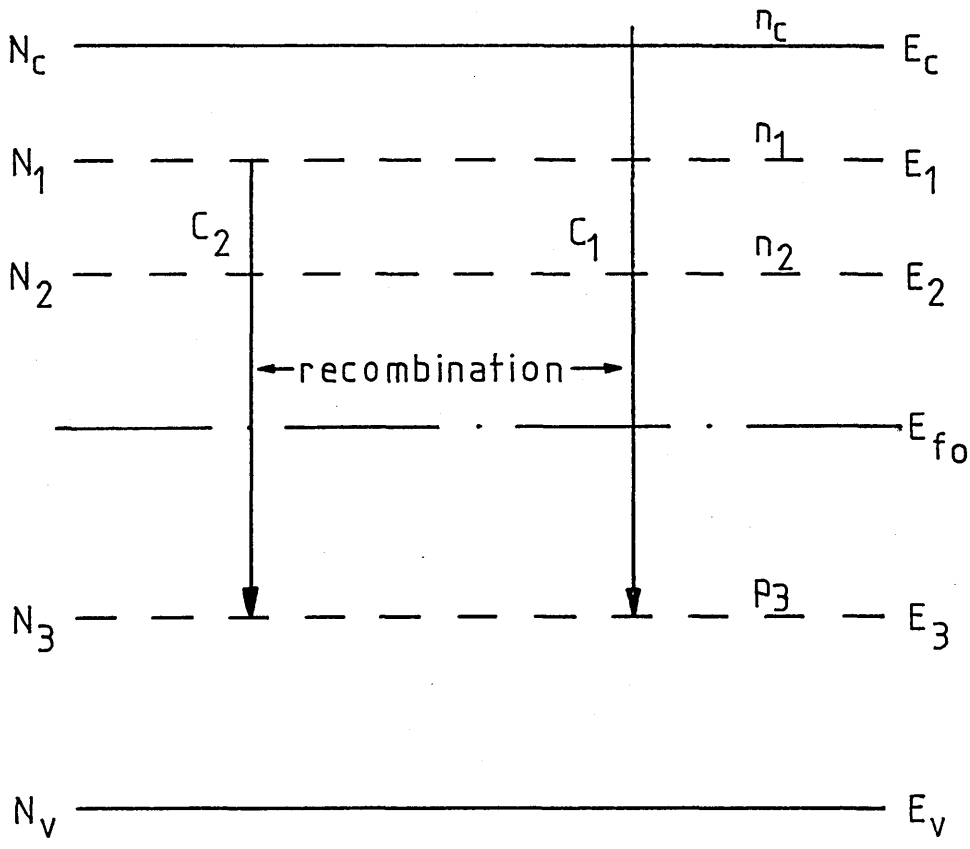

Figure 6.15. Application of the simplifying assumptions detailed in the text to the density of states distribution of figure 6.12, leads to the distribution shown here. The relevant coefficients associated with each of the energy levels are given in the figure. C_1 and C_2 are the recombination coefficients associated with the recombination paths shown.

photogenerated carriers will be in localised states. If it is assumed that the excess occupation of level 2 is considerably greater than that of level 1, application of the charge neutrality condition yields $n_2 \simeq p_3$. If recombination is from E_c to E_3, then

$$G = C_1 n_c p_3 \qquad - \qquad (6.7)$$

where G is the generation rate of free electron - hole pairs and C_1 is the relevant recombination coefficient. Under steady state conditions, n_2 and n_c are related by

$$\frac{n_c}{n_2} = \frac{N_c}{N_2} \exp\left(-\frac{E_c - E_2}{kT}\right) \qquad - \qquad (6.8)$$

Thus, combining equations 6.6, 6.7 and 6.8, together with the charge neutrality condition yields

$$\sigma_{ph} = e\mu_c \left(\frac{G N_c}{C_1 N_2}\right)^{\frac{1}{2}} \exp\left(-\frac{E_c - E_2}{2kT}\right) \qquad - \qquad (6.9)$$

This equation predicts a square - root relationship between the photocurrent and the photon flux, and a photocurrent activation energy of $(E_c - E_2)/2$. Thus, if it is assumed that firstly, the trap level at E_2 exists at an energy of 0.4 eV below the conduction band mobility edge in all of the sputtered specimens, and secondly, that the states at E_2 dominate the charge neutrality, then an activation energy of approximately 0.2 eV is expected from steady state photoconductivity measurements on all of the specimens studied. From table 6.2 it can be seen that, excepting specimen (x), this conclusion agrees favourably

with the experimental data.

The specimens in each of the three categories outlined in the previous section will now be discussed.

(i). Specimens in which E_μ and E_{ph} are approximately equal (O,+).

For these specimens, the above analyses gives a satisfactory fit to the steady state photocurrent data. However, it might be expected that the trap level at E_2 should be revealed in a transient photoconductivity experiment, leading to an observed electron drift mobility activation energy of 0.4 eV. It is proposed that this may not be the case for the reasons outlined below.

As discussed in this Chapter, the electron drift mobility was deduced from the initial rate of rise of the transient photoconductivity. If a semiconductor with two shallow trap levels (N_1 at 0.2 eV below E_c and N_2 at 0.4 eV below E_c) were to be suddenly illuminated, then a photocurrent rise curve similar to that shown in figure 6.16 might be expected. Now, in all of the transient rise measurements performed in this study, the drift mobility was deduced from the gradient of the photocurrent - time trace at times which were as short as practically possible. It can be seen from figure 6.16, that at very short times, the shallower traps (N_1) may determine the initial rate of rise of the photoconductivity, and the deduced drift mobility Arrhenius plot would yield a mobility activation energy of 0.2 eV. In the steady state, however, the 0.4 eV deep traps will dominate the transport, leading to a steady state bimolecular photocurrent activation energy also of 0.2 eV. Thus, by this argument, a 0.4 eV activation energy will never be

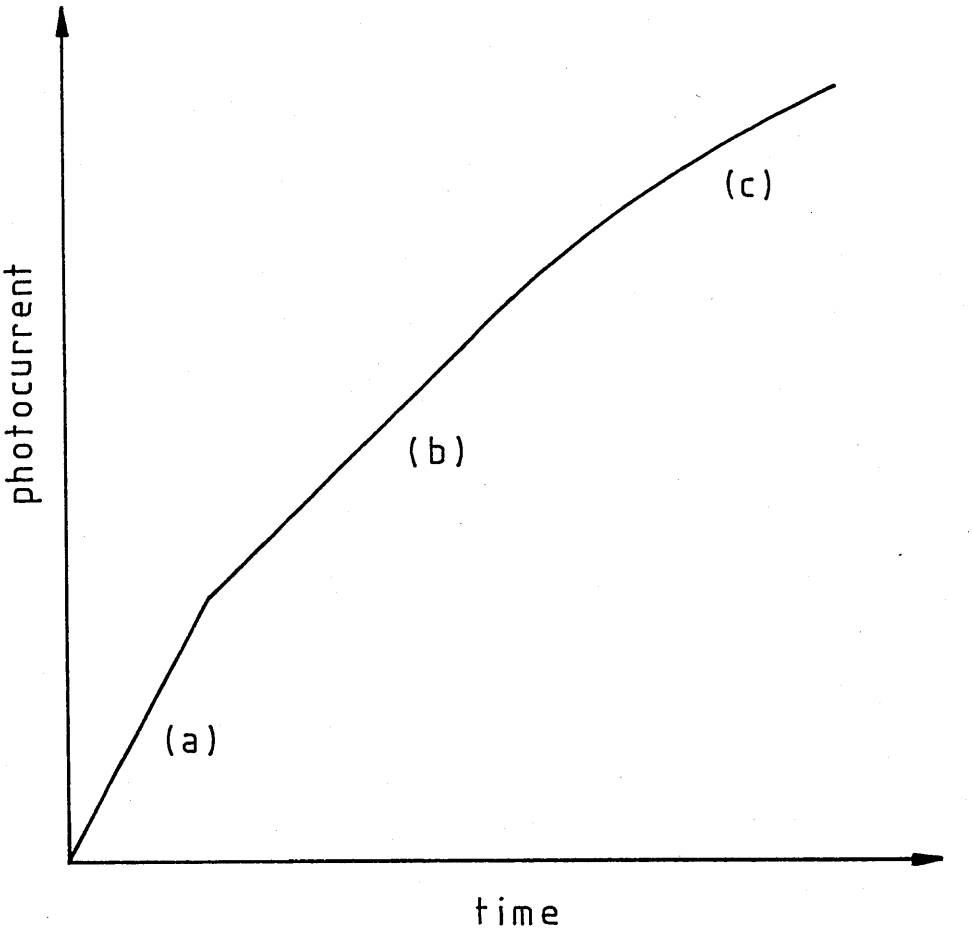

Figure 6.16. A typical transient photocurrent rise curve which may be expected from a specimen with the density of states distribution shown in figure 6.15.
(a). Slope determined by the 0.2 eV deep traps (N_1).
(b). Slope determined by the 0.4 eV deep traps (N_2).
(c). Recombination limited growth.

experimentally observed in these specimens.

The trap limited lifetime data of figure 6.10 will now be considered. - In the steady state, the magnitude of the photocurrent is determined by the product of the free carrier mobility (μ_0) and the free carrier recombination time (τ_f) as in

$$I_{ph} = \mu_0 \tau_f \qquad - \qquad (6.10)$$

If μ_0 can be considered temperature independent, then in the bimolecular region the steady state photocurrent activation energy (E_{ph}), and the activation energy of τ_f (E_{τ_f}) will be identical, i.e. $E_{ph} = E_{\tau_f} \simeq 0.2$ eV. Figure 6.10, however, shows the <u>experimentally observed</u> photo - decay time plotted as a function of inverse temperature. This photo - decay time will be longer than the free carrier recombination time by the ratio of trapped to free carriers, i.e.

$$\tau_{ph} = \tau_f \left(\frac{\text{trapped carrier density}}{\text{free carrier density}} \right) \qquad - \qquad (6.11)$$

where τ_{ph} is the observed photo - decay time. If in the initial part of the decay, the interchange with traps at E_1 is most rapid, then over the first part of the decay curve

$$\tau_{ph} \simeq \tau_f \left(\frac{n_1}{n_c} \right) \qquad (6.12)$$

and the observed τ_{ph} activation energy ($E_{\tau_{ph}}$) will be

$$E_{\tau_{ph}} = E_{\tau_f} - (E_c - E_1) = 0.2 - 0.2 = 0 \text{ eV} - (6.13)$$

Thus, a fairly temperature independent photo - decay time is expected. This conclusion is in agreement with the experimental data of figure 6.10. It is also worth noting that the magnitude of the term $(E_c - E_1)$ in equation 6.13 may be greater than, or less than 0.2 eV, depending upon the position in the mobility gap of the distribution of trapped carriers that dominate the photo - decay process. Thus, either a slightly increasing or a slightly decreasing photo - decay time with inverse temperature may be observed in the bimolecular region, the exact relationship being determined by the detailed "shape" of the density of states distribution. As can be seen from figure 6.10, both increasing and decreasing photo - decay times with 1/T have been experimentally observed.

For specimens in this category, an alternative description of the photoconductivity kinetics is possible. If it is assumed that the density of traps at N_2 is negligible (as has been suggested in section 6.4.3 for the specimens associated with this category), then following Spear et al (11) it is proposed that localised to localised transitions (from E_1 to E_3 as shown in figure 6.15) may dominate the recombination traffic. Under these conditions the charge neutrality condition yields $n_1 \simeq p_3$, and in the steady state

$$G = C_2 n_1 p_3 \qquad - \qquad (6.14)$$

where C_2 is the relevant recombination coefficient. Also, in the steady state n_c and n_1 are related by

$$\frac{n_c}{n_1} = \frac{N_c}{N_1} \exp\left(-\frac{E_c - E_1}{kT}\right) \qquad - \qquad (6.15)$$

Thus, combining equations 6.6, 6.14 and 6.15, together with the charge neutrality condition yields

$$\sigma_{Ph} = e\mu_c \left(\frac{G}{C_2}\right)^{\frac{1}{2}} \frac{N_c}{N_1} \exp\left(-\frac{E_c - E_1}{kT}\right) \quad - \quad (6.16)$$

This equation predicts the correct steady state photocurrent activation energy of 0.2 eV, together with a square - root photocurrent - photon flux dependence. Further, by an argument similar to that outlined above, it can be shown that this recombination model predicts a temperature independent photo - decay time and a drift mobility activation energy of $(E_c - E_1) = 0.2$ eV (in the bimolecular region) in agreement with experimental results.

(ii) Specimens in which E_{Ph} is considerably less than E_μ (■,◇,◆).

In these specimens, the steady state photocurrent data can be interpreted using the recombination model described by equation 6.9 (i.e. band to localised recombination from E_c to E_3). This leads to a photocurrent activation energy of 0.2 eV in agreement with experimental data. It is proposed that for specimens ◇ and ◆ , the transient photocurrent rise associated with the 0.2 eV deep traps occurs at too short a time to be experimentally resolvable. Thus, the slope of the photocurrent - time trace which is experimentally measured will be associated with the 0.4 eV deep traps, leading to a experimentally deduced drift mobility activation energy of 0.4 eV. For specimen ■ , the particular time scale over which the rate of rise of the transient photocurrent is computed may be associated with a transition region between the rise corresponding to the 0.2 eV deep traps and the rise

corresponding to the 0.4 eV deep traps. If the relative "time of measurement" remains unchanged over a given temperature span, then an activation energy of between 0.2 and 0.4 eV might be expected from a drift mobility Arrhenius plot. As seen from table 6.2, the specimen of interest yields a mobility activation energy of 0.30 eV in agreement with this hypothesis.

(iii). Specimens in which the drift mobility is singly activated over a limited temperature range but where the steady state photocurrent yields no unique activation energy (x).

In this particular specimen, it is proposed that over the temperature range of interest, no single transition path dominated the recombination kinetics. As the temperature is decreased, the details of the transport and / or the recombination traffic may change, leading to a photocurrent Arrhenius plot which is continuously curved. In the transient photoconductivity, however, if the relative "time of measurement" with respect to a given trap level remains fairly constant over a given temperature span, then it may be possible to obtain a singly activated mobility arrhenius plot over that temperature range. As can be seen from figures 6.9 and 6.13, this explanation is in reasonable agreement with the experimental data.

The following conclusions can be drawn from the discussion presented in this section.

(a). All of the steady state photoconductivity data obtained from

sputtered specimens of a - Si:H prepared in this laboratory can be interpreted using the density of states distribution shown in figure 6.12, together with the addition of suitable recombination centres. Results from this section, however, suggest that the discrete trap density should be situated at 0.42 $\pm$ 0.02eV below the conduction band mobility edge, as opposed to the spread in position of 0.30 to 0.42 eV which was deduced from transient photoconductivity measurements in isolation.

(b). No single process of transport and / or recombination can be used to universally characterise the photoconductivity in all of the specimens studied.

(c). In general, there is reasonable agreement between results obtained from steady state photoconductivity and from transient photoconductivity measurements.

6.5.4 OPTICAL ABSORPTION.

Optical transmission measurements were carried out on thin films of amorphous Silicon supported on Corning 7059 glass substrates. The optical transmission loss of the glass substrates was investigated and found to be constant over the complete photon energy range of interest. Before measurements were performed the optical transmission / reflection loss of the specimen configuration was estimated. This was achieved by performing optical transmission measurements at very low photon energies ($\simeq$ 1.1 eV). If the photon loss at that energy was found to be L %, then

all subsequent transmission measurements were loss corrected by multiplying the transmitted intensity by the factor 100/(100 - L). The optical absorption coefficient was calculated as described in Chapter 4.

Figure 6.17 shows the optical absorption coefficient (α) plotted as a function of photon energy ($h\nu$) for several specimens of amorphous Silicon. All of the specimens were hydrogenated and prepared under the same deposition conditions, except for the unhydrogenated specimen which is indicated. The same data are presented in figure 6.18, re - plotted on axes of $(\alpha h\nu)^{\frac{1}{2}}$ versus photon energy.

6.4.5.1 DISCUSSION

The optical absorption data shown in figure 6.17 are consistent with other measurements on a - Si:H in that there is significant experimental scatter in the results obtained from specimen to specimen. The general trends exhibited by all of the data are similar, however, and will be discussed below.

The experimental scatter in the optical absorption coefficient is much more significant at low photon energies (< 1.8 eV) than at high photon energies (> 1.8 eV). At high photon energies the data in figure 6.17 fit well to the quadratic relationship of equation 2.26, i.e.

$$\alpha h\nu = \text{const.}\ (h\nu - E_o)^2 \qquad - \quad (6.17)$$

as shown in figure 6.18. E_o defined from equation 6.17 may therefore be used as a measure of the experimental scatter at high photon energies.

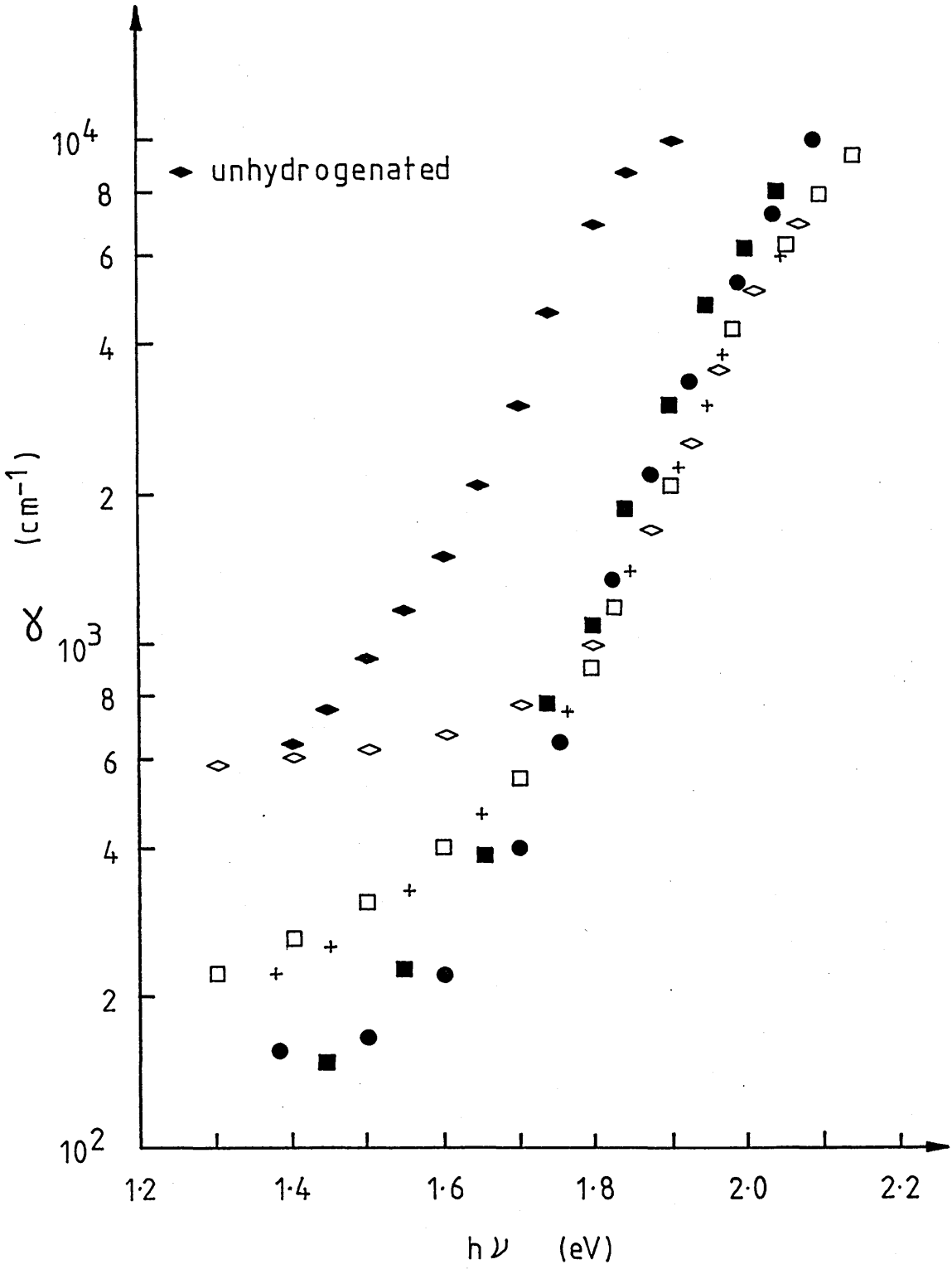

Figure 6.17. Optical absorption versus photon energy for specimens of a-Si:H prepared using the same deposition conditions.

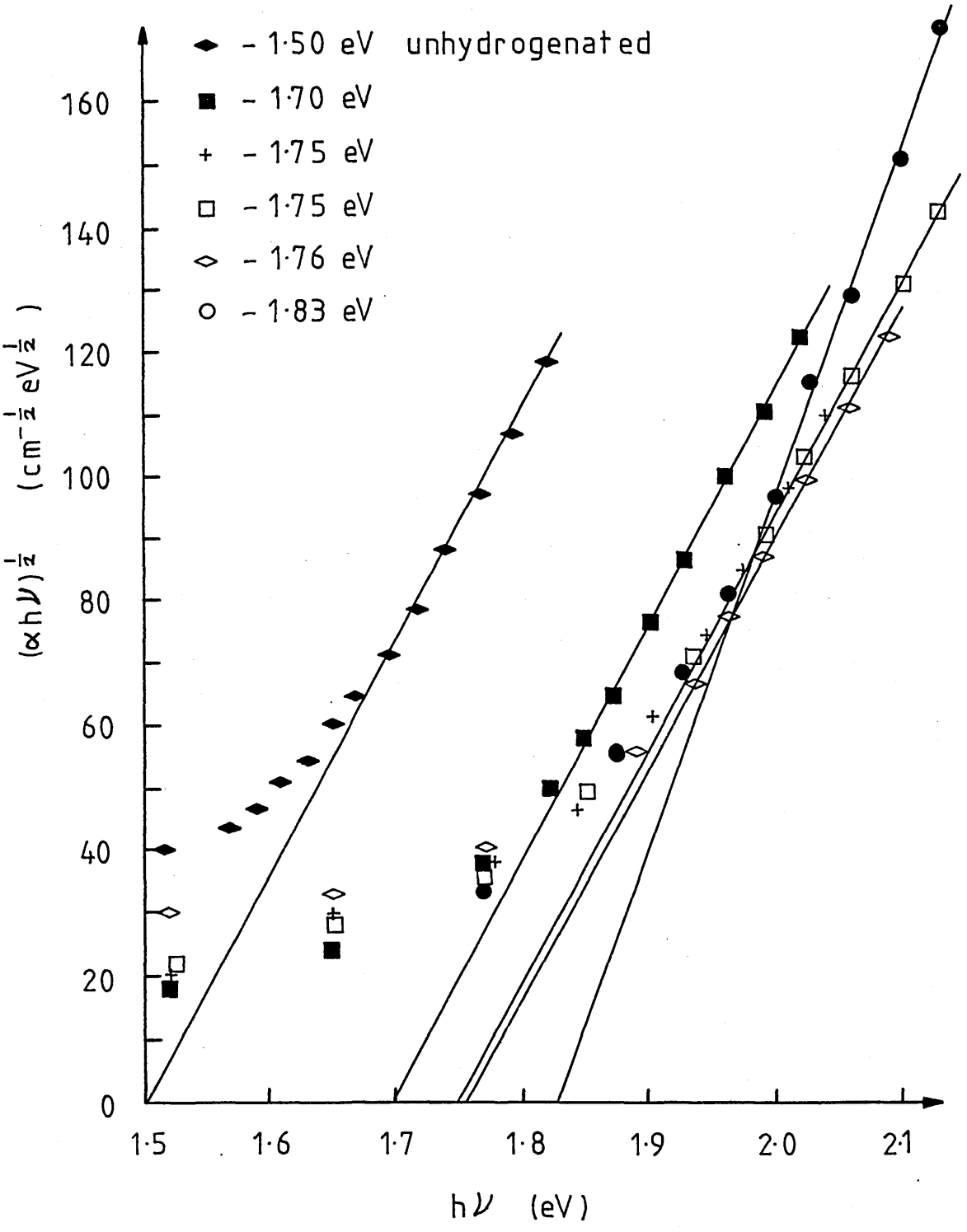

Figure 6.18. Data of figure 6.17 re-plotted on axes of $(\alpha h\nu)^{\frac{1}{2}}$ versus photon energy. The "optical gap" for each specimen is given in the figure.

From the insert on figure 6.18 it can be seen that E_o varies over the range 1.70 to 1.83 eV. These values agree favourably with similar measurements reported in the literature (13).

If E_o is assumed to be an optical gap separating extended states in the valence band and in the conduction band, then it is possible to explain the experimental scatter at high photon energies as involving an optical gap which is strongly dependent upon the conditions of film deposition. This fact has been shown to be the case, in a wider sense, by Freeman and Paul (13). They correlated optical gap measurements, defined in the above manner, with film deposition conditions such as substrate temperature and hydrogen partial pressure and found that the optical gap was strongly dependent upon both of these parameters. In the data presented in this study, however, all of the optical measurements were performed on specimens prepared using the same deposition conditions. At first sight, this suggests that E_o may be very sensitive to minute variations in deposition conditions. However, as pointed out in the previous sections, it is known that random amounts of impurity atoms are present in the films deposited in this laboratory. This unpredictable variable may account for much of the experimental scatter exhibited by the results.

Turning now to the optical absorption data at low photon energies (< 1.8 eV) it can be seen from figure 6.17 that the experimental scatter is much more pronounced in this region. This is probably due to the fact that in this photon energy range, the optical absorption is controlled by transitions involving localised states, the density of which is strongly related to film deposition conditions and (in particular for the

specimens prepared in this laboratory), to the level of impurity atoms within the film.

Finally, in conclusion of this section, it can be seen from figure 6.17 that at all photon energies, the optical absorption in the unhydrogenated material is considerably greater than that in all of the hydrogenated films. Furthermore, from figure 6.18 the optical gap defined from equation 6.17 for the unhydrogenated material is considerably smaller than the gaps deduced from the hydrogenated films. Thus, it appears that: (a). There is a large density of states in the mobility gap of unhydrogenated a - Si; and (b). that the optical gap of a - Si increases with increasing hydrogen film content. These conclusions are widely accepted and have been repeatedly reported in the literature.

SECTION C

6.5 ALUMINIUM DOPED AMORPHOUS SILICON - RESULTS

Specimens of Aluminium doped a - Si:H were prepared by co - sputtering strands of 99.999 % pure Aluminium wire with a polycrystalline Silicon target. The Aluminium wire, 1 mm in diameter, was cut into pieces 10 mm long and spread evenly over the entire target active surface area so as to ensure that, as far as possible, an even distribution of dopant material was generated in the deposited films. The sputtering conditions used for all of the depositions were a substrate temperature of approximately 250^{o}C, a Hydrogen and Argon partial pressure of 4 and 11 mTorr respectively and an r.f. power of 100 Watts.

Structural measurements were carried out on two representative doped specimens using a transmission electron microscope, and a range of electronic transport measurements were performed. In all of the Aluminium doped specimens it was found that the photoconductivity was quenched to a level that was below the resolution of the measurement system. Consequently, no measurements of steady state or of transient photoconductivity could be made. Time of flight experiments were attempted using a pulsed electron beam, but as with photoconductivity measurements, the transient signal generated was too small for detection. Only results from dark d.c. conductivity, thermoelectric power and optical absorption experiments were obtained.

6.5.1 STRUCTURE

Two films of Aluminium doped a - Si:H in the thickness range 100 to 200 Angstroms were deposited onto Carbon coated mica substrates. The films were "floated off" the substrates in distilled water and collected on fine copper grids. Prior to mounting in the electron microscope, (which had a resolution of about 50 Angstroms), the specimens were vacuum baked at 140^{o}C in order to reduce contamination effects. The two specimens considered were prepared using, (a) 50 and (b) 25 strands of Aluminium wire covering the active surface area of the target. These target area coverages corresponded to Aluminium - Silicon ratios of approximately (a) 8.5 % and (b) 4.1 % respectively. X - ray microanalyses of the films revealed that, to within an accuracy of $\pm$ 2 at. %, the atomic percentage of Aluminium in the deposited films was in agreement with figures deduced from target coverage calculations. This suggests that, to a first approximation, the sputtering rate of Aluminium and of Silicon is the same. In the following discussion, therefore, it will be assumed that there is a one to one correspondence between the Aluminium - Silicon coverage ratio of the target and the atomic percent of Aluminium in the deposited films. X - ray microanalyses also revealed Arsenic and Selenium impurities in the films, the concentrations of which varied from specimen to specimen over the range 1 to 3 at. %.

Observations of the film structure using an electron microscope suggest that both specimens are inhomogeneous. The electron micrograph displayed a two - phase mixture consisting of closely

spaced dark patches in a lightly shaded background. Electron diffraction analyses of the specimens revealed a diffraction pattern consisting of three broad diffuse halos (normally expected from an amorphous material) together with two to three well defined sharp rings. These observations suggest that the film structure may consist of a matrix of small crystalline Aluminium islands, embedded within an amorphous Silicon lattice. The electron diffraction pattern gives evidence for both the crystalline Aluminium structure and the amorphous Silicon lattice, while the "cermet" structure is evidenced by the electron micrograph. Dimensional measurements on the films revealed that the linear dimension of the Aluminium islands is about 50 Angstroms. It is interesting to note that structural measurements which are in agreement with those presented above have been reported by others. Tanaka et al (23) co - sputtered polycrystalline Silicon with Aluminium and found an X - ray diffraction pattern which contained rings corresponding to reflections with the Al(200) and Al(111) crystalline planes.

Note. No Aluminium doped specimens with dopant concentrations less than 1 at. % could be prepared. In all attempts to deposit such material the film began to peel away from the substrate soon after removal from the sputtering chamber. The film appeared to be under considerable strain, since "flakes" that became detached were propelled several centimeters away from the substrate. It is suggested that in these lightly doped specimens, the Aluminium may attempt to bond with the Silicon lattice creating considerable strain within the film. At high dopant levels, however, metallic islands are

formed, this leading to a much more relaxed structure. A similar deterioration in film quality with the addition of dopant material to r.f. sputtered a - Si:H has been observed by others (13).

6.5.2 DARK D.C. CONDUCTIVITY

Figure 6.19 shows an Arrhenius plot of the conductivity for four doped specimens of a - Si:H in which the Aluminium concentration ranges from 1.6 to 8.5 at. %. Table 6.3 gives details of the estimated Aluminium content of each film together with the corresponding room temperature conductivity and conductivity pre - exponential and activation energy. Included in figure 6.19 is conductivity data obtained from a representative undoped specimen prepared under the same deposition conditions as used for all of the doped material. No conductivity data could be obtained from specimen ◆, (the most lightly doped film), for reasons outlined in the previous section.

Figure 6.19 reveals a monotonic decrease in the conductivity activation energy as the dopant concentration is increased. The addition of approximately 8.5 at. % Aluminium to the amorphous Silicon is seen to result in an overall increase in the room temperature conductivity of about 5 orders of magnitude. The conductivity pre - exponential for all of the doped specimens lies in the range 5 to 30 $(\Omega\,cm)^{-1}$. This range is 2 to 3 orders of magnitude lower than the pre - exponential observed in the undoped material.

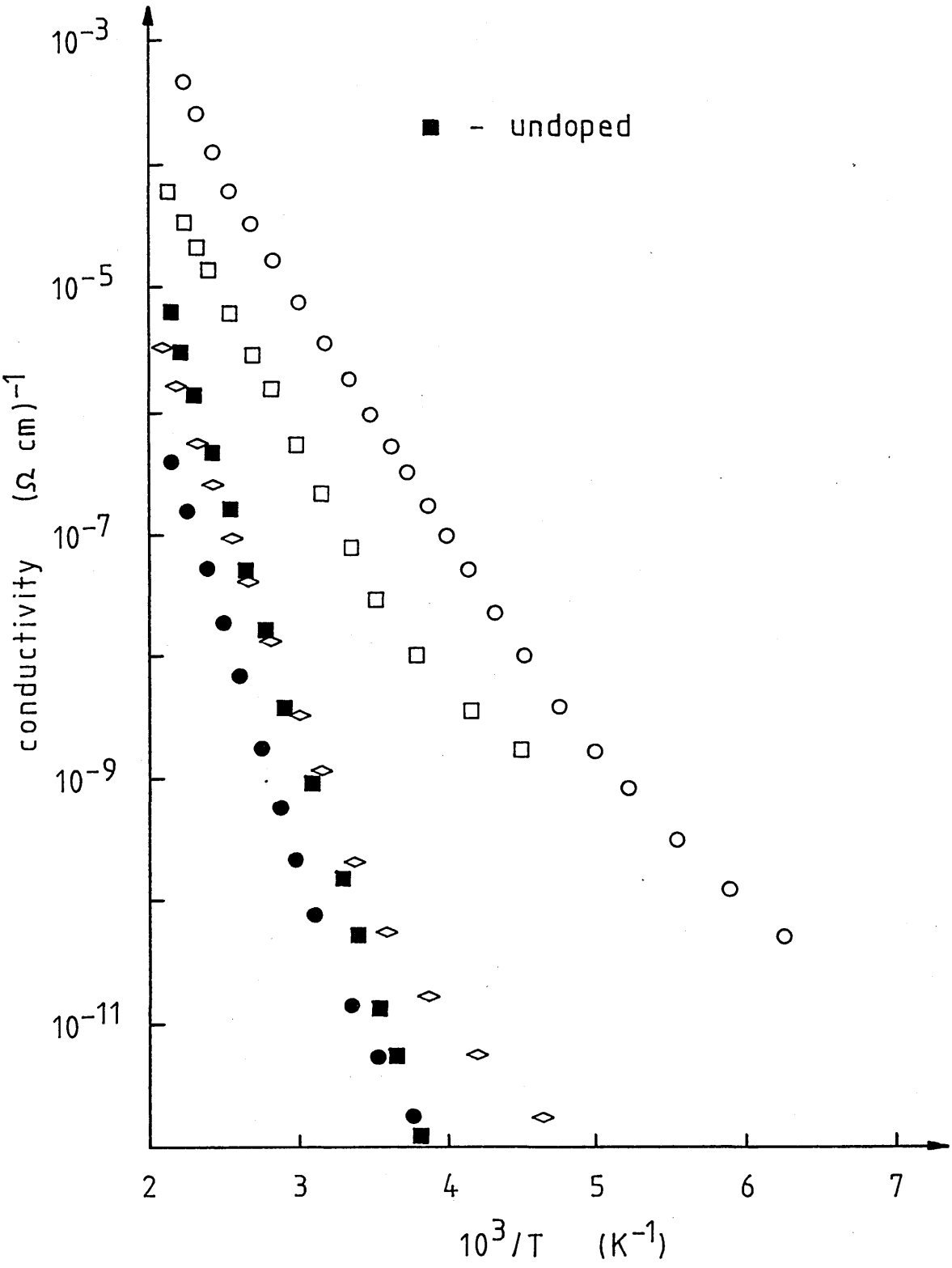

Figure 6.19. Arrenius plot of the conductivity for four Aluminium doped films of a-Si:H. Specimen details are given in table 6.3.

Specimen	Impurity at. %	σ_o $(\Omega\ cm)^{-1}$	E_σ (eV)	$\sigma_{R.T.}$ $(\Omega\ cm)^{-1}$
■	0	$3x10^{3}$	0.78	$7x10^{-11}$
◆	0.8	--	--	--
●	1.6	20	0.74	$1x10^{-11}$
◇	4.1	30	0.66	$2x10^{-10}$
□	5.8	10	0.50	$5x10^{-8}$
○	8.5	5	0.37	$1x10^{-6}$

Table 6.3.

Details of Aluminium doped specimens of a-Si:H investigated in this study.

6.5.3 OPTICAL ABSORPTION

Figure 6.20 shows the optical absorption coefficient (α), plotted as a function of photon energy ($h\nu$) for all of the Aluminium doped specimens prepared. The same data are presented in figure 6.21, re - plotted on axes of $(\alpha h\nu)^{\frac{1}{2}}$ versus photon energy. Both figures give data from a representative undoped specimen. From figure 6.21 it can be seen that in the high absorption region, all of the data fit well to the quadratic relationship described by equation 6.17. It can also be established from figures 6.20 and 6.21 that the optical absorption edge shifts towards lower photon energies with increasing film dopant concentration. The optical gap deduced for each of the doped films is given in the insert in figure 6.21.

6.5.4 THERMOELECTRIC POWER

Thermoelectric power measurements were performed using the experimental rig discussed in Chapter 5. The specimen holder was modified to accommodate two heater coils, between which the specimen was mounted. The temperature difference across the specimen was monitored using a Copper - Constantan thermocouple and the thermoelectric voltage developed between the specimen contacts was measured using a Keithley 610C electrometer.

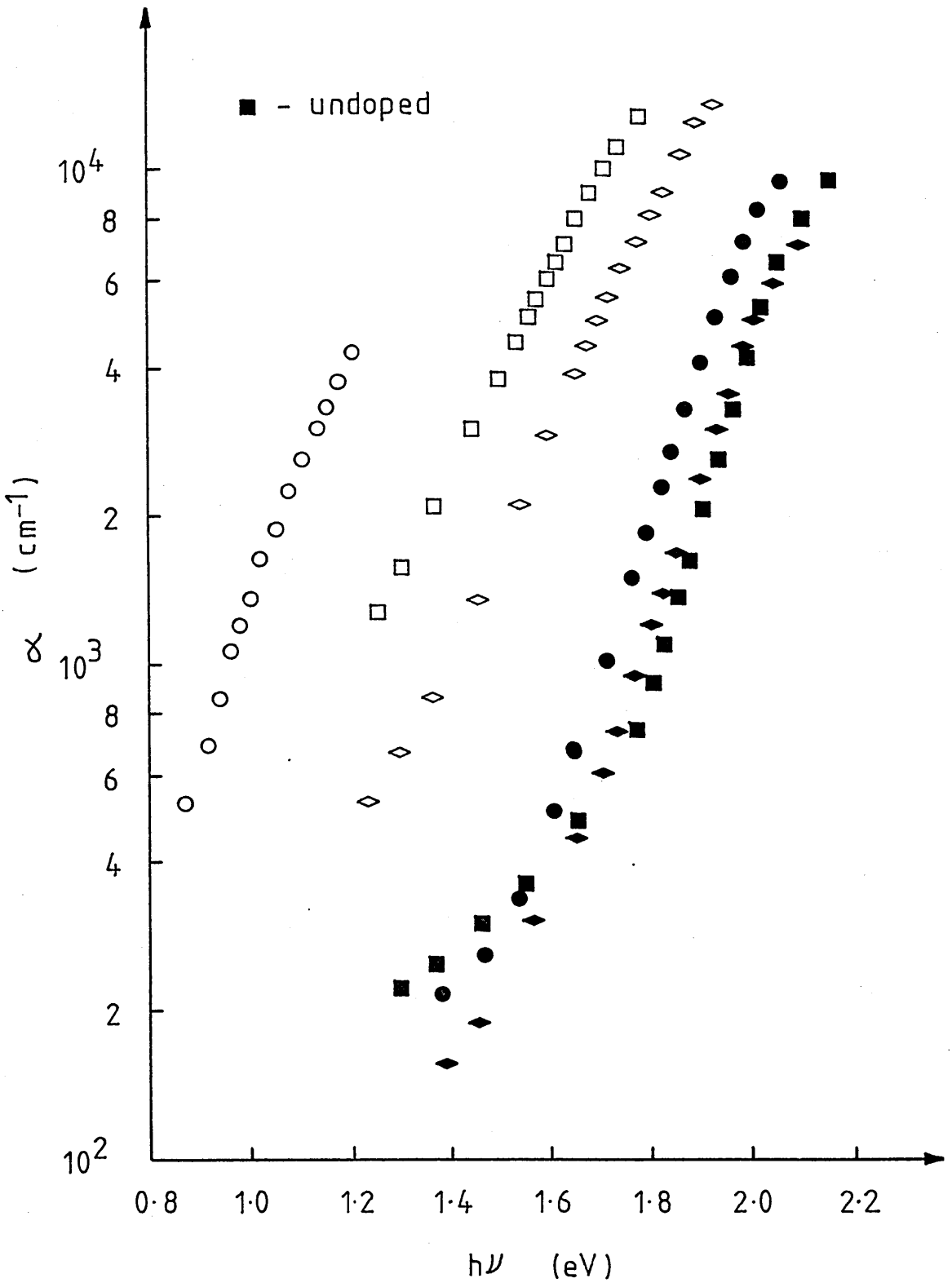

Figure 6.20. Optical absorption versus photon energy for Aluminium doped films of a-Si:H. Specimen details are given in table 6.3.

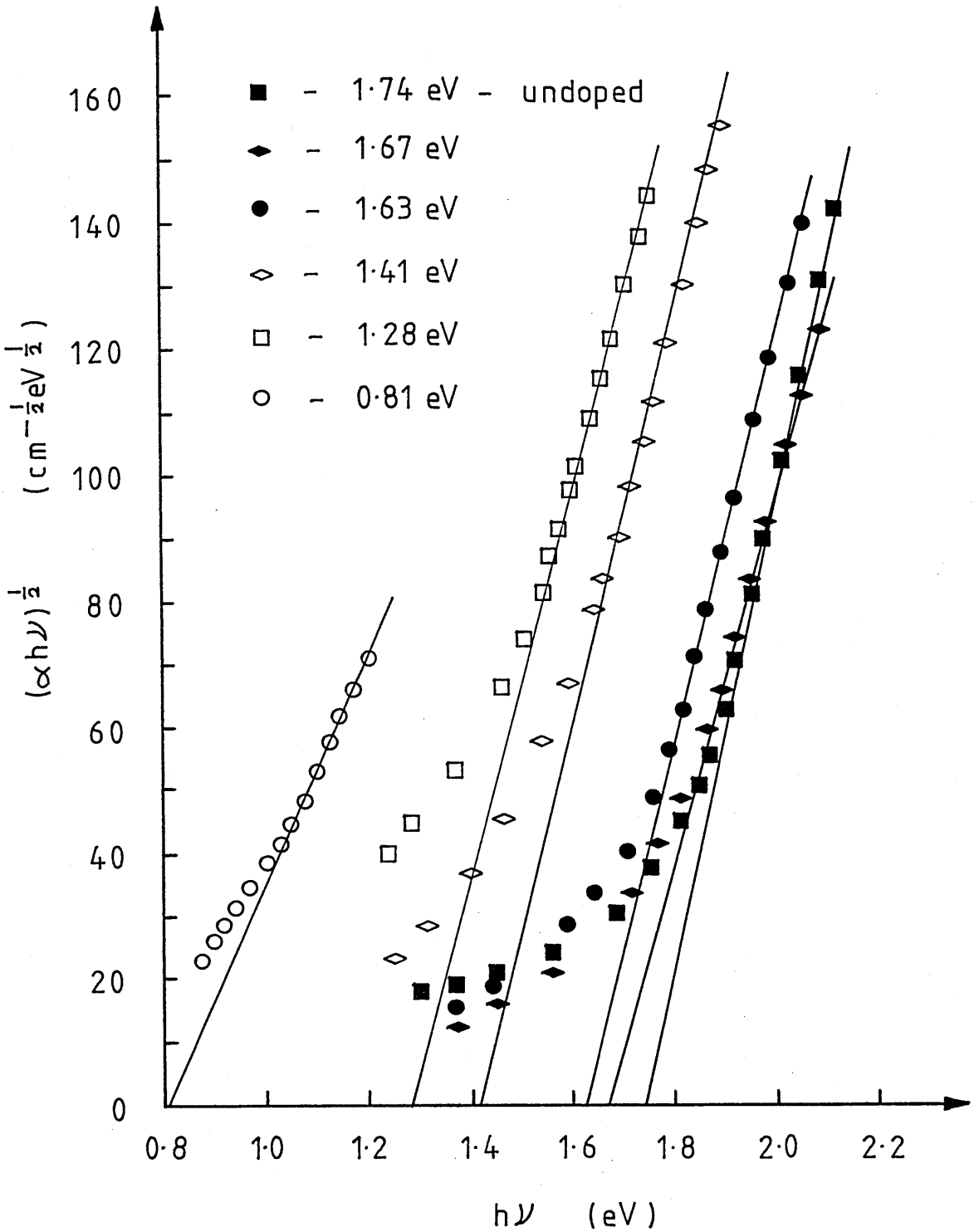

Figure 6.21. Optical absorption data of figure 6.20, re-plotted on axes of $(\alpha h\nu)^{\frac{1}{2}}$ versus photon energy. The "optical gap" deduced for each specimen is given in the figure.

Thermoelectric power measurements were attempted on all of the doped specimens, but due to the large level of electrical noise pick - up results could only be obtained from the most heavily doped film (specimen O). Measurements were performed on this film over the entire temperature range accessible, i.e. 250 K to 390 K. Figure 6.22 shows the thermoelectric power plotted as a function of inverse temperature for specimen O . It can be seen that the thermoelectric power is positive over the entire temperature range investigated.

6.6 DISCUSSION

Micrographs of Aluminium doped specimens have suggested a "cermet" structure. It must be remembered, however, that specimens on which structural measurements were carried out, are dimensionally substantially different from specimens used for electronic transport measurements. A film thickness of order 100 Angstroms was used for structural measurements, while transport data were collected from specimens in the thickness range 10^4 to 10^5 Angstroms. Detailed studies of cermet films (19) have shown that both the structure and the electronic transport properties of these materials are dramatically dependent upon film thickness. It has also been established that the local structure of sputter deposited cermet films may vary considerably in any given specimen. Thus, it is not possible with the data available to deduce with any certainty the exact structure of the films used in this study for the collection of electronic transport data. Considerable conjecture must therefore be applied in order to interpret the transport data presented in this

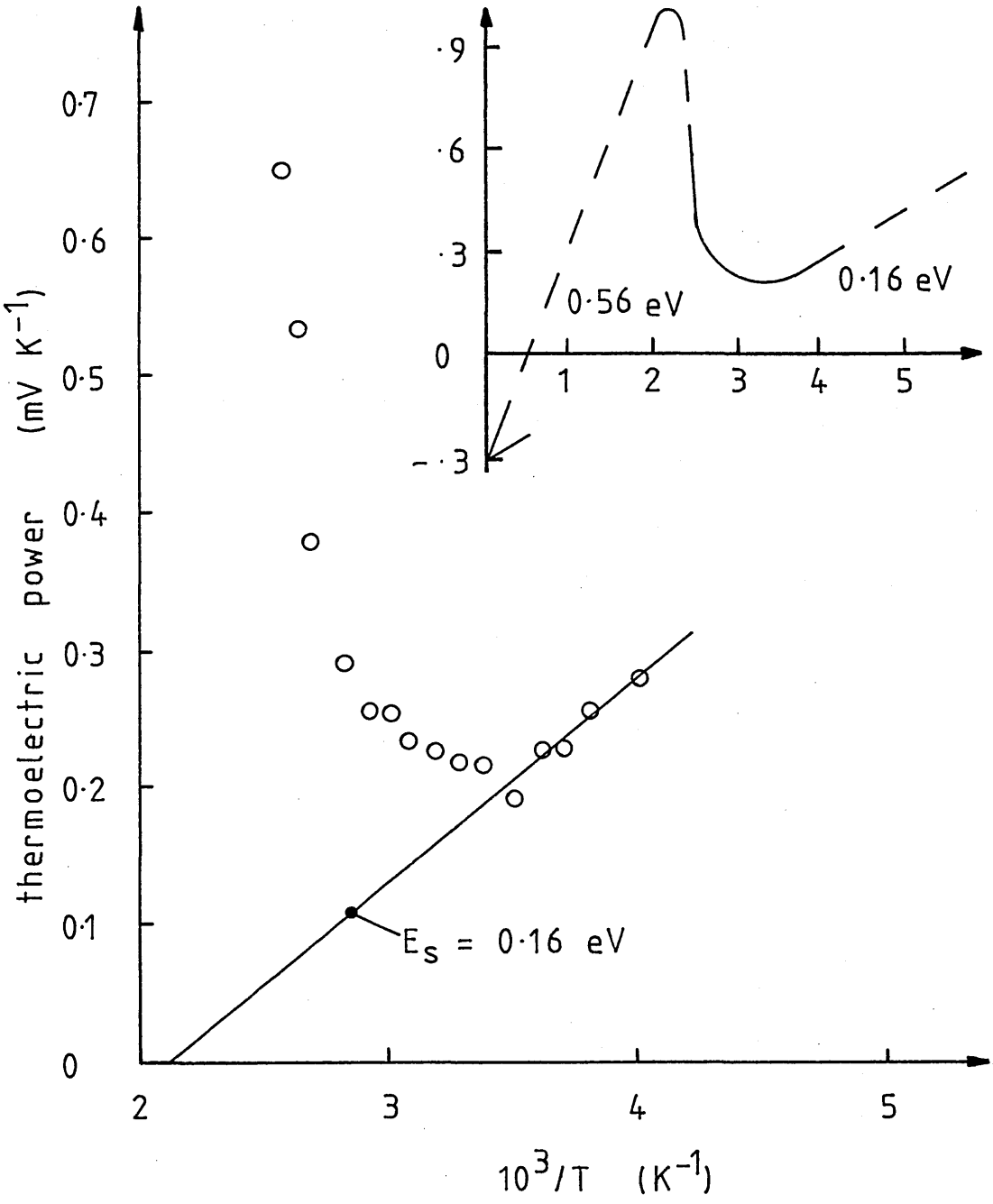

Figure 6.22. Thermoelectric power versus inverse temperature for an 8.5 at.% Aluminium doped specimen of a-Si:H. The figure insert is described in the text.

section.

In the broadest terms, it appears that there are three possible methods by which Aluminium can enter the Silicon lattice, namely; (a) as a substitutional dopant, (b) as a fully co - ordinated Silicon - Aluminium alloy, and (c) in isolated Aluminium islands similar to a cermet structure. It is also possible that the film structure may consist of a complex arrangement of two or more of these phases. In order to aid clarity too the discussion, each of the possibilities mentioned above will be analysed in terms of the electronic transport data presented.

(a). Substitutional Doping.

At first sight, the conductivity data of figure 6.19 suggests substitutional doping since there is an apparent shift in the Fermi level position, probably towards the valence band mobility edge, as the Aluminium concentration is increased. This hypotheses is quickly dispelled, however, when the conductivity data are considered in conjunction with optical absorption measurements. Figure 6.23 shows the optical gap (E_o), deduced from figure 6.21, plotted as a function of the dark conductivity activation energy, (E_σ), for all of the specimens considered. It is immediately evident from figure 6.23 that in all of the Aluminium doped films, the conductivity activation energy is around half the magnitude of the optical gap. Two possible explanations can be suggested in order to account for this observation. Firstly, if it is assumed that the dominant conduction

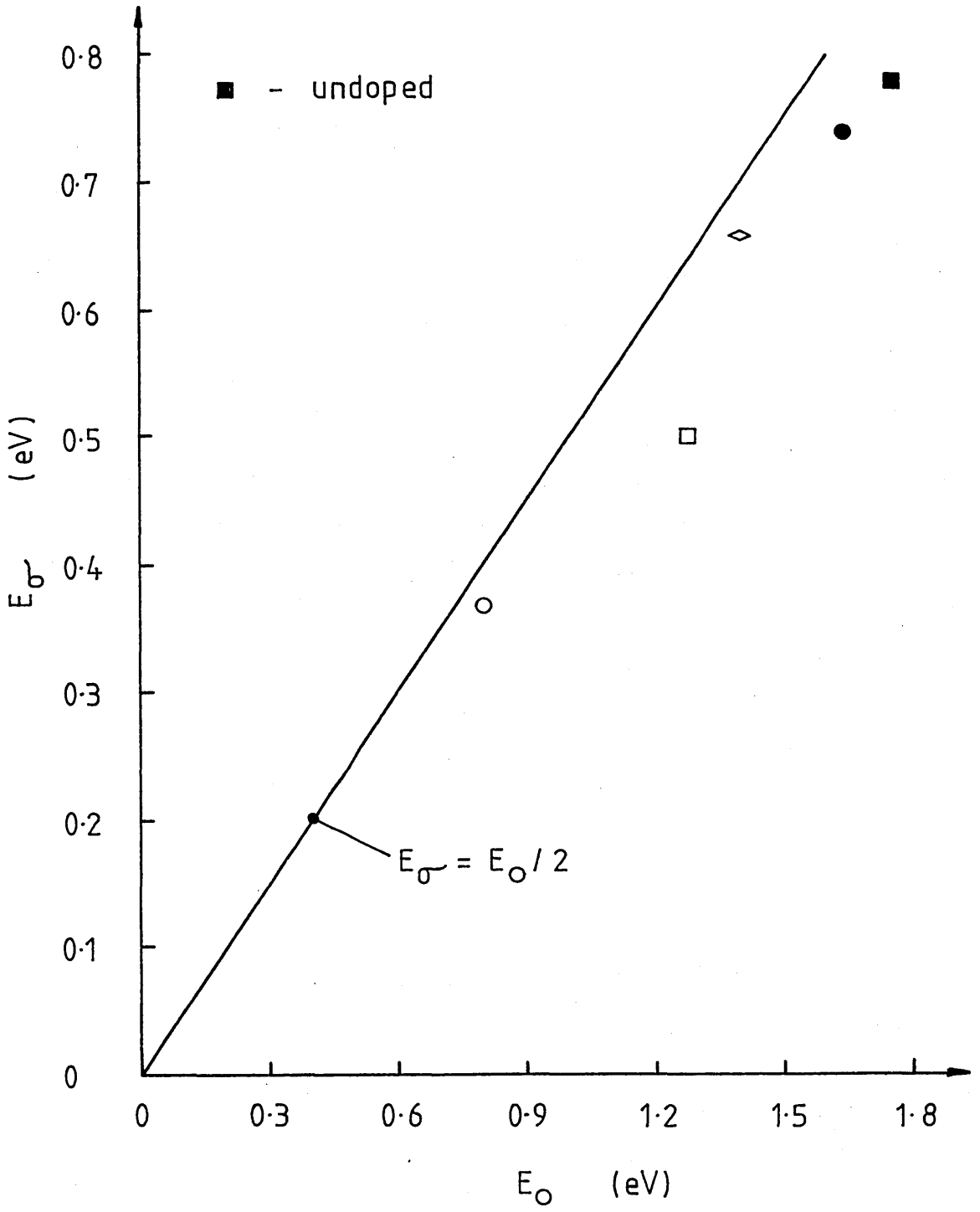

Figure 6.23. Optical gap (E_o), deduced from figure 6.21, plotted as a function of the dark conductivity activation energy, (E_σ), for all of the Aluminium doped films.

path at high temperatures is through extended states at E_c or E_v, then it must be concluded that the optical gap decreases and the Fermi level remains close to the mid - gap position as the Aluminium concentration is increased. Secondly, if it is assumed that the dominant conduction path at high temperatures is through localised states, then the activation energy to the conduction path and the magnitude of the optical gap must decrease in proportion as the Aluminium concentration is increased. As will be shown below, it is possible to differentiate between these two competing explanations by considering the thermoelectric power data generated from the most heavily doped specimen. One fact which is clear from the results presented in this section, however, is that substitutional doping in isolation cannot account entirely for all of the features observed in the experimental data. It must therefore be concluded that although a minority of the Aluminium atoms may be acting as substitutional dopants, the majority must be incorporated into the Silicon lattice in such a manner as to form a Silicon - Aluminium alloy or possibly a "cermet" structure.

The thermoelectric power data shown in figure 6.22 are positive in sign over the complete temperature range investigated. This suggests that the incorporation of Aluminium atoms into the Silicon lattice results in a material in which the electronic transport properties are dominated by holes. As will be shown below, a satisfactory fit to the experimental data can be obtained using a two - level transport model. At very high temperatures ($\geqslant$ 400 K), extended state conduction by holes in the valence band dominates the transport, while at lower temperatures the dominant conduction path is

through localised states situated between the Fermi level and the valence band mobility edge.

Figure 6.19 reveals that the conductivity Arrhenius plot for the most heavily doped specimen is not singly activated over the temperature range for which thermoelectric power data exist, indicating that no single conduction path dominates the transport in this temperature range. This implies that the thermoelectric power data of figure 6.22. will also be associated with a changing conduction mechanism. As pointed out in Chapter 2, no significance can be attached to the slope of the thermoelectric power versus inverse temperature plot in a temperature range where the conduction path is changing. Hence, in order to interpret the experimentally observed thermoelectric power data, an estimate must first be made of the conductivity activation energy at temperatures above the change - over region. Although considerable uncertainty exists in this result, a conductivity activation energy for $T \geqslant 400$ K of $E_\sigma = 0.56$ eV can be defined.

It is now possible to interpret the thermoelectric power data using the curve shown in the insert in figure 6.22. Applying a straight line approximation to the low temperature thermoelectric power data leads to an activation energy of $E_S = 0.16$ eV and an intercept on the thermoelectric power axis at $1/T = 0$ of $S_0 = -0.3$ mV K^{-1}. At temperatures greater than 400 K it is expected that the thermoelectric power data will approach the line with activation energy $E_S = 0.56$ eV and intercept $S_0 = -0.3$ mV K^{-1} as indicated in figure 6.22. This is due to the fact that for extended

state conduction S_o should equal the intercept deduced for localised state transport, and $E_S = E_\sigma$, (see Section 2.4). Thus, the dotted line indicates the thermoelectric power data that might be expected if the temperature range of measurement were to be extended, while the solid line depicts the actual experimental data obtained. It can be seen from figure 6.22 that this two - level transport model provides a satisfactory fit to the experimental data over the temperature range of interest. An additional piece of information which can be inferred from these experimental measurements is that there is a hopping energy of approximately $W = E_\sigma - E_S = 0.2$ eV associated with the conduction path through the localised states.

Turning now to the conductivity pre - exponential (σ_o) for all of the Aluminium doped films, it can be seen from table 6.3 that σ_o lies in the range 5 to 30 $(\Omega\ \text{cm})^{-1}$. This range is on the lower limit expected for extended state conduction but is about 1 to 2 orders of magnitude larger than the pre - exponential expected for a hopping mechanism (see Section 2.1). This suggests that there is a problem associated with the interpretation of the conductivity data around the room temperature region using a hopping mechanism. However, extended state transport appears also to be ruled out due to the finite difference between the thermoelectric power and the conductivity activation energies, and due to the transition at very high temperatures to a region of larger activation energy, (in the most heavily doped film).

Anderson and Paul (20) approached this problem and suggested that impurity related defect states in these heavily doped specimens may be partially or even completely delocalised. Such a situation would lead to an "apparent hopping conductivity pre - exponential" much larger than that theoretically expected from a phonon assisted hopping process. Although this possibility appears to be inconsistent with the fairly large difference between E_σ and E_s observed in practice, Anderson and Paul (21) have shown that the difference between E_σ and E_s (in undoped a - Si:H) can be correlated with structural inhomogeneities and does not necessarily imply a finite mobility activation energy. A similar argument can therefore be applied favorably to the experimental data presented in this study, since as discussed in section 6.5.1, the Aluminium doped films deposited in this laboratory have been found to contain significant structural inhomogeneities which could account for the finite difference between E_σ and E_s. It can therefore be concluded that a partially or even completely delocalised impurity band may exist above the valence band mobility edge in these heavily Aluminium doped specimens.

(b). Silicon - Aluminium Alloy.

The above discussion suggests that the creation of a Silicon - Aluminium alloy is a likely proposition. The experimental data suggest that the optical gap of this alloy is critically dependent upon the atomic ratio of Silicon to Aluminium, the optical gap decreasing with increasing Aluminium concentration. Conductivity data are in agreement with optical gap measurements in that the

conductivity activation energy is found to decrease, and the measured conductivity at all temperature increase, with increasing Aluminium concentration. Thermoelectric power in conjunction with conductivity measurements, suggest that electronic transport around room temperature in this alloy may be controlled by charge transfer through a partially or even completely delocalised impurity band. The major down - fall of this proposition is that structural measurements reveal a two phase mixture consisting of crystalline Aluminium islands embedded within an amorphous Silicon background lattice. In practice, however, the situation may be considerably more complex. It is probable that crystalline Aluminium islands exist, but the background lattice may be an Aluminium - Silicon alloy in which a minority of the Aluminium atoms act as substitutional dopants. In the discussion below, however, it will be suggested that the crystalline Aluminium islands do not have a major influence on the measured electronic transport properties of these Aluminium doped films.

(c). Cermet Structure.

Electronic conduction in cermet films can be divided into two well - defined categories. Firstly, in the metallic regime, the material behaves like a "dirty" metal; the resistivity is relatively low and the temperature coefficient of resistance (TCR) is positive. The conductivity is determined by scattering of electrons and by the geometric constraints of the current flow due to the meandering structure of the metallic continuum. A transition to the dielectric regime results from the break up of the metallic continuum into

isolated metal islands. In this regime, the conductivity results from tunneling of electrons between isolated metal grains; the resistivity is high and the TCR negative. Measurements on cermet films consisting of Gold or Silver in a $Si\ O_2$ matrix (22) have shown that the transition from the metallic to the dielectric regime occurs at a metal concentration of around 40 %. However, this figure is variable, and is critically dependent upon the details of film preparation, and upon the chemical properties of the constituent parts of the cermet.

For the material prepared in this laboratory it is suggested that cermet transport in the dielectric regime does not provide a realistic explanation for the experimental data. This is mainly due to the fact that any crystalline Aluminium islands which do exist in the host lattice will be inter - connected to many other metal islands by a relatively conductive Silicon - Aluminium alloy. Thus, instead of electrons (or holes) having to tunnel from one metal island to the next, (as occurs in real cermet films), charge transport between metal islands can take place by conduction through the semiconducting alloy, as previously described. Under these conditions, the electronic transport properties of the specimen will be dominated by the material of highest resistivity, which in all cases will be the Silicon - Aluminium alloy. Thus, it is proposed that even although there may be significant numbers of metallic islands within the material under test, the electronic transport properties of the background lattice will always be experimentally revealed, except under the conditions where a metallic continuum extends between the two test electrodes.

6.7 CONCLUSIONS

In this section it has been shown that the electronic transport properties of co - sputtered Silicon - Aluminium films can be interpreted in terms of an alloy with semiconducting characteristics. It has been suggested that even although there may be a large number of crystalline Aluminium islands within the films, these crystallites will only have a minor influence on the measured electronic transport properties. It is further suggested that in order to obtain a better understanding of the electronic processes occurring in these films, a detailed structural and chemical analysis must be performed on specimens which are dimensionally similar to those used for the collection of electronic transport data. Considerable work, therefore, still remains to be undertaken in this area.

6.8 ANTIMONY DOPED AMORPHOUS SILICON - RESULTS

Specimens of Antimony doped a - Si:H were prepared by co - sputtering spheres of 99.999 % pure Antimony shot with a polycrystalline Silicon target. Both the method of co - sputtering and the sputtering conditions used for all of the depositions were the same as described in Section 6.5.

Structural measurements were carried out on two representative doped specimens using a transmission electron microscope and a range of electronic transport measurements were performed. Results from dark d.c. conductivity and optical absorption experiments were obtained for each of the doped specimens. Due to very small signal levels, it was not possible to obtain steady state or transient photoconductivity measurements from the most heavily doped specimen. No thermoelectric power measurements were obtained due to the large level of electrical noise pick - up.

Note. In section 6.5.1 it was stated that very lightly Aluminium doped specimens of a - Si:H could not be successfully deposited due to the films flaking from the substrate. This flaking phenomenon was not observed with Antimony doped films and it was therefore possible to produce very lightly doped material from which photoconductivity data could be obtained.

6.8.1 STRUCTURE

The structure of two Antimony doped specimens in the thickness range 100 to 200 Angstroms were investigated. The specimens were prepared using (a) 1.2 % and (b) 0.6 % of the active surface area of the target covered with Antimony. X - ray microanalyses of the films revealed that the atomic percent of Antimony in the deposited material was less than about one half of the figures deduced from target coverage calculations. This suggests that, to a first approximation, the sputtering rate of Silicon is more than twice the sputtering rate of Antimony. In the following discussion, therefore, it will be assumed that the atomic percent of Antimony in the deposited films is one half of the figure deduced from target coverage calculations. X - ray microanalyses also revealed Arsenic and Selenium impurities in the films, the concentrations of which varied from specimen to specimen over the range 1 to 3 at. %.

Observations of the film structure using a transmission electron microscope revealed that both specimens are homogeneous down to a resolution of 50 Angstroms. Electron diffraction analyses of the specimens produced a diffraction pattern consisting of three broad diffuse halos, normally expected from an amorphous material. These observations suggest that Antimony is entering the amorphous Silicon lattice in a homogeneous manner.

6.8.2 DARK D.C. CONDUCTIVITY.

Figure 6.24 shows an Arrhenius plot of the conductivity for all of the Antimony doped specimens deposited. Table 6.4 gives details of the estimated Antimony content of each film together with the corresponding room temperature conductivity and the conductivity pre - exponential and activation energy. Included in figure 6.24 are conductivity data obtained from a representative undoped specimen prepared under the same deposition conditions as used for all of the doped material.

It can be seen from figure 6.24 that at low dopant levels (specimens ● , ◇ and □) there is no significant difference between the conductivity Arrhenius plots obtained from the doped and from the undoped material. All of these curves are singly activated over the complete temperature range of measurement, with an activation energy in the range 0.76 to 0.79 eV, and a conductivity pre - exponential ranging from 2×10^3 to 4×10^4 $(\Omega\,cm)^{-1}$. A significant change occurs in the conductivity Arrhenius plot with the addition of 0.6 at. % Antimony to the a - Si:H (specimen ○). This specimen yields two well defined conductivity activation energies; at high temperature 0.62 eV and at low temperatures 0.30 eV. No significant change occurs in the conductivity pre - exponential deduced from the high temperature slope (6×10^3 $(\Omega\,cm)^{-1}$), however, this lying in the range obtained for the more lightly doped films. The addition of approximately 0.6 at. % Antimony to the a - Si:H is seen to increase the room temperature conductivity by about 4 orders of magnitude.

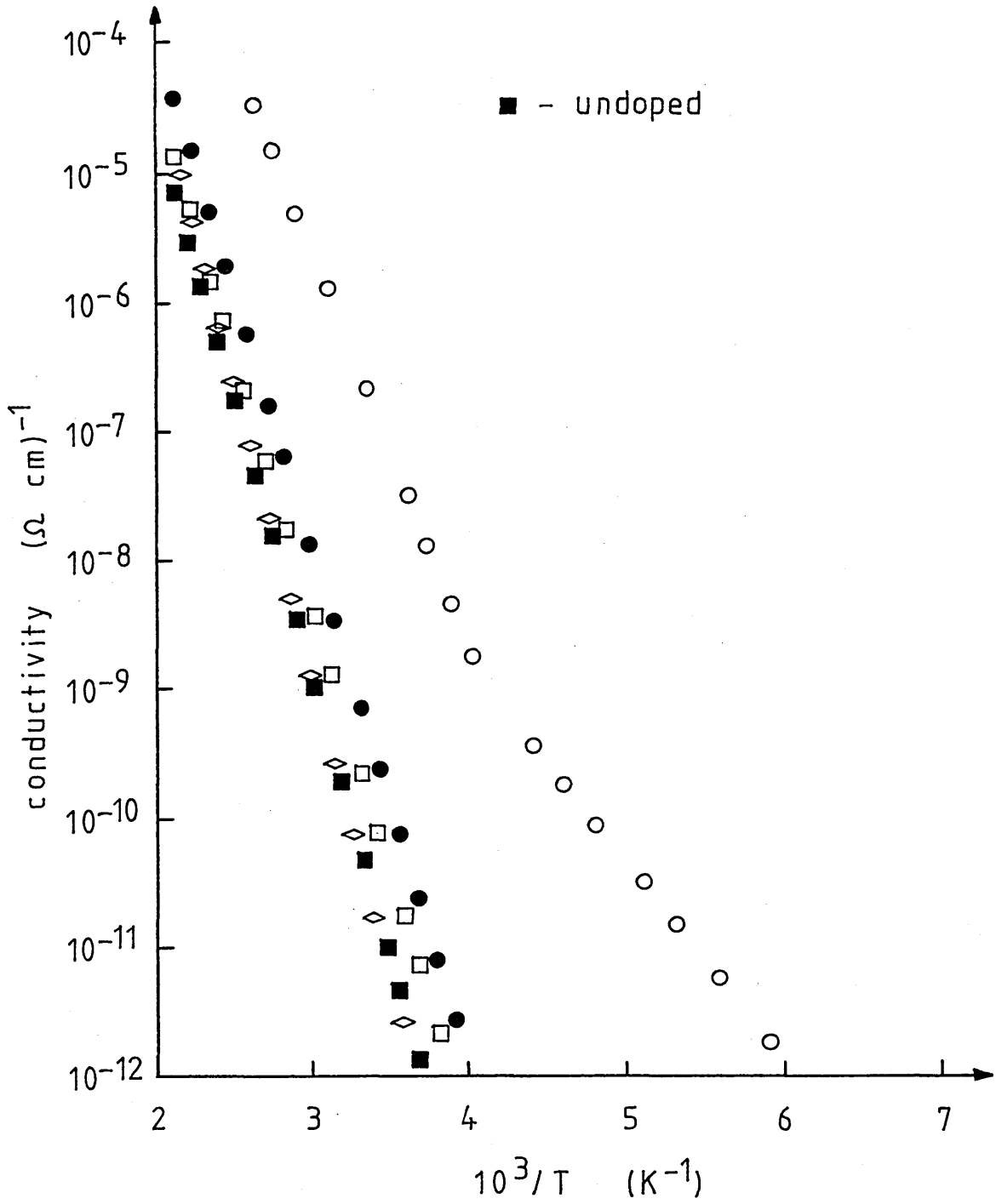

Figure 6.24. Arrenius plot of the conductivity for four Antimony doped films of a-Si:H. Specimen details are given in table 6.4.

Specimen	Impurity at. %	σ_o $(\Omega\ cm)^{-1}$	E_σ (eV)	$\sigma_{R.T.}$ $(\Omega\ cm)^{-1}$
■	0	$3x10^3$	0.78	$7x10^{-11}$
●	0.1	$5x10^3$	0.76	$8x10^{-10}$
◇	0.2	$4x10^4$	0.79	$7x10^{-11}$
□	0.3	$2x10^3$	0.76	$2x10^{-10}$
○	0.6	$6x10^3$	0.62	$3x10^{-7}$

Table 6.4.

Details of Antimony doped specimens of a-Si:H investigated in this study.

6.8.3 OPTICAL ABSORPTION

Figure 6.25 shows the optical absorption coefficient (α), plotted as a function of photon energy ($h\nu$) for all of the Antimony doped specimens prepared. The same data are presented in figure 6.26 re - plotted on axes of $(\alpha h\nu)^{\frac{1}{2}}$ versus photon energy. From figure 6.26 it can be seen that in the high absorption region all of the data fit well to the quadratic relationship described by equation 6.17, and an optical gap, E_o, can be defined for each of the films. The deduced optical gaps are shown in the insert in figure 6.26. From figures 6.25 and 6.26 it can also be seen that the optical absorption edge shifts monotonically towards lower photon energies with increasing film dopant concentration.

6.8.4 STEADY STATE PHOTOCONDUCTIVITY

Figure 6.27 shows plots of the steady state photocurrent versus inverse temperature for the 0.1, 0.2 and 0.3 at. % Antimony doped specimens. Due to the very small signal levels no results were obtained from the most heavily doped film (0.6 at. % Antimony). For comparison, curve ■ is a plot of the photocurrent versus inverse temperature for the "worst" undoped specimen prepared (see figure 6.13).

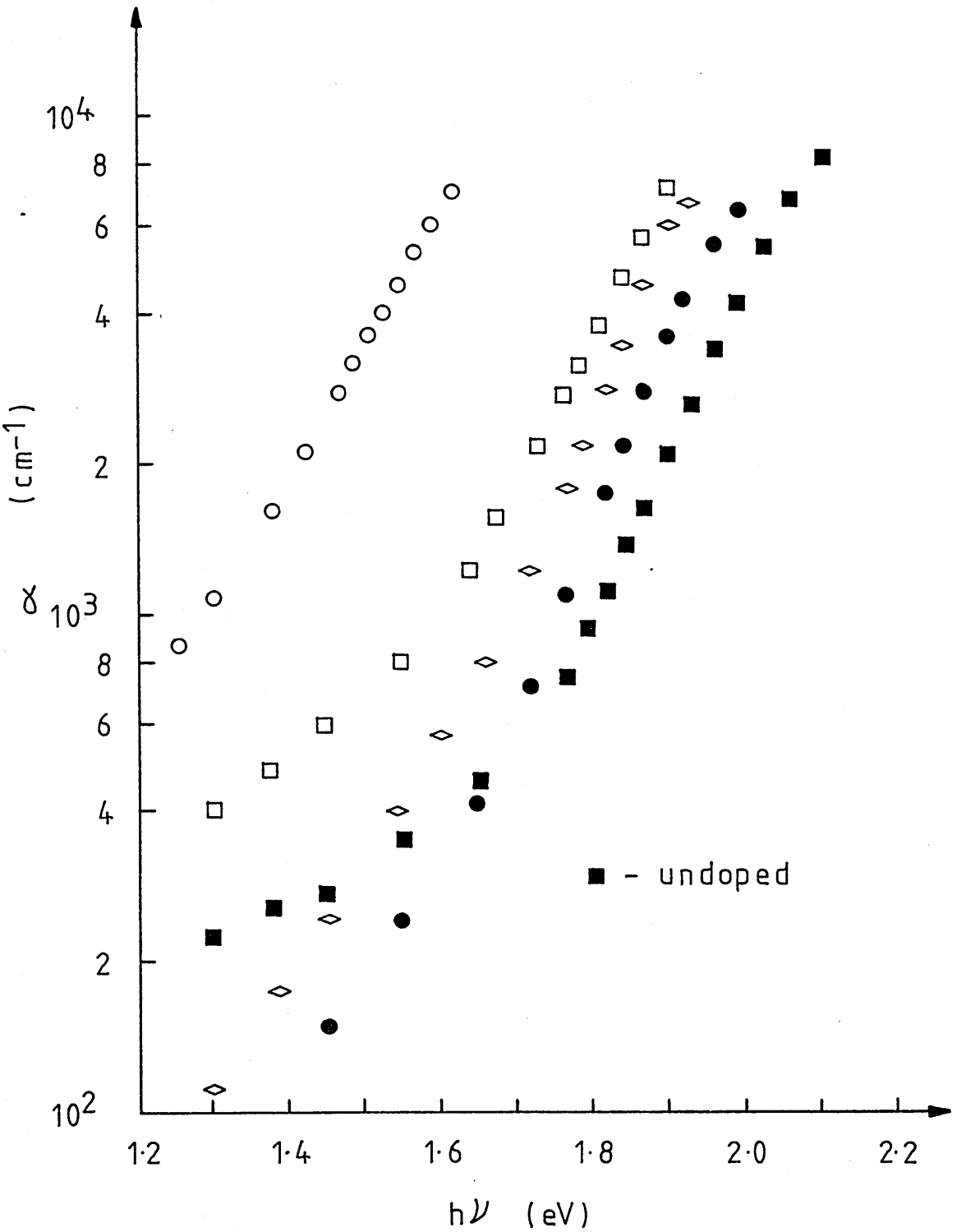

Figure 6.25. Optical absorption versus photon energy for Antimony doped films of a-Si:H. Specimen details are given in table 6.4.

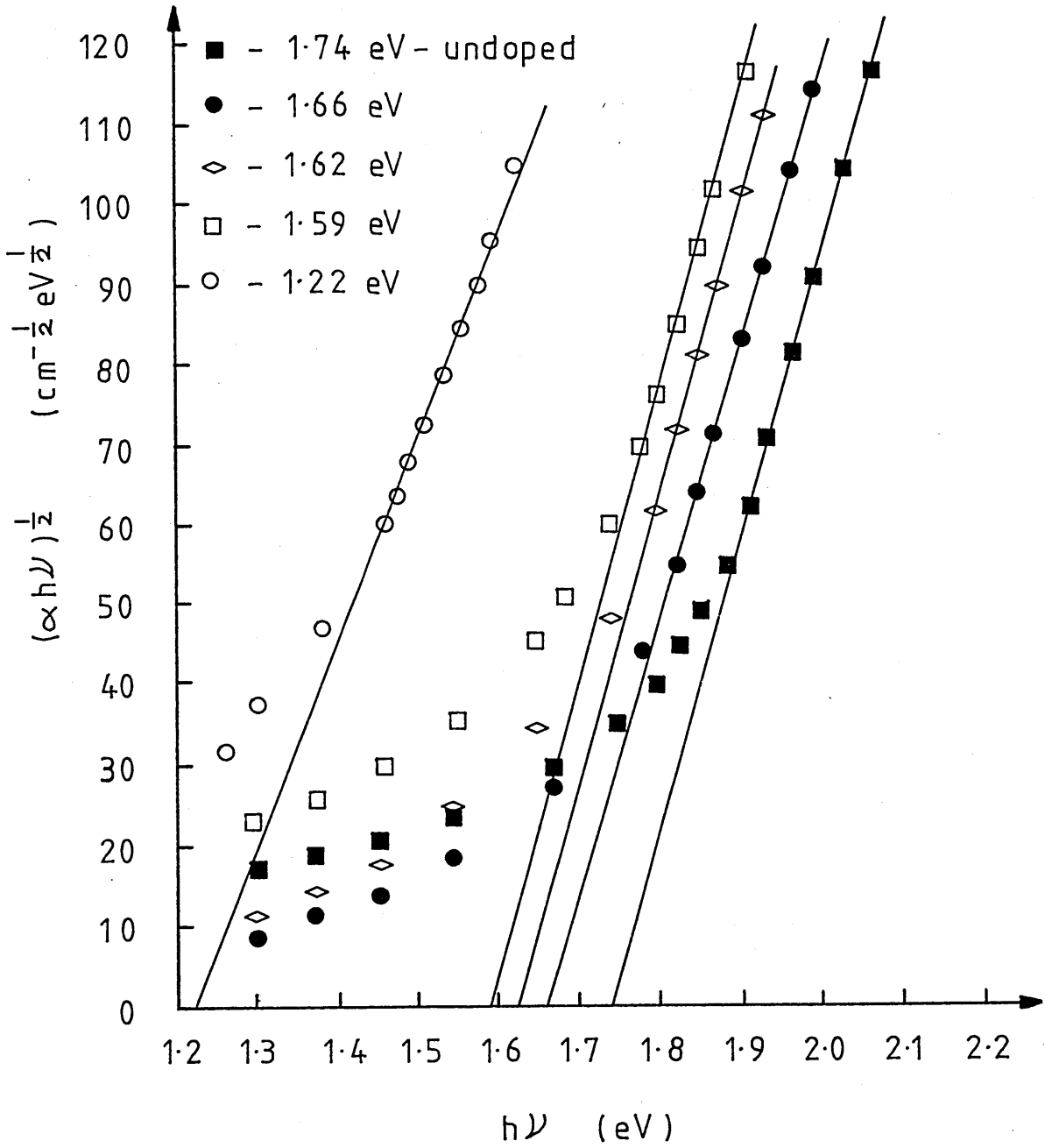

Figure 6.26. Optical absorption data of figure 6.25, re-plotted on axes of $(\alpha h\nu)^{\frac{1}{2}}$ versus photon energy. The "optical gap" deduces for each specimen is given in the figure.

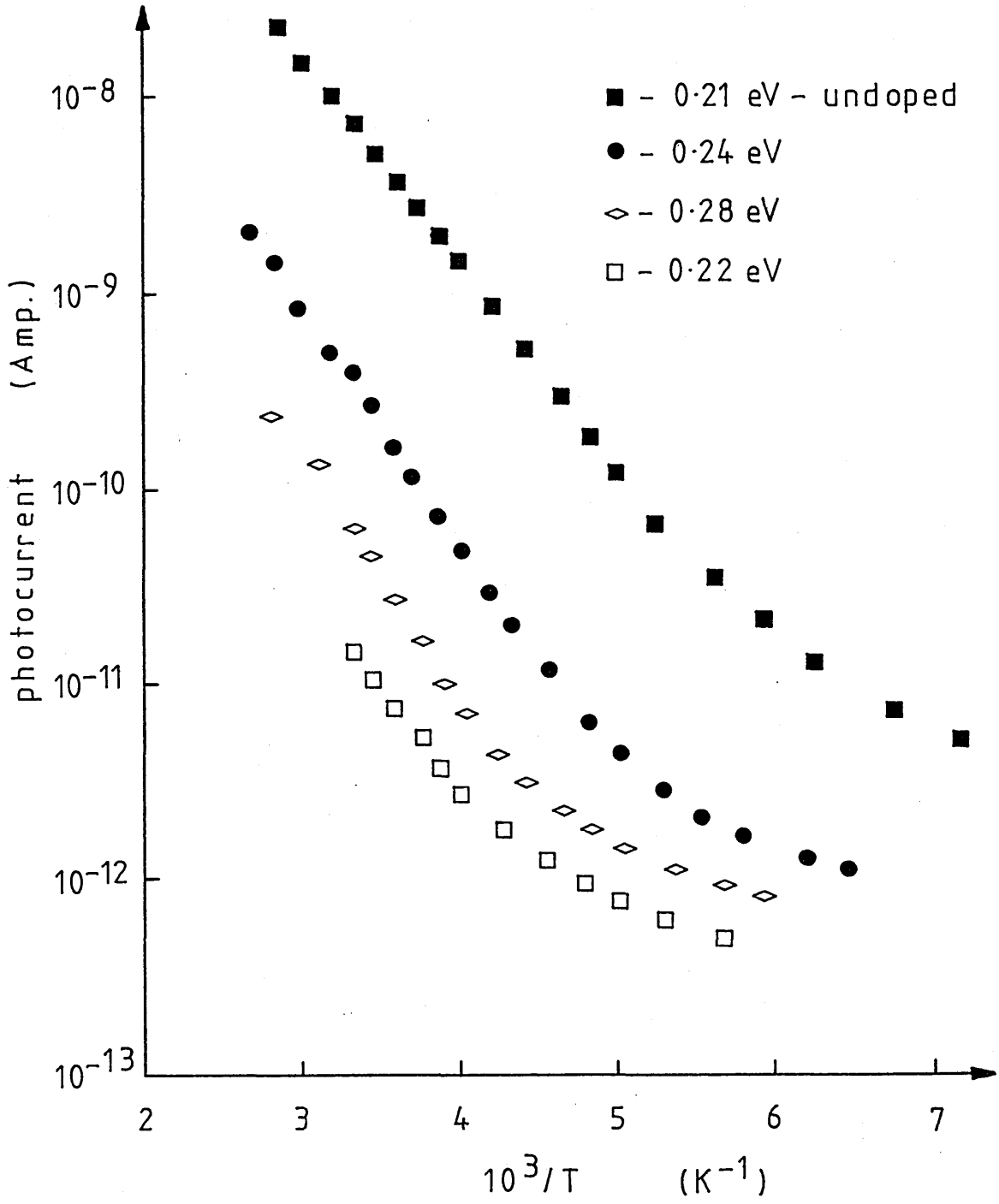

Figure 6.27. Photocurrent versus inverse temperature for Antimony doped films of a-Si:H. For comparison, the undoped specimen with the lowest photoconductivity is shown. Activation energies deduced from the high temperature linear regions are given in the figure.

Figure 6.27 reveals two temperature regions for all of the doped specimens. At high temperatures the photocurrent plots are singly activated with activation energies in the range 0.21 to 0.28 eV. At low temperatures the photocurrent plots display continuous curvature towards lower effective activation energies with decreasing temperature. The magnitude of the photocurrent at all temperatures decreases monotonically with increasing dopant concentration. The addition of approximately 0.3 at. % Antimony to the a - Si:H is seen to reduce the room temperature photocurrent by between 3 and 6 orders of magnitude (compared with the various curves of figure 6.13).

6.8.5 TRANSIENT PHOTOCONDUCTIVITY

Figure 6.28 shows plots of the carrier drift mobility and the trap limited carrier lifetime versus inverse temperature for the most lightly doped film of a - Si:H (0.1 at. % Antimony). Again, due to very small signal levels, no transient photoconductivity data could be obtained for the more heavily doped specimens. From figure 6.28 it can be seen that the mobility is singly activated over the entire temperature range investigated, with an activation energy of $E_{\mu} = 0.39$ eV. The room temperature mobility is approximately 5×10^{-10} $cm^2 V^{-1} s^{-1}$, this value being about three orders of magnitude lower than the lowest room temperature mobility observed in the undoped material. The trap limited carrier lifetime lies in the range 3×10^{-3} to 2×10^{-2} seconds. These values are comparable with the longest lifetimes observed in the undoped material.

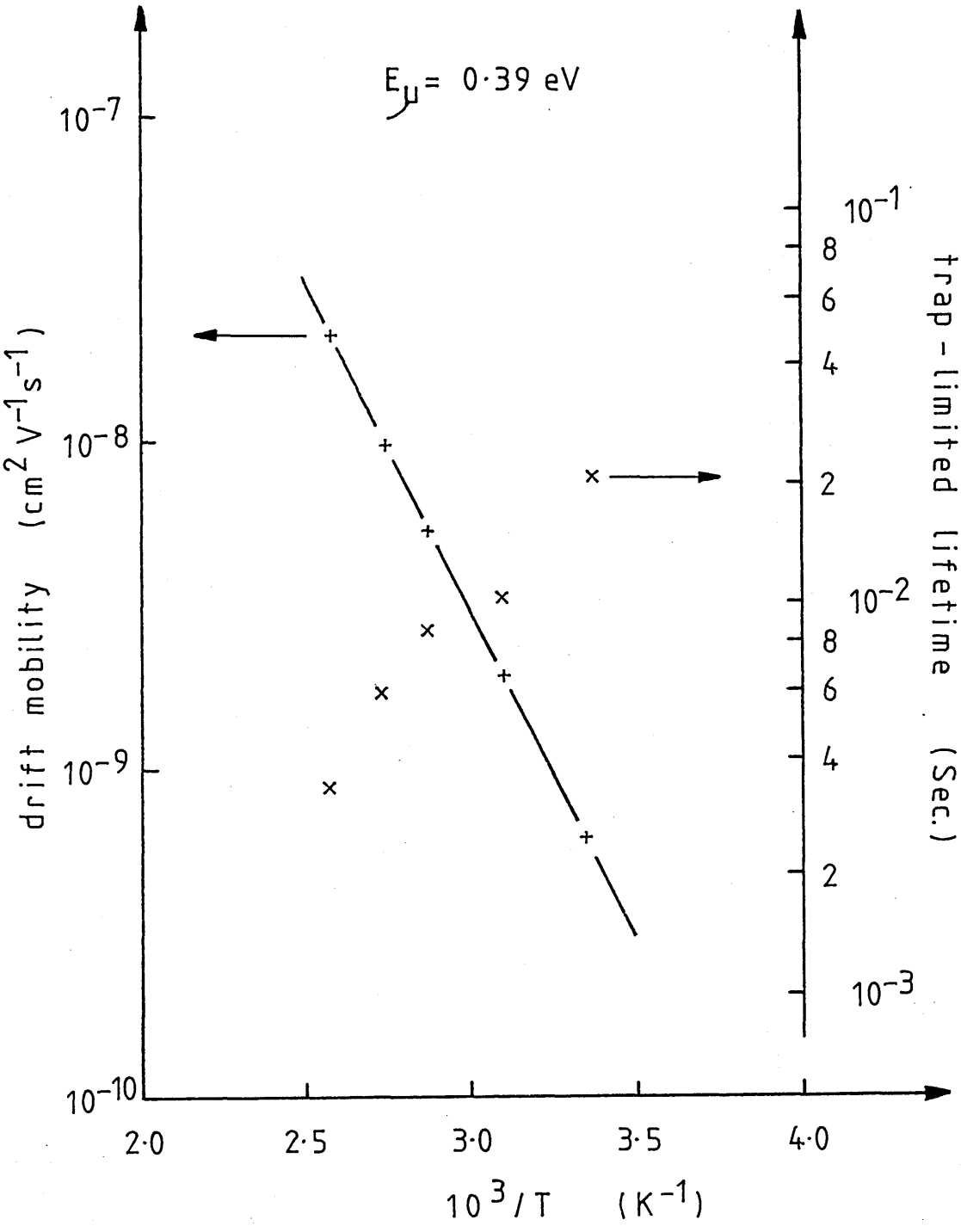

Figure 6.28. Drift mobility and trap limited lifetime versus inverse temperature for the 0.1 at.% Antimony doped film.

6.9 DISCUSSION

Figure 6.24 reveals no significant change in the dark d.c. conductivity of a - Si:H with the addition of small amounts of Antimony ($\leqslant$ 0.3 at. %). Any real change in material characteristics, however, may be obscured by the large and variable concentration of Arsenic and Selenium impurities that have been found to exist in these films. For larger dopant concentrations ($\simeq$ 0.6 at. %), the high temperature conductivity activation energy shows a marked decrease in value and a new low temperature region, with a well defined activation energy of 0.30 eV, is established. The large value of conductivity pre - exponential ($\geqslant 2 \times 10^{3}$ $(\Omega\,\mathrm{cm})^{-1}$) obtained from all of the doped specimens suggests that the conductivity is dominated by carriers (assumed to be electrons) moving in extended states at E_c. The well defined low temperature activation energy for specimen O , indicates that Antimony doping may introduce an impurity associated level of localised states in the mobility gap, at an energy of around 0.3 eV below the conduction band mobility edge. However, since no steady state or transient photoconductivity measurements could be obtained for specimen O , the existence of such a localised peak could not be verified.

Figure 6.26 shows that the optical gap reduces with increasing dopant concentration. By comparing the deduced optical gap, E_o, and the measured conductivity activation energy, E_σ, it can be established that the Fermi level is situated around mid - gap in all of the doped specimens. It is therefore suggested that Antimony is not acting as

an effective substitutional dopant for these particular specimens of r.f. sputtered a - Si:H. It is proposed that the reduction in the conductivity activation energy with increasing dopant concentration is due to a corresponding reduction in the magnitude of the optical gap. It therefore seems likely that the majority of Antimony atoms are entering the a - Si:H lattice in a fully co - ordinated manner, resulting in the deposition of an amorphous Silicon - Antimony alloy. It can thus be established that the optical gap of the alloy decreases with increasing Antimony concentration.

The steady state photocurrent data of figure 6.27 imply a decreasing photo - response with increasing Antimony concentration. This is probably due to an increase in the density of recombination centres as the Antimony concentration is increased. From figure 6.28 a room temperature $\mu\tau$ product of around 10^{-11} $cm^2 V^{-1}$ can be defined for specimen ● . This $\mu\tau$ product is 1 to 2 orders of magnitude less than corresponding data obtained from the "worst" undoped material. The long trap - limited carrier lifetime and the small measured drift mobility are probably due to a large density of trapping centres.

The well defined activation energies obtained from the photocurrent Arrhenius plots of figure 6.27 can be explained in terms of either band to localised or localised to localised recombination (as described in section 6.4.4.1). The well defined drift mobility activation energy of E_μ = 0.39 eV obtained from figure 6.28, however, suggests that trapping centres are likely to exist well below the conduction band mobility edge. In the steady state it is probable that the deepest traps will contain the majority of the photogenerated

charge implying that band to localised recombination may provide the best fit to the experimental data.

6.10 CONCLUSIONS

Clearly, it has not been possible with the limited data available to provide a detailed interpretation of the electronic transport properties of these Antimony doped a - Si:H films. However, it has been possible to identify some likely processes which may be occurring. It has been shown that substitutional doping is unlikely to occur in this material. More probably, the Antimony is entering the a - Si:H lattice in a fully co - ordinated manner, leading to an amorphous Silicon - Antimony alloy. The optical gap of this alloy has been shown to decrease with increasing Antimony concentration. Photoconductivity measurements have suggested that there is a decrease in the photo - response as the Antimony concentration is increased. This is probably due to an increase in the density of states within the mobility gap, as the Antimony concentration is increased.

REFERENCES CHAPTER 6

(1) Pfister G., Phys. Rev. Lett. 36, 271, (1976).

(2) Grunwald H.P., Blankney R.M., Phys. Rev. 165, 1006, (1968). [For example]

(3) Pfister G., Scher H., Proc. 7th Int. Conf. on Amorphous and Liquid Semiconductors, (Ed. Spear W.E.), p.197, (1977).

(4) Marshall J.M., Phil. Mag. B36, 4, 959, (1977).

(5) Marshall J.M., Sharp A.C., J. Non-Cryst. Sol. 35 - 36, 99, (1980).

(6) Sharp A.C., Marshall J.M., J. Phys. C, Solid State Phys. 14, 761, (1981).

(7) Anderson D.A., Paul W., Phil. Mag. B44, 2, (1981).

(8) Mort J. et al, Appl. Phys. Lett. 45, 16, 1348, (1981).

(9) Anderson D.A., Moustakas T., Paul W., Proc. 7th Int. Conf. on Amorphous and Liquid Semiconductors, (Ed. Spear W.E.), (1977).

(10) Kirby P.B., Paul W., Phys. Rev. B25, 8, 5373, (1982).

(11) Spear W., Loveland R.J., Al-Sharbaty A., J. Non-Cryst. Sol. 13, 55, (1974).

(12) Anderson D.A., Spear W., Phil. Mag. 36, 695, (1977).

(13) Freeman E.C., Paul W., Phys. Rev. B20, 2, 716, (1979).

(14) Jones D.I., LeComber P.G., Spear W.E., Phil. Mag. B36, 541, (1977).

(15) Allan D., Phil. Mag. B38, 4, 381, (1978).

(16) Marshall J.M., Private Communication, (1984).

(17) Spear W.E., LeComber P.G., J. Non-Cryst. Sol. 8 - 10,

727, (1972).

(18) Marshall J.M., Street R.A., Thompson M.J., Phys. Rev. B29, 4, 2331, (1984).

(19) Coutts T.J., in "Electrical Conduction in Thin Metal Films" (American Elsivier), (1974).

(20) Anderson D.A., Paul W., Phil. Mag. B45, 45, 1, (1981).

(21) Anderson D.A., Paul W., J. Phys. Soc. Japan, 49, Suppl. A, 1197, (1982).

(22) Cohen R.W., Cody G.D., Coutts M.D., Abeles B., Phys. Rev. B8, 3689, (1973).

(23) Tanaka T. et al, J. Vac. Soc. Japan, 23, 12, (1980).

(24) Kirby P.B., Paul W., Phys. Rev. B29, 2, 826, (1984).

(25) Paul W., Anderson D.A., Solar Energy Materials 5, 229, (1981).

CHAPTER 7

CONCLUSIONS

Computer - based equipment has been developed for the capture and analyses of fast transient current pulses generated from a time of flight experiment. The equipment has been thoroughly tested using the well characterised material amorphous Selenium. Time of flight measurements obtained from amorphous Selenium suggest that a trap - limited band transport mechanism is the most likely to occur. It has further been suggested that the electronic structure of amorphous chalcogenide semiconductors may be influenced to a measurable degree by the method of film preparation.

An r.f. sputter deposition system capable of preparing thin films of doped and undoped amorphous Silicon has been commissioned. Dark d.c. conductivity, electron drift mobility, transient and steady state photoconductivity and optical absorption experiments have been carried out on specimens of amorphous Silicon prepared in this system. The variation of the dark d.c. conductivity with hydrogen partial pressure has been measured and found to be consistent with similar measurements reported in the literature. In general, experimental data obtained from specimens of amorphous Silicon prepared under seemingly identical deposition conditions have been found to vary widely from specimen to specimen. This variation has been interpreted in terms of a density of states distribution which is critically dependent upon the conditions of film deposition. Further, it has

been proposed that random amounts of impurity atoms which have been found to exist in specimens deposited in this laboratory may have a determining influence on the density of states distribution and hence on the measured electronic transport properties. Experimental data have been interpreted in terms of localised conduction band tail states extending to approximately 0.2 eV below the conduction band mobility edge, and a discrete set of localised states situated at 0.4 eV below the conduction band mobility edge. It has been suggested that the extent of the tail states and the density of the discrete states are critically dependent upon the conditions of film deposition and upon the level of impurity atoms within the material.

P - type doping was attempted by co - sputtering strands of Aluminium wire with a polycrystalline Silicon target. The Silicon - Aluminium films deposited were found to contain crystalline Aluminium islands embedded within an amorphous background lattice. It was suggested that the background lattice is an amorphous Silicon - Aluminium alloy. Electronic transport measurements revealed that with increasing impurity concentration there was a monotonic decrease in both the conductivity activation energy and the optical band gap. Thermoelectric power measurements on the most heavily doped film suggested that electronic transport around room temperature in all of the Silicon - Aluminium films is dominated by phonon assisted hopping through localised states situated between the Fermi level and the valence band mobility edge. The above results were interpreted in terms of the electronic transport properties of an amorphous Silicon - Aluminium alloy. It was suggested that the vast majority of the Aluminium atoms did not enter the amorphous Silicon as substitutional

dopants. Consequently, co - sputtering Aluminium and Silicon was found not to be an effective means of preparing p - type material.

N - type doping was attempted by co - sputtering spheres of Antimony shot with a polycrystalline Silicon target. The material prepared was found to be homogeneous to a resolution of 50 Angstroms. Electronic transport measurements revealed that for impurity concentrations up to about 3 at. % there was no significant change in the temperature dependence of the conductivity. For larger impurity concentrations the high temperature conductivity activation energy displayed a marked decrease in value, and a new low temperature region to the conductivity Arrhenius plot was established. The optical band gap was found to monotonically decrease with increasing impurity concentration. The results were interpreted in terms of the electronic transport properties of a Silicon - Antimony alloy. In conclusions similar to those reached for the Aluminium impurities it was suggested that Antimony was not entering the amorphous Silicon lattice as a substitutional dopant and that co - sputtering Antimony and Silicon was not an effective means of preparing n - type material.

In general, the results presented in this thesis suggest that, with the necessary equipment, it is relatively simple to prepare thin films of amorphous Silicon by r.f. sputter deposition. However, in order to prepare material of high quality, the optimisation of the many alterable sputter parameters must be carried out. This involves a detailed characterisation of a large number of specimens which have been prepared over a wide range of deposition conditions, followed by a choice of sputter parameters which lead to the deposition of the

highest quality material. Clearly, due to the large number of alterable and inter - related parameters which exist within a sputter deposition system, this characterisation procedure is a time consuming and extensive process which lends itself to much compromise.

In conclusion, the results presented in this thesis show that the material prepared in this laboratory is not of the high quality required for device applications and presently achievable using the glow discharge process. It is proposed that, in part, this may account for the poor response obtained from attempts at electronic doping. It is suggested that prior to further attempts at doping an optimisation study must be carried out in order to improve the quality of the base undoped material.

APPENDIX I

System Program For NASCOM
MICRO - COMPUTER.

```
;************************************************************
;
;     PROGRAM: DEC-SYS MONITOR (VER 1.2) FOR NASCOM 2
;
;     AUTHOR:  HENRY S. FORTUNA
;
;     DATE:    SEPTEMBER 1980
;
;************************************************************
;
;
; ABSTRACT
; ========
;
; THIS PROGRAM CONTAINS ROUTINES WHICH ENABLE NASCOM TO :
; 1) COMMUNICATE WITH THE DEC-20
; 2) LOAD AND STORE INTEL HEX FILES ON THE DEC-20
; 3) ASSIST IN EPROM PROGRAMMING WITH THE SOFTY MICRO
; 4) SUPPORT A REAL TIME CLOCK
; 5) TRANSFER DATA FROM DATALAB DL905 TRANSIENT ANALYSER TO
;    NASCOM MEMORY
;
;       LOADED AT 0D000H
;       APPROX. SIZE 1.5K BYTES
;
        ORG     0D000H
;       ==============
;
;
;************************************************************
;
;       PROGRAM EQUATES
;
;************************************************************
;
ADDHB   EQU 0009H       ; ADD HL TO BC
ARG1    EQU 0C0CH       ; NASCOM RAM
ARG3    EQU 0C10H       ;     "
ARGN    EQU 0C0BH       ;     "
ARGS    EQU 0060H       ; NASCOM SUB.
SPACE   EQU 0020H       ; ASCII SPACE
B2HEX   EQU 0068H       ; NASCOM SUB.
BEL     EQU 0007H       ; ASCII BELL
BLINK   EQU 007BH       ; NASCOM SUB.
CLSCR   EQU 000CH       ; ASCII CLEAR SCREEN
CR      EQU 000DH       ; ASCII RETURN
CRLF    EQU 006AH       ; NASCOM SUB.
CURSOR  EQU 0C2 H       ; POSITION IN VIDEO RAM
DEL     EQU 007FH       ; ASCII DELETE
```

```
ERR     EQU 006BH       ; NASCOM SUB.
ESC     EQU 001BH       ; ASCII ESCAPE
IM2     EQU 5EEDH       ; MODE 2 INT.
INLIN   EQU 0063H       ; NASCOM SUB.
ITAB    EQU 0C80H       ; INTERRUPT TABLE
IVEC    EQU 000CH       ; INT. VECTOR
KIN     EQU 0061H       ; NASCOM SUB.
LDDE    EQU 5BEDH       ; Z-80 (LD DE,(MEM) )
LDCUR   EQU 53EDH       ; Z-80 (LD (MEM),DE )
LDIA    EQU 47EDH       ; Z-80 (LD I,A)
LDIR    EQU 0B0EDH      ; Z-80 INSTR.
NAS     EQU 005BH       ; NASCOM SUB.
NSAV    EQU 0C21H       ; NASCOM RAM
NUM     EQU 0064H       ; NASCOM SUB.
NUMN    EQU 0C20H       ; NASCOM RAM
PAC     EQU 0006H       ; PORT A CONTROL
PAD     EQU 0004H       ;   "    DATA
PBC     EQU 0007H       ; PORT B CONTROL
PBD     EQU 0005H       ;   "    DATA
PMASK   EQU 007FH       ; PARITY MASK
RETI    EQU 4DEDH       ; Z-80 (RETI)
RCLOCK  EQU 0C82H       ; CLOCK IN RAM
VCLOCK  EQU 0BF0H       ; CLOCK IN VIDEO
RLIN    EQU 0079H       ; NASCOM SUB.
SBCHB   EQU 42EDH       ; SUB BC FROM HL
SBCHD   EQU 52EDH       ; SUB DE FROM HL
SCAN    EQU 0062H       ; NASCOM SUB.
SERO    EQU 006FH       ;    "
SOUT    EQU 006DH       ;    "
SPAC    EQU 0069H       ;    "
SRLIN   EQU 0070H       ;    "
TBCD3   EQU 0066H       ;    "
TDEL    EQU 005DH       ;    "
TOPLIN  EQU 0BCAH       ; NASCOM RAM
ULINE   EQU 005FH       ; ASCII '_'
;
;
;*************************************************************
;
;       ENTRY POINT
;
;*************************************************************
;
START:  MVI     A,CLSCR
        RST     6               ; CLEAR SCREEN
        LXI     H,HEAD          ; POINT TO HEADING
        LXI     D,TOPLIN        ;    "    TOPLINE OF VDU
        LXI     B,11            ; LOAD NO. OF CHARS.
        DW      LDIR            ; WRITE HEADING
        RST     3
```

```
        DB      CRLF            ; NEWLINE
INP:    MVI     A,'>'
        RST     6               ; PROMPT
        RST     3
        DB      BLINK           ; WAIT FOR INPUT
        CPI     'A'
        JZ      TA              ; TRANS. ANALYSER
        CPI     'C'
        JZ      CLOCK           ; SET REAL TIME CLOCK
        CPI     'E'
        JZ      EXE             ; EXECUTE
        CPI     'F'
        JZ      FILLF           ; FILL RAM WITH 0FFH
        CPI     'H'
        JZ      DECIO           ; LOGGING DEC I/O
        CPI     'L'
        JZ      DECIO           ; LOGGING DEC I/O
        CPI     'N'
        JZ      MON             ; JMP TO NAS-SYS
        CPI     'R'
        JZ      READ            ; READ HEX FILE FROM DEC
        CPI     'S'
        JZ      SOFTY           ; WRITE TO SOFTY
        CPI     'T'
        JZ      DONE            ; NON-LOGGING DEC I/O
        CPI     'V'
        JZ      VERIFY          ; VERIFY RAM BLOCKS
        CPI     'W'
        JZ      WRITE           ; WRITE HEX FILE TO DEC
        RST     3
        DB      ERR             ; OTHERWISE GIVE ERROR
        JMP     INP             ; RE-PROMPT
;
;
;       DEC-SYS ROUTINES
;       ================
;
;*************************************************************
;
;       ANALYSE - A START ADDRESS FOR THE DATA FROM THE
;                 ANALYSER IS REQUIRED. IF THERE IS NO INPUT
;                 THEN 1000H IS ASSUMED. A SPACE STARTS THE
;                 TRANSFER,ANYTHING ELSE RETURNS TO DEC-SYS.
;                 PORT A : D0-D7 INPUT FROM ANALYSER
;                 PORT B : D0 WORD REQUEST TO  "
;                          D1 DATA READY FROM  "
;                          D2 DIGITAL O/P REQUEST TO ANALYSER
;                          D3    "     "  ENABLE  "     "
;                          D4-D7 UNUSED
;
```

```
;************************************************************
;
TA:     MVI     A,01001111B
        OUT     PAC             ; SET A AS INPUTS
        MVI     A,11001111B
        OUT     PBC             ; SET B TO BIT CONTROL
        MVI     A,00000010B
        OUT     PBC             ; ALL O/P'S EXCEPT BIT 2
        XRA     A
        OUT     PBD             ; WRITE 0'S TO B
TA1:    RST     3
        DB      CRLF
        RST     5
        DB      'ADDR ? ',00H   ; PROMPT STORAGE ADDRESS
        RST     3
        DB      INLIN           ; GET ADDRESS
        LXI     H,7
        DAD     D               ; ADD 7 TO DE FOR
        XCHG                    ; RLIN ROUTINE
        RST     3
        DB      RLIN            ; EXAMINE INPUT
        JC      TA1             ; IF INVALID REPROMPT
        LXI     H,1000H         ; SET POINTER
        LDA     ARGN            ; GET NO. OF I/P ARGUMENTS
        ORA     A
        JZ      TA2             ; IF NONE DON'T ALTER POINTER
        LHLD    ARG1            ; OTHERWISE ALTER POINTER
TA2:    PUSH    H
        RST     3
        DB      BLINK           ; WAIT FOR KBD. I/P
        POP     H
        CPI     SPACE           ; IS IT A SPACE ?
        JNZ     START           ; IF NOT ABORT TRANSFER
        LXI     D,3FFH          ; SET TRANSFER COUNT
        MVI     A,00001000B
        OUT     PBD             ; ENABLE DIGITAL O/P
        MVI     A,00001100B
        OUT     PBD             ; REQUEST MEMORY TRANSFER
TA3:    IN      PBD
        ANI     02H             ; DATA READY HI ?
        JZ      TA3             ; NO,CHECK AGAIN
        IN      PAD             ; YES,READ DATA
        MOV     M,A             ; STORE IT
        INX     H               ; INC. POINTER
        DCX     D               ; DEC. TRANSFER COUNT
        MOV     A,E
        ORA     D               ; COUNT = 0 ?
        JZ      TAF             ; THEN FINISHED
        MVI     A,00001101B
        OUT     PBD
```

```
        MVI     A,00001100B
        OUT     PBD             ; OTHERWISE PULSE WORD REQ.
        JMP     TA3             ; LOOP
TAF:    XRA     A
        OUT     PBD             ; DISABLE DIG O/P & REQ.
        JMP     WRITE           ; READY TO WRITE TO DEC
;
;
;*************************************************************
;
;       CLOCK - SETS THE REAL TIME CLOCK. ENTER 4 DIGITS FOR
;               HOURS & MINUTES THEN ANY KEY TO START CLOCK.
;
;*************************************************************
;
CLOCK:  DI                      ; DISABLE INTERRUPTS
        DW      IM2             ; SET INT. MODE 2
        LXI     H,CINT          ; POINT TO INT. ROUTINE
        SHLD    ITAB            ; STORE ROUTINE ADDRESS
        MVI     A,IVEC          ; MSB OF INT. TABLE ADDRESS
        DW      LDIA            ; A => CPU INT. REGISTER
        LXI     H,ICLOCK        ; POINT TO INITIALISATION
        CALL    WCLOCK          ; WRITE TO VIDEO RAM
        LXI     H,ICLOCK
        LXI     D,RCLOCK        ; POINT TO COPY IN WORK RAM
        LXI     B,8             ; SET COUNT
        DW      LDIR            ; COPY INIT. TO WORK RAM
        LXI     H,RCLOCK        ; POINT TO COPY IN WORK RAM
        MVI     C,2
CL0:    MVI     B,2
CL1:    PUSH    H
        PUSH    B
        RST     3
        DB      BLINK           ; INPUT HOURS & MINUTES
        POP     B
        POP     H
        RST     6
        MOV     M,A
        INX     H
        DCR     B
        JNZ     CL1
        INX     H
        DCR     C
        JNZ     CL0
        LXI     H,RCLOCK
        CALL    WCLOCK          ; WRITE CLOCK TO VDU
        RST     3
        DB      BLINK           ; WAIT FOR ANY KEY
        RST     3
        DB      CRLF
```

```
        EI                      ; ENABLE INTERRUPT
        JMP     START
CINT:   PUSH    H               ; START OF INTERRUPT ROUTINE
        PUSH    D
        PUSH    B
        PUSH    PSW             ; SAVE ALL REGISTERS
        LXI     H,RCLOCK+7      ; POINT TO SECOND'S UNITS
        MVI     B,35H           ; SET B TO ASCII '5'
        MVI     C,39H           ; SET C TO ASCII '9'
        MOV     A,C
        CMP     M               ; IS SU = 9 ?
        JNZ     CINT2           ; INC. IF NOT
        MVI     M,30H           ; ELSE ZERO SU
        DCX     H               ; POINT TO SECOND'S TENS
        MOV     A,B
        CMP     M               ; IS ST = 5 ?
        JNZ     CINT2           ; INC. IF NOT
        MVI     M,30H           ; ELSE ZERO ST
        DCX     H
        DCX     H               ; POINT TO MINUTE'S UNITS
        MOV     A,C
        CMP     M               ; IS MU = 9 ?
        JNZ     CINT2           ; INC. IF NOT
        MVI     M,30H           ; ELSE ZERO MU
        DCX     H               ; POINT TO MINUTE'S TENS
        MOV     A,B
        CMP     M               ; IS MT = 5 ?
        JNZ     CINT2           ; INC. IF NOT
        MVI     M,30H           ; ELSE ZERO MT
        DCX     H
        DCX     H               ; POINT TO HOUR'S UNITS
        MVI     A,33H
        CMP     M               ; IS HU = 3 ?
        JNZ     CINT1
        DCR     A
        DCX     H               ; POINT TO HOUR'S TENS
        CMP     M               ; IS HT = 2 ?
        INX     H               ; POINT TO HOUR'S UNITS
        JNZ     CINT1
        MVI     A,30H           ; HOURS = 23
        MOV     M,A
        DCX     H
        MOV     M,A             ; ZERO THE HOURS
        JMP     CINT3
CINT1:  MOV     A,C             ; HOURS NOT = 23
        CMP     M               ; IS HU = 9 ?
        JNZ     CINT2           ; INC. IF NOT
        MVI     M,30H           ; ELSE ZERO HU
        DCX     H               ; POINT TO HOUR'S TENS
CINT2:  INR     M
```

```
CINT3:  LXI     H,RCLOCK        ; POINT TO CLOCK IN RAM
        CALL    WCLOCK          ; WRITE TO VDU
        POP     PSW
        POP     B
        POP     D
        POP     H               ; RESTORE REGISTERS
        EI                      ; ENABLE INTERRUPTS
        DW      RETI
;
;
;***************************************************************
;
;       DECIO - TURNS THE NASCOM INTO A TERMINAL FOR THE
;               DEC-20. IF NOT LOGGED ON,DECIO LOGS INTO
;               <PHYSR-HF> (H COMMAND) OR <PHYSR-STEP>
;               (L COMMAND) ^B RETURNS TO DEC-SYS.
;
;***************************************************************
;
DECIO:  MOV      D,A                    ; SAVE L OR H
        MVI     A,CR
        RST     3
        DB      SERO            ; SEND CR TO DEC
SCANS:  RST     3
        DB      SRLIN           ; CHECK FOR DEC REPLY
        JNC     SCANS           ; WAIT FOR REPLY
        ANI     PMASK           ; MASK PARITY
        RST     6
        CPI     BEL             ; WAS CHAR. A BELL ?
        JNZ     DONE            ; IF NOT,LOGGED ON ALREADY
        RST     3
        DB      TDEL            ; DELAY
        MVI     A,03H
        RST     3
        DB      SERO            ; SEND ^C TO DEC
        RST     3
        DB      TDEL
        MOV     A,D             ; H OR L INTO A
        LXI     H,LOGH          ; POINT TO LOGON DATA FOR HF
        MVI     B,25H           ; LOAD NO. OF CHARS.
        CPI     'L'             ; WAS L ENTERED ?
        JNZ     DONE4           ; IF NOT,LOGON HF
        LXI     H,LOGL          ; OTHERWISE LOGON STEP
        INR     B
        INR     B               ; ALTER COUNT TO 27H
DONE4:  RST     3
        DB      SOUT            ; SEND THEM TO DEC
DONE:   LHLD    CURSOR          ; POINT TO CURSOR
        MOV     B,M             ; SAVE DATA IN B
        MVI     M,ULINE         ; WRITE ULINE TO VIDEO RAM
```

```
DONE1:  PUSH    H
        PUSH    B
        RST     3
        DB      KIN             ; ANY DATA FROM KEYBOARD ?
        POP     B
        POP     H
        JNC     NOCHAR          ; NON CARRY MEANS NO DATA
        CPI     02H             ; IS IT A ^B ?
        JZ      START           ; YES,GOTO DEC-SYS
        CPI     08H             ; IS IT BACKSPACE ?
        JNZ     DONE2           ; IF NOT,CHECK FURTHER
        MVI     A,DEL           ; SET A TO DELETE
        JMP     DONE3
DONE2:  CPI     17H             ; IS IT CH ? (ESC)
        JNZ     DONE3           ; IF NOT,SEND IT
        MVI     A,ESC           ; SET A TO ESCAPE
DONE3:  RST     3
        DB      SERO            ; SEND TO DEC
        MOV     M,B             ; OVERWRITE CURSOR
NOCHAR: RST     3
        DB      SRLIN           ; ANY DATA FROM DEC ?
        JNC     DONE1           ; NO,THEN LOOP
        ANI     PMASK           ; YES, MASK PARITY
        MOV     M,B             ; OVERWRITE CURSOR
        RST     6               ; PRINT IT
        JMP     DONE            ; LOOP
;
;
;***************************************************************
;
;       EXE - WHEN A VALID HEX NO. IS INPUT TO THIS ROUTINE
;             THE STACK IS SET TO 1000H,THE SCREEN CLEARED
;             AND EXECUTION COMMENCES AT THE ADDRESS.
;
;***************************************************************
;
EXE:    RST     3
        DB      CRLF            ; NEWLINE
EXE2:   RST     5
        DB      'ADDR ? ',00H   ; PROMPT THE ADDRESS
        RST     3
        DB      INLIN           ; GET ADDRESS
        LXI     H,6
        DAD     D               ; ADD 6 TO DE
        XCHG                    ; FOR RLIN ROUTINE
        RST     3
        DB      RLIN            ; EXAMINE INPUT
        JC      EXE2            ; IF INVALID REPROMPT
        LDA     ARGN            ; GET NO. OF I/P ARGS.
        ORA     A
```

```
        JZ      START           ; IF NONE GOTO DEC-SYS
        LXI     SP,1000H        ; OTHERWISE SET STACK
        MVI     A,0CH
        RST     6               ; CLEAR SCREEN
        RST     3
        DB      ARGS            ; GET ADDRESS IN HL
        PCHL                    ; JUMP TO ADDRESS
;
;
;************************************************************
;
;       FILLF - FILL'S A 1K BLOCK OF RAM WITH 0FFH. THIS IS
;               USED BEFORE LOADING A HEX FILE FROM THE DEC
;               PRIOR TO TRANSFERRING THE BLOCK TO SOFTY
;               FOR EPROM PROGRAMMING. IF NO BYTE IS ENTERED
;               AFTER THE ADDRESS,0FFH IS ASSUMED.
;
;************************************************************
;
FILLF:  RST     3
        DB      CRLF            ; NEWLINE
F1:     RST     5
        DB      '? ',00H        ; PROMPT START ADDRESS
        RST     3
        DB      INLIN           ; GET ADDRESS
        INX     D               ; ALTER DE FOR RLIN
        RST     3
        DB      RLIN            ; EXAMINE INPUT LINE
        JC      F1              ; IF INVALID,REPROMPT
        LDA     ARGN            ; GET NO. OF I/P ARGS.
        ORA     A
        JZ      START           ; IF NONE GOTO DEC-SYS
        RST     3
        DB      ARGS            ; ADDRESS => HL,FILL BYTE => E
        LXI     B,400H          ; COUNT = 1024
        CPI     1               ; 1 ARGUMENT ?
        JNZ     F2
        MVI     E,0FFH          ; YES,FILL BYTE = 0FFH
F2:     MOV     A,E
        MOV     M,A             ; WRITE BYTE TO RAM
        INX     H               ; INC. RAM POINTER
        DCX     B               ; DEC. COUNT
        MOV     A,B
        ORA     C
        JNZ     F2              ; IF BC NON-ZERO,LOOP
        JMP     START           ; OTHERWISE GOTO DEC-SYS
;
;
;************************************************************
;
```

```
;       MON - JUMPS TO NAS-SYS MONITOR.
;
;*************************************************************
;
MON:    RST     3
        DB      NAS
;
;
;*************************************************************
;
;       READ - READS AN INTEL HEX FILE FROM THE DEC. IF AN
;              OFFSET IS ENTERED IT IS ADDED TO ALL THE
;              ADDRESS'S SPECIFIED IN THE HEX DATA BLOCKS.
;              IF THE FILE GIVEN DOES NOT EXIST ON THE DEC
;              THE FILENAME PROMPT IS REPEATED. AS THE FILE
;              IS BEING READ THE ADDRESS OF THE LAST LOCATION
;              OF THE BLOCK JUST LOADED IS WRITTEN TO THE
;              SCREEN. ^C ABORTS.
;
;*************************************************************
;
READ:   RST     3
        DB      CRLF            ; NEWLINE
READ1:  RST     5
        DB      'OFFSET ? ',00H ; PROMPT
        RST     3
        DB      INLIN           ; GET OFFSET
        LXI     H,0008H
        DAD     D               ; ADD 8 TO DE
        XCHG                    ; FOR NUM
        RST     3
        DB      NUM             ; CHECK OFFSET,SAVE IN NSAV
        JC      READ1           ; IF INVALID,REPROMPT
READ5:  RST     5
        DB      'FILE ? ',00H   ; PROMPT
        RST     3
        DB      INLIN           ; GET FILENAME
        LXI     H,7
        DAD     D               ; ADD 7 TO DE
        MOV     A,M             ; GET 1ST CHAR. OF FILENAME
        CPI     SPACE
        JZ      START           ; IF A SPACE,GOTO DEC-SYS
        XCHG                    ; SAVE IN DE
        LXI     H,MESS1         ; POINT TO 'RUN' MESSAGE
        MVI     B,3
        RST     3
        DB      SOUT            ; SEND TO DEC
        XCHG                    ; GET FILENAME POINTER BACK
READ2:  MOV     A,M             ; GET FILENAME CHAR.
        CPI     SPACE
```

```
        JZ      READ3           ; IF A SPACE,ALL SENT
        RST     3
        DB      SERO            ; OTHERWISE SEND TO DEC
        INX     H               ; INC. POINTER
        JMP     READ2           ; LOOP
READ3:  LXI     H,MESS2
        MVI     B,5
        RST     3
        DB      SOUT            ; SEND '.HEX' TO DEC
READ4:  RST     3
        DB      SRLIN           ; DATA FROM DEC ?
        JNC     READ4           ; IF NOT,LOOP
        ANI     PMASK           ; OTHERWISE MASK PARITY
        CPI     ':'
        JZ      READ6           ; IF ':',FOUND START OF DATA
        CPI     '%'
        JNZ     READ4           ; IF NOT '%',LOOP FOR MORE DATA
        RST     3
        DB      TDEL            ; OTHERWISE FILE NOT FOUND,
        RST     3               ; DELAY FOR ERROR MESS. FROM
        DB      TDEL            ; DEC
        IN      1               ; DISCARD LAST DATA FROM DEC
        JMP     READ5           ; REPROMPT FILENAME
READ6:  LHLD    NSAV            ; OFFSET IN HL
        CALL    REC             ; READ REST OF 1ST BLOCK
        JNC     READ            ; FINISHED IF NC
READ7:  CALL    RECORD          ; READ DATA BLOCK
        JNC     READ            ; FINISHED IF NC
        JMP     READ7
;
;
;************************************************************
;
;       SOFTY - LOADS A 1K BLOCK OF RAM FROM NASCOM TO
;               SOFTY FOR EPROM BURNING.
;               PORT A : D0-D7 O/P DATA TO SOFTY
;               PORT B : D0 TRI-STATE BUFFER ENABLE O/P
;                        D1 I/P BUFFER FULL (IBF) FROM SOFTY
;                        D2 STROBE TO SOFTY
;                        D3-D7 UNUSED
;
;************************************************************
;
SOFTY:  MVI     A,00001111B
        OUT     PAC             ; SET PORT A FOR O/P
        MVI     A,11001111B
        OUT     PBC             ; SET PORT B FOR BIT CONTROL
        MVI     A,00000010B
        OUT     PBC             ; SET PB1 FOR I/P
        MVI     A,11111111B
```

```
        OUT     PAD             ; SET A O/P'S HI
        OUT     PBD             ; SET B O/P'S HI
        RST     3
        DB      CRLF            ; NEWLINE
SOFT1:  RST     5
        DB      'ADDR ? ',00H   ; PROMPT START OF RAM
        RST     3
        DB      INLIN           ; GET ADDRESS
        LXI     H,6
        DAD     D               ; ADD 6 TO DE FOR RLIN
        XCHG
        RST     3
        DB      RLIN            ; CHECK ADDRESS
        JC      SOFT1           ; IF INVALID,REPROMPT
        LDA     ARGN            ; GET NO. OF ARGS.
        ORA     A
        JZ      START           ; IF NONE,GOTO DEC-SYS
        MVI     A,11111110B
        OUT     PBD             ; ENABLE BUFFERS
        LHLD    ARG1            ; GET START ADD. IN HL
        LXI     B,1024D         ; SET COUNT
SOFT2:  IN      PBD
        ANI     02H             ; GET IBF FROM SOFTY
        JNZ     SOFT2           ; IF HI,LOOP
        MOV     A,M             ; GET DATA TO BE TRANSFERRED
        OUT     PAD             ; PRESENT TO SOFTY I/P
        MVI     A,11111010B
        OUT     PBD
        MVI     A,11111110B
        OUT     PBD             ; WRITE DATA PULSE
        INX     H               ; INC. RAM POINTER
        DCX     B               ; DEC. COUNT
        MOV     A,B
        ORA     C
        JNZ     SOFT2           ; LOOP IF COUNT NON-ZERO
        MVI     A,11111111B
        OUT     PBD             ; DISABLE BUFFERS
        JMP     SOFT1
;
;
;*************************************************************
;
;       VERIFY - COMPARES 2 BLOCKS OF MEMORY EACH 1K LONG.
;                THE 2 START ADDRESSES ARE ENTERED. THEY
;                MUST DIFFER BY AT LEAST 400H AND THE
;                SMALLER ADDRESS MUST BE THE FIRST INPUT.
;                IF AN ERROR IS FOUND THE ADDRESSES AND
;                DATA ARE DISPAYED. ANY KEYBOARD CHARACTER
;                CONTINUES THE COMPARISON. ^C ABORTS.
;
```

```
;************************************************************
;
VERIFY: RST     3
        DB      CRLF            ; NEWLINE
V1:     RST     5
        DB      'ADDRS ? ',00H  ; PROMPT ADDRESSES
        RST     3
        DB      INLIN           ; GET THEM
        LXI     H,7
        DAD     D               ; ADD 7 TO DE FOR RLIN
        XCHG
        RST     3
        DB      RLIN            ; VALID HEX INPUT ?
        JC      V1              ; IF NOT RE-PROMPT
        LDA     ARGN            ; GET NO. OF ARGS. INPUT
        ORA     A
        JZ      START           ; IF NONE,GOTO DEC-SYS
        DCR     A
        JZ      V1              ; IF 1,RE-PROMPT
        RST     3               ; GET 1ST ADDRESS IN HL
        DB      ARGS            ; GET 2ND IN DE
        XCHG                    ; SWOP,HL SHOULD BE > DE
        DW      SBCHD           ; SUB DE FROM HL
        JC      V1              ; IF DE > HL,REPROMPT
        LXI     D,400H          ; HL CONTAINS DIFFERENCE
        DW      SBCHD           ; SUB 400H FROM HL
        JC      V1              ; IF HL < 400H,REPROMPT
        RST     3
        DB      ARGS            ; RE-LOAD ARGS.
        LXI     B,400H          ; SET COUNT
V2:     LDAX    D               ; GET DATA FROM RAM
        CMP     M               ; COMPARE WITH OTHER RAM
        JNZ     MISS            ; IF UNEQUAL,PRINT ERROR
V3:     INX     D
        INX     H               ; INC. RAM POINTERS
        DCX     B               ; DEC. COUNT
        MOV     A,B
        ORA     C
        JNZ     V2              ; IF B NON-ZERO,LOOP
        JMP     V1
MISS:   PUSH    B
        RST     3
        DB      TBCD3           ; PRINT HL
        MOV     A,M             ; GET DATA
        RST     3
        DB      B2HEX           ; PRINT IT
        RST     3
        DB      SPAC            ; PRINT SPACE
        XCHG                    ; OTHER ADDRESS INTO HL
        RST     3
```

```
        DB      TBCD3           ; PRINT HL
        MOV     A,M             ; GET DATA
        RST     3
        DB      B2HEX           ; PRINT IT
        XCHG                    ; SWAP BACK
        RST     3
        DB      CRLF            ; NEWLINE
        PUSH    H
        PUSH    D
V4:     RST     3
        DB      SCAN            ; SCAN KBD.
        JNC     V4              ; IF NOTHING,LOOP
        POP     D
        POP     H
        POP     B
        CPI     03H
        JNZ     V3              ; IF NOT ^C,CONTINUE
        JMP     START           ; OTHERWISE GOTO DEC-SYS
;
;
;*************************************************************
;
;       WRITE - WRITES A HEX FILE TO THE DEC IN INTEL FORMAT.
;               THE 2 ADDRESS LIMITS OF THE DATA TO BE
;               WRITTEN ARE ENTERED,THE SMALLER FIRST.
;               THE DESIRED FILENAME FOR THE DATA IS THEN
;               ENTERED AND THE DATA WILL BE WRITTEN TO
;               'FILENAME.HEX'. AS THE DATA IS WRITTEN THE
;               ADDRESS OF THE LAST BYTE WRITTEN IS DISPLAYED
;               ON THE SCREEN. IF RETURN IS GIVEN IN REPLY
;               TO EITHER OF THE PROMPTS THE ROUTINE RETURNS
;               TO DEC-SYS. ^C ABORTS.
;
;*************************************************************
;
WRITE:  RST     3
        DB      CRLF            ; NEWLINE
WRT1:   RST     5
        DB      'LIMITS ? ',00H ; PROMPT
        RST     3
        DB      INLIN           ; GET LIMITS
        LXI     H,8
        DAD     D               ; ADD 8 TO DE FOR RLIN
        XCHG
        RST     3
        DB      RLIN            ; CHECK LIMITS
        JC      WRT1            ; IF INVALID,RE-PROMPT
        LDA     ARGN            ; GET NO. OF ARGS.
        ORA     A
        JZ      START           ; IF NONE,GOTO DEC-SYS
```

```
        CPI     1
        JZ      WRT1            ; IF 1, RE-PROMPT
        RST     3
        DB      ARGS            ; GET ARGS. IN HL AND DE
        XCHG                    ; HL SHOULD > DE
        DW      SBCHD           ; SUB DE FROM HL
        JC      WRT1            ; IF DE > HL,RE-PROMPT
        INX     H               ; MODIFY DATA COUNT
        SHLD    ARG3            ; SAVE COUNT
        RST     5
        DB      'FILE ? ',00H   ; PROMPT FILENAME
        RST     3
        DB      INLIN           ; GET IT
        LXI     H,7             ; ADD 7 TO DE TO POINT TO
        DAD     D               ; START OF FILENAME
        MOV     A,M
        CPI     SPACE
        JZ      START           ; IF SPACE,GOTO DEC-SYS
        XCHG                    ; START OF FILNAME => DE
        LXI     H,MESS3         ; POINT TO 'RUN WR'
        MVI     B,7             ; LOAD NO. OF CHARS.
        RST     3
        DB      SOUT            ; SEND MESSAGE TO DEC
        XCHG                    ; POINT HL TO FILENAME
WRT3:   MOV     A,M             ; GET FILENAME CHAR.
        CPI     SPACE
        JZ      WRT4            ; IF SPACE,FINISHED
        RST     3
        DB      SERO            ; OTHERWISE SEND TO DEC
        INX     H               ; INC. POINTER
        JMP     WRT3            ; LOOP
WRT4:   MVI     A,CR
        RST     3
        DB      SERO            ; SEND RETURN TO DEC
WRT5:   RST     3
        DB      SRLIN
        JNC     WRT5            ; WAIT FOR DATA FROM DEC
        ANI     PMASK           ; MASK PARITY
        CPI     '*'
        JNZ     WRT5            ; WAIT FOR ASTERISK
        RST     3
        DB      ARGS            ; HL= START DE=FINISH BC=COUNT
        XCHG
        PUSH    B
        POP     H
SEND6:  LXI     B,16            ; NOW HL=COUNT DE=START BC=16
        DW      SBCHB           ; SUB 16 FROM COUNT
        JNC     SEND1           ; IF COUNT >= 16,OK
        DB      ADDHB           ; ADD 16 BACK ON
        MOV     C,L             ; SAVE COUNT IN BC
```

```
        JMP     SEND3
SEND1:  JNZ     SEND2           ; JUMP IF COUNT NON-ZERO
SEND3:  XRA     A
        STA     ARGN            ; ZERO ARGN AS FLAG FOR COUNT=0
SEND2:  MVI     A,':'
        RST     3
        DB      SERO            ; SEND START OF DATA BLOCK
        XRA     A
        STA     NUMN            ; ZERO CHECKSUM
        MOV     A,C
        CALL    SENDA           ; SEND BYTE COUNT
        MOV     A,D
        CALL    SENDA           ; SEND HI ADDRESS BYTE
        MOV     A,E
        CALL    SENDA           ; SEND LO ADDRESS BYTE
        XRA     A
        CALL    SENDA           ; SEND 00
SEND4:  LDAX    D               ; GET DATA BYTE
        CALL    SENDA           ; SEND IT
        INX     D               ; INC. POINTER
        DCR     C               ; DEC. COUNT
        JNZ     SEND4           ; LOOP IF MORE DATA TO SEND
        LDA     NUMN
        MOV     B,A             ; CHECKSUM TO B
        XRA     A
        SUB     B               ; FORM 2'S COMPLEMENT IN A
        CALL    SENDA           ; SEND IT
        MVI     A,CR
        RST     3
        DB      SERO            ; SEND RETURN
        PUSH    B
        XCHG                    ; POINTER TO HL
        PUSH    D
        DW      LDDE
        DW      CURSOR
        RST     3
        DB      TBCD3           ; WRITE HL TO SCREEN
        DW      LDCUR
        DW      CURSOR
        POP     D
        XCHG                    ; SWOP BACK
        POP     B
SEND8:  RST     3
        DB      SRLIN
        JNC     SEND8
        ANI     PMASK
        CPI     '*'
        JNZ     SEND8           ; WAIT FOR AST. FROM DEC
        PUSH    H
        PUSH    D
```

```
        RST     3
        DB      KIN
        JNC     SEND5           ; IF NO KEY,CONTINUE
        CPI     03H
        JZ      SEND9           ; IF ^C,ABORT
SEND5:  POP     D
        POP     H
        LDA     ARGN            ; GET COUNT FLAG
        ORA     A
        JNZ     SEND6           ; IF NOT ZERO,SEND MORE
SEND9:  LXI     H,MESS4         ; POINT TO EOF BLOCK
        MVI     B,12            ; LOAD COUNT
        RST     3
        DB      SOUT            ; SEND TO DEC
SEND7:  RST     3
        DB      SRLIN
        JNC     SEND7
        ANI     PMASK
        CPI     40H
        JNZ     SEND7           ; WAIT FOR @
        JMP     WRITE
;
;
;*************************************************************
;
;       SUBROUTINES
;
;*************************************************************
;
; FUNCTION: BYTE
; DESCRIPTION: BYTE READS 2 ASCII CHARS. FROM THE SERIAL PORT
;              AND CONVERTS THEM TO A HEX BYTE IN THE A REG.
;              D REG. MUST CONTAIN THE CHECKSUM ON ENTRY AND
;              IS UPDATED WITH THE BYTE RECEIVED.
; INPUTS: D - CHECKSUM
; OUTPUTS: A - BYTE RECEIVED
;          D - UPDATED CHECKSUM
; CALLS: CONV,SRLIN
; DESTROYS: A,C,F/F'S
;
BYTE:   RST     3
        DB      SRLIN
        JNC     BYTE            ; LOOP IF NO SERIAL I/P
        ANI     PMASK           ; MASK PARITY
        CALL    CONV            ; CONVERT ASCII TO HEX
        RLC
        RLC
        RLC
        RLC                     ; SHIFT TO HI PART OF A
        MOV     C,A             ; SAVE IN C
```

```
BYTE2:  RST     3
        DB      SRLIN
        JNC     BYTE2           ; WAIT FOR 2ND ASCII BYTE
        ANI     PMASK
        CALL    CONV            ; CONVERT TO HEX
        ORA     C               ; BUILD HEX BYTE IN A
        MOV     C,A             ; SAVE IN C
        ADD     D               ; ADD IN CHECKSUM
        MOV     D,A             ; UPDATE
        MOV     A,C             ; MOVE HEX TO A
        RET
;
;
;************************************************************
;
; FUNCTION: CONV
; DESCRIPTION: CONV CONVERTS AN ASCII BYTE IN A TO ITS BINARY
;              EQUIVALENT. IT ASSUMES THAT THE ASCII BYTE IS
;              A VALID HEX CHARACTER.
; INPUTS: A - ASCII BYTE
; OUTPUTS: A - HEX BYTE
; CALLS: NOTHING
; DESTROYS: A,F/F'S
;
CONV:   SUI     '0'
        CPI     10H
        RM                      ; RETURN IF 0...9
        SUI     07H             ; CONVERT A..F TO 10..15
        RET
;
;
;************************************************************
;
; FUNCTION: RECORD
; DESCRIPTION: RECORD READS A BLOCK OF DATA FROM THE DEC IN
;           INTEL FORMAT AND LOADS IT INTO NASCOM MEMORY WITH
;           AN APPROPRIATE OFFSET WHICH CAN BE ZERO. IF THERE
;           IS A CHECKSUM ERROR THE OUTPUT FROM THE DEC IS
;           SUPPRESSED AND AN ERROR MESSAGE OUTPUT. THE
;           ROUTINE RETURNS WITH THE CARRY RESET ON AN ERROR
;           OR AT EOF AND SET OTHERWISE.
; INPUTS: NONE WHEN CALLED AS RECORD BUT
;         A - ':'
;         HL - OFFSET ADDRESS WHEN CALLED AS REC.
; OUTPUTS - CARRY = 0 ON ERROR OR EOF
;                 = 1 OTHERWISE
; CALLS: BYTE,ERR,SERO,SRLIN,TBCD3,TDEL
; DESTROYS: A,B,C,D,E,H,L,F/F'S
;
RECORD: LHLD    NSAV            ; GET OFFSET IN HL
```

```
RECO:   RST     3
        DB      SRLIN
REC:    MVI     B,':'
        SUB     B
        JNZ     RECO            ; LOOP IF NOT ':'
        MOV     D,A             ; ZERO CHECKSUM
        CALL    BYTE            ; GET BYTE COUNT
        JZ      REC2            ; IF ZERO, END OF FILE
        MOV     E,A             ; SAVE COUNT IN E
        CALL    BYTE            ; GET HI ADDRESS
        PUSH    PSW             ; SAVE ON STACK
        CALL    BYTE            ; GET LO ADDRESS
        POP     B               ; HI ADDRESS => B
        MOV     C,A             ; LO ADDRESS =>C
        DAD     B               ; ADD OFFSET
        CALL    BYTE            ; GET ZERO BYTE
REC1:   CALL    BYTE            ; GET DATA BYTE
        MOV     M,A             ; SAVE
        INX     H               ; INC. RAM POINTER
        DCR     E               ; DEC. COUNT
        JNZ     REC1            ; LOOP IF MORE
        CALL    BYTE            ; GET CHECKSUM
        JNZ     REC3            ; ERROR IF CHECKSUM NON ZERO
        DW      LDDE
        DW      CURSOR
        RST     3
        DB      TBCD3           ; PRINT ADDRESS
        DW      LDCUR
        DW      CURSOR
        RST     3
        DB      KIN
        JNC     OK              ; CONTINUE IF NO KBD I/P
        CPI     03H
        JNZ     OK              ; CONTINUE IF NOT ^C
REC3:   MVI     A,0FH
        RST     3
        DB      SERO            ; OTHERWISE SEND ^O TO DEC
REC4:   RST     3
        DB      SRLIN
        ANI     PMASK
        CPI     '@'
        JNZ     REC4            ; WAIT FOR @
        RST
        DB      ERR             ; PRINT ERROR MESSAGE
REC2:   RST     3
        DB      TDEL            ; DELAY
        IN      1               ; DISCARD LAST DATA
        STC                     ; SET CARRY
        CMC                     ; RESET CARRY
        RET
```

```
OK:     STC                     ;SET CARRY
        RET
;
;
;************************************************************
;
; FUNCTION: SENDA
; DESCRIPTION: SENDS THE A REG. AS 2 ASCII BYTES TO THE DEC
;              AND UPDATES A CHECKSUM HELD IN NSAV.
; INPUTS: A - HEX BYTE TO BE SENT
; OUTPUTS: NONE
; CALLS: SERO
; DESTROYS: A,F/F'S
;
SENDA:  PUSH    PSW             ; SAVE COPY ON STACK
        RRC
        RRC
        RRC
        RRC                     ; HI NIBBLE => LO NIBBLE
        ANI     0FH             ; ZERO BITS 4-7
        CPI     0AH
        JM      SENDB           ; JUMP IF 0..9
        ADI     07H             ; PARTIAL CONV. TO A..F
SENDB:  ADI     30H             ; CONVERSION TO ASCII 0..9,A..F
        RST     3
        DB      SERO            ; SEND TO DEC
        POP     PSW             ; GET COPY
        PUSH    PSW             ; SAVE AGAIN
        ANI     0FH             ; MASK
        CPI     0AH
        JM      SENDC
        ADI     07H
SEND :  ADI     30H             ; CONVERT AGAIN
        RST     3
        DB      SERO            ; SEND TO DEC
        POP     PSW             ; GET COPY
        PUSH    H
        LXI     H,NUMN          ; POINT TO CHECKSUM
        ADD     M               ; ADD M TO A
        MOV     M,A             ; UPDATE CHECKSUM
        POP     H
        RET
;
;
;************************************************************
;
; FUNCTION: WCLOCK
; DESCRIPTION: COPIES CLOCK FROM MEMORY TO VIDEO RAM
; INPUTS: HL - START ADDRESS OF DATA TO BE CCOPIED
```

```
; OUTPUTS: NONE
; CALLS: NOTHING
; DESTROYS: A,B,C,D,E,H,L,F/F'S
;
WCLOCK: LXI     D,VCLOCK        ; POINT TO CLOCK IN VIDEO RAM
        LXI     B,8             ; SET COUNT
        DW      LDIR            ; WRITE TO VDU
        RET
;
;
;*****************************************************************
;
;       MESSAGE TABLE
;
;*****************************************************************
;
HEAD:   DB      'DEC-SYS 1.2'
ICLOCK: DB      '00:00:59'
LOGH:   DB      'TER '
        DB      'WIDTH '
        DB      '48',CR
        DB      'LOG '
        DB      'PHYSR-HF '
        DB      'RXHF2 4544'
        DB      CR
LOGL:   DB      'TER '
        DB      'WIDTH '
        DB      '48',CR
        DB      'LOG '
        DB      'PHYSR-STEP '
        DB      'ZHT2F 4544'
        DB      CR
MESS1:  DB      'TY '
MESS2:  DB      '.HEX',CR
MESS3:  DB      'RUN WR',CR
MESS4:  DB      ':0000000000',CR
;
;
        END
;
;*****************************************************************
@
```

APPENDIX II

DEC - SYSTEM - 20 Control Program
for Accepting Data From NASCOM.

```
00100   INPUT FILE$
00200   OPEN FILE$+".HEX" FOR OUTPUT AS FILE 1
00300   PRINT "*"
00320   INPUT A$ \ PRINT #1,A$
00360   IF LEFT$(A$,3)=":00" THEN GOTO 400  ELSE GOTO 300
00400   CLOSE
01000   END
@
```

APPENDIX III

Routine For Converting a File of Hexadecimal Numbers into a File of Decimal Numbers.

```
00100 INPUT "NAME HEX FILE",FILE$
00200 OPEN FILE$+".HEX" FOR INPUT AS FILE 1,INVALID 1100
00300 OPEN FILE$+".DAT" FOR OUTPUT AS FILE 2
00400 IFEND #1 GOTO 1300
00500 INPUT #1,DATA$
00600 IF LEFT$(DATA$,3)=":00" GOTO 1300
00650 DATA$=RIGHT$(DATA$,10)
00700 FOR LOOP=1 TO 16
00710 N=ASCII(MID(DATA$,1,1))
00740 IF N<65 THEN N=N-48 ELSE N=N-55
00750 NUMB=N*16
00760 N=ASCII(MID(DATA$,2,1))
00770 IF N<65 THEN N=N-48 ELSE N=N-55
00780 NUMB=NUMB+N
00790 PRINT #2,NUMB
00795 DATA$=RIGHT$(DATA$,3)
00800 NEXT LOOP
00870 GOTO 400
01100 PRINT "FILE NOT FOUND"
01200 GOTO 100
01300 CLOSE
01400 END
@
```

APPENDIX IV

Graph Plotting Routine Using
"GHOST" Graphics Package.

```
      IMPLICIT INTEGER(D)              ! D IS INTEGER
      DIMENSION D(1024),X(1024),Y(1024)
      DOUBLE PRECISION NAME,FNAME,ADT,ADT2
      LIN = 0   ;   LOG = 0
      CALL DATE(ADT)   ;   CALL TIME(T)
      WRITE(5,113)ADT,T
113   FORMAT(1H ,A9,20X,A5)
      WRITE(5,100)
100   FORMAT(1H0,' LINEAR PLOT ? (Y/N) ',$)
      READ(5,200)A
200   FORMAT(A1)
      IF (A.EQ.'Y') LIN = 1
      WRITE(5,101)
101   FORMAT(1H+,' LOG/LOG PLOT ? (Y/N) ',$)
      READ(5,200)A
      IF(A.EQ.'Y') LOG = 1
      IF (LOG < 1 .AND. LIN < 1) GOTO 901
      WRITE(5,102)
102   FORMAT(1H+,' ENTER .DAT FILENAME ',$)
      READ(5,201)NAME
201   FORMAT(A8)
      OPEN(UNIT=20,FILE=NAME,ACCESS='SEQIN')
      MIN = 256
      DO 300 I = 0,1023
      READ(20,202)V
202   FORMAT(G)
      D(I) = INT(V)
      IF (D(I).GT.MIN)GOTO 300
      MIN = D(I)
      MINX = I
300   CONTINUE
      WRITE(5,109)
109   FORMAT(1H+,' INPUT DATE (SEE ABOVE,NO LOWERCASE) ',$)
      READ(5,203)ADT2
203   FORMAT(A9)
      WRITE(5,110)
110   FORMAT(1H+,' TEMP ? ',$)
      READ(5,202)V
      ITEMP = INT(V)
      WRITE(5,111)
111   FORMAT(1H+,' FIELD ? ',$)
      READ(5,202)V
      IFIELD = INT(V)
      WRITE(5,112)
112   FORMAT(1H+,' SAMPLE TIME ? ',$)
      READ(5,202)TS
      IF (LIN < 1)GOTO 902
      DO 301 I = 0,1023
      X(I) = I
```

```
      Y(I) = D(I)
301   CONTINUE
      WRITE(5,104)
104   FORMAT(1H ,' LINEAR PLOT'/'  ==========')
      CALL PAPER(1)
      CALL MAP(0.0,1023.0,0.0,255.0)
      CALL AXES
      CALL PLACE(7,1)
      CALL UNDLIN(1)
      CALL TYPECS('LINEAR PLOT',11)
      CALL UNDLIN(0)
      CALL CTRMAG(15)
      CALL PLACE(37,1)
      CALL HLINFD(1)
      CALL TYPECS(ADT2,9)
      CALL SPACE(3)
      CALL TYPECS(T,5)
      CALL PLACE(65,36)
      CALL TYPECS('TEMP  ',6)
      CALL TYPENI(ITEMP)
      CALL TYPECS(' K',2)
      CALL PLACE(65,37)
      CALL HLINFD(1)
      CALL TYPECS('FIELD ',6)
      CALL TYPENI(IFIELD)
      CALL TYPECS(' V',2)
      CALL PLACE(65,39)
      CALL TYPECS('T',1)
      CALL SUFFIX
      CALL TYPECS('S',1)
      CALL NORMAL
      CALL SPACE(4)
      CALL HSPACE(1)
      CALL TYPENF(TS,1)
      CALL SPACE(1)
      CALL CTRSET(4)
      CALL TYPENC(23)
      CALL CTRSET(1)
      CALL TYPECS('S',1)
      CALL PLACE(65,40)
      CALL HLINFD(1)
      CALL TYPECS(NAME,6)
      CALL TYPECS('.HEX',4)
      DO 302 I = 0,1023,3
      CALL POINT(X(I),Y(I))
302   CONTINUE
      CALL GREND
      IF(LOG < 1) GOTO 999
902   WRITE(5,105)
105   FORMAT(1H ,' LOG/LOG PLOT'/'  ===========')
```

```
      IF (LIN < 1)GOTO 903
      WRITE(5,106)
106   FORMAT(1H ,' GRID FILE NAME (0-5 CHARS):',$)
      READ(5,201)FNAME
      CALL FILNAM(FNAME)
903   LAST = D(1023) + 1
      J = 0
      ICNT = 0
      DO 303 I = MINX,1023
      J = J + 1
      Y(J) = LAST - D(I)
      X(J) = J
303   CONTINUE
      CALL CTRMAG(20)
      CALL PAPER(1)
      DO 305 I = 1,10
      WRITE(5,108)X(I),Y(I)
108   FORMAT(2G)
305   CONTINUE
      CALL MAPXYL(1.0,1023.0,1.0,255.0)
      CALL AXEXYL
      CALL PLACE(7,1)
      CALL UNDLIN(1)
      CALL TYPECS('LOG/LOG PLOT',12)
      CALL UNDLIN(0)
      CALL CTRMAG(15)
      CALL PLACE(37,1)
      CALL HLINFD(1)
      CALL TYPECS(ADT2,9)
      CALL SPACE(3)
      CALL TYPECS(T,5)
      CALL SPACE(6)
      CALL TYPECS('TEMP  ',6)
      CALL TYPENI(ITEMP)
      CALL TYPECS(' K',2)
      CALL PLACE(60,3)
      CALL TYPECS('FIELD ',6)
      CALL TYPENI(IFIELD)
      CALL TYPECS(' V',2)
      CALL PLACE(60,4)
      CALL HLINFD(1)
      CALL TYPECS('T',1)
      CALL SUFFIX
      CALL TYPECS('S',1)
      CALL NORMAL
      CALL SPACE(4)
      CALL HSPACE(1)
      CALL TYPENF(TS,1)
      CALL SPACE(1)
```

```
        CALL CTRSET(4)
        CALL TYPENC(23)
        CALL CTRSET(1)
        CALL TYPECS('S',1)
        CALL PLACE(60,6)
        CALL TYPECS(NAME,6)
        CALL TYPECS('.HEX',4)
        DO 304 I = 1,J
        IF(Y(I).GT.0.5)GOTO 904
        ICNT = ICNT + 1
        WRITE(5,115)ICNT,X(I),Y(I)
115     FORMAT(1H ,3G)
        GOTO 304
904     CALL POINT(X(I),Y(I))
304     CONTINUE
        CALL GREND
        WRITE(5,114)ICNT
114     FORMAT(1H0,I3,' POINTS NOT PLOTTED')
999     WRITE(5,107)
107     FORMAT(1H0)
        STOP
901     WRITE(5,103)
103     FORMAT(1H ,'NO PLOTS')
        STOP
        END
@
```